

345-72

N72-31778

NASA CR-120853

# CASE FILE COPY

## A GRAPHITE-LINED REGENERATIVELY COOLED THRUST CHAMBER

by

V. R. Stubbs

Aerojet Liquid Rocket Company  
Sacramento, California 95813

Prepared for

NATIONAL AERONAUTICS AND SPACE ADMINISTRATION

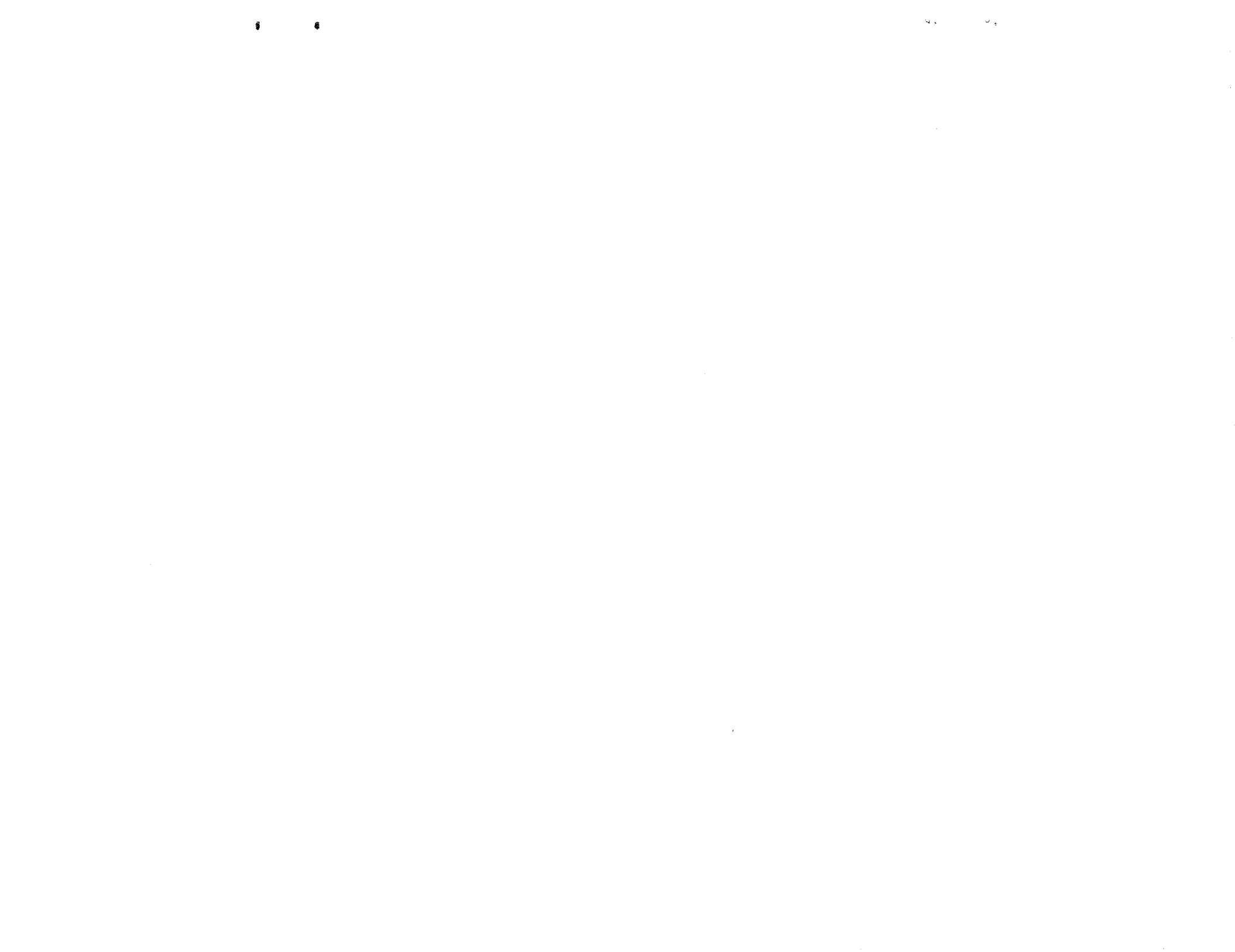


NASA Lewis Research Center

Contract NAS 3-13315

R. A. Duscha, Project Manager

1. Report No. NASA CR-120853		2. Government Accession No.		3. Recipient's Catalog No.	
4. Title and Subtitle A GRAPHITE-LINED REGENERATIVELY COOLED THRUST CHAMBER				5. Report Date	
				6. Performing Organization Code	
7. Author(s) V. R. Stubbs				8. Performing Organization Report No.	
				10. Work Unit No.	
9. Performing Organization Name and Address Aerojet Liquid Rocket Company P.O. Box 13222 Sacramento, California 95813				11. Contract or Grant No. NAS 3-13315	
				13. Type of Report and Period Covered Contractor Report	
12. Sponsoring Agency Name and Address National Aeronautics and Space Administration Washington, D.C. 20546				14. Sponsoring Agency Code	
15. Supplementary Notes Project Manager, R. A. Duscha, NASA Lewis Research Center, Cleveland, Ohio					
16. Abstract  Design concepts, based on use of graphite as a thermal barrier for regeneratively cooled FLOX-methane thrust chambers, have been screened and concepts selected for detailed thermodynamic, stress, and fabrication analyses. A single design employing AGCarb-101, Aerojet's fibrous graphite composite material, for a thermal barrier liner and an electroformed nickel structure with integral coolant passages was selected for fabrication and testing. The fabrication processes and the test results are described and illustrated.					
17. Key Words (Suggested by Author(s)) Thrust chamber Thermal barriers Graphite-lined thrust chamber Electroformed nickel thrust chamber			18. Distribution Statement Unclassified - Unlimited		
19. Security Classif. (of this report) Unclassified		20. Security Classif. (of this page) Unclassified		21. No. of Pages 260	22. Price* \$3.00



## FOREWORD

The work described herein was performed for NASA/LeRC under Contract NAS 3-13315, titled "Contract for Regeneratively Cooled Graphite-Lined Thrust Chamber." Mr. R. A. Duscha was the NASA/LeRC project manager.

The program manager was Dr. N. E. Van Huff and the project manager Mr. R. C. Schindler. Mr. V. R. Stubbs, the author of this report, was project engineer. Thermodynamic studies were performed by Messrs. L. Schoenman and J. C. Cunningham. Stress analyses were performed by J. W. Starr and P. J. Krusi.



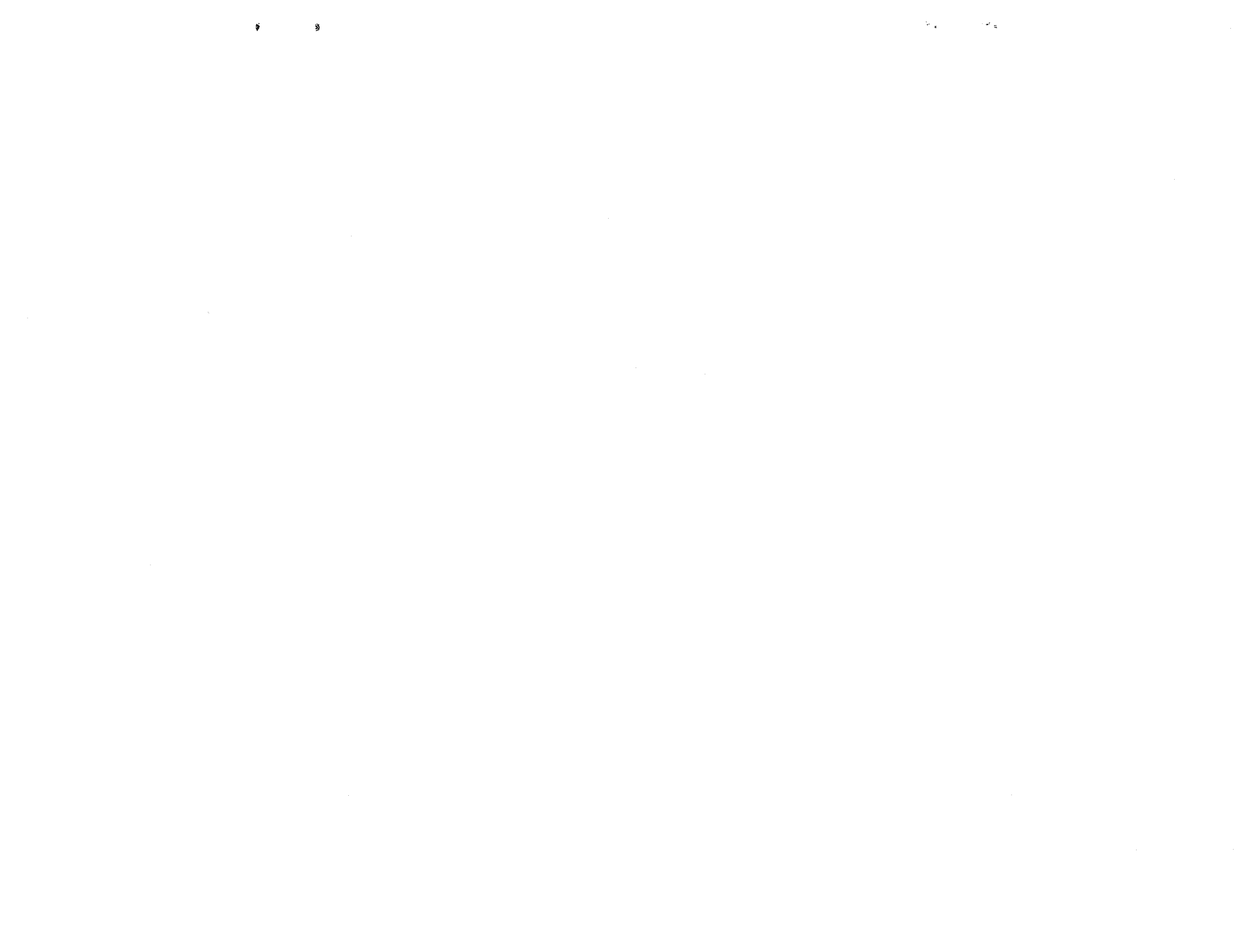


TABLE OF CONTENTS

	<u>Page</u>
I. Summary	1
A. Objectives	1
B. Summary of Tasks I Through V	1
C. Conclusions and Recommendations	3
II. Introduction	4
A. Background	4
B. Objectives	4
C. Design Requirements	4
D. Approach	5
III. Task I - Design and Evaluation	6
A. Subtask 1. Preliminary Conceptual Designs	6
B. Subtask 2. Design Evaluation	6
C. Subtask 3. Uncooled Chamber Designs	41
D. Subtask 4. Final Design	50
IV. Task II - Fabrication	68
A. Uncooled Chamber Fabrication	68
B. Cooled Chamber Fabrication	68
V. Task III - Facility Preparation and Injector Checkout	93
A. Facility Preparation	93
B. Injector Checkout Firing	93
VI. Task IV - Cooled Chamber Tests	99
A. Test Conditions	99
B. Test Results, Cooled Chamber Testing	101
C. Posttest Analysis	102
D. Analysis of Test Results	111
VII. Conclusions	117
References	119

APPENDICES

	<u>Appendix</u>
Thermal and Mechanical Evaluations of AGCarb Material	A
Structural Analysis of Regeneratively Cooled AGCarb Graphite-Lined Thrust Chamber	B
Distribution List	C

TABLE LIST

<u>Table</u>		<u>Page</u>
I	Summary of Minimum Margins of Safety, Workhorse Chamber No. 1159375	48
II	Summary of Minimum Margins of Safety, Copper Workhorse Chamber No. 1158763	49
III	Test Results, Graphite-Lined Workhorse Thrust Chamber	98
IV	Summary of Major Parameters of Cooled Tests	106
V	Pulse Test	107

FIGURE LIST

<u>Figure</u>		<u>Page</u>
1	Electroformed Jacket AGCarb Liner, Drawing 1158932	7
2	Pyrolytic Graphite Insert, Cylindrical Shell, Drawing 1158920	8
3	Axial Segmented Graphite, Drawing 1159044	9
4	AGCarb Liner Nickel Segmented Shell, Drawing 1158544	10
5	AGCarb Liner, Copper Milled Passages, Drawing 1158941	11
6	Channeled Graphite Liner, Nickel Shell, Drawing 1158546	12
7	Coolant Flow Characteristics, Concept I	15
8	Thickness vs Temperature at Axial Distance = 8.0 in.	16
9	Interface Contact Coefficient for Graphite	17
10	Coolant Channel Analysis	18
11	Steady-State Temperature Profiles, Concept I	21
12	Transient and Steady-State Temperature Profiles, Concept I	22
13	Steady-State Solution for Axial Distance = 13.50 in.	23
14	Transient and Steady-State Temperature Profiles, Concept II	27
15	Coolant Flow Conditions, Axially Segmented Graphite Chamber	32
16	Interchannel Fluid Mixing Ribs	33
17	Transient and Steady-State Temperature Profiles, Concept III	34
18	Combustion Chamber, Workhorse, Uncooled, Drawing 1159375	42
19	Combustion Chamber Assembly, Copper Workhorse, Drawing 1158763	44
20	Temperature Profile at 6 sec and 8 sec	45
21	Copper Heat Sink Chamber Temperature Response at Throat	46
22	Channel Design Effects on Nickel Temperature	52
23	Liner and Channel Wall Temperature Variation for Constant Channel Width Design	53
24	Three Channel Designs	55
25	Channel Design Summary - 100 Channels	57
26	Liner, Combustion Chamber, Drawing 1159524	58
27	Combustion Chamber, Drawing 1159525	27
28	Combustion Chamber Assembly, Drawing 1159636	61
29	Thermal Parameters for 100-Channel Chamber Design	63
30	Test Specimens After Graphitization and Before Machining	66

FIGURE LIST (cont.)

<u>Figure</u>		<u>Page</u>
31	Test Specimen as Shipped to Southern Research Corporation	67
32	Manufacturing Flow Chart	71
33	Discrepancy Analysis	72
34	Throat Segments Premolded and Machined	73
35	Exit Segments Bonded, Cured and Rough Machined	74
36	Cylindrical Segments Cured and Rough Machined	75
37	Components in Assembly Position	76
38	Liner Assembly Prior to OD Machining	77
39	SN 2 Showing Delamination in Exit Section	80
40	Graphite Liner in "Setup" Position for Electroforming	81
41	Crack Indication - Dye Penetrant	82
42	Electroformed Chamber Contour Machined to "K" Diameter	84
43	Milling Coolant Channels	85
44	Chamber with Core Material in Slots Before Closeout Electroforming	86
45	Electroform Repair, Aft Flange SN 1	88
46	Electroform Repair, Aft Flange SN 2	89
47	SN 2 After Final Machining	90
48	Pattern Flow Test	91
49	FLOX/Methane Test Setup, Test Stand J-4	94
50	Graphite-Lined Workhorse Chamber on Test Stand	96
51	Graphite-Lined Workhorse Chamber, Posttest	97
52	J-4 Test Stand	103
53	Thrust Chamber SN 2 on Test Stand	104
54	Posttest First Run, 5.5 sec	105
55	Posttest No. 13 Cylindrical Section	108
56	Posttest No. 14 Exit End Showing Carbon Deposit	109
57	Posttest No. 14 Exit End After Cleaning Liner	110
58	Temperature Transients at the Throat, Test No. 14	112
59	Predicted vs Actual Temperature Conditions	114
60	Predicted vs Actual Transient Temperature Conditions	116

I. SUMMARY

A. OBJECTIVES

The objective of Contract NAS 3-13315 was to demonstrate the feasibility of operating a graphite-lined regeneratively cooled thrust chamber with the FLOX-methane propellant combination. This was to be preceded by a three-part program which included design concept evaluation and analysis, thrust chamber fabrication, and facility preparation and injector checkout.

B. SUMMARY OF TASKS I THROUGH V

Task I consisted of the development of 12 conceptual designs and their initial screening. This was followed by analysis of the six most promising concepts, which are described below.

Concept I - Electroformed jacket, AGCarb liner.- This design consists of a fibrous graphite liner over which is an electroformed nickel shell containing coolant passages.

Concept II - Pyrolytic graphite insert, cylindrical shell.- This design features a composite, replaceable liner of various graphite materials, including a series of pyrolytic graphite washers at the throat area.

Concept III - Axial segmented graphite.- This thrust chamber is constructed of 42 axial wedge-shaped graphite sections separated by nickel coolant fins.

Concept IV - AGCarb liner, nickel segmented shell.- In this design, a fibrous graphite liner and electroformed nickel shell are used as in Concept I; however, in this design, the shell is in three segments, permitting the liner or any segment to be replaced.

Concept V - AGCarb liner, copper milled passages.- This design employs a fibrous graphite liner electroformed or plasma sprayed copper with milled passages, a split copper throat segment, and a cylindrical structural shell.

Concept VI - Channeled graphite liner, nickel shell.- In this design, a bulk graphite liner is grooved on the outside diameter to form axial coolant passages. The outside shell is electroformed nickel.

Concept I was selected for detailed design and fabrication. A program was accomplished to further characterize the AGCarb gas-side material prior to the completion of the design. This program tested AGCarb material specimens of

I, B, Summary of Tasks I Through V (cont.)

the exact configuration to be used to obtain mechanical properties data. The specimens were fabricated by San Rafael Plastics Company and testing performed by Southern Research Corporation (see Appendix A for test data).

Task I also included the design of an uncooled workhorse or "streak" chamber and a copper heat sink chamber which could be used for injector evaluation. These designs were completed including heat transfer and stress analyses.

Task II consisted of the fabrication of the uncooled and regeneratively cooled thrust chambers. The workhorse chamber consisted of a stainless steel housing which contained an ATJ graphite liner. Two extra liners were fabricated for use as replacements. The copper heat sink chamber contained an AGCarb throat insert which was intended to permit firing durations up to 8 sec. An equivalent all-copper throat was calculated to provide a 2- to 3-sec duration capability. Two spare AGCarb throat inserts were fabricated.

Task III consisted of two subtasks: (1) Facility Preparation and (2) Injector Checkout Firing. The first subtask included the buildup of a propellant feed system on an existing test stand. This system contained a heat exchanger to cool gaseous methane to  $-120^{\circ}\text{F}$  ( $189^{\circ}\text{K}$ ). The second subtask consisted of six test firings of the workhorse thrust chamber to check the facility operation and ensure that the injector was functioning properly. Test firing of the heat sink chamber was deleted to permit additional duration testing of the cooled thrust chamber.

The tests with the workhorse chamber demonstrated proper functioning of the facility and injector. Six tests were performed with a total duration of 23 sec. There was no streaking or erosion of the thrust chamber. Slight soot deposits were evident on the chamber wall.

In Task IV, one of the two cooled thrust chambers fabricated was tested for a total duration of 540 sec. This test series consisted of 22 start and stop cycles including a cycling test which consisted of eight pulses of 5 sec on and 2 sec off. The thrust chamber was inspected after each test and throat measurements taken. The throat diameter measurements varied from 1 to 2 mils (0.0254 to 0.0762 mm) under prefire diameter measurements, indicating an absence of throat erosion and slight varying soot buildup. Heavy soot deposits were noted in the cylindrical section of the thrust chamber. These deposits varied in thickness from a few mils up to 1/8 of an inch (3.17 mm). Variations in thermocouple readings indicated a continual buildup and flaking off of layers of soot occurred during the test firing. The lack of thrust chamber deterioration during the test series resulted in the decision to accomplish the demonstration using a single unit. The untested second thrust chamber was delivered to NASA Lewis Research Center.

## I, B, Summary of Tasks I Through V (cont.)

Task V included monthly reports, posttest analyses, and the final report. Posttest analyses were limited to X-ray to determine throat area thermocouple location and posttest measurements and visual inspection.

### C. CONCLUSIONS AND RECOMMENDATIONS

(1) The fabrication and operation of a fibrous graphite thermal barrier contained within an electroformed nickel coolant jacket was demonstrated to be feasible using FLOX-methane propellants. The thermal, mechanical, and chemical properties of the fibrous graphite composite material are sufficiently well defined. Fabrication techniques for the fibrous graphite material and the electroformed nickel processing are sufficiently state-of-the-art that further development would be necessary only if there were substantial departures from the size and geometry of the units tested. Changes in propellant which significantly alter the chemical environment to which the graphite was exposed could require further gas-side material development.

(2) It is recommended that further testing be performed with existing hardware to define the failure limits of the design. This should include testing at increased chamber pressure and higher mixture ratios to increase heat flux while reducing coolant flow.

(3) Since the mechanical capability and thermal shock advantages of the fibrous graphite - regeneratively cooled nickel thrust chamber are established, it is also recommended that studies be initiated to investigate the use of fibrous graphite in applications with propellant combinations other than FLOX-methane. This investigation would have the twofold objective of defining the chemical environment capabilities of fibrous graphite and improving its corrosion resistance to combustion products of other propellant combinations.



## II. INTRODUCTION

### A. BACKGROUND

The employment of high-energy propellants in liquid bipropellant thrust chambers has resulted in indications that regenerative cooling of metal-walled thrust chambers is inadequate at the higher heat flux environment. The design limitations of conventional regeneratively cooled engines employing tubular designs have been overcome by the use of nontubular coolant passages in high conductivity materials such as copper and nickel. Although these concepts permit the designer greater flexibility in tailoring flow rate and velocity of coolant to suit heat input predictions, thermal barrier systems will further improve heat flux capability.

Graphite and fibrous graphite composite materials have a demonstrated ability to withstand temperatures of 5000°F (3033°K) while subjected to a HF environment. These properties result in these materials being prime candidate thermal barrier materials. This program was structured to combine the features of nontubular construction with the use of graphitic thermal barrier materials to produce a regeneratively cooled thrust chamber with a heat flux capability and reliability beyond that attainable with metal or refractory-coated metal structures.

### B. OBJECTIVES

The objectives of this program were to determine both analytically and experimentally the feasibility and limits of combining regenerative cooling technique with a passive high temperature, thermal resistant material such as graphite.

### C. DESIGN REQUIREMENTS

The design requirements established were as follows:

Thrust	= 5000 lb
Chamber pressure	= 500 psia
Area ratio	= 100 (may be tested with reduced expansion)
Propellants	= FLOX-liquid methane
Mixture ratio	= 5.25
Coolant mode	= Regenerative using fuel
Injector	= To be supplied
Coolant temperature at inlet	= 250°R (139°K)

II, C, Design Requirements (cont.)

Coolant temperature rise = 1450°F (max) (1061°K)  
Coolant pressure at outlet = Two times chamber pressure  
Coolant pressure drop = Minimum  
Gas-side wall temperature = 4000°F (max) (2477°K)  
Gas-side material = Graphite or graphitic

D. APPROACH

The program was divided into five major tasks with subtasks as shown. This enumeration was established as the project work plan. The descriptions and discussions in the succeeding sections will follow the sequence noted.

REPORTING CATEGORY

TASK I - DESIGN AND EVALUATION

1. Preliminary Conceptual Design
2. Design Evaluation
3. Uncooled Chamber Designs
4. Final Designs

TASK II - THRUST CHAMBER FABRICATION

5. Uncooled Chambers Fabrication
6. Cooled Chambers Fabrication

TASK III - FACILITY PREPARATION AND INJECTOR CHECK

7. Facility Preparation
8. Injector Checkout Firing

TASK IV

9. Cooled Chamber Tests

TASK V

10. Posttest Analysis
11. Monthly Reports
12. Final Report

### III. TASK I - DESIGN AND EVALUATION

#### A. SUBTASK 1. PRELIMINARY CONCEPTUAL DESIGNS

Prior to development and screening of conceptual designs, candidate materials were listed and their thermal and mechanical properties categorized. The properties of the propellants were obtained and considerable study and analysis were performed on published results of other NASA FLOX-methane programs. Methods of analysis were established for the heat transfer and stress analyses planned, and a preliminary heat transfer and stress analysis was performed on the electroformed nickel-AGCarb liner design concept as a method of confirming the models and computer programs.

Twelve design concepts were identified for further study. Performance and fabrication considerations reduced these to six concepts which included the desirable features of the original twelve. These are presented in Figures 1 through 6 and discussed in the next section of this report.

#### B. SUBTASK 2. DESIGN EVALUATION

Program requirements included the analysis of candidate designs in sufficient detail to permit prudent selection of two designs for fabrication and testing. Each candidate was examined for fabrication feasibility, thermal limitations, and structural adequacy. Problem areas and deficiencies were identified for each concept and considered in a final rating to determine the concepts to be recommended for design and fabrication. The results of the study indicated that three of the six concepts studied were feasible. One of these was recommended for final design, fabrication, and testing. The three designs are designated as: (I) Electroformed Jacket, AGCarb Liner, (II) Pyrolytic Graphite Insert, and (III) Axially Segmented Graphite, Cylindrical Shell. The final review by NASA resulted in selection of the AGCarb liner-electroformed nickel concept for final design and fabrication. It was further agreed that, in lieu of design and fabrication of a second concept, further characterization of AGCarb mechanical and thermal properties was desirable.

The following paragraphs summarize the design studies of each of the six design concepts. Each concept is identified and considered individually. The structural analyses performed are not included in this report due to the fact that the analyses were preliminary and carried only to the point of determining basic feasibility and identifying problem areas. A complete analysis of the final design, which illustrates the methods of analysis employed, is presented in Appendix B.

##### 1. Concept I. Electroformed Jacket, AGCarb Liner (Figure 1)

###### a. Description and Fabrication Approach

The design consists of an AGCarb fibrous graphite flame liner encased in an electroformed nickel regenerative cooling jacket. Neither the liner nor jacket are replaceable individually. A flat wrap parallel to the



Figure 2. Combustion Chamber Pyrolytic Graphite Insert Cylindrical Shell

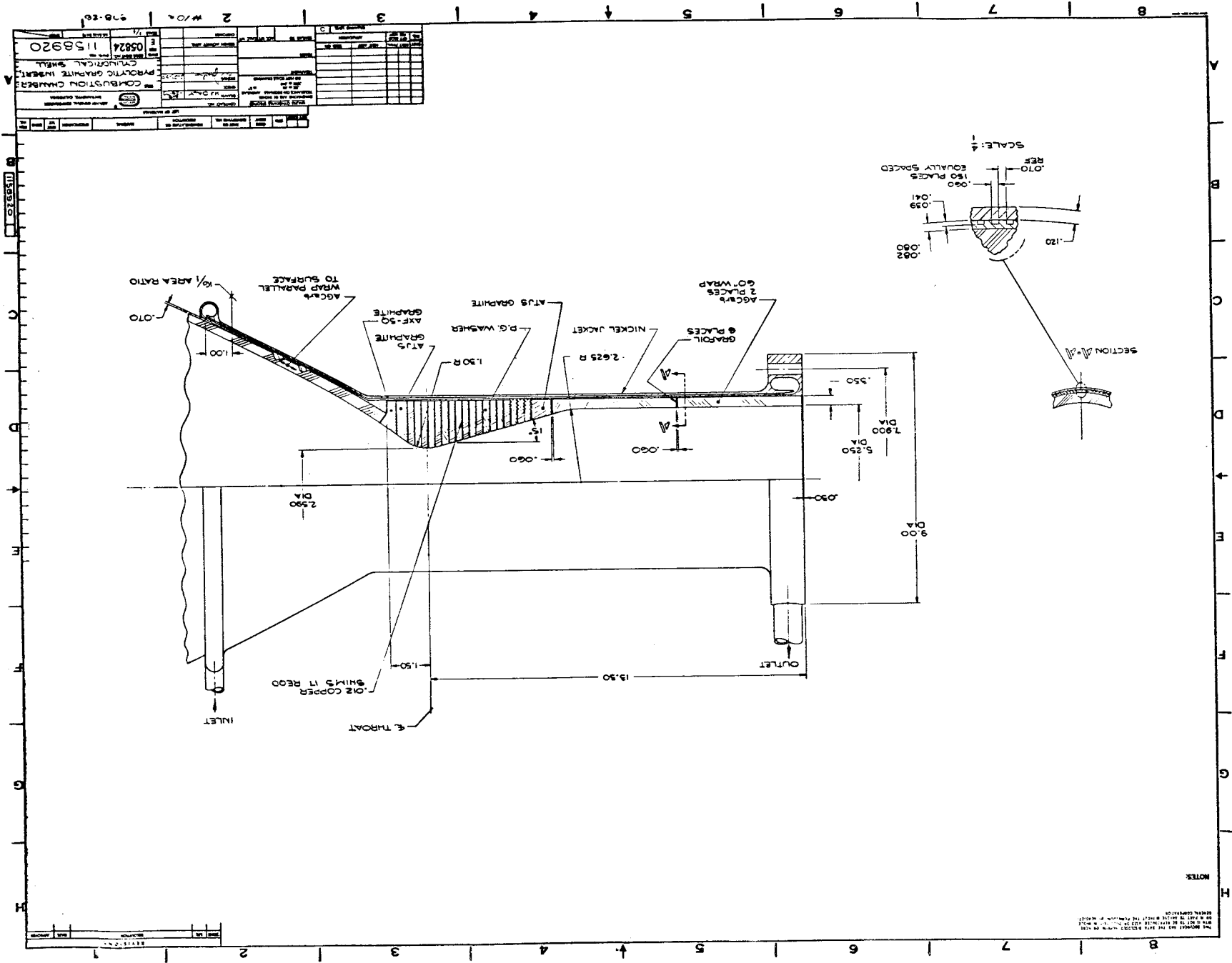
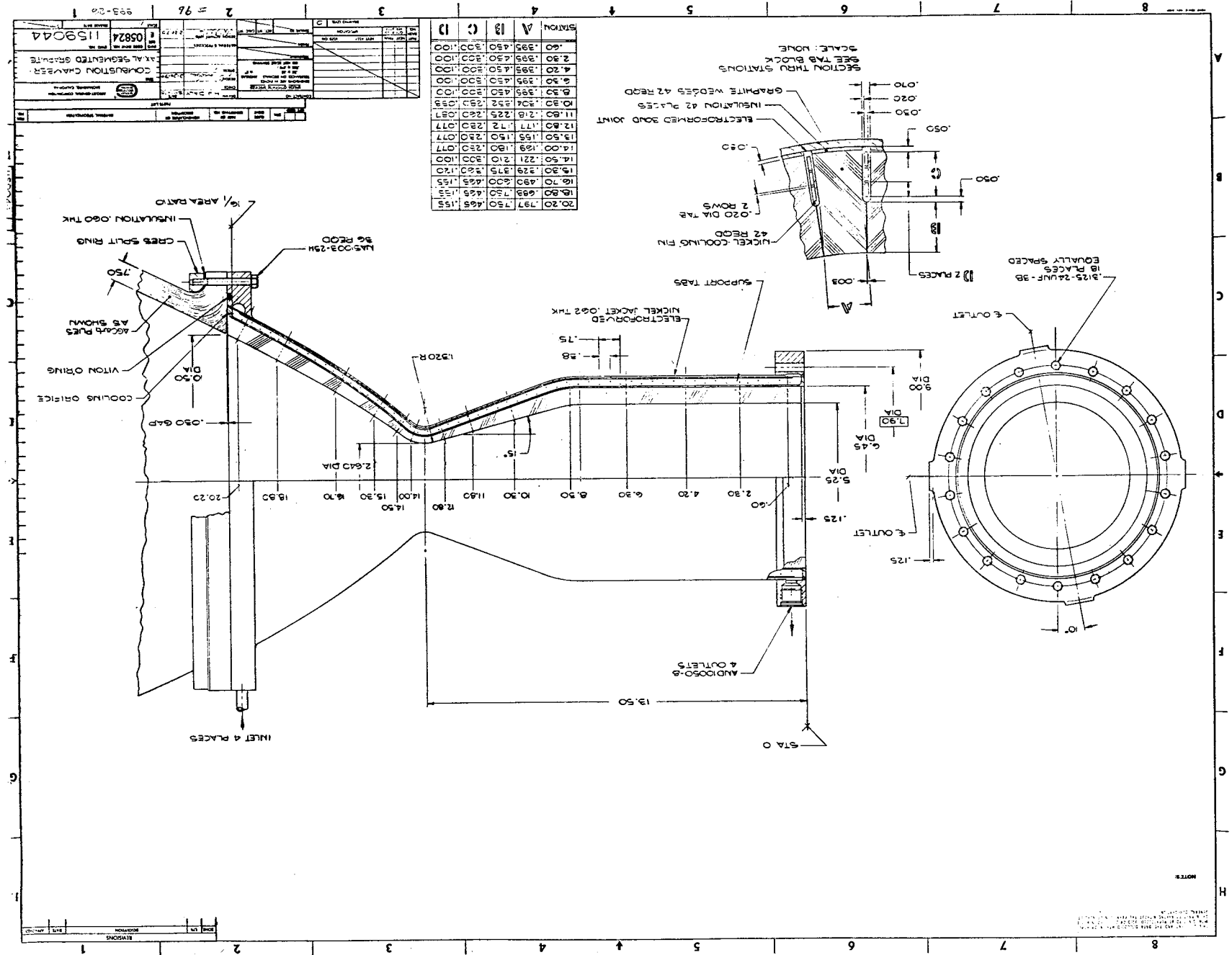


Figure 3. Combustion Chamber Axial Segmented Graphite









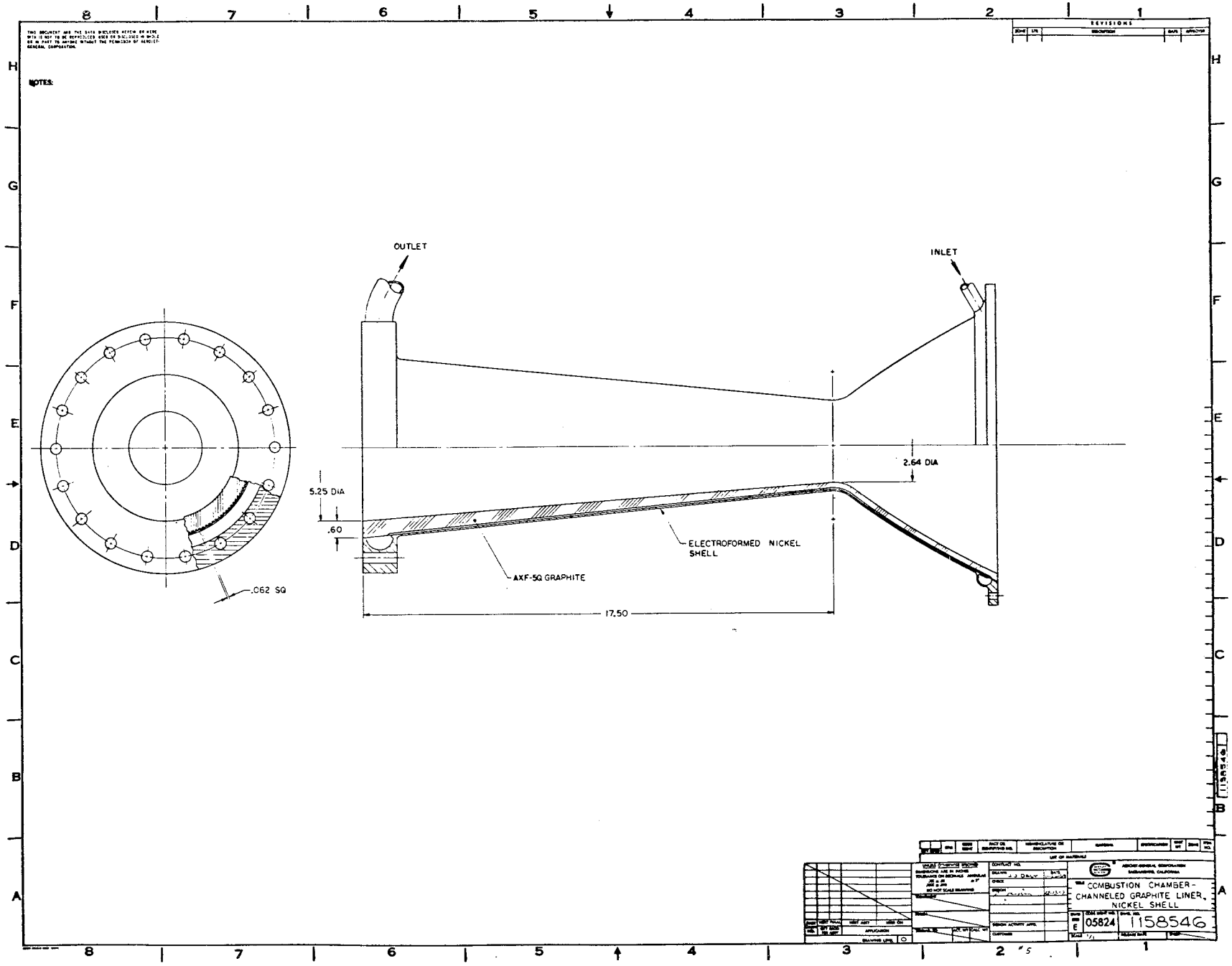


Figure 6. Combustion Chamber Channeled Graphite Liner, Nickel Shell

### III, B, Subtask 2. Design Evaluation (cont.)

surface is the preferred fabrication method for the AGCarb liner. This results in a thin wall in the throat area which is not desirable from a handling standpoint. There would also be a reduction in conductivity should a delamination occur. For these reasons, a 60° to the surface layup angle was selected. For ease of fabrication, construction is of four axial segments. The throat area segment is made by compression molding. The others are made using 45° bias tape wrapped 60° to the surface to area ratio 2.8:1 where a flat wrap parallel to the surface is used. At area ratio 16:1, the regenerative jacket ends and the liner becomes a free-standing, radiation-cooled nozzle.

This design is lightweight in that the AGCarb and nickel jacket are at minimum thickness. The jacket is electroformed onto the graphite, permitting the jacket to follow the liner contour exactly. The electroforming also produces a joint of minimum thermal resistance. AGCarb was chosen for the flame liner because it is readily fabricated in large sections and is less brittle than the bulk graphites. AGCarb is an Aerojet-developed fibrous graphite composite material having superior strength and higher density and conductivity than other fibrous graphites. Nickel was selected for the cooling jacket because of its compatibility with the methane and the combustion products, its ability to be electroformed, and its good conductivity and reasonable strength at elevated temperatures.

The fabrication technique to be followed will be to electroform a layer of nickel over the AGCarb liner. The layer will be at least 0.080 in. (2.03 mm) thick. Cooling channels will be milled into the nickel layer. The cooling channels will be filled with a low melting temperature core material and then covered with a 0.060 in. (1.524 mm) or greater layer of nickel after which the wax core material is removed. Flanges and inlet and outlet manifolds will be attached by electron beam welding.

#### b. Thermal Analysis

##### (1) Thermal and Hydraulic Summary

The thrust chamber shown in Figure 1 is regeneratively cooled to an area ratio of 16:1. Coolant enters at an area ratio of 4 and flows aft through 75 channels which are 0.1 in. (2.54 mm) deep and 0.078 in. (1.98 mm) wide to an exit area ratio of 16:1. At this point, the coolant turns around and flows back up to the 4:1 area ratio through the same quantity of adjacent channels of the same configuration. The depth of the channels carrying the coolant at this point is reduced linearly to 0.040 in. (1.015 mm) at a station slightly downstream of the throat. The channel depth is maintained at 0.040 in. (1.015 mm) from this point to the injector. At an axial station of 12.2 in. (0.31 m), the channel width is increased from 0.078 in. (1.98 mm) to 0.094 in. (2.39 mm) in order to minimize pressure drop. This larger channel carries the fluid to an axial station of 10.1 in. (0.256 m) where the rib

### III, B, Subtask 2. Design Evaluation (cont.)

thickness reaches 0.120 in. (3.025 mm). At this point, the 75 0.094-in.-wide (2.39 mm) channels are bifurcated into 150 channels 0.062 in. (1.575 mm) wide to further reduce pressure drop. The pressure drop for this design is 170 psi ( $1.172 \times 10^3 \text{ N/m}^2$ ). The maximum and minimum rib thickness are 0.160 in. (4.075 mm) at the exit and 0.0445 in. (1.131 mm) at the throat.

Rib thickness in the chamber is 0.064 in. (1.630 mm). The liner thickness has been sized to maintain gas-side wall temperatures at approximately 4500°F (2750°K) and the nickel below 1250°F (950°K). The coolant discharge temperature at steady-state conditions is 300°F (422°K). Coolant mass velocity ( $\dot{w}/A$ ), temperature, and pressure profiles along the axis of the chamber are presented in Figure 7.

#### (2) Steady-State Thermal Conditions

Thermal analysis of this concept was conducted in two phases involving several design iterations. Liner thickness and coolant velocities were first hand calculated for the chamber, throat, and exit nozzle stations to determine the effect of AGCarb-101 thickness and orientation on wall temperatures. The results of the chamber station analysis are presented in Figure 8. Design variables considered in the analysis were: liner thicknesses of 0.25 to 0.35 in. (6.36 to 8.90 mm); fiber orientations of 30 and 60° with the hot gas stream; and two states of interface contact, full thermal contact and a contact coefficient of 5500 Btu/hr-ft<sup>2</sup>-°F (17,300 W/hr-m<sup>2</sup>) based on data of Figure 9. The results of this analysis, shown in Figure 8, demonstrated that maximum wall temperature was not sensitive to substantial variations in liner wall thicknesses and contact resistances. This analysis also demonstrated that the 60% fiber orientation angle produced more favorable gas-side temperatures than the shallower angle.

Selection of the liner thickness was based on previous test histories of Aerojet's AGCarb chambers wherein this material experienced numerous thermal cycles to temperatures exceeding 5000°F (3033°K). The thickness selected for the analysis was 0.35 in. (8.9 mm) in the chamber, 0.130 in. (3.3 mm) at the throat, and 0.60 in. (15.2 mm) at an exit area ratio of 4.0. These resulted in gas-side wall temperatures of approximately 4500°F (2760°K), 4700°F (2860°K), and 4400°F (2700°K), respectively, at these locations, assuming that the electroforming process provides full thermal contact.

The selected liner configuration simplified fabrication by use of linear tapers between these calculated locations.

The 150/75 1-1/2 pass coolant channel arrangement selection is based on the parametric analysis detailed in Figure 10 where it is shown that the number of channels does not significantly influence thermal profiles. The specific channel width conforms to standard tool sizes and the

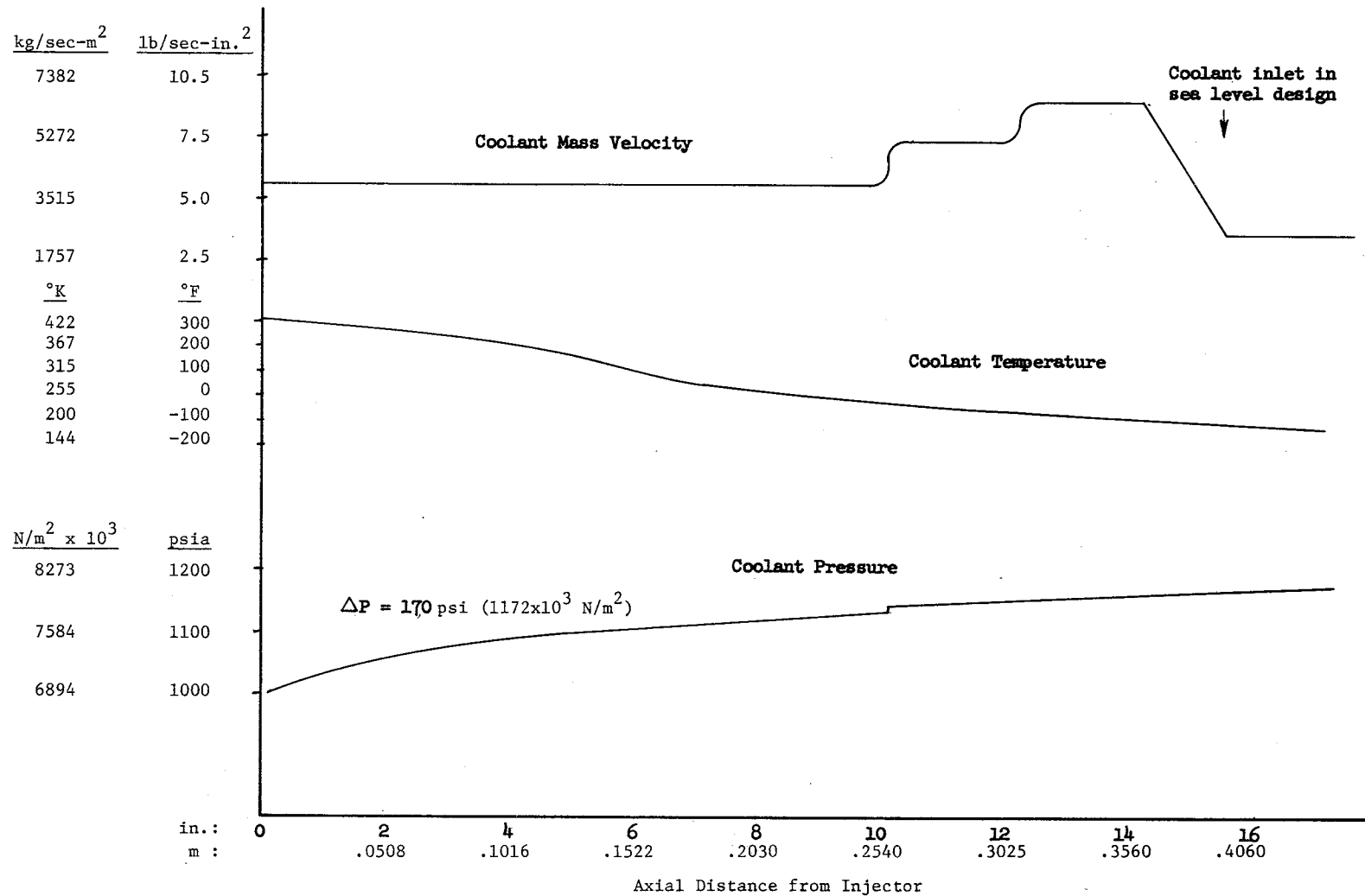


Figure 7. Coolant Flow Characteristics, Concept I

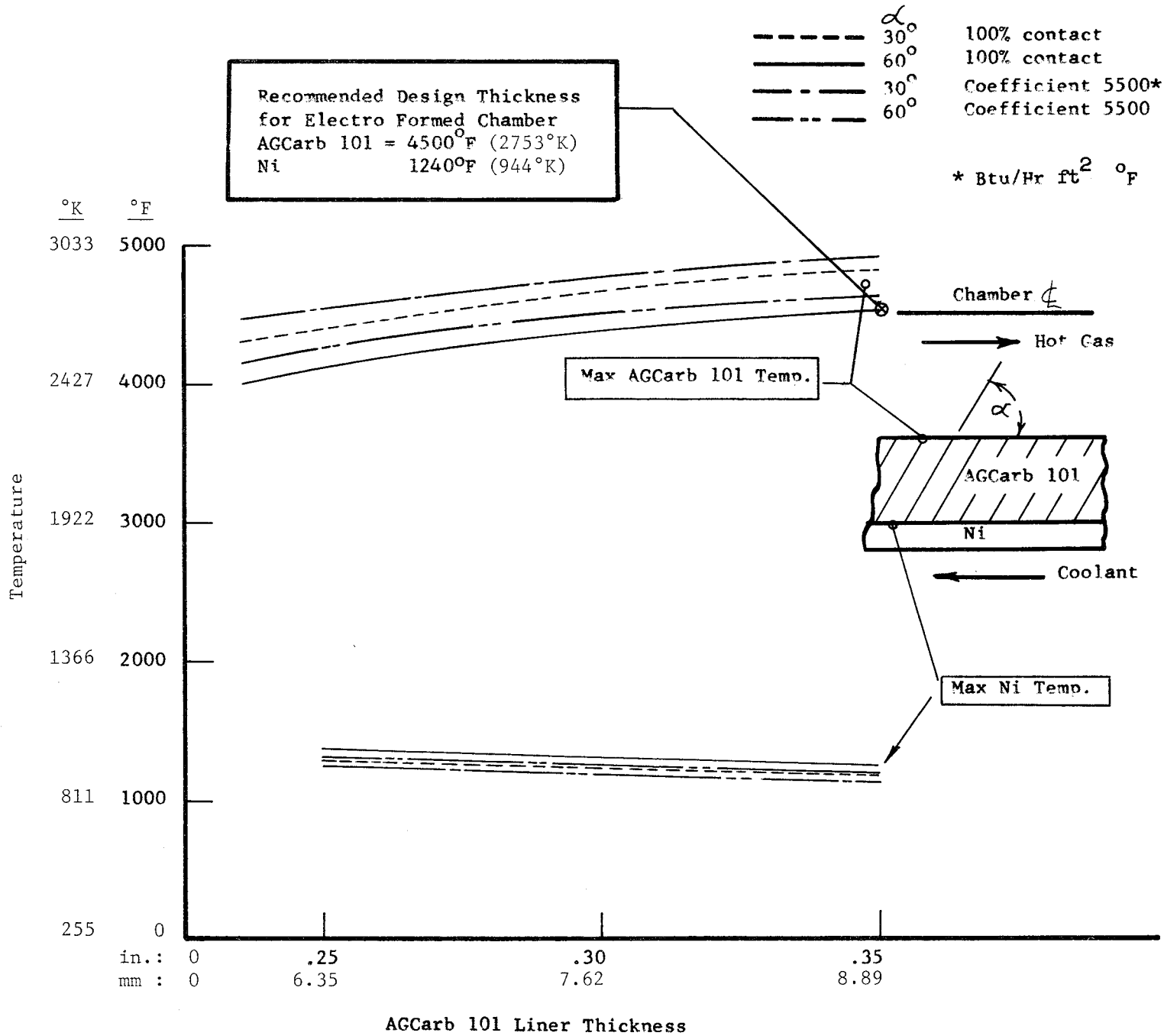


Figure 8. Thickness vs Temperature at Axial Distance = 8.0 in.

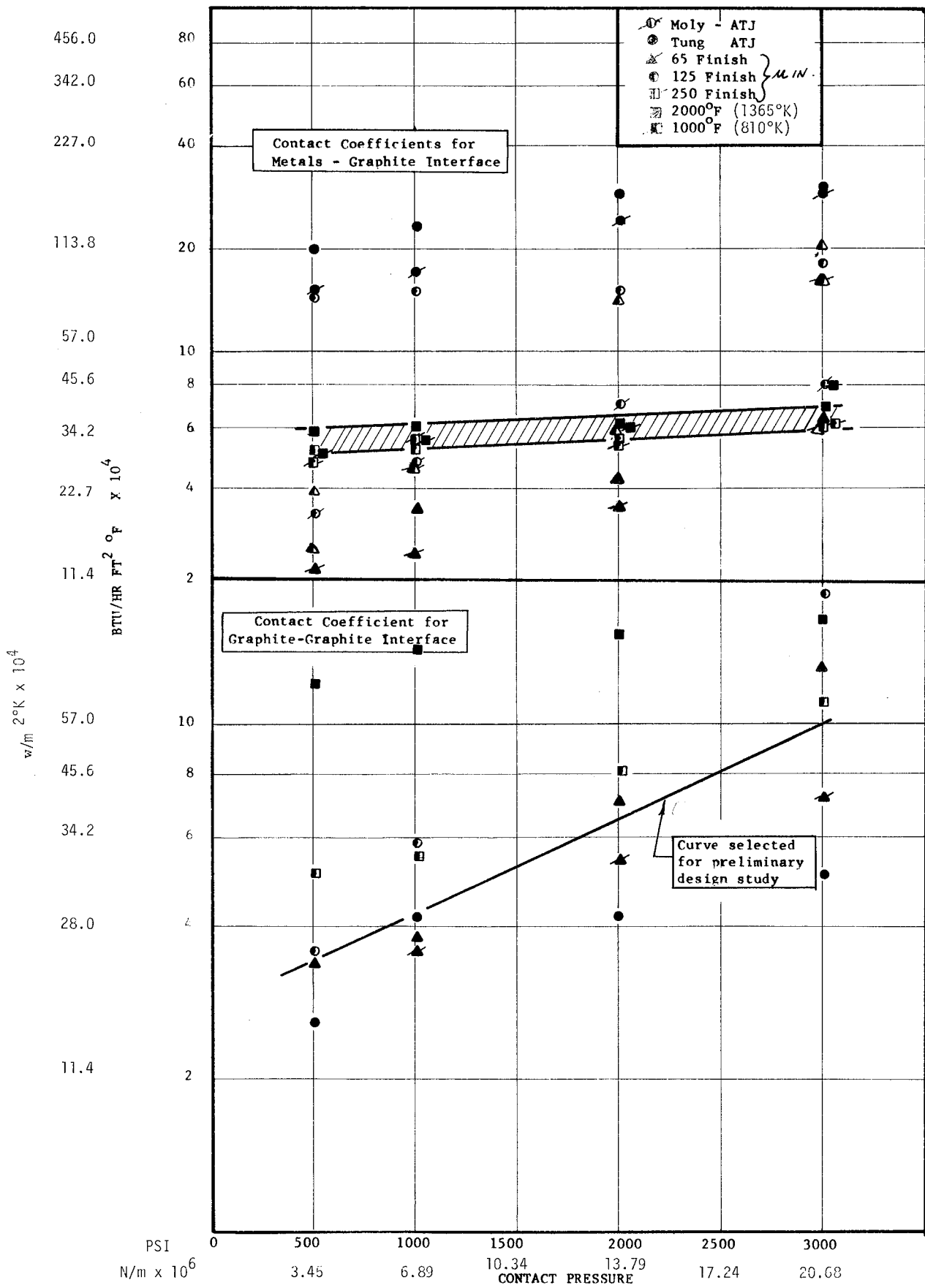


Figure 9. Interface Contact Coefficient for Graphite

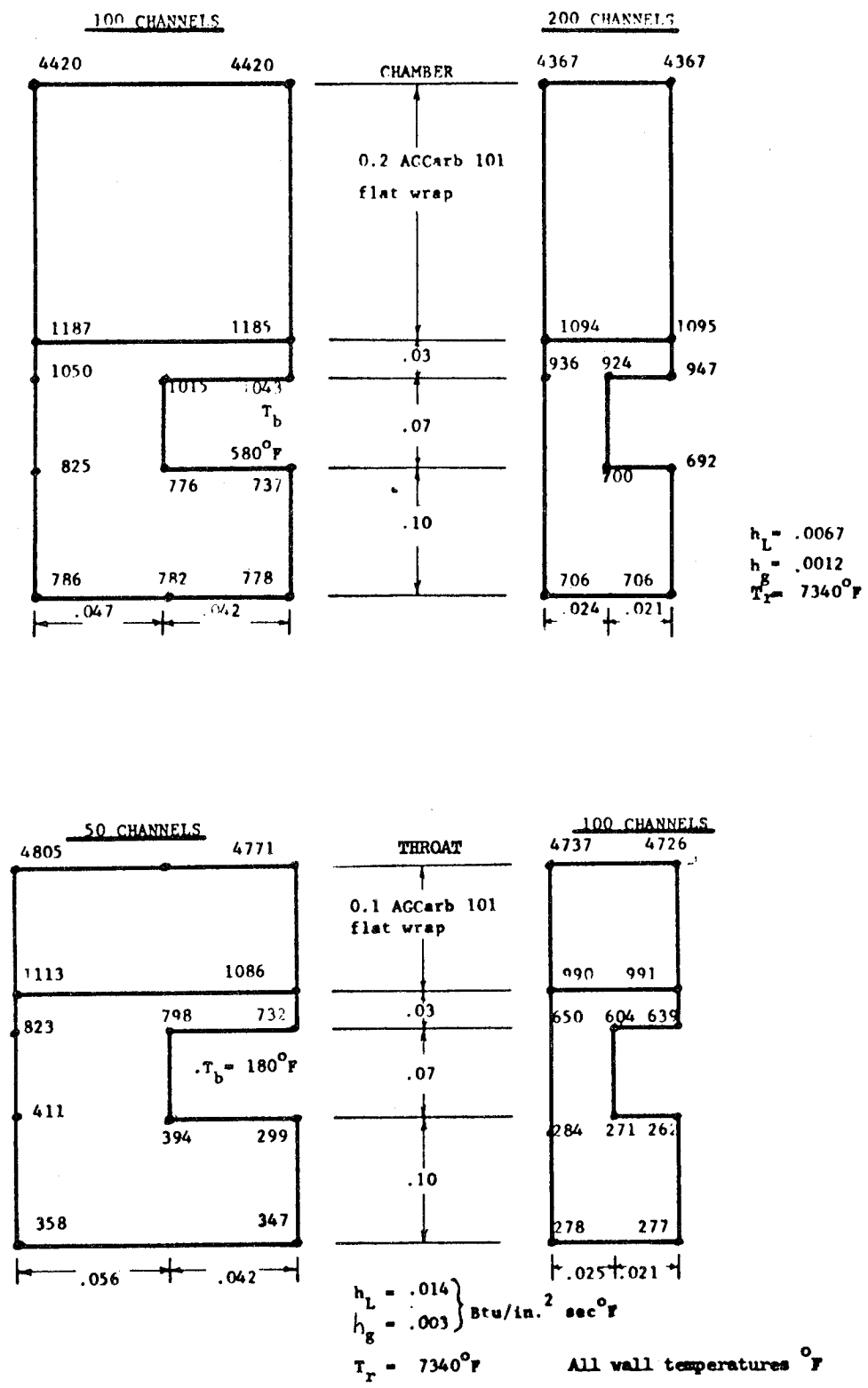
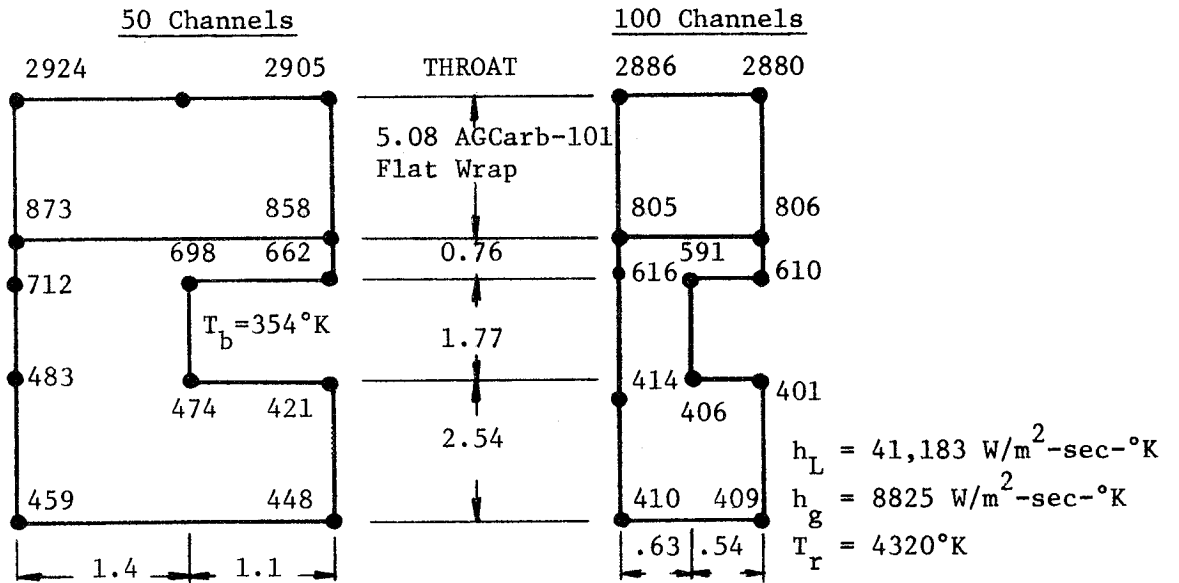
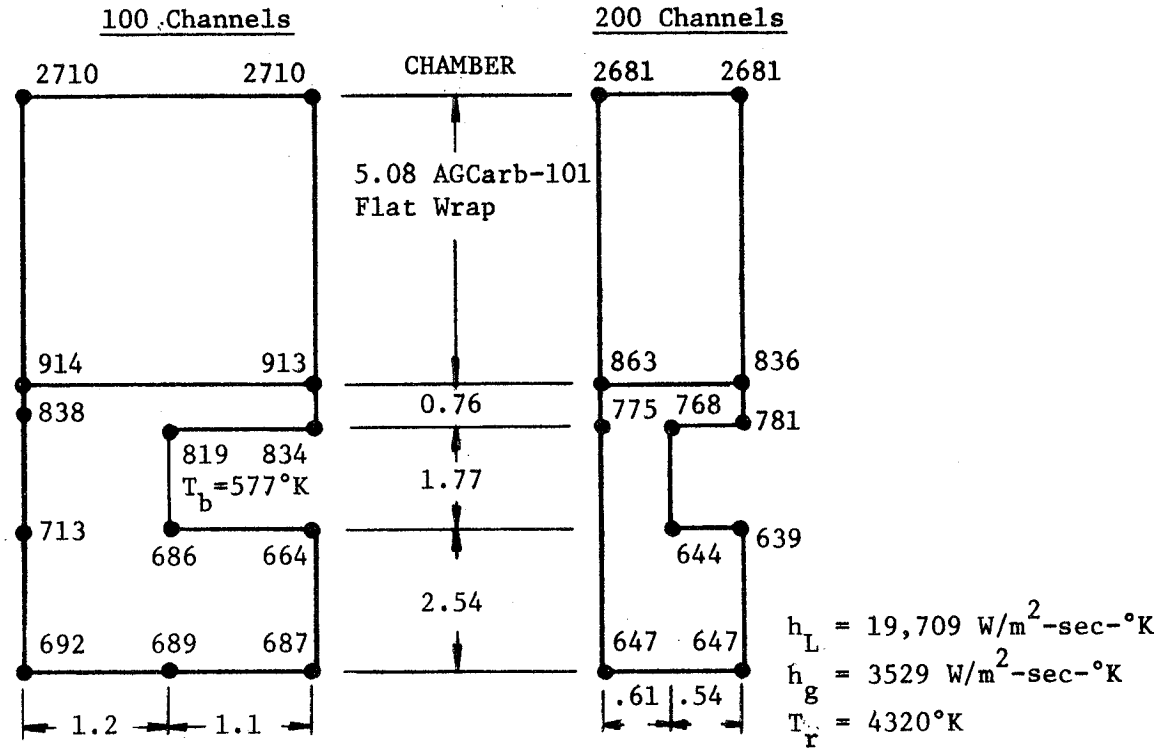


Figure 10a. Coolant Channel Analysis



Dimensions in millimeters  
Wall temperatures in °K

Figure 10b. Coolant Channel Analysis (SI Units)



### III, B, Subtask 2. Design Evaluation (cont.)

depth is varied to provide the required coolant mass velocity. Bifurcations and variations in the channel width were employed as the method of preventing the rib width from becoming either too large or too small. It was desired to hold the minimum rib width at about 0.050 in. (1.27 mm). The actual minimum achieved in this design is 0.0445 in. (1.13 mm) at the throat station. The maximum allowable rib width is a function of the heat flux and coolant velocity; larger rib widths are both acceptable and desirable in the low flux zones in order to make better use of the deeper coolant channels. Excessive rib widths in the high flux zones would have caused locally high nickel wall temperatures.

#### (3) Transient Thermal Conditions

The three-dimensional steady-state and transient thermal analyses conducted on this design consider the influence of the parameters discussed on the resulting temperature profiles. The results of the final thermal analysis for the selected design are presented in Figures 11 and 12. The first is a summary figure depicting the steady-state axial profiles on the various surfaces and interfaces which also defines the significant dimensions employed in the analysis. Figure 12 provides the summary of the transient analysis showing the rate at which the flame surface, nickel interface, and coolant bulk temperature at the discharge end approaches the final steady-state temperatures. Figure 13 is typical of the 15 thermal maps constructed, which provide a detailed three-dimensional thermal profile for the design described in Figure 11. Each of these 15 maps represents the chamber cross-section at an axial distance from the injector noted at the top of the page. As can be seen from the format, these use direct computer printouts in pictorial form.

#### (4) Transient Thermal Characteristics

Review of the transient temperatures for this design (initial temperature at  $-200^{\circ}\text{F}$  [ $145^{\circ}\text{K}$ ]) indicates that steady-state thermal conditions are first achieved in the throat, with the forward and aft ends trailing because of lower heat fluxes and thicker graphite liners. Since maximum inside to outside temperature differentials are experienced at steady-state operations, a structural analysis of the transient is not considered necessary.

#### c. Summary

Since the fabrication of the AGCarb liner could encounter delaminations during the graphitization process, three sets of components should be fabricated to ensure that at least two sets survive the entire fabrication cycle. The fabrication techniques used in producing the entire assembly are state-of-the-art and problems are expected to be minimal.

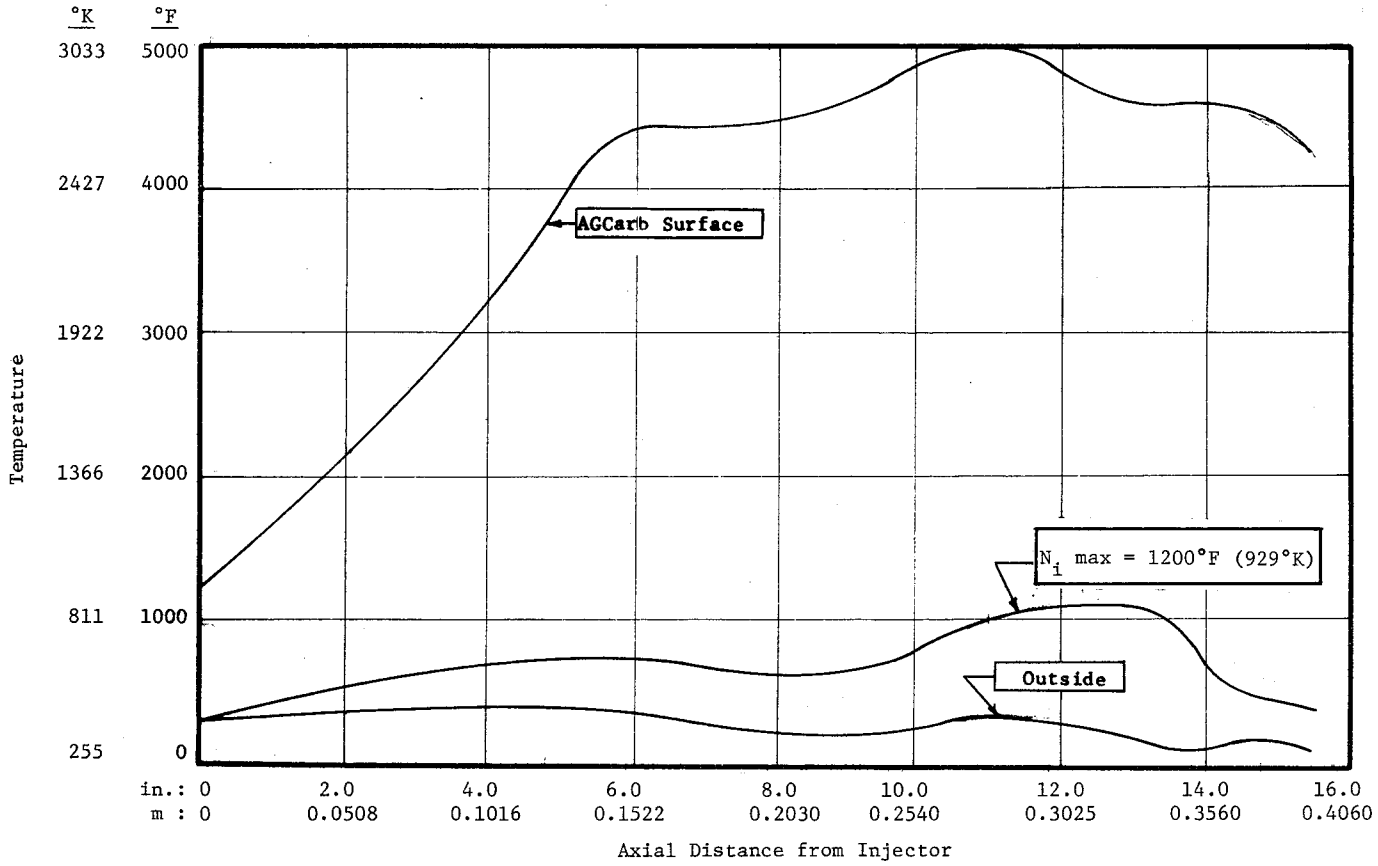
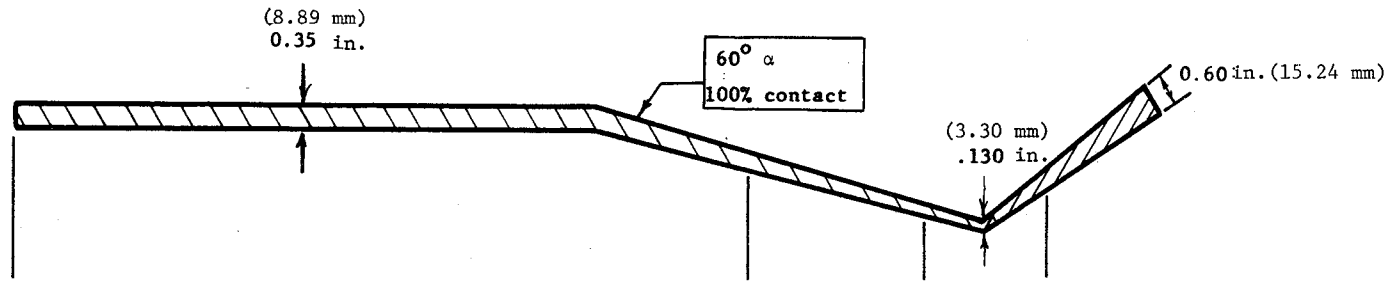


Figure 11. Steady-State Temperature Profiles, Concept I

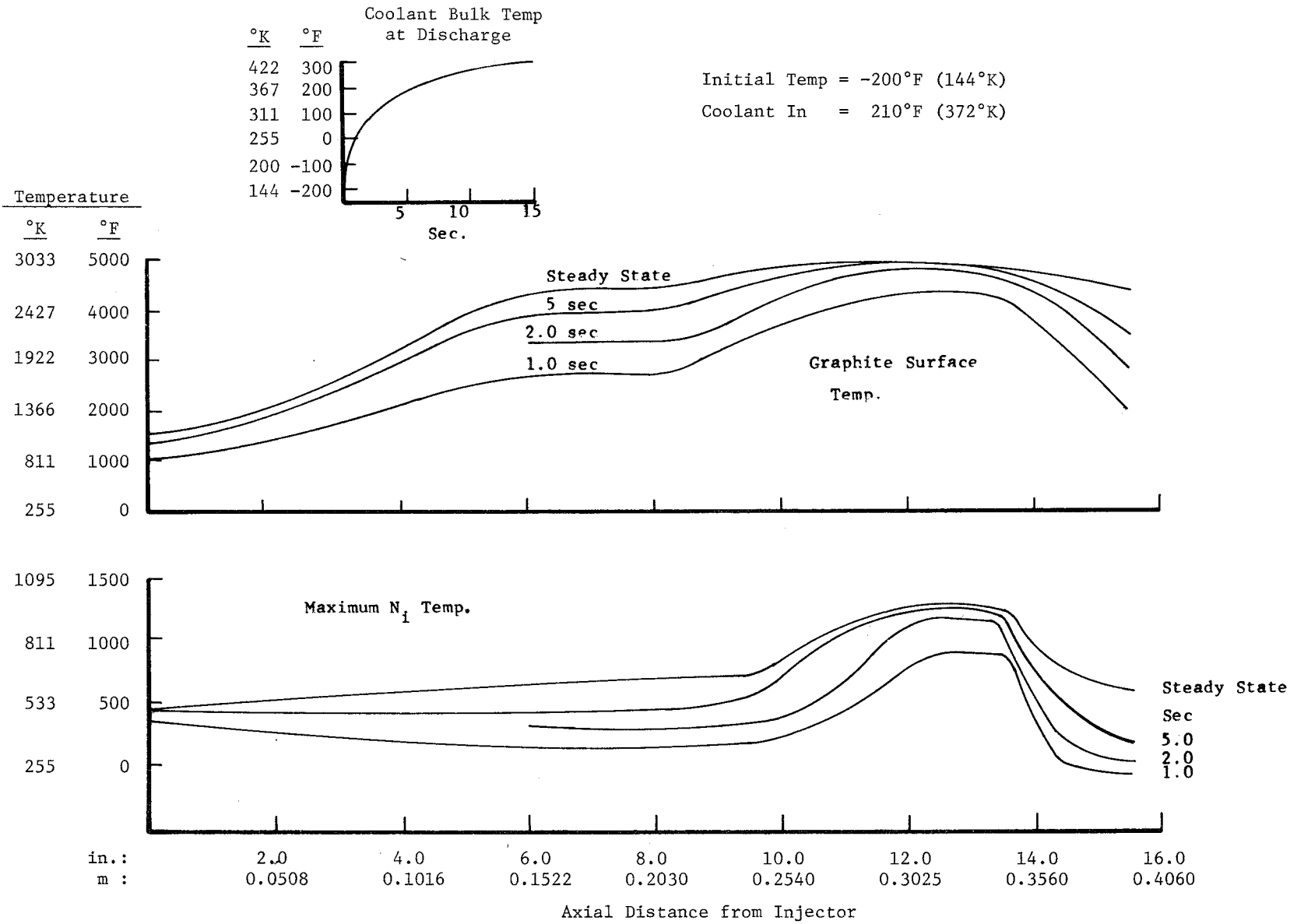


Figure 12. Transient and Steady-State Temperature Profiles, Concept I

\*\*\*\*\*

TIME 1.00000+01 DTIMEU 0.00000 CSGMIN( 0) 0.00000 DTMPC(

STEADY STATE SOLUTION FOR AXIAL DISTANCE= 13.50IN.

NICKEL

```

-----
*
* 259.5      245.5      237.6*
THICK = .060 IN
*
* 307.4      245.7      212.6*
-----
*
* 352.9      292.6*
*
* 428.4      355.7      * -90.3 BULK TEMP. DEG-
*
* 551.1      453.4*
-----
*
* 721.5      809.0      858.2*
THICK = .040 IN
*
* 1198.6     1220.5     1232.8*
-----
*
* 1199.5     1221.5     1234.2*
*
* 2235.1     2238.9     2241.0*
THICK = .130 IN
*
* 3406.5     3407.3     3407.7*
*
* 4742.3     4743.5     4744.2*
-----
*****

```

7390.0 RECOVERY TEMP-F

HG = .00317( BTU/IN-SEC-F)

HL = .00633( BTU/IN-SEC-F)

HL = .00668( BTU/IN-SEC-F)

HL = .00698( BTU/IN-SEC-F)

HL = .00575( BTU/IN-SEC-F)

HL = .00736( BTU/IN-SEC-F)

V.F. = .02857

TOTAL HEAT IN= 34.1069 TOTAL HEAT OUT= 33.870

RADIATION HEAT = .2479

Figure 13. Steady-Stage Solution for Axial Distance = 13.50 in.

### III, B, Subtask 2. Design Evaluation (cont.)

The thermal analysis performed indicates reasonable temperatures can be maintained if the jacket and liner surfaces remain in contact. If separation occurs, an increase in temperature will result due to the addition of a thermal resistance at the interface. Available data on contact resistance indicate that a minimum contact pressure of 500 psi ( $3447 \times 10^3 \text{ N/m}^2$ ) is required to permit a reasonable prediction of contact resistance. The preliminary stress analysis performed indicates the contact pressure to be 492 psi ( $3392 \times 10^3 \text{ N/m}^2$ ) in the chamber section and 200 psi ( $1380 \times 10^3 \text{ N/m}^2$ ) in the throat. A transient analysis at one second predicts values of 492 psi ( $3392 \times 10^3 \text{ N/m}^2$ ) in the throat and 818 psi ( $5640 \times 10^3 \text{ N/m}^2$ ) in the chamber. This did not include the effect of a preload of approximately 34 psi ( $234 \times 10^3 \text{ N/m}^2$ ) due to the shrinkage of the electroformed nickel upon cooling from the bath temperature of 130°F (328°K) to ambient. The predicted thermal loads are based on the expansion properties of pure wrought nickel. These agree with the room temperature properties of electroformed nickel as published by Electroforms Inc. However, it is reported by Kura, et al. (Ref 1), that other investigators have found the coefficient of linear expansions of electroformed nickel at room temperature to be  $3.1 \times 10^{-6}$  to  $6.3 \times 10^{-6}$  in./in./°F ( $1.72 \times 10^{-6}$  to  $3.5 \times 10^{-6}$  m/m/°K). This compares to 7.4 (4.12) for pure wrought nickel. The use of pure nickel properties is therefore conservative in that lower interface pressures are predicted than might occur.

The stress analysis performed for this design indicates margins of safety calculated to be all positive except in the nozzle area. Those which are below 0.2 dictate a reassessment of properties data or local redesign to gain greater margins.

#### 2. Concept II. Pyrolytic Graphite Throat Insert, Cylindrical Shell (Figure 2)

##### a. Description and Fabrication Approach

This design features a composite replaceable inner liner of various graphite materials which were selected for their specific thermal and structural properties. The liner is contained in a precompressed state (shrunk fit) within a cooled cylindrical metal shell. Shell materials considered are Nickel 200, Hastelloy B, and Columbium 103. The nozzle extension is attached to the metal case by electron beam welding.

##### (1) Liner Material Selection

The liner in the chamber section is AGCarb-101 formed from a 45° bias tape wrapped at an angle of 60° to the direction of gas flow. This is followed by: a short section of ATJS at the start of the convergent section, a series of pyrolytic graphite washers in the throat section, and additional bulk graphite downstream of the throat. The exit nozzle is formed from flat-wrap AGCarb-101.

### III, B, Subtask 2. Design Evaluation (cont.)

Grafoil is used at all joints except between the pyrolytic graphite washers. The Grafoil is used to distribute joint loads uniformly and take up tolerances of individual parts. During firing, each washer undergoes a nonuniform expansion ranging from about 0.010 in. (0.254 mm) on the flame surface to nearly nothing on the cooled surface. To allow for this, a 0.012-in. (0.302 mm) copper disc is positioned between each pyrolytic graphite disc as shown in the drawing. The main function of the shim is to keep the washers tight at all times and allow for the expansion of the pyrolytic graphite in the axial direction at the flame surface. Consideration is also given to substituting Grafoil for the copper since Grafoil has higher temperature capability and can be compressed more than the copper.

The AGCarb-101 chamber liner is used because of its demonstrated excellent erosion resistance, its availability in large sizes, and because it results in a desirably thin assembly due to its low thermal conductivity. Where the convergent section begins, ATJS is used because the material thickness increase in this area results in the need for a higher conductivity material to keep the surface temperature below 4500°F (2756°K). At the point where the surface temperature significantly exceeds 4500°F (2756°K), the material is changed to higher conductivity pyrolytic graphite. Bulk graphite is again used downstream of the throat. The nozzle extension is a parallel-to-surface wrapped - AGCarb liner with an electroformed nickel shell. The nozzle extension assembly is welded to the chamber to provide a smooth flow path between components as well as a minimum amount of material.

#### (2) Jacket Material Selection

The cylindrical jacket will be made from Nickel 200, Columbian C-103, Columbian C-129, or a composite where the inner shell will be Nickel 200 and the outer shell Hastelloy B. A combination of Nickel 200 for the inner and outer shell with a reinforcing jacket of Hastelloy B or columbium was also considered.

#### (3) Coolant Channels

The coolant circuit in this design consists of a single-pass 150-channel arrangement. Coolant enters at a 16:1 exit nozzle area ratio and proceeds toward the injector. Channel cross sections are 0.078 in. (1.98 mm) wide, 0.050 in. (1.27 mm) deep at the inlet and remain constant to an area ratio of 4:1 downstream of the throat. At this point, the coolant mass velocity is increased by reducing each channel to a width of 0.062 in. (1.51 mm) and a depth of 0.040 in. (1.02 mm). These dimensions are maintained constant to the discharge end at the injector face in order to simplify fabrication. Channel width in the forward chamber region could be increased to reduce coolant pressure drop; this was not recommended because it increases fabrication costs and reduces the structural safety factors. The coolant pressure drop for this design is 153 psi ( $1055 \times 10^3 \text{ N/m}^2$ ).

III, B, Subtask 2. Design Evaluation (cont.)

b. Thermal Analysis

(1) Steady-State and Transient Wall Temperatures

Thermal analysis of this design was conducted employing the analytical procedure and models developed for Concept I. The thermal design goals and actual design achievements are summarized as follows:

	<u>Goal</u>	<u>Thermal Contact</u>	
		<u>Best Estimate</u>	<u>Maximum</u>
Maximum gas-side temperature	4000-5000°F (2500-3040°K)	5350°F (3240°K)	5150°F (3125°K)
Maximum jacket temperature	1250°F (950°K)	930°F (775°K)	1020°F (825°K)
Interface contact pressure	1000 psi min (6894x10 <sup>3</sup> N/m <sup>2</sup> )	200 psi (1378x10 <sup>3</sup> N/m <sup>2</sup> ) nickel 400 psi (2758x10 <sup>3</sup> N/m <sup>2</sup> ) columbium	

Axial steady-state and thermal transient temperature profiles for the gas-side, graphite-nickel interface and backside of the coolant jacket are provided in Figure 14. An insert to this figure provides the coolant bulk temperature at the discharge of the jacket as a function of time.

The configuration of this design is dictated by the requirements for maintaining a cylindrical outer shell and a chamber diameter compatible with 5.25 in. (0.1333 m) injector face diameter. The throat diameter is in accordance with thrust and chamber pressure specifications. These criteria result in a minimum diameter for the cylindrical shell of 5.950 in. (0.1511 m), which in conjunction with the chamber contour result in a prescribed thickness for the graphite liner in all locations except the divergent nozzle.

The thermal design options are reduced to selecting the type of graphite to be employed at each station and the coolant velocities. The thickest graphite sections are in the throat where the walls are 1.67 in. (0.0422 m). A high thermal conductivity material such as pyrolytic graphite was therefore selected for this location. With these restrictions and an assumed contact coefficient of 5500 Btu/ft<sup>2</sup>-hr-°F (31,219 W/hr-m<sup>2</sup>-°K), gas-side wall temperature in the throat region is predicted to be 5350°F (3227°K). Although higher than desired, this temperature is not considered excessive. Analyses showed that, if perfect contact between the graphite and jacket could be attained, the predicted maximum graphite temperature would drop to 5150°F (3116°K) and additional reduction in wall temperatures could be attained by increasing the coolant velocity. This, however, would be at the expense of increased coolant pressure drop and fabrication complexity.

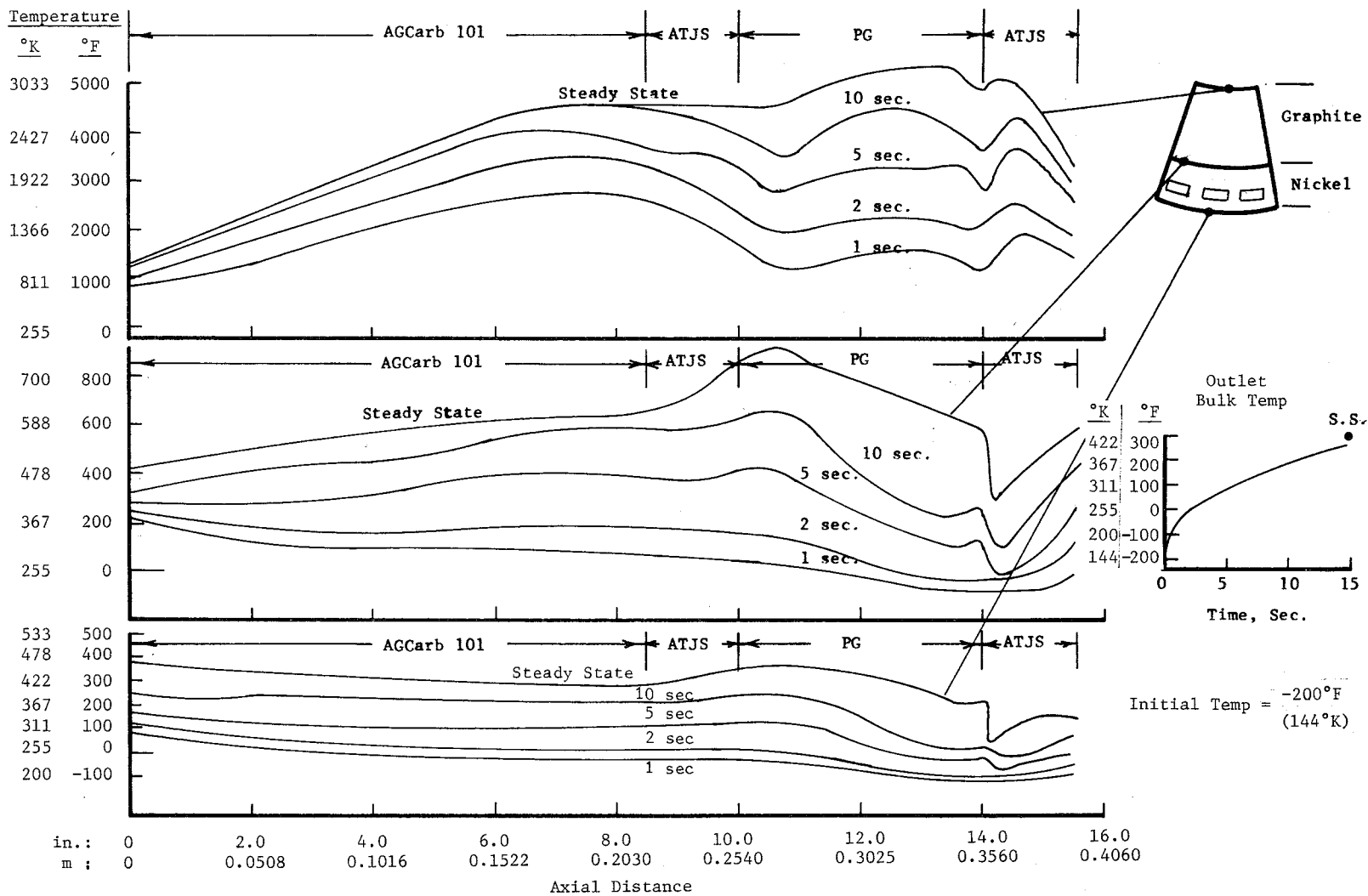


Figure 14. Transient and Steady-State Temperature Profiles, Concept II



### III, B, Subtask 2. Design Evaluation (cont.)

Thermal analyses were conducted for a nickel coolant jacket. The maximum temperature predicted for this material is 930°F (722°K) at an axial station of 10.6 in. (0.269 m) from the injector face. This temperature could rise to 1020°F (822°K) if perfect thermal contact between the liner and the shell were realized. The predicted temperatures also apply to a columbium shell since its thermal properties are very similar to nickel. A composite shell consisting of a nickel inner sleeve and a Hastelloy B outer sleeve would run slightly hotter on the inner wall and slightly cooler on the outer surface because of the lower thermal conductivity of the Hastelloy material.

#### (2) Potential Problem Areas

An analytical uncertainty is encountered in this design at the interface behind the pyrolytic graphite throat discs. The uncertainty is in the degree of thermal contact which could be achieved because of the low interface compressive loads predicted by the structural analysis.

#### (3) Thermal Advantages

The design employing the pyrolytic graphite throat insert in disc form is considered to have the highest durability, be most suitable for use at higher chamber pressures, and have the least pressure drop. Durability is considered maximum because the substantial thickness of graphite in the throat would preclude the possibility of changing the thermal characteristics if small amounts of flame surface wear should take place. The design can be uprated with slight modifications to very high chamber pressure by converting the pyrolytic graphite washer throat to a combined regeneratively and transpiration-cooled design. The pressure drop is lowest with this design because the heat flux to the coolant is considerably reduced due to the large radial heat conduction effects.

#### c. Summary

Fabrication of the cylindrical jacket and the liner components as shown is relatively simple and no problems are anticipated; however, as evident from the stress analysis, the nickel outer shell yields and may result in a decrease in contact pressure after the first cycle, which would result in higher temperatures in both the graphite and jacket. The following options are available in the event re-analysis confirms that nickel yields excessively:

- (1) The use of columbium as both the inner and outer coolant jacket shells.

### III, B, Subtask 2. Design Evaluation (cont.)

- (2) The use of a columbium jacket over the nickel coolant jacket.
- (3) The use of a Hastelloy B jacket over the nickel coolant jacket.

The use of columbium complicates the joint of the cylindrical chamber to the nozzle. A relatively simple Nickel 200 to electroformed nickel joint is shown. With Option (1), electroformed copper would be used over the AGCarb for the nozzle. Columbium and copper would be welded with the electron beam process. This is not, however, easily accomplished and would require some experimentation to develop the proper joint design, establish the strength, and develop the process. Options (2) or (3) were better solutions to the joint problem where electroformed nickel would be electron beam welded to Nickel 200.

The structural analysis indicates the use of nickel is questionable; columbium provides adequate margins but increases costs and fabrication problems. Hastelloy B was not analyzed, but a comparison of its tensile and thermal expansion properties indicates it may be acceptable. The joint at the cylindrical section to the nozzle extension was not analyzed. A bolted flange joint with seals was considered but set aside in favor of the relatively simple nickel-to-nickel welded joint shown.

### 3. Concept III. Axially Segmented Graphite (Figure 3)

#### a. Description and Fabrication Approach

A unique concept is presented in the axially segmented design. The chamber is made from 42 axial, wedge-shaped graphite sections with cooling fins located between each graphite wedge.

This design is simple to fabricate in large quantities. The graphite wedges can be cut from standard-size plate with little waste. The cooling fins can be etched using Aerojet's platelet photoetching technique to achieve the exact flow pattern desired. The fins can be sealed by diffusion bonding or brazing a flat strip over the etched manifolds. Diffusion bonding is the preferred method to preclude blocking channels with braze alloy; however, the absence of available equipment of the required size would necessitate the use of brazing. Plugging and other braze flow problems can be minimized by the use of electroless nickel plating of the components to be brazed. The use of electroless nickel as the braze alloy has been successfully used by Aerojet on several recent programs. The advantage of the electroless nickel technique is that the quantity and location of alloy can be controlled. Each individual cooling fin can be X-ray inspected and water flowed to determine the flow rate at rated conditions prior to assembly into the chamber.

### III, B, Subtask 2. Design Evaluation (cont.)

After assembly of the graphite wedges and cooling fins, the entire assembly will be covered with an electroformed nickel shell. The shell acts to hold all the components in place, prevent external leakage, and is the structural support for the assembly. Manifolds to feed each fin will also be formed by electroforming. A significant feature of this design is that, should the graphite develop cracks, heat flow and structural integrity would not be affected. Insulation placed between the graphite wedges and the electroformed shell will reduce heat flow to the shell. Candidate insulation materials are the graphite felts.

The wedges and fins are held in place by steel bands at at least four locations with the locations masked and the electroforming to a thickness of 0.020 inch (0.51 mm) done between the bands. Following removal of the bands the electroforming is continued. A machine cut can be taken to achieve constant thickness or the first area to be electroformed can be masked until a thickness of 0.020 inch (0.51 mm) was attained in the original band areas. A slight preload is also attained in the electroforming process due to shrinkage of the shell on cooling from 130°F (328°K) to ambient.

Consideration was also given to alternate fabrication approaches. Using a conical chamber design, it is possible to fabricate a shell by spinning. Assembly of the coolant fins and graphite wedges from the inside would present a problem in that the taper would prevent the final segment or wedge from being installed.

Another method considered for applying an outer shell is the ribbon wrap and braze technique accomplished by Solar on some NASA chambers several years ago. Although reasonably successful, the technique is not considered state of the art.

#### b. Thermal Analysis

##### (1) Design Analysis

The axially segmented design is cooled via 42 radially oriented fins that are compressed between an equal number of bulk graphite wedges running the axis of 16:1 regeneratively cooled portion of the chamber. The configuration of the 42 sections was based on a minimum graphite thickness of 0.2 inches (5.08 mm) at the throat. Coolant enters the fins at an area ratio of 16:1 and flows toward the injector through 42 coolant passages (one in each fin). No bifurcations are required for this design. Each fin consists of a 0.030-inch (0.76 mm) wide coolant channel with a 0.020-inch (0.51 mm) thick nickel or copper side cover plates with the coolant mass velocity controlled by varying the effective channel height. Each coolant channel contains structural supports to prevent collapse of the side cover plates under compression load. These supports, however, are not bonded so that the hydraulic load within the coolant channels (1000 psi) ( $6894 \times 10^3 \text{ N/m}^2$ ) can

### III, B, Subtask 2. Design Evaluation (cont.)

force the walls against the graphite, ensuring good contact pressure when the engine is running. Figure 15 summarizes the hydraulic characteristics of this design. Two pressure and temperature profiles are shown. One corresponds to the configuration of Drawing 1159044 (Figure 3) which is not optimized for wall temperature in the divergent nozzles. The second curve corresponds to a uniform wall temperature of 4500°F (2755°K).

The problem of temperature stratification along the radius of the coolant stream was circumvented by placing continuous intra-channel mixing devices along the flow path as shown in Figure 16. The mixing device consists of a 0.005-inch (0.127 mm) high vane on the side walls which produces an upward flow along one side of the channel and a downward flow on the other, causing a slow rotation of the flow within each fin. This device would result in increased pressure drop. The use of copper for the fin material would help minimize temperature stratification.

#### (2) Steady State Analysis

Analyses were conducted for ATJS and AXF-5Q grade graphites. Transient and steady state axial temperature profiles for this design are presented in Figure 17 using AFX-5Q properties. Maximum gas-side wall temperatures are calculated to be about 4500°F (2755°K) in the chamber, 4600°F (2811°K) at the throat, and 3000°F (1922°K) at the 16:1 exit plane. The maximum temperatures of 5000°F (3033°K) for the region upstream at the throat result from the assumption of a linear variation in graphite thickness between the chamber and the throat and simultaneous changes in the coolant mass velocity (see Figure 15). This linear variation is not a fabrication limit for this concept and, in the process of optimizing, the wall thickness and coolant channel height would be reduced to provide a temperature value equal to or less than the throat temperature.

Maximum backside temperatures for this design are predicted to be 750°F (672°K) at the midpoint of the chamber. The temperature of the nickel case can be controlled by placing a low conductivity material between the graphite and the electroformed case while maintaining good contact between the case and the fins. The temperatures shown in Figure 17 are based on an analysis without such insulation and therefore represent a maximum temperature.

Calculations made to determine contact pressures indicated pressures of 500 to 1000 psi ( $3447 \times 10^3 \text{ N/m}^2$ ) ( $6894 \times 10^3 \text{ N/m}^2$ ) in the throat area and 200 to 300 psi ( $1378 \times 10^3$  to  $2068 \times 10^3 \text{ N/m}^2$ ) in the chamber section. This analysis conservatively neglected the effects of three factors, all of which tend to increase interface pressures. These are: (1) tube expansion under internal pressure of coolant, (2) preload due to contraction of the electroformed nickel upon cooldown from a bath temperature of 130°F (328°K) to ambient, and (3) preload obtained in assembly by wedging the last keystone fin into place.

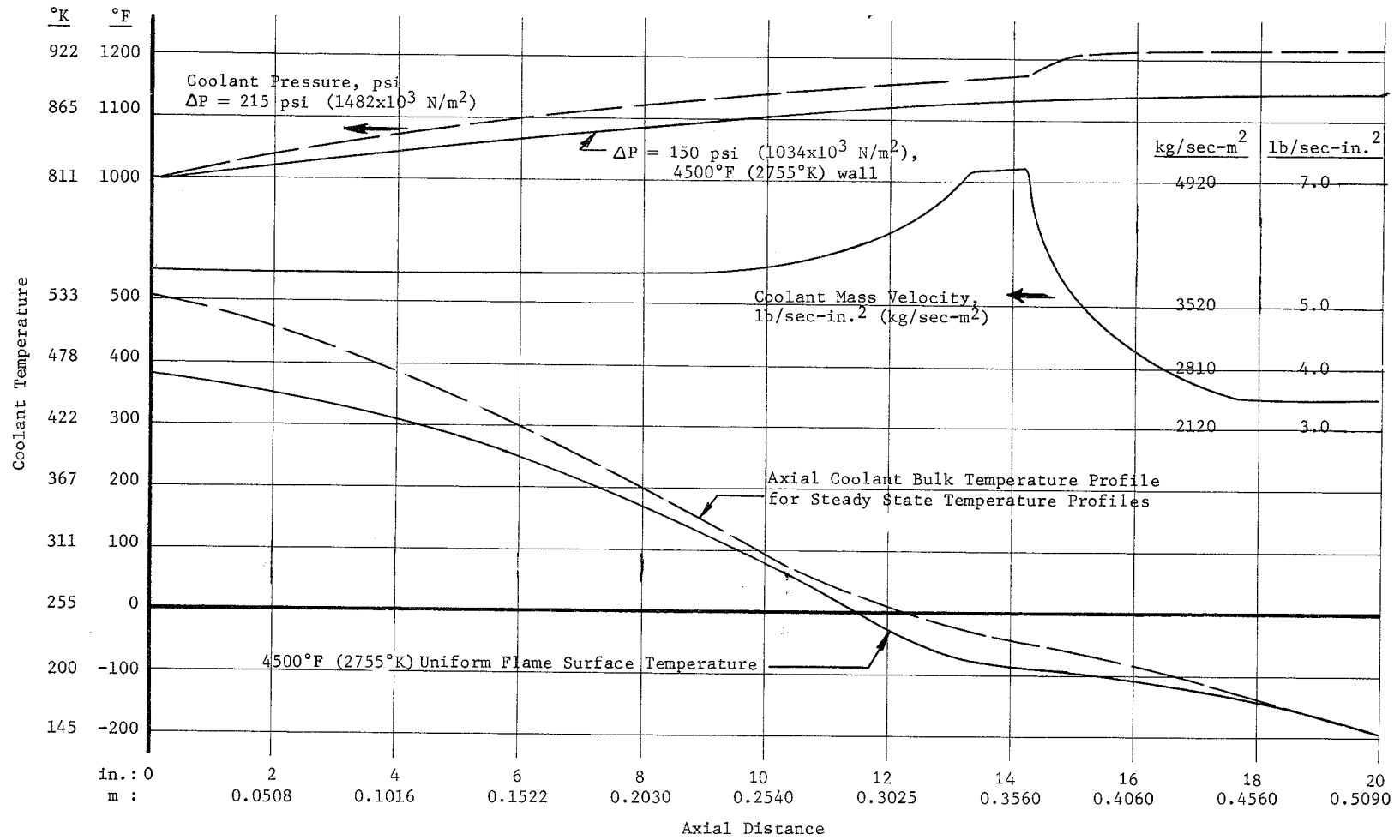


Figure 15. Coolant Flow Conditions, Axially Segmented Graphite Chamber

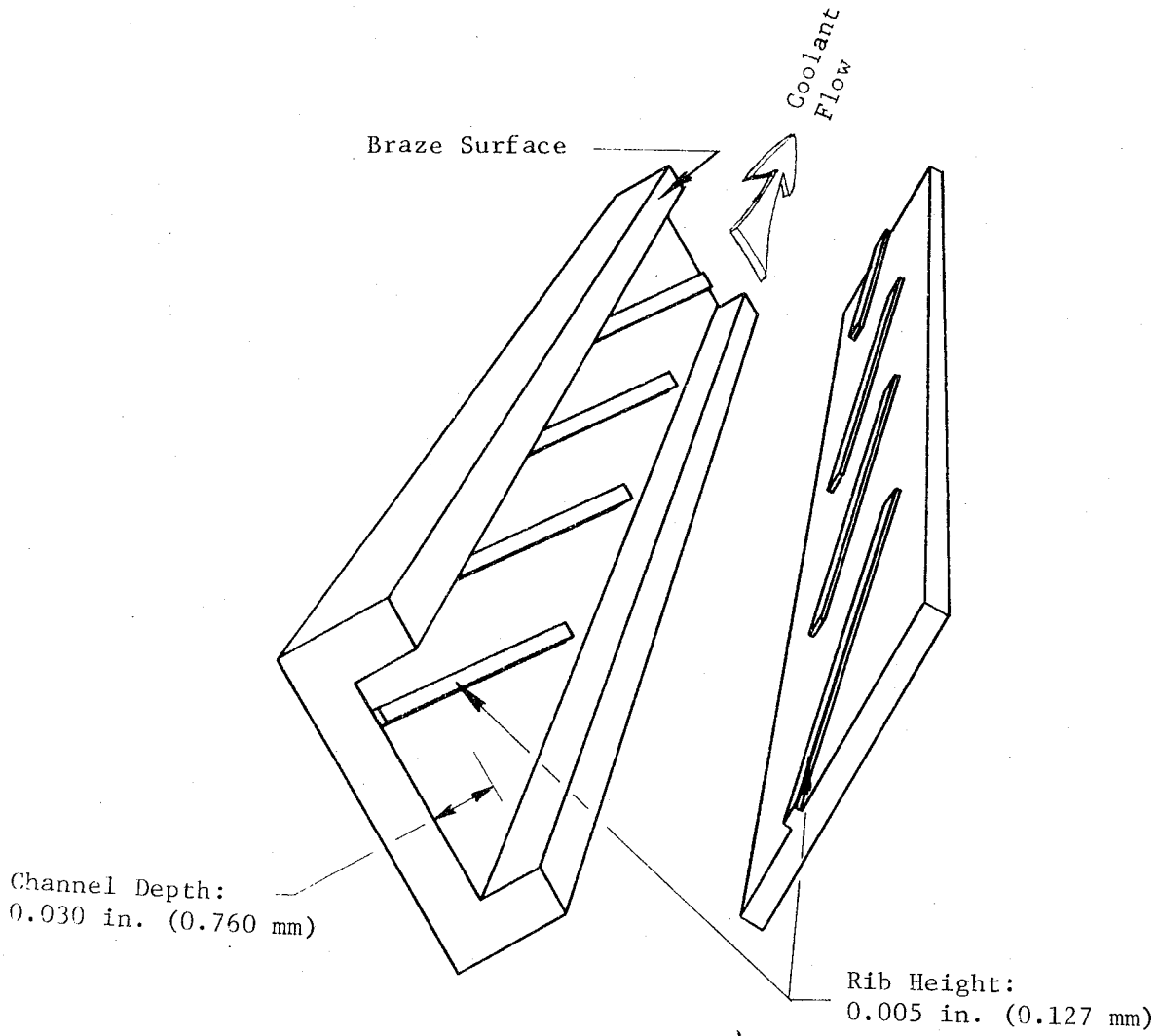


Figure 16. Interchannel Fluid Mixing Ribs

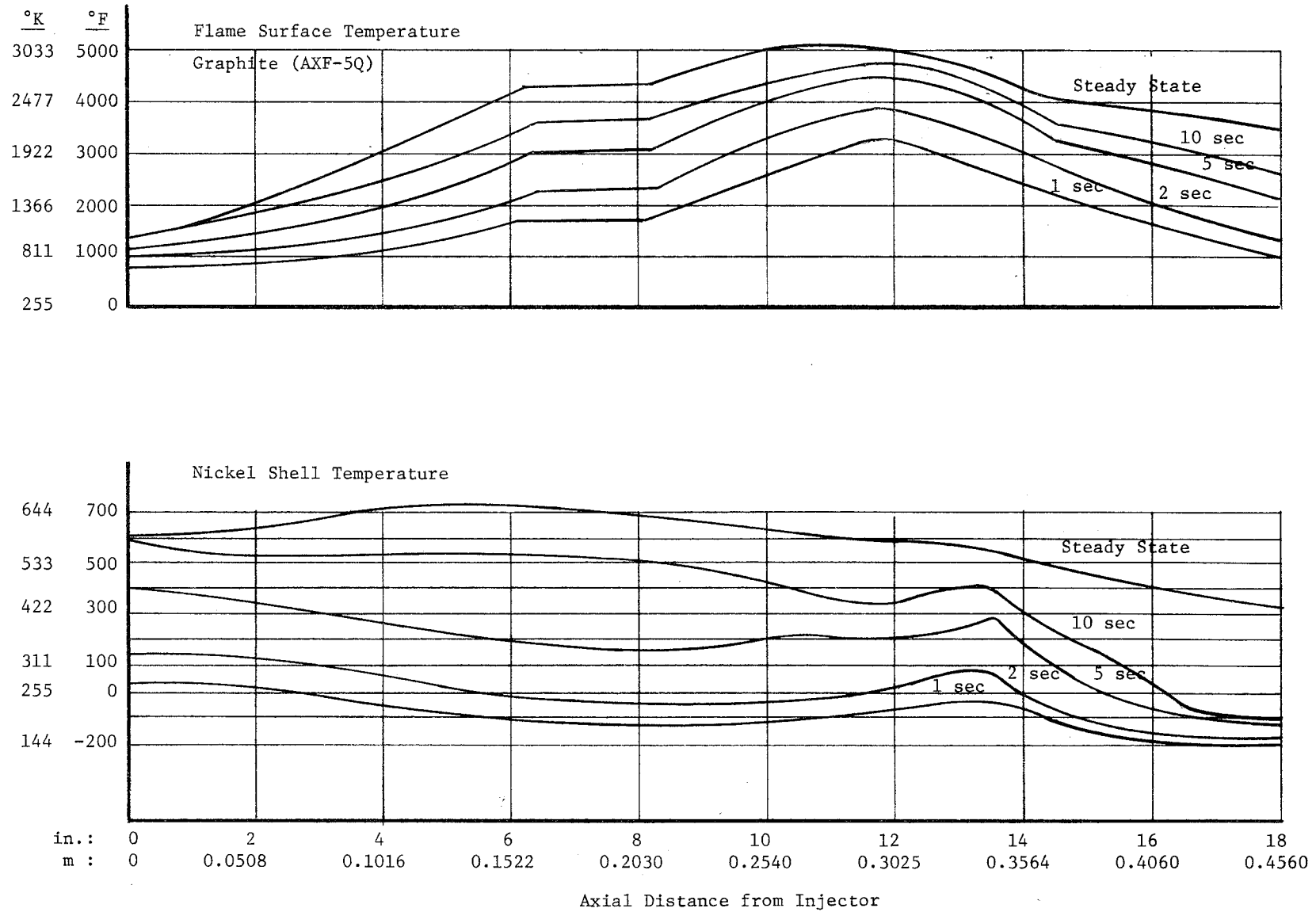


Figure 17. Transient and Steady-State Temperature Profiles, Concept III

### III, B, Subtask 2. Design Evaluation (cont.)

An additional gain can be made in interface pressure by substituting copper in place of nickel as the fin material. Two advantages are realized by this action: one is the increase in expansion due to the higher coefficient of copper ( $9.8 \times 10^{-6}$  in./in./°F) ( $5.44 \times 10^{-6}$  m/m/°K) (4.12) for nickel, and the second is the theoretical improved heat transfer resulting from increased surface contact due to the lower yield strength of copper.

In comparison with other concepts, the fabrication operations of this concept probably require tighter controls. This can be interpreted as a somewhat higher development risk factor which may be outweighed by an improved potential for high  $P_c$  and larger chambers.

#### (3) Transient Analysis

The transient analysis shown in Figure 17 shows that this design has a long start transient. The slow heating rates are due to the thick graphite walls employed in the chamber and in the exit nozzle. Design optimization would require a tradeoff between coolant bulk temperature rise and pressure drop at steady state operation and time to achieve steady state conditions. In the current configuration, the graphite wall at the 16:1 area ratio is 1.315 inches (33.4 mm) thick and has a flame surface temperature of 3100°F (1977°K). Figure 17 shows the nozzle to heat very slowly downstream of the throat. Increasing the wall thickness to provide a 4500°F (2755°K) surface temperature is calculated to reduce the pressure drop at steady state conditions from the current value of 215 psia ( $1,482 \times 10^3$  N/m<sup>2</sup>) ( $1,034 \times 10^3$  N/m<sup>2</sup>); however, this would make the engine heavier and slower responding. A possible solution to this is to employ a thinner AGCarb-101 in the exit nozzle or place an insulator between the fins and the graphite.

This design is capable of operating at chamber pressures higher than 500 psia ( $3,447 \times 10^3$  N/m<sup>2</sup>) because the graphite liner could be made thinner and the coolant pressure drop is not excessive. Very high pressure operation could be achieved if small amounts of film coolant are added at the start of the convergent nozzle. In fact, if the throat recovery temperature were reduced to 5000°F (3033°K) by local film cooling, the pressure level at which the engine could operate would be controlled completely by structural considerations.

#### c. Summary

This concept has many more component parts than other concepts considered. However, cost estimates from machining, photoetching and brazing vendors show that, in spite of the number of pieces involved, overall costs are reasonable. All processes are state of the art and experimentations to develop the assembly technique would be minimal. The machining



### III, B, Subtask 2. Design Evaluation (cont.)

of the graphite wedges would require close dimensional, flatness and parallelity tolerances. This requirement increases the cost of fabrication considerably and makes this a major cost item. It is felt, however, that the use of tape controlled machine tools with automatic gauging devices would provide a means for reducing machining cost to a more reasonable figure when quantity production is considered.

The raw material for the graphite wedges, AFX-5Q produced by Poco Graphite, Inc., is an equally high cost item. A reduction in cost on a quantity basis cannot be predicted at this time; however, the potential exists. The key to the apparent feasibility of the design is the relatively high thermal expansion of AFX-5Q. No competitive graphite product has the thermal expansion required to obtain high pressure at the fin-wedge interface.

Small disparities due to local warpage or distortion occurring during brazing of the fins would be eliminated by Blanchard grinding both sides. This operation is not expensive and would not affect performance as thickness is not critical to heat transfer where nickel or copper are used.

The thermal analysis indicates all temperatures to be within design limits. Thermal gradients are less in this design than in the other concepts considered and, due to its configuration, the potential exists to hold average temperature lower than competing designs. Success, however, would be highly dependent on the ability to hold the mating surfaces in intimate contact at a minimum of 500 psi ( $3,447 \times 10^3 \text{ N/m}^2$ ) loading.

#### 4. Concept IV, AGCarb Linner, Nickel Segmented Shell, (Figure 4)

##### a. Description and Fabrication Approach

This design consists of an AGCarb-lined thrust chamber with a nickel regenerative cooling jacket and has replaceable liner and cooling jacket segments.

The AGCarb liner is continuous from the injector to an area ratio of 16:1 in the nozzle extension. The cooling jacket is designed in three pieces to surround the liner like a clam shell. The pressure vessel loads are carried by restraining bands which hold the shell segments together. Because the AGCarb material is slightly porous, the assumption was made that the shell must be leak tight. The joint between segments are sealed by a copper crush gasket backed by a steel stiffening strip. The retaining bands are spaced one inch apart between centers. An AGCarb flat-wrapped nozzle extension is attached by bolting to the cooling jacket at 16:1 area ratio.

### III, B, Subtask 2. Design Evaluation (cont.)

Nickel was selected for the cooling jacket segments because of its high thermal conductivity and reasonable strength at the temperatures to be encountered.

Two fabrication approaches were considered. One requires close tolerance forming of the inner and outer wall from sheet materials. After machining channels in the inner shell, the two are brazed together. To meet the tolerances that would have to be held to permit even a reasonable fit to the graphite liner, the inner contour would have to be machined. This could result in thick and thin areas, depending on the accuracy held in the forming and brazing operations. The second approach is to electroform the jacket on a mandrel that has been machined to the same contour template used in machining the graphite liner outside contour. With this approach, deviations up to 3 mils (0762 mm) could be expected; this is considered unacceptable.

A solution to the match machining problem is to use the liner as the electroforming mandrel, employ a mold release and three plastic strip separators. The three segments would then be stripped from the mandrel, leaving only a loss of approximately  $5 \times 10^{-5}$  inches ( $0.1270 \times 10^{-5}$  mm) radially, representing the mold release material. While this approach alleviates the contact resistance problem for the first assembly, there would be a contour matching problem when the liner was replaced. The replaceability feature of the concept would therefore be lost eliminating advantages over the concepts which electroformed directly on the graphite liner.

#### b. Thermal Analysis

Ideally, thermal profiles for the segmented shell design are quite similar to those shown in Figures 11, 12, and 13. The only difference is the degree of thermal contact which could be achieved between the AGCarb-101 liner and the segmented coolant jacket. As shown in Figure 9, only slight temperature differences are realized if a good mechanical, rather than metallurgical, contact is attained at the interface. If this contact could be attained, this design would be thermally acceptable.

#### c. Stress Analysis

Preliminary analysis indicates the need for circumferential retaining bands at least every inch as shown in the drawing. The axial seal design was reviewed and leakage was predicted at 500 psi ( $3447 \times 10^3$  N/m<sup>2</sup>) unless more bands or heavier longitudinal stiffener were employed. Fabrication analysis predicted that maintaining contact between the liner and the shell by precision machining to match the contours would have little chance for success. For this reason, stress analysis was suspended.

### III, B, Subtask 2. Design Evaluation (cont.)

#### d. Summary

The fabrication of the segmented jacket concept is simple and no major problems are anticipated. The heat transfer analysis performed for the AGCarb liner, electroformed nickel jacket concept applies also to this concept with the addition of a contact resistance factor that results in an increase in liner average temperature of approximately 300°F (422°K) based on the assumption that a precision fit has been obtained in the matching contours. This is not considered to be a reasonable assumption since a method of match-machining to a no-tolerance condition is not available. Although the replaceability feature of the concept is attractive, the above mentioned heat transfer situation resulted in the basic concept being judged not feasible.

#### 5. Concept V, AGCarb Liner, Copper Milled Passage (Figure 5)

##### a. Description and Fabrication Approach

This copper jacket design is similar to the electroformed nickel concept shown except that the fabrication approach has been changed in an attempt to reduce the dependence on electroforming.

In this design, the AGCarb is covered with a layer of copper by either electroforming or plasma spraying, channels milled into the copper, and a stainless steel cylinder brazed over the outside to close the channels. In the throat section, a split copper ring is used to fill the area between the copper channel area and outside jacket. In the original concept, the coolant channels followed the cylinder wall, with the copper split ring conducting heat to the coolant. Thermal analyses indicate the copper would melt. The approach shown in Figure 5 is an attempt to salvage the original concept.

##### b. Thermal Analysis

Thermal profiles for this design are similar to those presented in Figures 11, 12, and 13. The similarity exists because the thermal characteristics of the graphite liner and the coolant velocity control the temperature profiles, while the thermal properties of the metal shell provide only second order effects.

##### c. Stress Analysis

Analysis performed on the AGCarb liner electroformed nickel design indicates a marginal condition insofar as contact pressure is concerned. Since the expansion of copper is greater than nickel, this condition would be aggravated. For this reason, no further analysis was performed.

### III, B, Subtask 2. Design Evaluation (cont.)

#### d. Summary

The attempt in this design to employ a stainless steel outer shell of cylindrical shape as a means of obtaining a milled channel design which was not entirely dependent on electroforming resulted in higher estimated costs to produce than the electroformed nickel AGCarb liner design as well as fitup problems and greater weight. Additionally, the stress analysis performed on the nickel design indicated a marginal but feasible condition in regard to interface contact pressure in the event of separation. The copper will separate from the liner during brazing due to the  $\alpha\Delta T$  of the two materials. Also, since the  $\alpha$  of copper exceeds that of nickel, it was concluded that the contact would be close to nonexistent at steady-state conditions. It was concluded that this design is not feasible.

#### 6. Concept VI. Channeled Graphite Liner, Nickel Shell (Figure 6)

##### a. Description and Fabrication Approach

The channeled graphite design is aimed at being light-weight and as simple as possible. It consists of a graphite liner which is grooved on the outside diameter to form cooling passages. The outside shell is electroformed nickel. The significant advantage of this design in terms of heat transfer is the elimination of an interface (contact resistance) between jacket and liner which exists on the other designs.

AXF-5Q and ATJS graphite are the candidate liner materials; AXF-5Q (POCO) is not available in the size billet required although the company states that larger size billets will be available in the future. The other candidate material, ATJS, manufactured by Union Carbide, is available in cylindrical sizes 17 in. (0.432 m) in diameter and 14 in. (0.356 m) long and in rectangular sizes 24 in. (0.610 m) by 20 in. (0.508 m) by 9 in. (0.228 m). These would be adequate for a test chamber with an area ratio of 4:1 but would not make the flight size design with area ratio 16:1.

Fibrous graphite was another possible material but, because of its low conductivity, would be thin (about 0.125 in. (3.18 mm) at the throat); machining the cooling channels would weaken the material significantly. The porosity problem of graphite would be solved by pyrolytic graphite infiltration of gas-side and backside surfaces. It may be possible to compression mold a fibrous graphite such as AGCarb with the plies normal to the chamber axis. This would increase the thickness of the material and minimize the weakening of the structure attendant to machining coolant channels on its back surface.

An electroformed nickel jacket 0.060 in. (1.52 mm) thick closed the machined channels in the graphite. Flanges and manifolds are attached by electron beam welding.

### III, B, Subtask 2. Design Evaluation (cont.)

#### b. Thermal Analysis

Thermal profiles for this design are quite similar to those calculated for axially segmented graphite designs (presented in Figures 15 and 17) since both designs employ bulk graphite and provide good thermal contact between the graphite and the coolant. Detailed thermal analyses were not performed for this design because it was rejected for other than thermal reasons.

#### c. Stress Analysis

Preliminary stress analysis and design review of this concept indicated that a crack or local failure of the graphite liner would probably result in a catastrophic failure. The coolant channels in the graphite create stress raisers to some extent and, in fibrous graphite, the fibers would be interrupted, causing loss of hoop strength. A marginal situation also exists in maintaining a compressive rather than tensile load at the graphite to nickel interface. The  $\Delta T$  between the graphite and jacket is less than where the coolant is entirely in the jacket. The relative movement due to thermal expansion of the two components, therefore, is greater and tends to approach a tensile rather than compressive load. Separations at the interface would undoubtedly occur due to the combination of tensile and axial shear stresses to permit interchannel leakage and loss of velocity in the throat area.

#### d. Summary

For the reasons noted in c above, this concept is not considered feasible.

### III, Task I - Design and Evaluation (cont.)

#### C. SUBTASK 3. UNCOOLED CHAMBER DESIGNS

##### 1. Basic Design Description

Two workhorse thrust chambers were designed: a streak chamber to obtain compatibility information on the injector and to check the facility, and a heat sink chamber to obtain thermal data and characterized engine startup transients. Each design was thermally and structurally analyzed to verify its integrity and to assure that a maximum amount of usable data would be obtained to aid in the evaluation of flight designs. The completed designs are shown in Figures 18 and 19.

The streak chamber was a graphite liner of ATJ material in a steel retaining shell. ATJ was chosen because of its mechanical properties and availability in the size required. Its moderate density would result in its showing any injector-induced streaking. The liner was designed to be replaceable to enable reuse of the steel shell. One shell and two liners were fabricated. The graphite thickness was selected on the basis of providing sufficient heat sink to permit a run duration of 8 seconds. This duration was considered to be sufficient to characterize the chemical and gas dynamic compatibility of the injector. The results of the thermal analysis for this design for 6 seconds and 8 seconds are shown in Figure 20.

The copper heat sink chamber was designed to obtain engine performance and thermal data. The copper thickness was selected to provide sufficient heat sink for 6 seconds of operation; however, the desired duration could not be achieved in the throat section using copper alone. A throat insert of AGCarb fibrous graphite was used as a heat barrier to the copper at the throat to achieve 6 seconds run duration. The graphite insert design did not simulate the operation of the regeneratively cooled hardware because the copper backup undergoes greater temperature gradients and expansion than the regenerative jacket. One complete copper assembly was fabricated along with two spare graphite inserts.

The copper in the throat section was a brazed assembly of four parts. Gaps were provided between the parts to reduce two-dimensional heat flow which would affect thermal data. Thermocouples were incorporated to measure gas-side temperatures of the copper and backside temperatures of the graphite. The gas-side thermocouples were brazed in place; backside thermocouples were spring loaded to conform to the movement of the throat insert. The predicted temperature response at the throat is shown in Figure 21.

##### 2. Structural Analysis

Structural analyses of the two workhorse chambers were conducted to determine their capability to withstand the mechanical and thermal environments to be imposed during six cycle - six second duration repetitive use.

Figure 18. Combustion Chamber-Workhorse, Uncooled

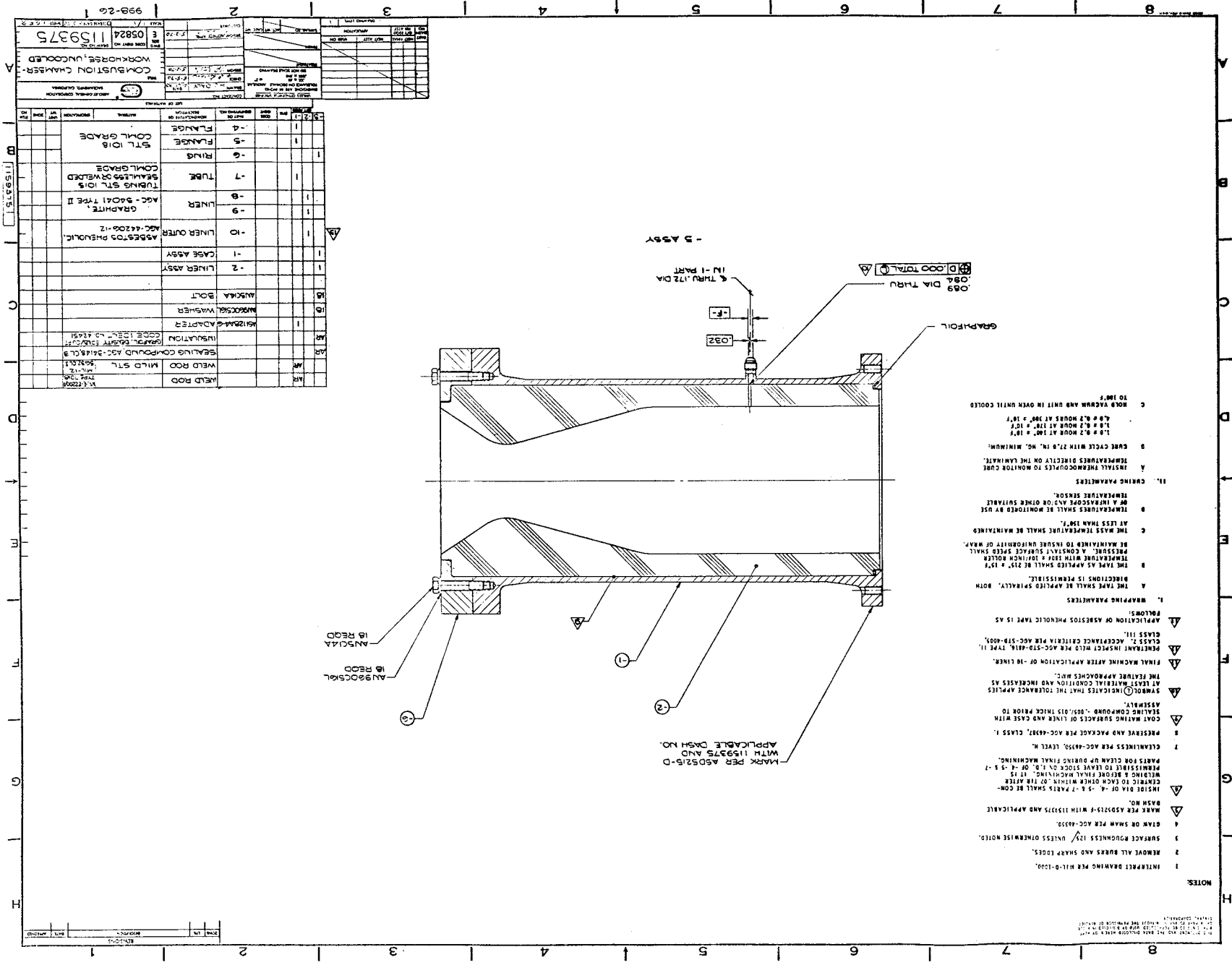
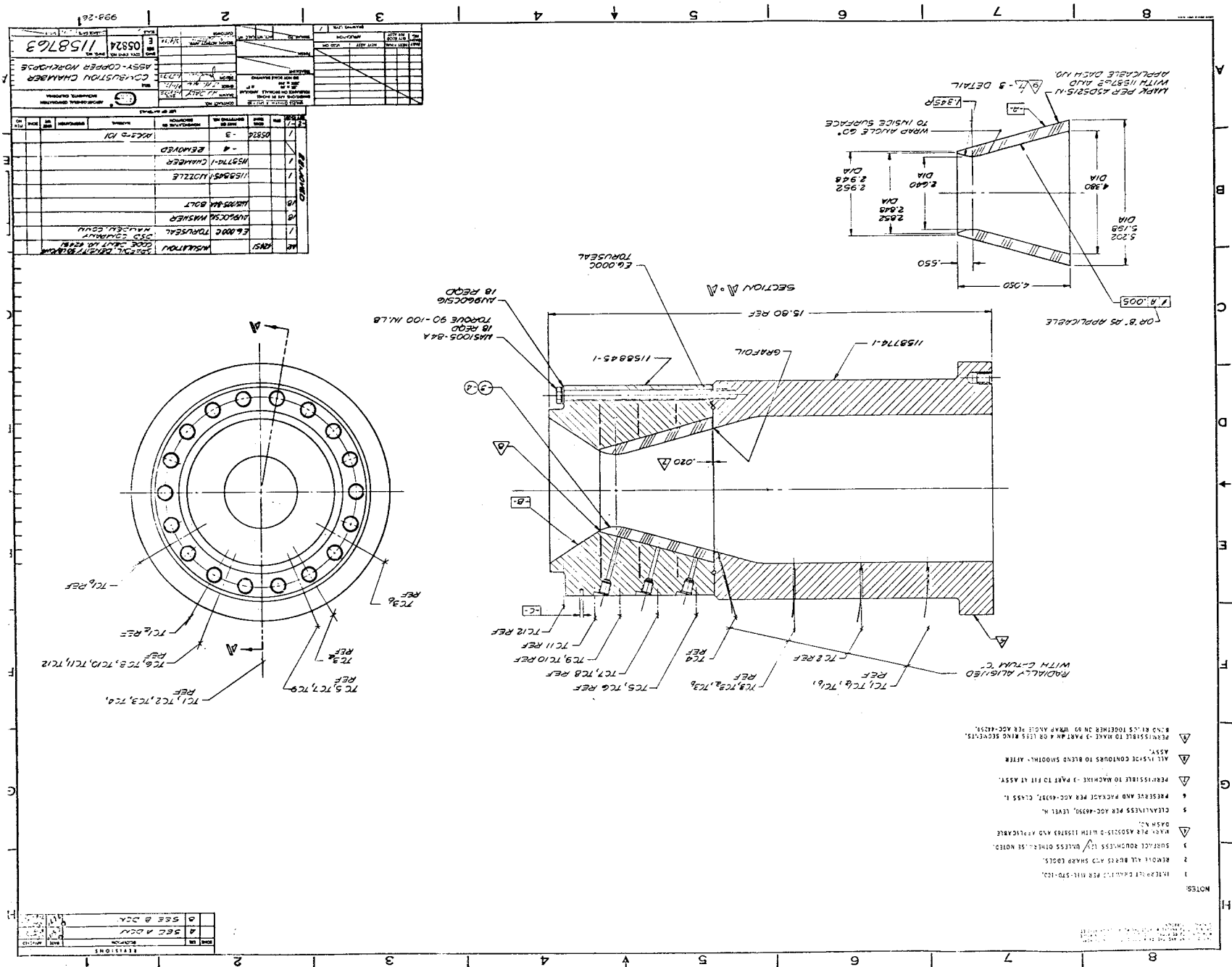






Figure 19. Combustion Chamber Assy-Copper Workhorse



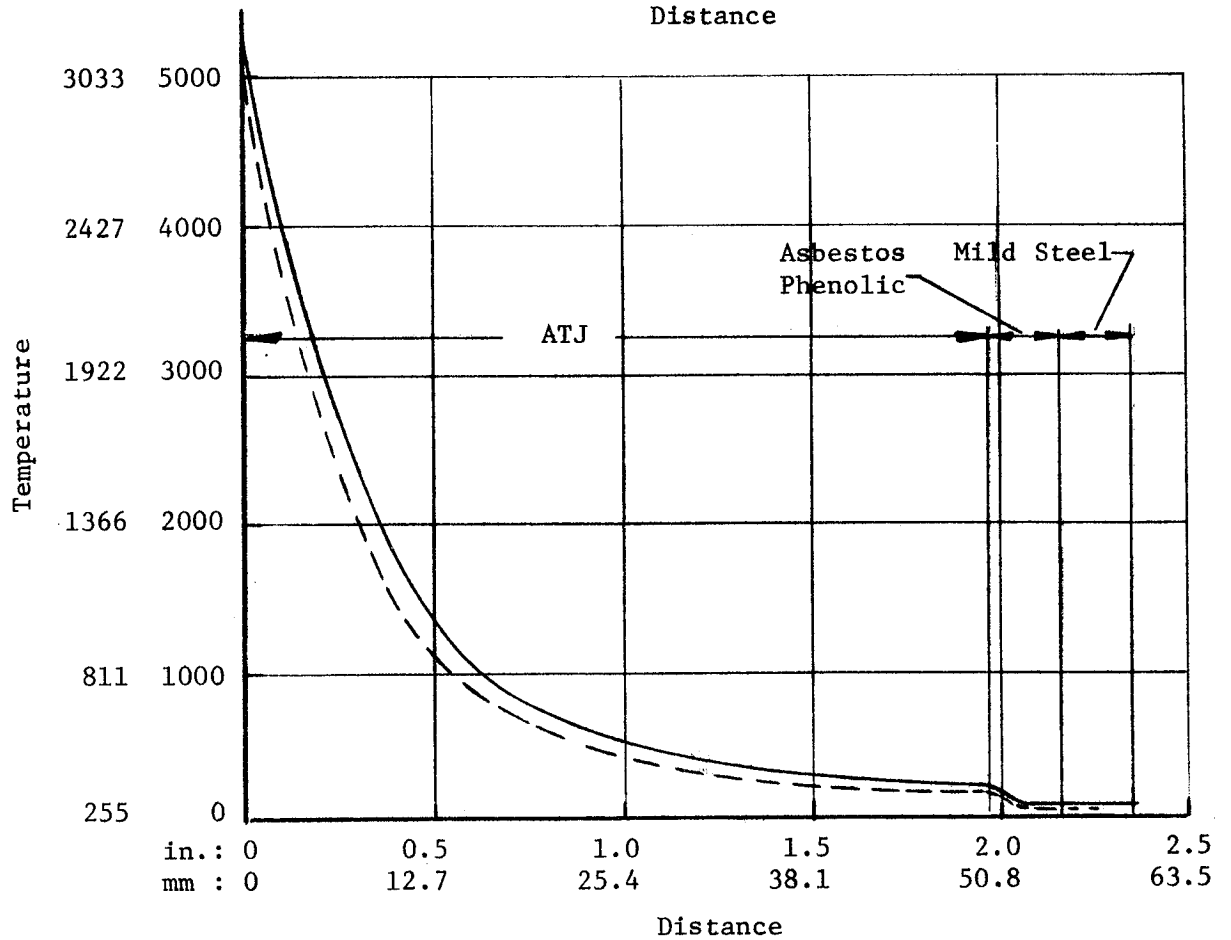
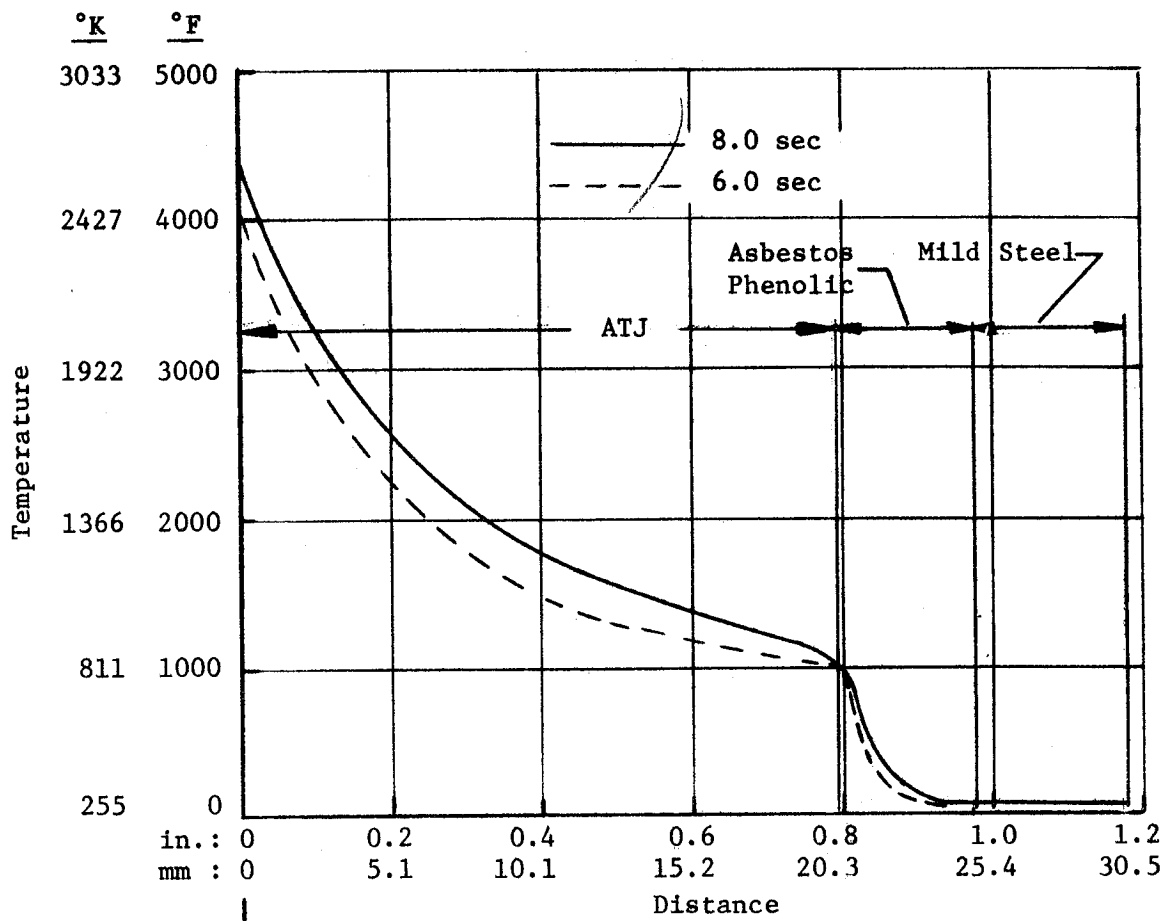


Figure 20. Temperature Profile at 6 sec and 8 sec

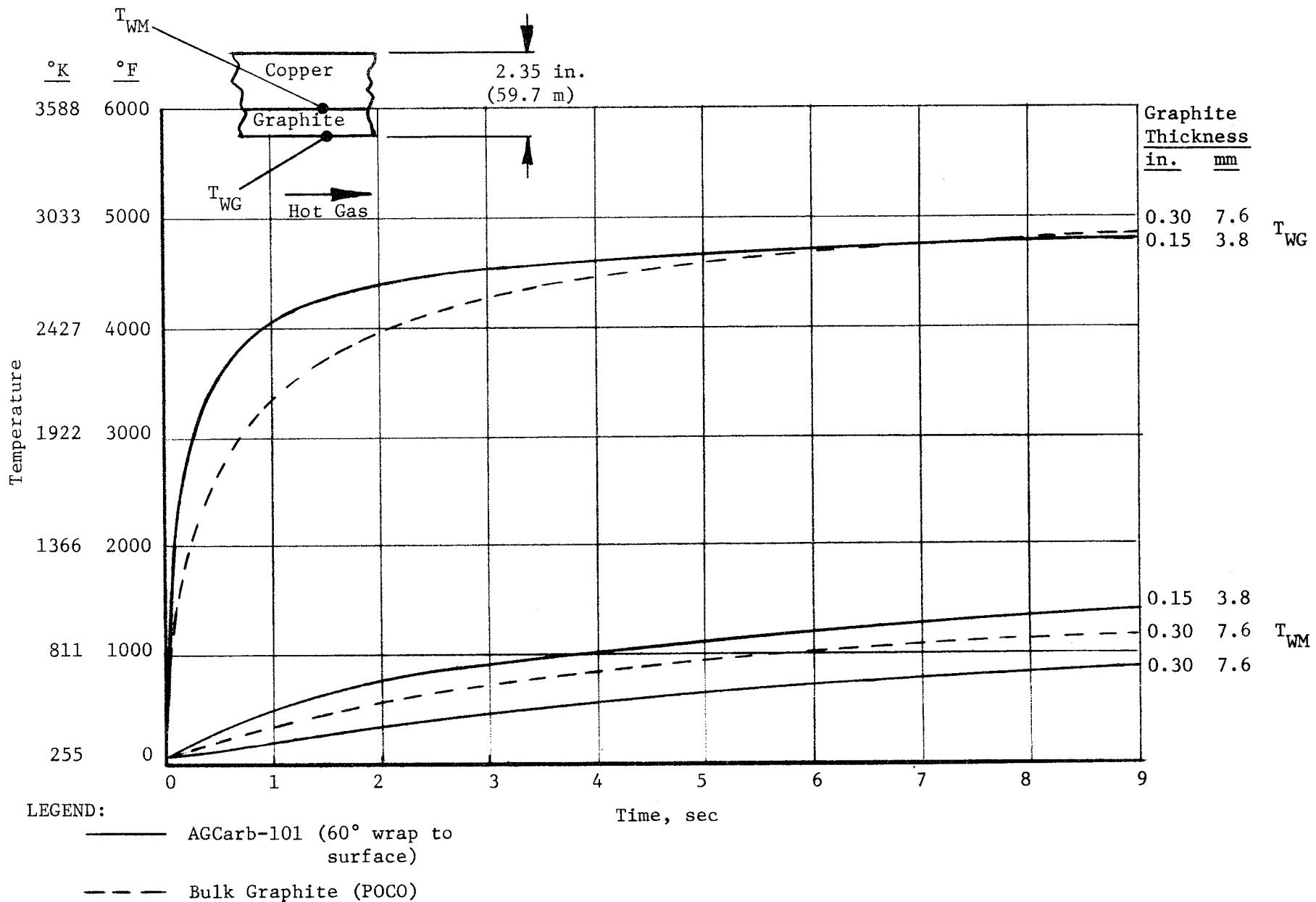


Figure 21. Copper Heat Sink Chamber Temperature Response at Throat

### III, C, Subtask 3. Uncooled Chamber Designs (cont.)

The bulk graphite liner-stainless steel shell configuration (ref Drawing No. 1159375) had a minimum margin of safety of +0.10 in the ATJ graphite throat section. The margins of safety are listed in Table I.

The AGCarb liner-copper shell workhorse engine (ref Drawing No. 1158763) was determined to be an acceptable configuration. Although the thermal limits resulted in the AGCarb liner being subjected to a high radial thermal gradient, any less severe thermal gradient compromised the purpose of the engine. The calculated meridional tension stresses on the backside of the AGCarb liner indicated that one or two circumferential cracks were likely. A shear lip was incorporated in the copper throat support to prevent spalling and ejection of the aft portion of the AGCarb insert. The combination of the copper shear lip and an 0.020 in. (0.508 mm) longitudinal gap at the forward end of the AGCarb insert was intended to prevent excessive longitudinal separation as circumferential cracks developed. The margins of safety are shown in Table II.

TABLE I

SUMMARY OF MINIMUM MARGINS OF SAFETY  
WORKHORSE CHAMBER NO. 1159375

<u>Component</u>	<u>Type of Stress</u>	<u>Applied Stress</u>	<u>Allowable Stress</u>	<u>Margin of Safety</u>
Stainless steel shell	Hoop tension	10,000 psi (68.94x10 <sup>6</sup> N/m <sup>2</sup> )	30,000 psi (206.84x10 <sup>6</sup> N/m <sup>2</sup> )	+2.00
Forward flange bolts	Tension	2080 lb (934 kg)	4000 lb (1814 kg)	+0.92
Forward flange	Bending	3750 psi (25.85x10 <sup>6</sup> N/m <sup>2</sup> )	25,500 psi (175.81x10 <sup>6</sup> N/m <sup>2</sup> )	+5.80
Aft flange bolts	Tension	1960 lb (889 kg)	4400 lb (1995 kg)	+1.25
Aft flange	Bending	3050 psi (21.02x10 <sup>6</sup> N/m <sup>2</sup> )	25,500 psi (175.81x10 <sup>6</sup> N/m <sup>2</sup> )	+7.40
Aft flange tab	Bending	9300 psi (64.12x10 <sup>6</sup> N/m <sup>2</sup> )	25,500 psi (175.81x10 <sup>6</sup> N/m <sup>2</sup> )	+1.75
ATJ graphite throat	Hoop tension	500 psi (3.44x10 <sup>6</sup> N/m <sup>2</sup> )	3450 psi (23.79x10 <sup>6</sup> N/m <sup>2</sup> )	+5.90
ATJ graphite forward throat	Merid. tension	2500 psi (17.23x10 <sup>6</sup> N/m <sup>2</sup> )	2750 psi (18.95x10 <sup>6</sup> N/m <sup>2</sup> )	+0.10
ATJ graphite throat	Effective compression	8300 psi (57.22x10 <sup>6</sup> N/m <sup>2</sup> )	9100 psi (62.74x10 <sup>6</sup> N/m <sup>2</sup> )	+0.10

TABLE II

SUMMARY OF MINIMUM MARGINS OF SAFETY  
COPPER WORKHORSE CHAMBER NO. 1158763

<u>Component</u>	<u>Type of Stress</u>	<u>Applied Stress</u>	<u>Allowable Stress</u>	<u>Margin of Safety</u>
Copper barrel section	Hoop tension	2360 psi (16.27x10 <sup>6</sup> N/m <sup>2</sup> )	3300 psi (22.75x10 <sup>6</sup> N/m <sup>2</sup> )	+0.40
Forward flange and throat bolts	Tension	740 lb (335 kg)	1650 lb (748 kg)	+1.22
Forward flange	Bending	1520 psi (10.48x10 <sup>6</sup> N/m <sup>2</sup> )	3300 psi (22.75x10 <sup>6</sup> N/m <sup>2</sup> )	+1.17
AGCarb throat	Hoop tension	3700 psi (25.51x10 <sup>6</sup> N/m <sup>2</sup> )	9200 psi (63.43x10 <sup>6</sup> N/m <sup>2</sup> )	+1.48
AGCarb throat	Merid. tension	See Summary		
AGCarb throat	Hoop compression	5700 psi (39.30x10 <sup>6</sup> N/m <sup>2</sup> )	7300 psi (50.33x10 <sup>6</sup> N/m <sup>2</sup> )	+0.28

### III, Task I - Design and Evaluation (cont.)

#### D. SUBTASK 4. FINAL DESIGN

Work under Subtask 2, Design Evaluation, culminated with selection by NASA of one of the three design concepts recommended by Aerojet as attractive and feasible based on the analyses performed. The concept selected was the fibrous graphite (AGCarb) liner with an electroformed nickel coolant jacket.

In discussions with the NASA project manager prior to start of final design, it was agreed that final design effort should include analyses with the objective of (1) reducing the predicted gas-side temperature of the liner and (2) simplifying coolant channel configurations by eliminating bifurcations and employing a constant width channel in a single pass system. It was agreed also that, to increase confidence in temperature predictions and stress analyses, additional AGCarb thermal and mechanical property data were required. Certain specific property data related to the exact wrap angle were considered desirable to confirm values previously factored and extrapolated from existing data. The final design task was therefore divided into four phases:

- (1) Final design using existing thermal and mechanical properties data for AGCarb.
- (2) Material characterization of AGCarb for specific properties related to configuration.
- (3) Structural analysis using new AGCarb properties and revision to design as required.
- (4) Review of new thermal property data and changes in design to conform as required.

The paragraphs immediately following summarize design efforts under these headings.

#### 1. Final Design Using Existing Thermal and Mechanical Properties Data for AGCarb

##### a. General

The thrust chamber configuration considered in this analysis was based on the design concept shown in Figure 1 and described under Design Evaluation. To permit testing at sea level, the nozzle was terminated at area ratio 4:1. The methane coolant temperature for this version was adjusted to simulate nozzle cooling to area ratio 16:1. This was to be accomplished by cooling methane to  $-120^{\circ}\text{F}$  ( $188^{\circ}\text{K}$ ) rather than using the  $-210^{\circ}\text{F}$  ( $139^{\circ}\text{K}$ ) methane employed for a flight configuration. The  $90^{\circ}\text{F}$  ( $305^{\circ}\text{K}$ ) temperature increase represents the bulk temperature rise between area ratio 16:1 and area ratio 4:1.

III, D, Subtask 4. Final Design (cont.)

The chamber and coolant conditions established for the analysis are:

Maximum nickel temperature	1200°F (922°K)
Maximum graphite temperature	4700°F (2866°K)
Chamber pressure	500 psia ( $3.45 \times 10^6$ N/m <sup>2</sup> )
Mixture ratio	5.75
Thrust	5000 lb (22,240 N)
Coolant supply temperature	-120°F (189°K)
Coolant supply pressure	As required to obtain 1000 psi ( $6.87 \times 10^6$ N/m <sup>2</sup> ) discharge pressure

b. Parametric Studies

The studies were begun by parametrically investigating the effects of various coolant channel design parameters, such as land-width and channel-width, on the nickel channel and AGCarb-101 liner temperatures. Typical curves for the high heat flux throat and chamber regions are shown in Figures 22 and 23. From the results of these parametric studies, a nickel channel design providing for 100 coolant channels and a coolant flow area of 0.130 in.<sup>2</sup> (8.385 mm<sup>2</sup>) at the throat was selected. The parametric studies also showed that AGCarb-101 liner thickness ranges of 0.130 in. (3.302 mm) to 0.150 in. (3.810 mm) at the throat and 0.250 in. (6.35 mm) to 0.300 in. (7.62 mm) in the chamber region were necessary to maintain the nickel shell temperatures at acceptable levels at these chamber locations.

The parametric studies assumed that the channel width would be maintained constant throughout the chamber. Since the parametric studies indicated this to be a feasible design approach, a channel width was selected for the design. A width of 0.0325 in. (0.826 mm) was found to satisfy thermal requirements and also provide a sound mechanical structure besides being a standard milling cutter size.

c. Channel and Liner Design Selection

With the number of coolant channels and the channel width fixed, only the channel height could be varied to change the local methane velocity in the coolant passages. Varying channel height is employed to increase the methane velocity in the high heat flux zones of the chamber where increased methane cooling is required. Tailoring the coolant velocity



- NOTES: (1) See Figure 23 for Nomenclature.  
 (2)  $W_c/A_f$  in  $\text{lb/in.}^2\text{-sec}$  ( $\text{kg/m}^2\text{-sec}$ )  
 (3) Methane coolant flow rate ( $W_c$ ): 2.05  $\text{lb/sec}$  (0.929  $\text{kg/sec}$ )

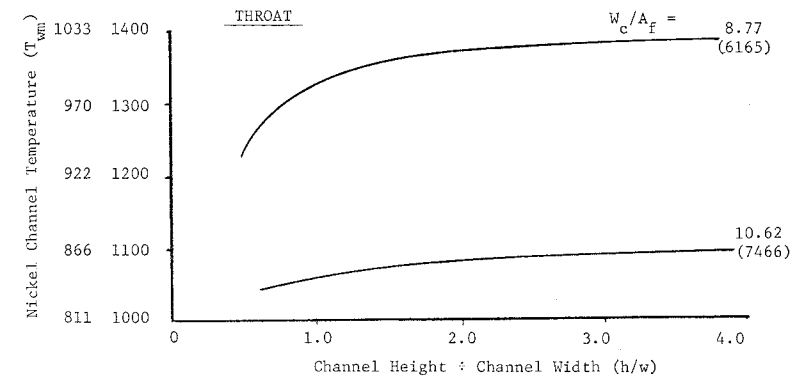
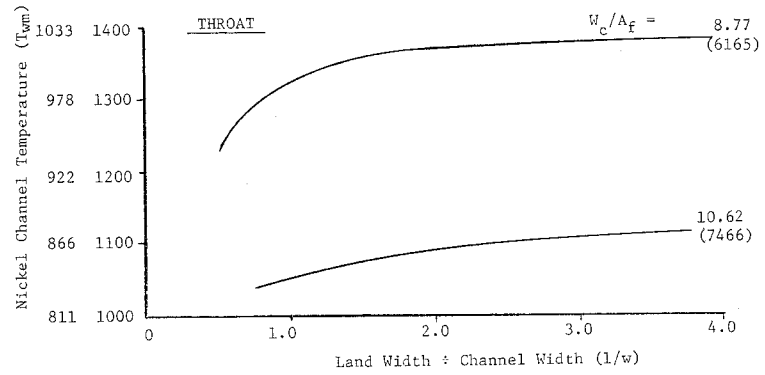
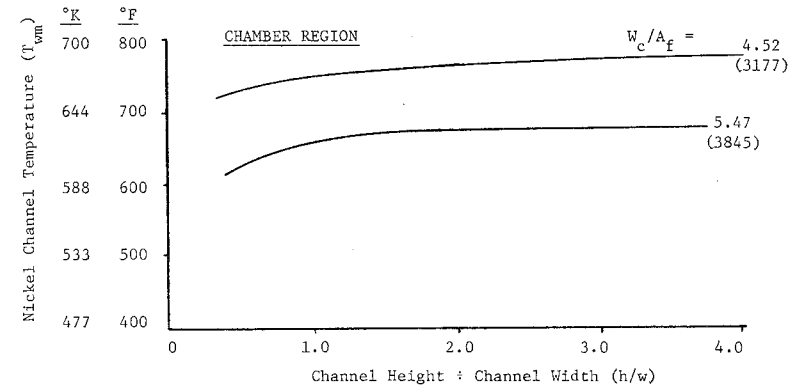
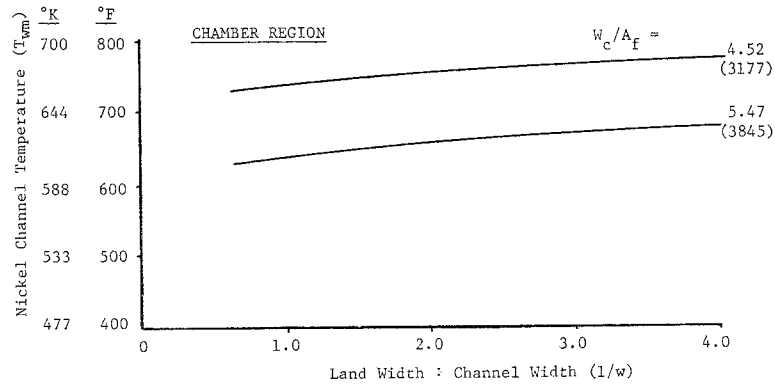
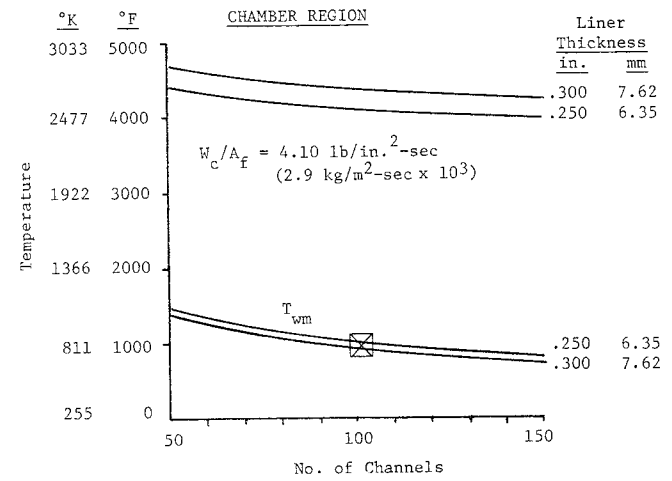
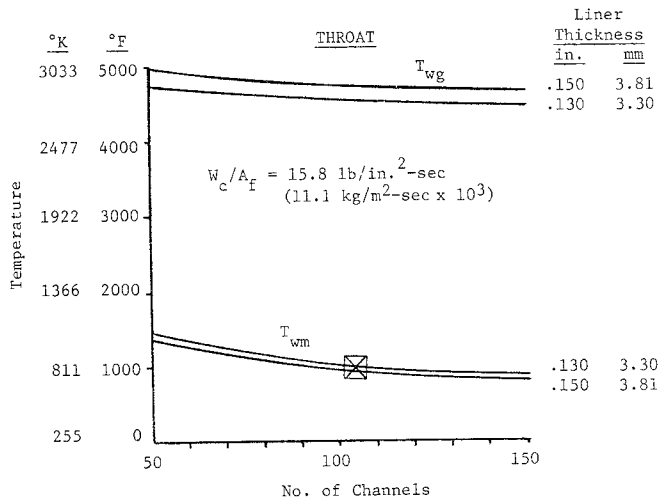


Figure 22. Channel Design Effects on Nickel Temperature



$W_c$  = Coolant flow rate  
 $A_f$  = Coolant flow area

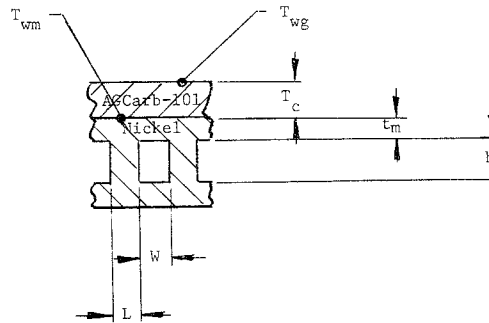


Figure 23. Liner and Channel Wall Temperature Variation for Constant Channel Width Design

### III, D, Subtask 4. Final Design (cont.)

Design B; however, the Design B linear channel height taper upstream of the throat produces high nickel channel temperatures upstream of the throat. Design C, which provides for a constant channel height and liner thickness in the high heat flux region, is seen to produce flat graphite and nickel temperature curves throughout the high heat flux throat region. It was concluded from the temperature curves that a chamber design incorporating the features of Design C would be the most efficient thermal design since it eliminated the liner and channel temperature peaks in the high heat flux throat region.

#### d. Recommended Design

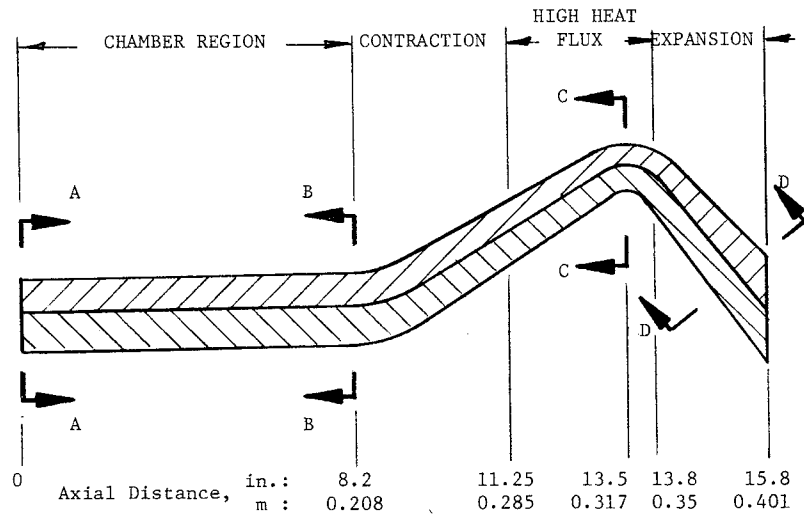
The chamber design recommended for fabrication is shown on Figure 25. The channel dimensions, land width and liner thickness in the chamber, which have been divided into four heating zones, are tabulated. As shown, this design provides for 100 coolant channels that are a constant 0.0325 in. (0.826 mm) wide. In accordance with the discussions in b and c above, both the channel height and graphite liner thickness were tapered to tailor the local cooling design to the heating conditions throughout the chamber.

Beginning at the forward end of the chamber, the channel height and liner thickness are maintained constant at 0.150 in. (3.810 mm) and 0.30 in. (7.62 mm), respectively, throughout the cylindrical length. The constant channel size and liner thickness were selected to cool the most severe heating conditions encountered in this portion of the chamber and ignores injector barrier cooling effects\*. In the contraction region of the chamber, the channel height and liner thickness are tapered linearly along the contour to the beginning of the high heat flux zone which begins at axial distance 11.25 in. (0.286 m). The channel height of 0.040 in. (1.02 mm) and liner thickness of 0.13 in. (3.30 mm) at this location are then held constant beyond the throat to axial distance 13.8 in. (0.351 m). In the expansion zone, the channel height and liner thickness are again tapered to values of 0.150 in. (3.810 mm) and 0.45 in. (11.43 mm), respectively. The final design engineering drawings conforming to the recommended design (Figure 25) are shown in Figures 26 through 28.

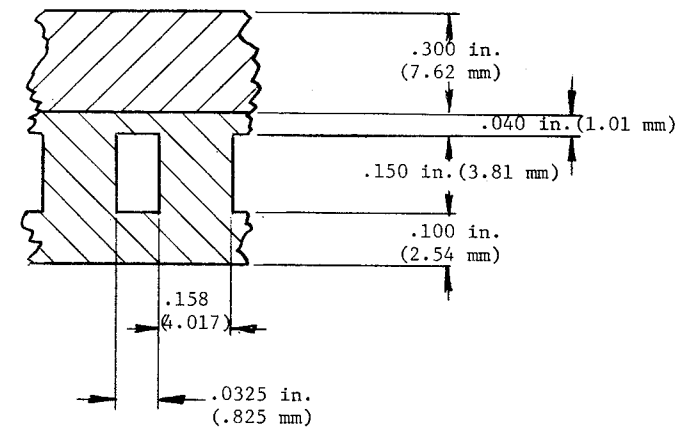
The predicted thermal parameters for the recommended 100-channel design are summarized on Figure 29. The maximum liner and nickel channel temperatures are 4700°F (2866°K) and 1150°F (894°K), respectively. The coolant pressure drop was calculated as 268 psi ( $1848 \times 10^3 \text{ N/m}^2$ ) and included a 22 psi ( $151 \times 10^3 \text{ N/m}^2$ ) velocity head loss at the injector end of the chamber. The 246 psi ( $1696 \times 10^3 \text{ N/m}^2$ ) frictional pressure drop was

---

\*Neglecting barrier cooling will permit the chamber to be tested with injectors which do not provide barrier cooling.



SECTION A-A, B-B AND D-D



CHANNEL DESIGN SUMMARY - 100 CHANNELS

LOCATION:	CHAMBER		CONTRACTION	
	in.	mm	in.	mm
Graphite Liner	.30	7.62	.30-.13	7.62-3.30
Channel Height	.150	3.81	.150-.040	3.81-1.01
Channel Width	.0325	.825	.0325	.825
Land Width	.150	3.81	.150-.100	3.81-2.54

LOCATION:	HIGH HEAT FLUX		EXPANSION	
	in.	mm	in.	mm
Graphite Liner	.13	3.30	.13-.45	3.30-11.42
Channel Height	.040	1.01	.040-.150	1.01-3.81
Channel Width	.0325	.825	.0325	.825
Land Width	.100-.061	2.54-1.54	.067-.150	1.70-3.81

SECTION C-C

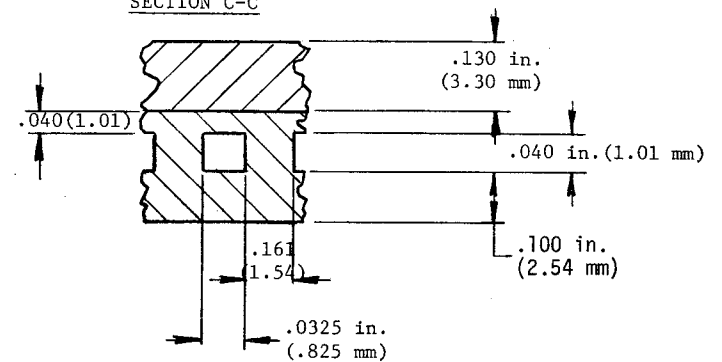
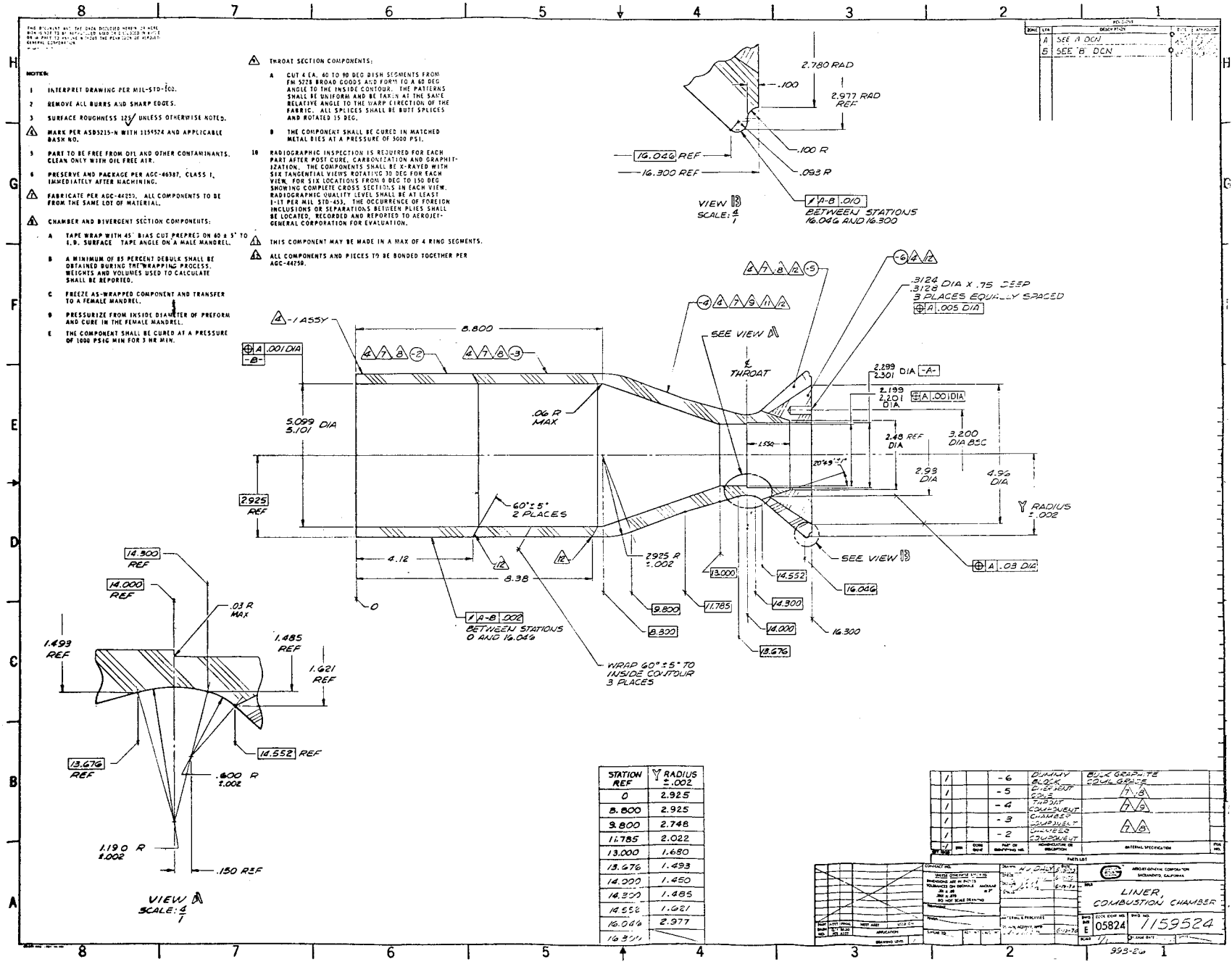


Figure 25. Channel Design Summary - 100 Channels







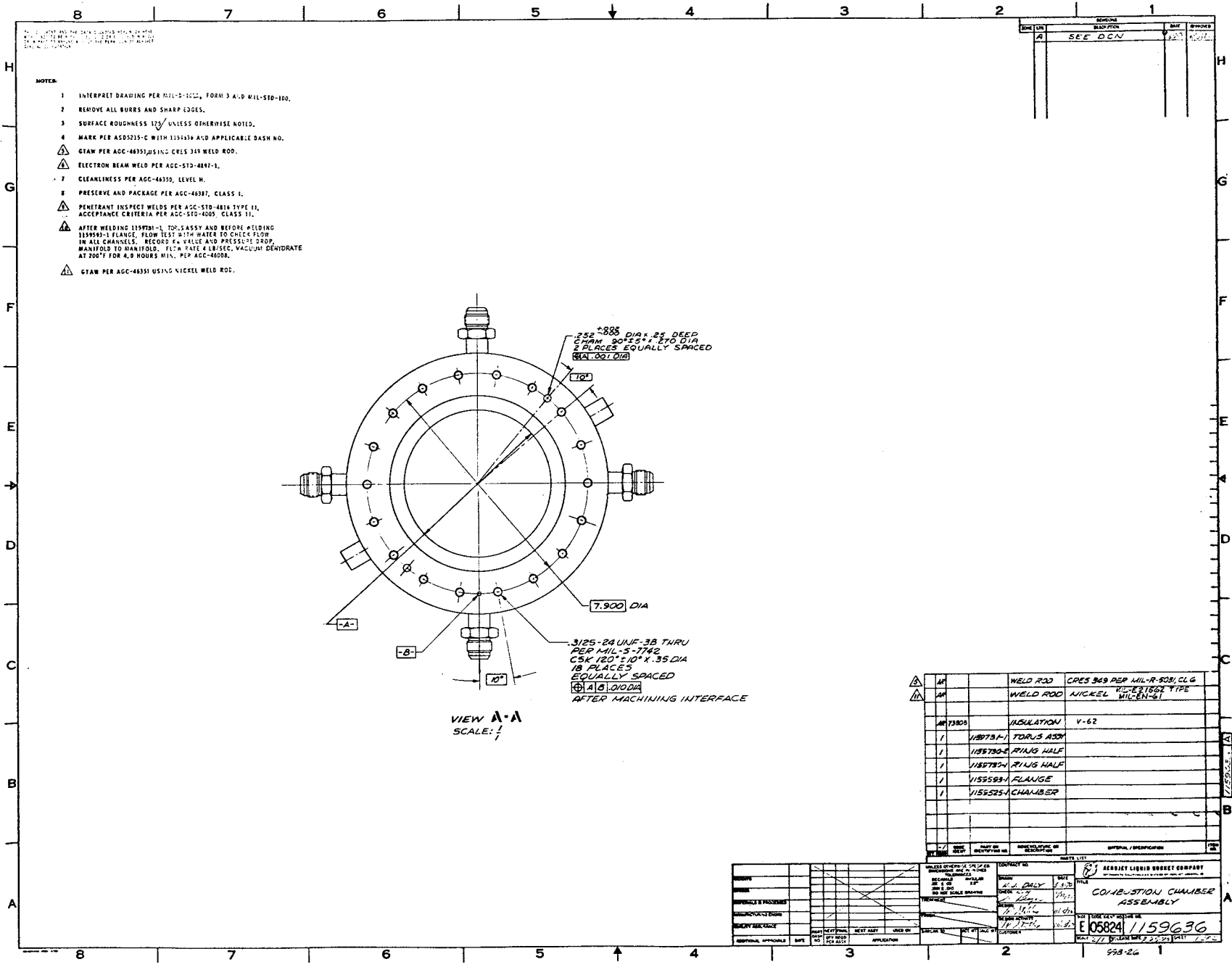


Figure 28. Combustion Chamber Assembly





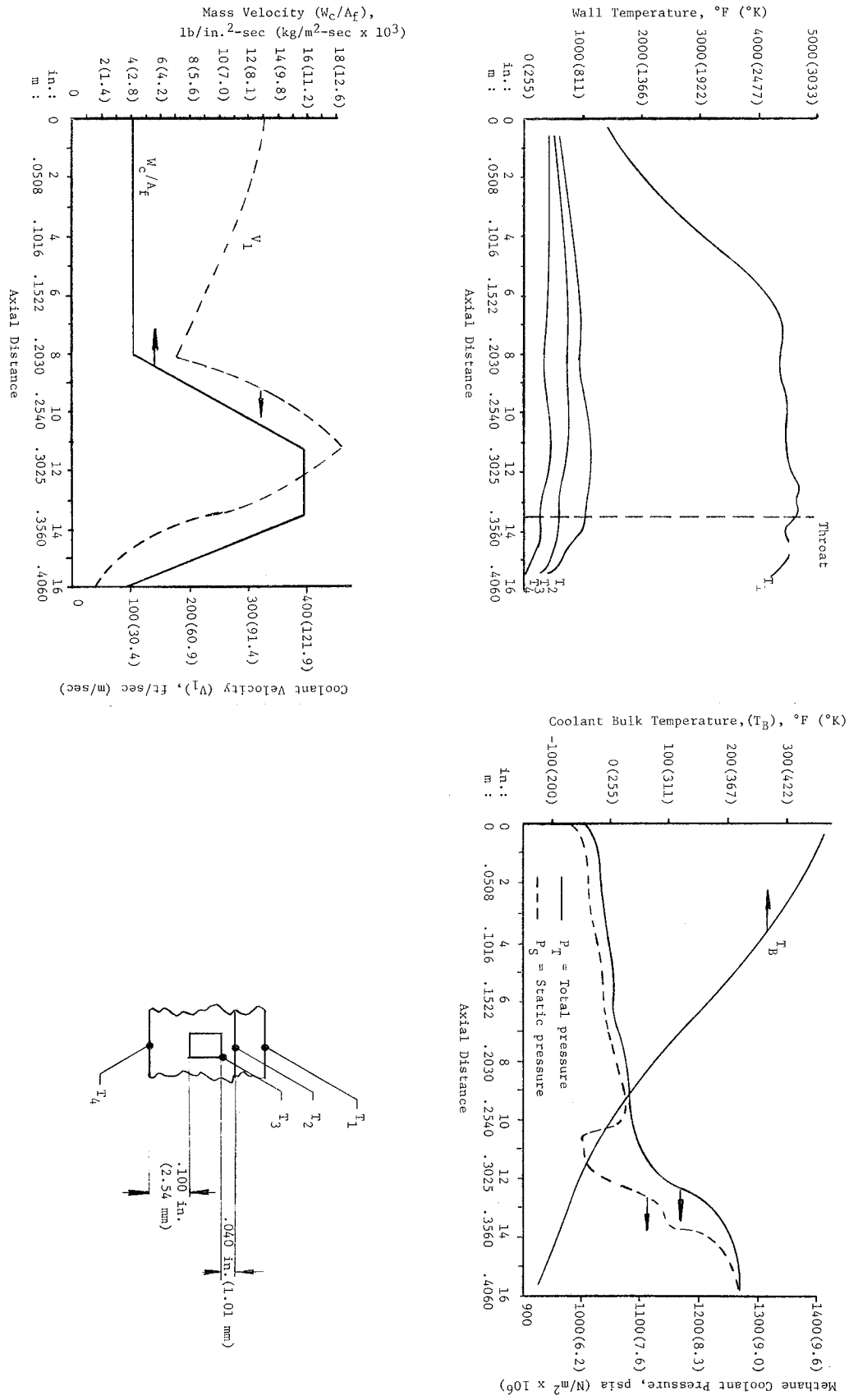


Figure 29. Thermal Parameters for 100-Channel Chamber Design

III, D, Subtask 4. Final Design (cont.)

calculated using a conventional isothermal friction factor approach and may be conservatively high compared to  $\Delta P$  calculations which include the effects of coolant temperature drop in the viscous boundary layer.

2. Material Characterization - AGCarb Fibrous Graphite Liner

The liner (Figure 26) consists of four segments. The two forward segments are tape wrapped with 45° bias tape 60° to the chamber contour. The throat segment is compression molded split discs of carbon cloth rotated so splits are not coincident. The aft section is tape wrapped similar to the cylindrical section. Existing thermal and mechanical property data (Ref 2) were based on flat panels with properties tested with or against the grain. Due to the uncertainty of factoring these data to obtain value for the 60° tape wrap segments and the heterogeneous pattern of the throat segment, a test program was planned to obtain these values by direct testing. The test plan shown below carries the original test numbers. Missing numbers represent tests cancelled because of cost limitations.

Test No.	Specimen No.	Type	Data	No. of Tests - Temperature		
				RT	3000°F	5000°F
1	1	Tensile (chamber hoop)	Ultimate Modulus Poisson's ratio Stress-strain curve	3	3	3
4	4	Compression (throat hoop)	Ultimate Modulus Stress-strain curve Poisson's ratio	3	3	3
5	12	Tensile (throat hoop)	Ultimate Modulus Poisson's ratio Stress-strain curve	3	3	3
7	13	Block compr.	Ultimate Modulus Stress-strain curve	12	12	12
14	9,14	Therm. Conduc. (chamber radial)	Btu/in./sec/°F	1	1	1
15	10,15	Therm. Conduc. (throat radial)	Btu/in./sec/°F	1	1	1

### III, D, Subtask 4. Final Design (cont.)

The specimens were fabricated by San Rafael Plastic Company in the size and configuration shown on Figure 1 of Appendix A. Figure 30 (foreground) shows some specimens prior to final machining. Figure 31 shows specimens as shipped to Southern Research Corporation, who was selected as a testing source due to their 5000°F (3033°K) temperature capability. Results obtained by Southern Research Corporation are summarized in this report under Appendix A. The mechanical properties values reported were used in performing the structural analysis described below and in Appendix B.

#### 3. Structural Analysis

A structural analysis of the final design was completed by the ALRC Structural Engineering Section. A summary of results is made below and the complete analysis is included in this report as Appendix B.

##### Summary

(1) The structure will develop marginal hoop compressive stresses in the AGCarb throat liner. However, the AGCarb is in a state of compression and is contained by the nickel shell with the local shear stresses within allowable values. Therefore, the condition is considered acceptable.

(2) The structure will develop excessive shear stresses in the aft AGCarb liner at the aft retaining flange. Since this is a very local condition, it is anticipated that the liner will probably delaminate locally (interlaminar) but not completely fracture. A possible means of alleviating this local excessive stress condition would be to provide an axial expansion relief, e.g., a Grafoil material insert.

Due to scheduling problems, chamber fabrication was started before completion of the final stress analysis and had proceeded beyond the point where a design change could be made. (Post test examination indicated no evidence of the predicted local shear failure.)

#### 4. Thermal Data Review

Thermal data from the AGCarb testing were compared to the values used in the original analysis to establish the graphite liner wall thickness and found to be within what was considered measuring error range. The chamber wall temperature profile using the new data was compared to original predictions. Graphite gas-side temperature at the throat was nearly identical. At 2 in. (0.051 m) upstream of the throat, the revised profile was approximately 70 F (36°K) higher. Since these differences were not considered significant, no revisions were made to the engineering drawings.

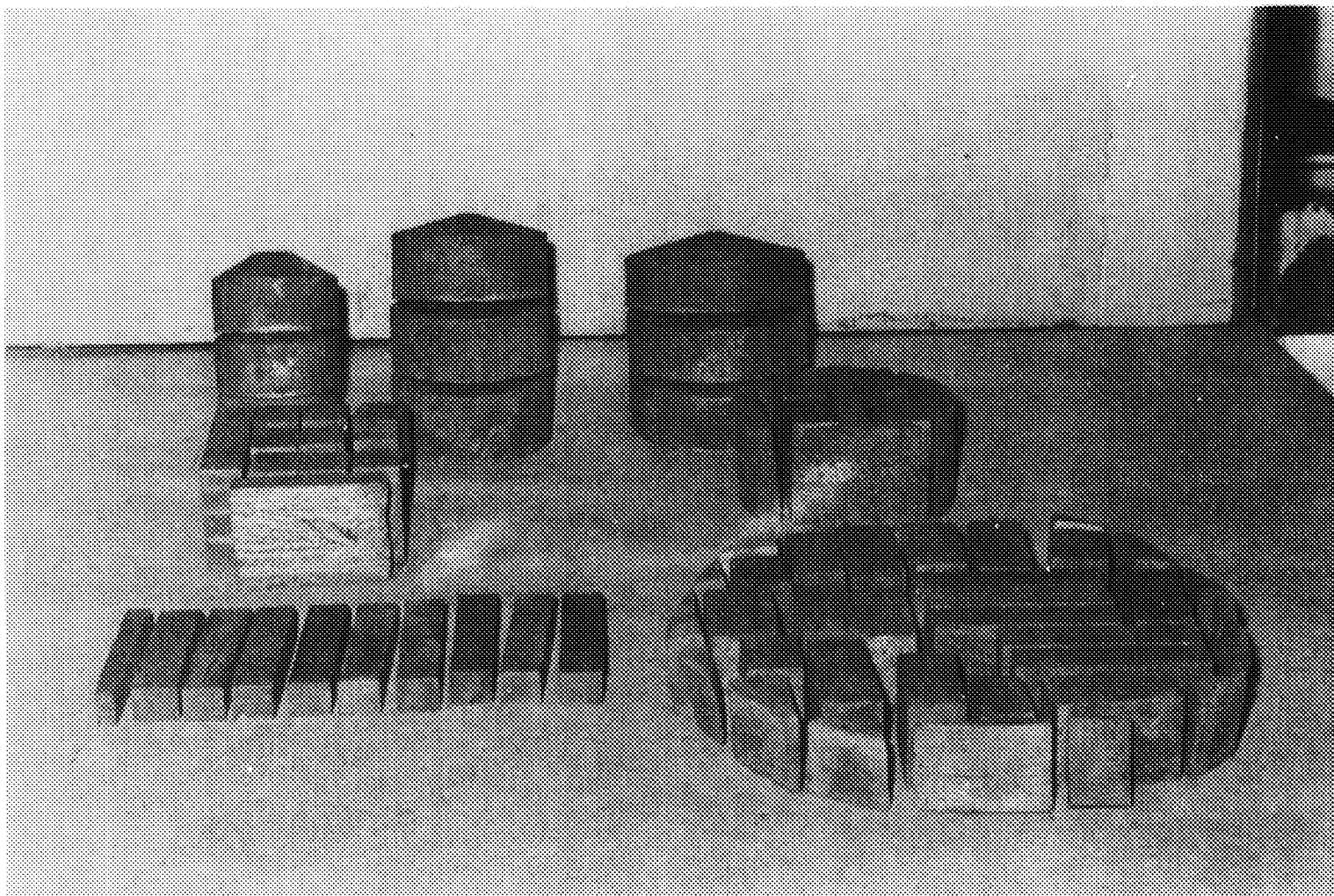


Figure 30. Test Specimens After Graphitization and Before Machining

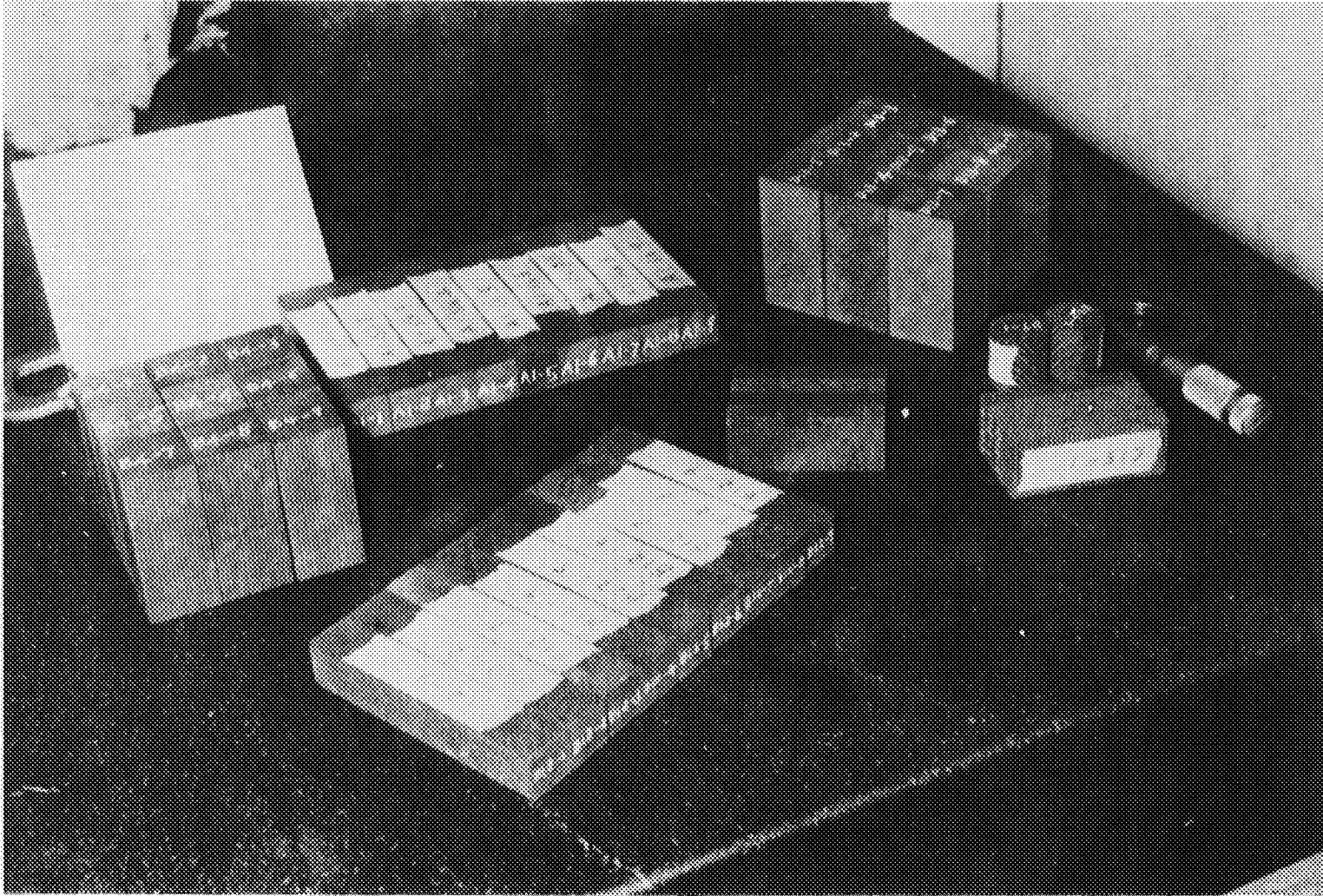


Figure 31. Test Specimen as Shipped to Southern Research Corporation

#### IV. TASK II - FABRICATION

##### A. UNCOOLED CHAMBER FABRICATION

The designs of the streak chamber and the copper heat sink chamber are described in Section III,C. Figures 18 and 19 depict the final designs. Fabrication of these test chambers was straightforward and required no unique methods. No problems were encountered in fabrication or assembly. Extreme care was taken in fitting the AGCarb insert into the copper chamber throat to ensure that maximum contact would be obtained at the copper-graphite interface. This was accomplished by machining identical tapers, pressing the insert into position, rotating to lap the surfaces, then trimming the insert to length after fitup.

##### B. COOLED CHAMBER FABRICATION

###### 1. Approach

The Work Plan submitted at program start in conformance with contractual requirements stipulated that make or buy decisions for fabrication of cooled chamber components would depend on the configuration selected and the materials used. It was planned that, if AGCarb was selected as the liner material, fabrication would be by an outside subcontractor performing under Aerojet specifications and surveillance. Likewise, if electroformed nickel were to be used, the work would be performed by an outside electroforming shop under Aerojet specifications and surveillance. Contracts were to include provision for continuous engineering surveillance by Aerojet personnel during fabrication.

When the AGCarb liner-electroformed nickel jacket concept was selected as the primary concept, an overall manufacturing plan was developed incorporating the fabrication and quality control specifications noted above with other control and contractual documents and a tooling plan. The essential control documents, their functions and interrelation are explained in the following sections.

###### 2. Subcontractor Selection

During the preliminary design phase, discussions were held with several potential subcontractors and informal proposals received. San Rafael Plastics was selected for AGCarb fabrication on the basis of previous work done for Aerojet and their contributions to the proposal and the design.

A survey of potential electroforming sources and discussions with these companies with NASA personnel participating resulted in selection of Electroforms Inc., Gardena, California, as the electroforming subcontractor. Since several machining operations were anticipated between stages of electroforming, it was considered prudent to have the electroforming vendor responsible

#### IV, B, Cooled Chamber Fabrication (cont.)

for both intermediate and final machining. Machining of the slots also required special skills and equipment; an agreement was made after a surveillance visit to permit the subcontracting of slot machining to Huevil Profiling Company, Gardena, California.

### 3. Fabrication Control

#### a. Parameters

Critical aspects of the selected design were considered to be (1) maintenance of a complete bond and/or intimate contact between the nickel jacket and the fibrous graphite liner and (2) close dimensional control of the coolant channels in the machining and subsequent electroforming of the outer shell. The first of these is critical because any loss of interface contact or any discrepancy that tended to lower interface pressure at temperature would increase contact resistance and thereby appreciably increase the graphite liner temperature. This aspect was discussed in the design evaluation section of this report. Close dimensional control of channel size is critical because of the relationship between coolant velocity,  $\Delta P$ , and temperature rise. Experience with the electroformed chamber constructed and tested under NASA Contract NAS 3-7971 (Ref 3), where pressure drop exceeded that predicted by a factor of 3, plus some subscale work under other programs indicated that the process of electroforming over the core material, which is subsequently melted out, is suspect in that any of three discrepancies that could occur would increase  $\Delta P$ . These are (1) loss of channel height dimension due to erosion of the wax filler during cleaning for final electroforming, (2) excessive surface roughness of the channel closeout nickel due to roughness of the core material, and (3) loss of coolant flow due to core material that is not entirely removed in the melting and flushing steps.

Another critical area in the manufacturing process is the dimensional control of the inner shell thickness, rib height, and outer shell thickness. Since these dimensions were not directly measurable due to the method of fabrication, they were controlled by basic dimensions and tooling templates.

To control the overall fabrication process including the critical aspects noted above, several control documents and mechanisms were initiated. These included purchase order contracts, process specifications, engineering drawings, master tooling template, manufacturing flow chart, and discrepancy analysis. The function of the purchase order and engineering drawings needs no explanation; however, a brief explanation of the other controls is made in the following paragraphs.



#### IV, B, Cooled Chamber Fabrication (cont.)

##### b. Process Specifications

(1) A specification covering the manufacture of AGCarb materials was prepared and made a part of the contractual document negotiated with San Rafael Plastics for fabrication of chamber liners (see Figure 26).

(2) In order to control chemical and mechanical properties of electroformed nickel, a development specification, AGC-44259, was written and made a part of the contractual document with the electroforming subcontractor. The specification, as written, was adequate to handle the major aspects of quality control; however, problems in welding the electroformed nickel suggest a revision is needed to require closer control over elements detrimental to welding. The welding problems are discussed in the next section.

##### c. Manufacturing Flow Chart

The fabrication process followed the sequence depicted in the Manufacturing Flow Chart (Figure 32). The philosophy of the fabrication sequence was based on (1) the use of internal mandrels that were fixed and stayed with the assembly through all the electroforming and machining operations; (2) the use of master tooling templates; and (3) machining of the graphite ID to final contour after electroforming, OD machining, and removal of the mandrel.

The inspection operation, symbol  $\triangle C$  in the flow chart, refers to critical inspection points as determined by the discrepancy analysis. A summary of the discrepancy analysis study is shown in Figure 33. The historical summary of the actual fabrication problems to follow will permit a comparison to anticipated problems.

##### d. Master Tooling

Referring to Figures 27 and 28, it can be seen that dimensions are established by a system of coordinate dimensioning. The X coordinate represents the chamber axis and the Y coordinate the radii from the axis. To effectively coordinate all machining operations and ensure that dimensional tolerances were held, a master contour template to the graphite inner contour was constructed. All other templates were coordinated to this master. Each had the end of the part scribed to locate it axially to the reference surface of the mandrel.

#### 4. Historical Summary

##### a. Introduction

This section provides a historical account of the fabrication operation with the object of highlighting problem areas and presenting solutions and recommendations to provide a guide for subsequent

## MANUFACTURING PLAN GRAPHITE LINED THRUST CHAMBER

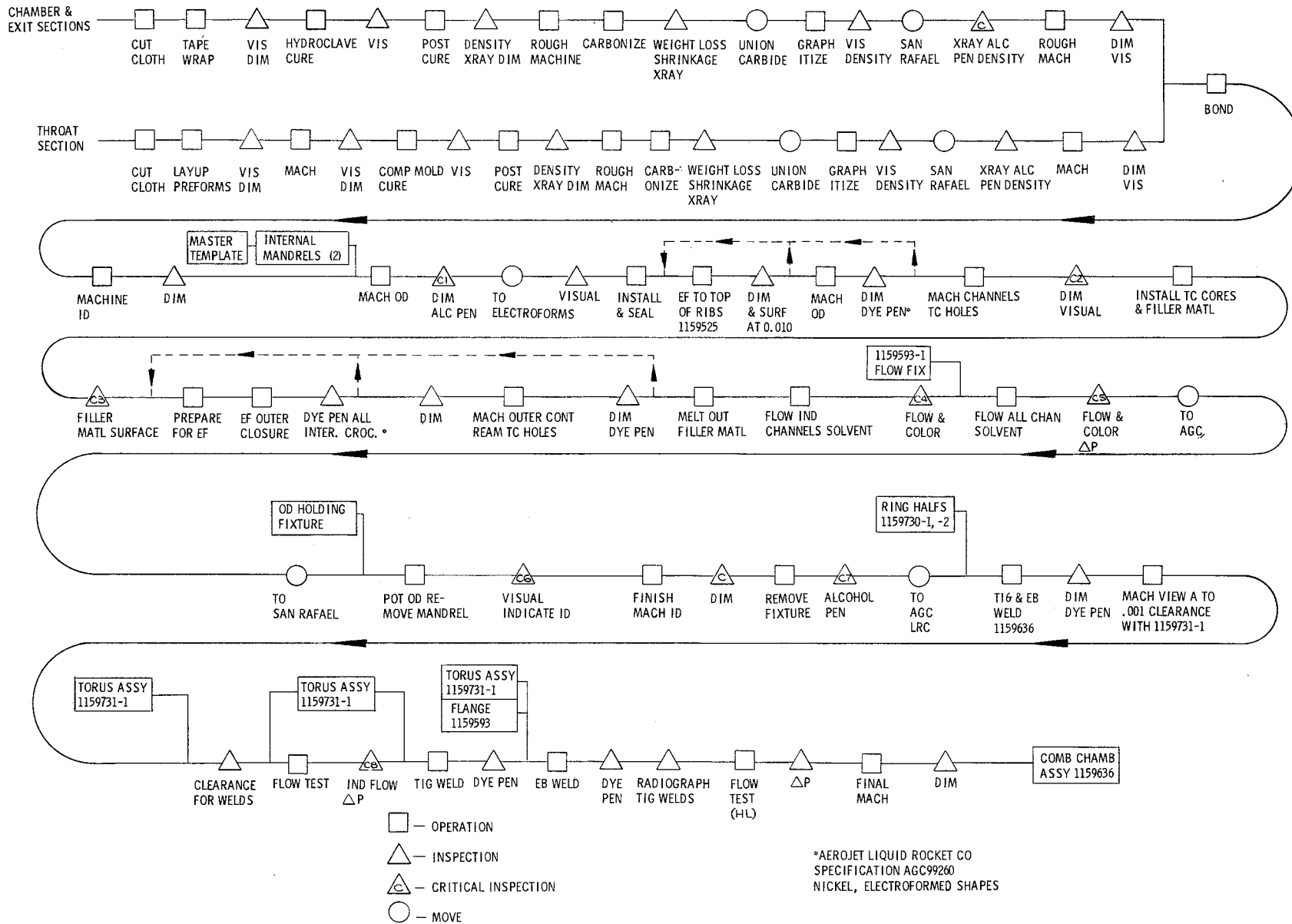


Figure 32. Manufacturing Flow Chart

<u>Inspection Code</u>	<u>Possible Discrepancy</u>	<u>Anticipated Disposition</u>
C1	1. Dimensionally undersize	Compensate on ID.
	2. Alcohol penetrant shows cracks or delaminations	Minor - Repair with C-34 cement. Major - Use spare throat section.
C2	1. Channel dimensionally out of tolerance	Slightly undersize.- Refer to heat transfer studies; allow max. graphite temp 5000°F, max. Ni temp 1500°F, max. ΔP 400 psia. Oversize - Operate with increased fuel flow.
C3	1. Filler material excessively rough or below rib height	Refill and reprocess.
C4	1. Individual channel low flow	Flow 24 hours with hot solvent. Use a wire or "pipe cleaner". X-ray. If local area, remove closure locally and repair by electroforming. If no X-ray indication, machine off total closure and reprocess.
C5	1. Individual channel low flow	Repeat mechanical steps in C4 above. Calculate maximum temperatures; compare to allowable.
	2. ΔP excessive	Repeat mechanical cleaning in C4 above. Calculate maximum temperatures and compare to allowable. Increase inlet pressure (max. 1400 psia). X-ray and make local or total repair.
C6	1. Liner out of round, so liner thickness out of tolerance	Calculate maximum temperatures at thicker than print areas. If excessive, stress relieve at 350°F for 4 hours. Reinspect. If still excessive, press to round out.
C7	1. Alcohol penetrant shows cracks or delaminations	Minor - Repair with C-34 cement. Major - Part will function with fairly large delamination as it will close up on firing and heat transfer is only slightly affected. A major loss of material would require local insertion of repair AGCarb material.
C8	1. Individual channel low flow	Compare data to that obtained on C4 and C5 inspections. Increased ΔP or obstructions can be attributed to contaminants incurred during processing. Repeat mechanical cleaning of C4 above. X-ray and make local repair.
	2. ΔP excessive	Repeat mechanical cleaning of C4 above. X-ray and make local or total repair.

Figure 33. Discrepancy Analysis

#### IV, B, Cooled Chamber Fabrication (cont.)

design efforts using the materials and fabrication techniques employed. The manufacturing plan depicted in the Manufacturing Flow Chart was followed quite closely. Documentation required by the engineering drawings and specifications was maintained in a central file for review if required during the post-test analysis subtask. Some expected discrepancies occurred. Several unanticipated problems arose and were solved by joint action between the subcontractors and Aerojet. The NASA project manager was advised of all problems as they occurred and participated in the solutions. Although the account that follows notes several problem areas, it should be emphasized that the subcontractors involved (San Rafael Plastics Co., who produced the AGCarb liner and machined the liner ID after electroforming, and Electroforms Inc., who did the electroforming and related machining) were extremely diligent in their efforts to ensure the success of the program.

##### b. Fabrication of AGCarb Liner

###### (1) Fabrication

The thrust chamber liners were fabricated to Drawing 1159524 shown in Figure 26 and the specifications referenced on the drawing. In addition, the subcontractor manufacturing plan was reviewed and approved before start of fabrication.

As noted on the Manufacturing Flow Chart (Figure 32), the liner construction was of four segments; the two forward segments and the aft segment were tape wrapped and the throat segment compression molded. The photographs in Figures 34 and 35 provide a pictorial account of some of the in-process fabrication steps. Figure 34 shows the throat segments as made from disk cutouts premolded and machined to varying angles to centerline. Figure 35 shows the three throat segments cured and rough machined prior to carbonizing. Figure 36 shows the cylindrical segment in the same condition and Figure 37 shows the position of the segments in an assembly following the carbonizing operation. Following carbonizing in which the resins are decomposed to essentially pure carbon, the parts were sent to Union Carbide for their proprietary "Code 88" graphitizing treatment at 5000°F (3033°K). The resultant product is AGCarb-101, Aerojet's designator for fibrous graphite.

Assembly of the components was preceded by rough machining the OD and finish machining the ends for fitup to each other. After bonding, the ID was machined to suit the mandrel and the OD was machined to final contour using the master contour template and the internal mandrel. Figure 38 shows the bonded assembly before installation of the internal mandrel.

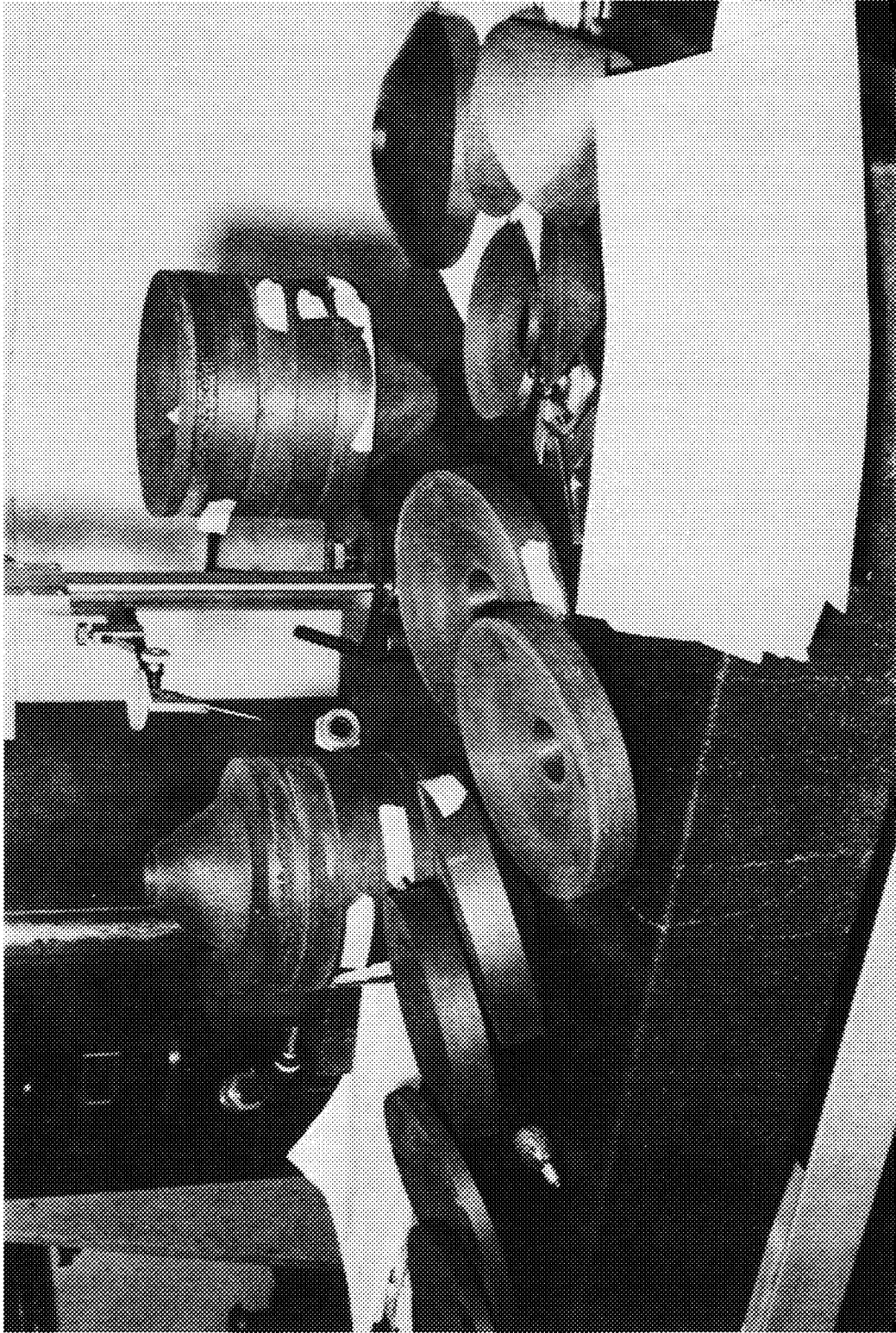


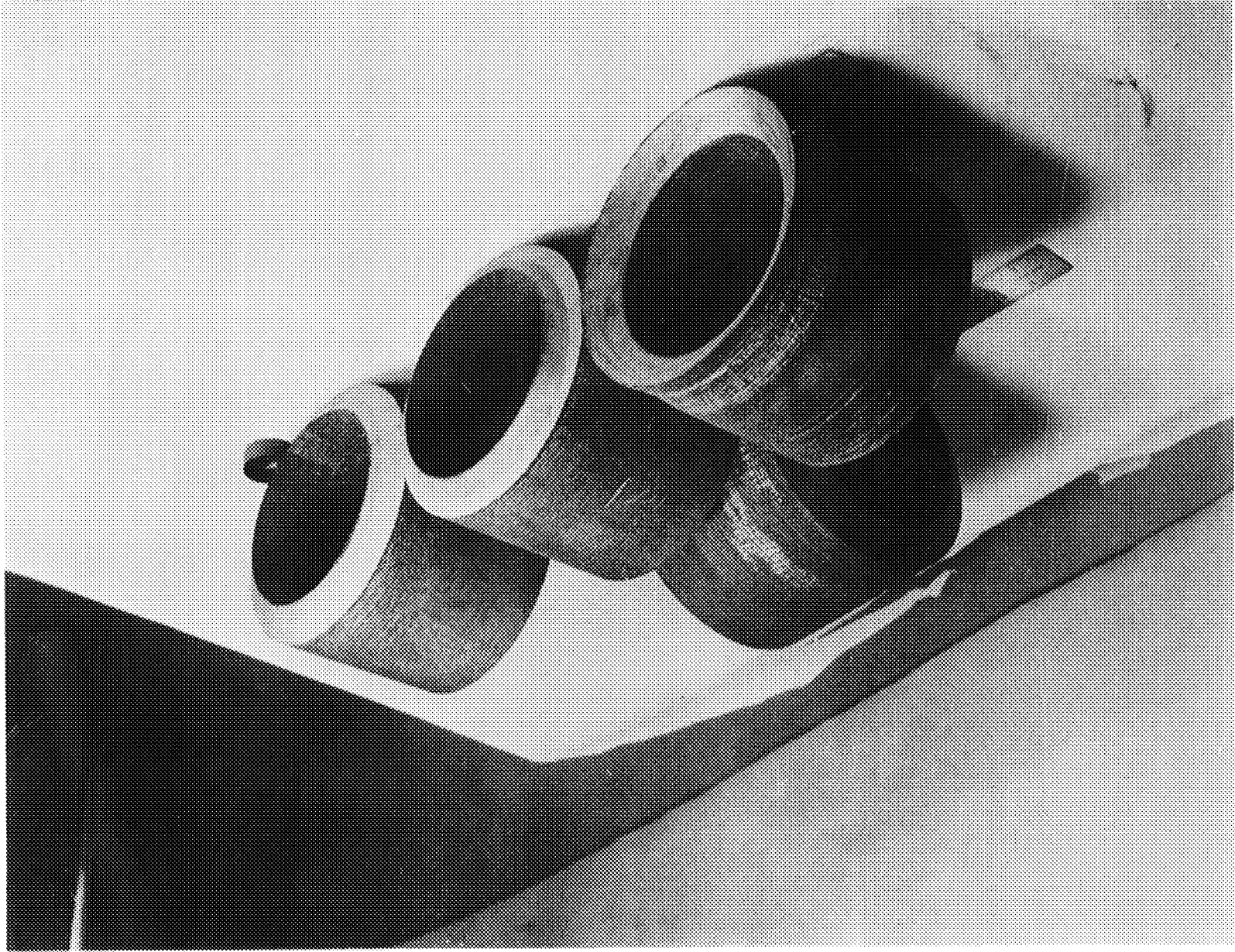
Figure 34. Throat Segments Premolded and Machined



Figure 35. Exit Segments Bonded, Cured and Rough Machined



Figure 36. Cylindrical Segments Cured and Rough Machined



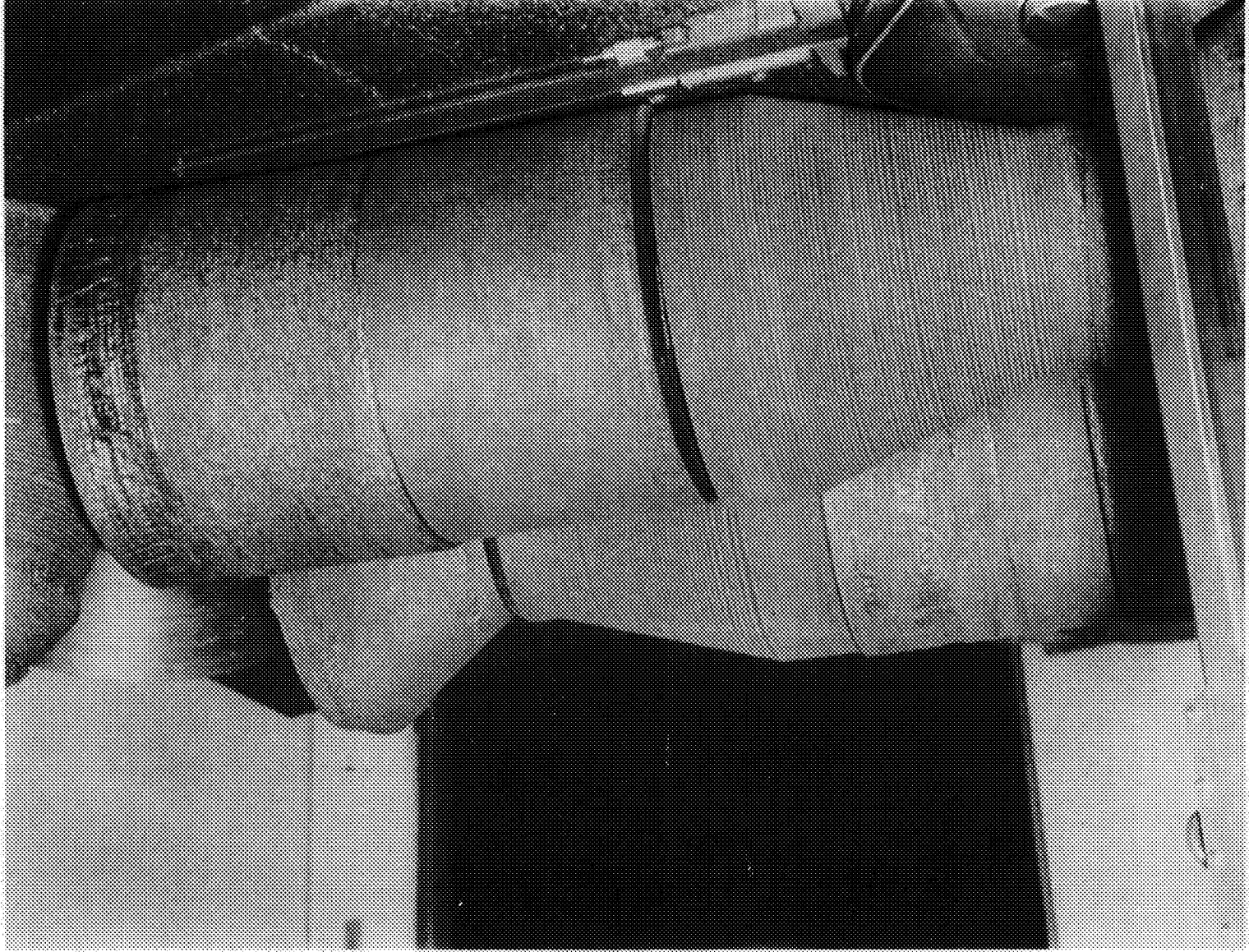
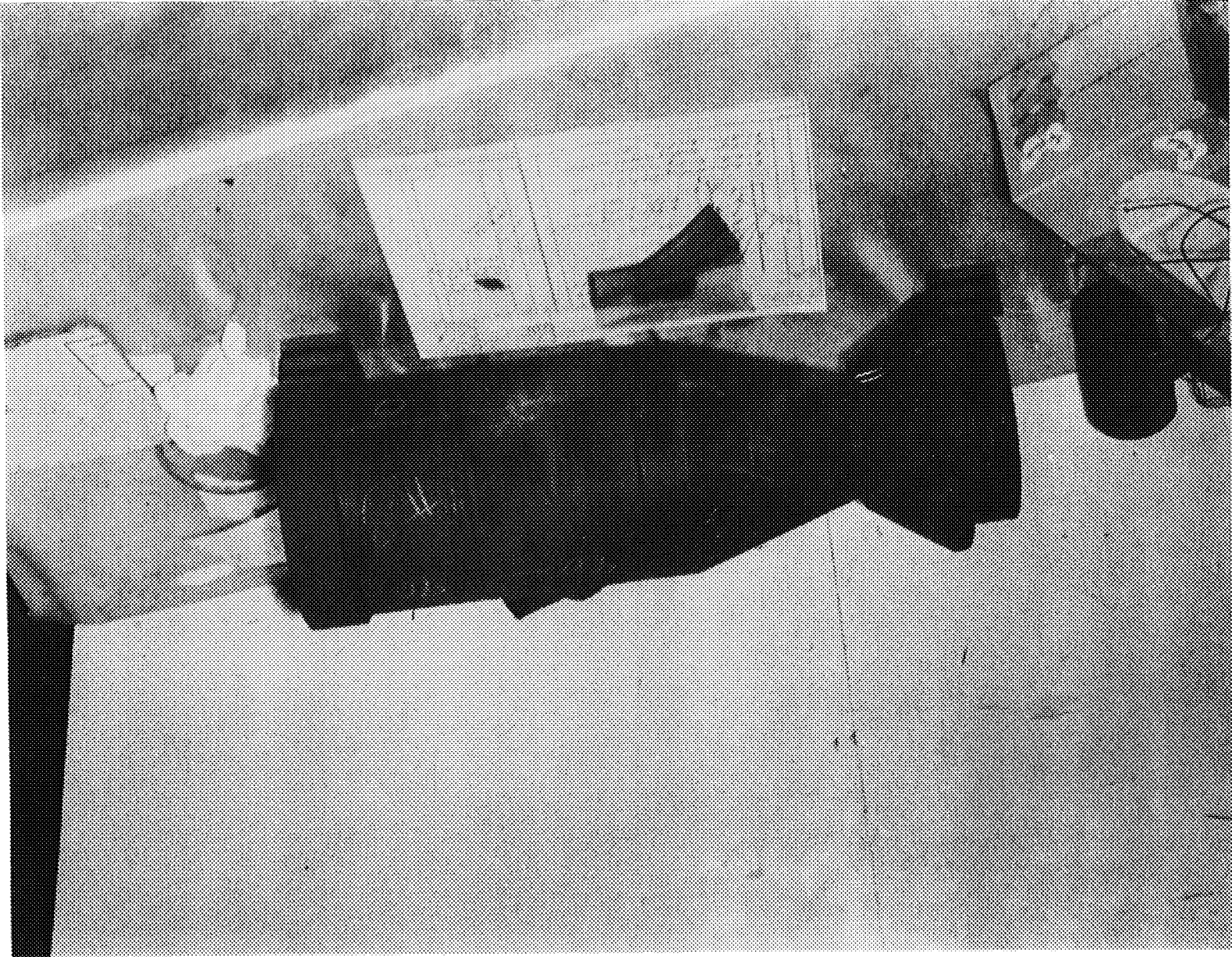


Figure 37. Components in Assembly Position



Figure 38. Liner Assembly Prior to OD Machining



#### IV, B, Cooled Chamber Fabrication (cont.)

##### (2) Problems in Liner Fabrication

As anticipated, delaminations were indicated in several components by the alcohol penetrant and X-ray inspections performed. No extensive delaminations were noted. Some indications appearing in inspections prior to rough machining were not evident in later inspections. At the last inspection before assembly, a delamination was noted in one exit section. Final machining of the ID exposed this delamination to where it became easily visible to the eye as can be noted in Figure 39. Although this delamination was somewhat more extensive than anticipated, the delamination was not considered critical because (1) heat flow to the cooling jacket is not affected by delamination due to the 60° to surface construction and (2) this area is in axial compression during firing and tends to close up. As can be seen in postfire photographs, the delaminations did not enlarge.

Other problems in liner fabrication were in relation to shrinkage allowance in the axial direction. One throat section and one cylindrical section component on final machining did not have sufficient stock. Since a spare throat section had been fabricated for such contingencies, the spare was used. To complete the cylindrical section, a 0.30 in. (7.62 mm) piece of bulk graphite was bonded to the forward end of the cylindrical section. This dummy piece was subsequently machined off after electroforming.

An obvious conclusion is that more shrinkage allowance must be added in the axial direction. Excess material can be machined off but, due to the length of the fabrication cycle, a requirement to fabricate new parts covers an unacceptable schedule situation.

##### c. Fabrication of the Electroformed Nickel Jacket

###### (1) Fabrication

Figure 40 shows the liner and mandrel after OD machining mounted in the holding rack prior to initial electroforming operation at the Electroform Inc. plant. Note the Plexiglas current shield at the forward end and the masking on the mandrel end plate at the aft end. The chamber was positioned vertically in the plating tank and agitated horizontally.

The first electroforming operation plated nickel on the graphite liner to a height equivalent to the top of the ribs (Figure 27). After machining to the proper contour, the nickel was dye penetrant inspected. A crack was found in the metal about 0.50 in. from the aft end (see Figure 41). This area was removed by machining. Although not visible, it was assumed that a slight separation existed in the graphite and that the nickel had failed to bridge. Repair plating was done at a lower current density until it was evident the plating was continuous. Dye penetrant inspection after this repair showed no indications.



Figure 39. SN 2 Showing Delamination in Exit Section

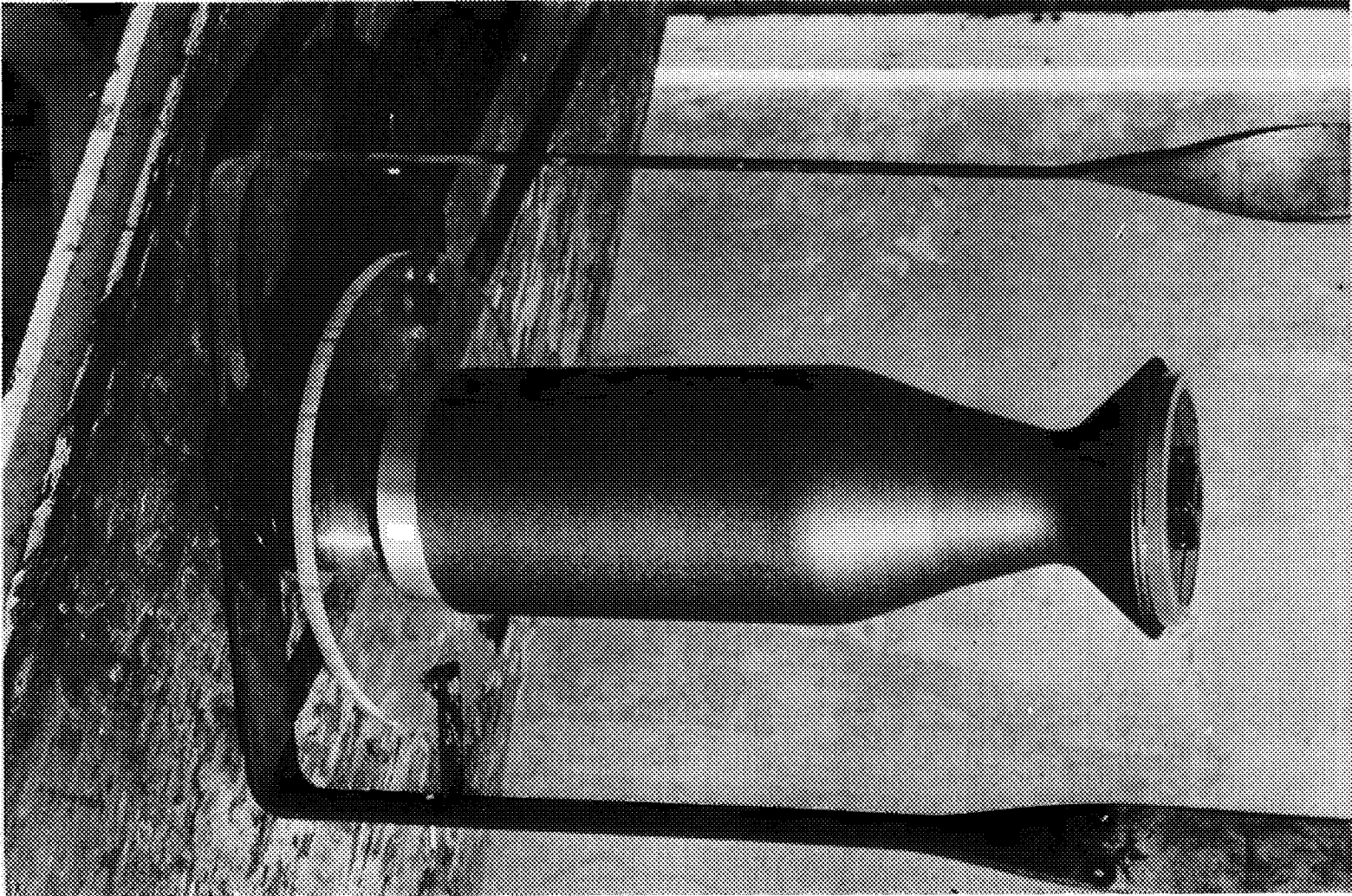
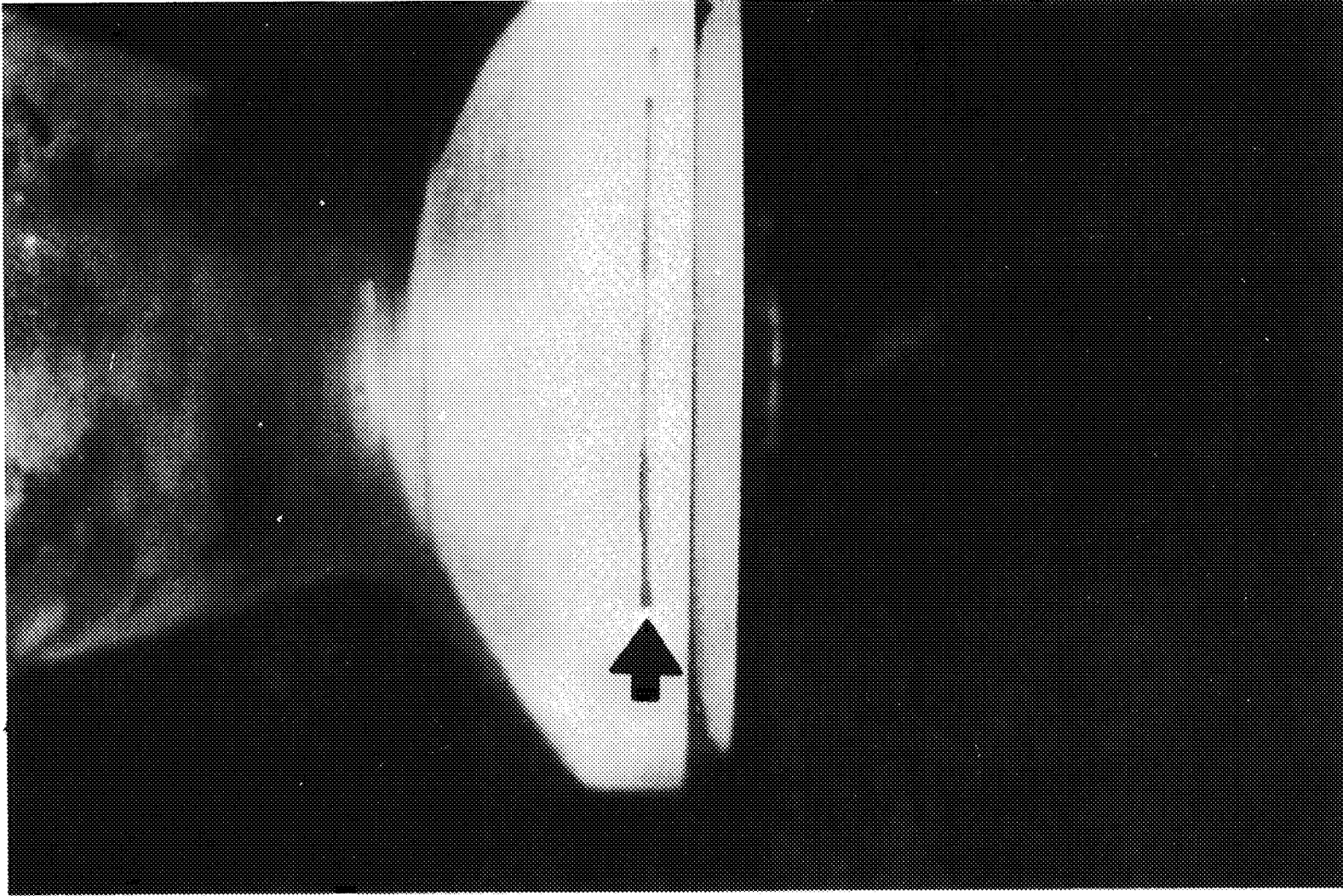


Figure 40. Graphite Liner in "Setup" Position for Electroforming



Figure 41. Crack Indication - Dye Penetrant



#### IV, B, Cooled Chamber Fabrication (cont.)

Figure 42 shows chamber SN 1 after electroforming and machining to the rib height and contour ("K" diameter, Drawing 1159525). Milling of the coolant channels was accomplished on a vertical milling machine with a Man-Au-Trace cam follower which traced the slotting template. Figure 43 shows the slotting operation equipment with the slotted chamber held between a dead center and an indexing head. Figure 44 shows the coolant channels milled and filled with low melting point core material.

Following machining of the coolant channels, the chamber was prepared for electroforming of the outer shell. This is a critical operation in the processing as any discrepancy can result in lack of bond between the ribs and the outer shell. The basic process steps are:

- (1) Fill channels with meltable core material.
- (2) Clean rib tops by light vapor blast.
- (3) Chemically clean and rinse.
- (4) Cathodic treatment.
- (5) Nickel plate.
- (6) Machine using appropriate tracer template.
- (7) Machine end configurations.
- (8) Dye penetrant inspect.
- (9) Remove core material.
- (10) Flow test.

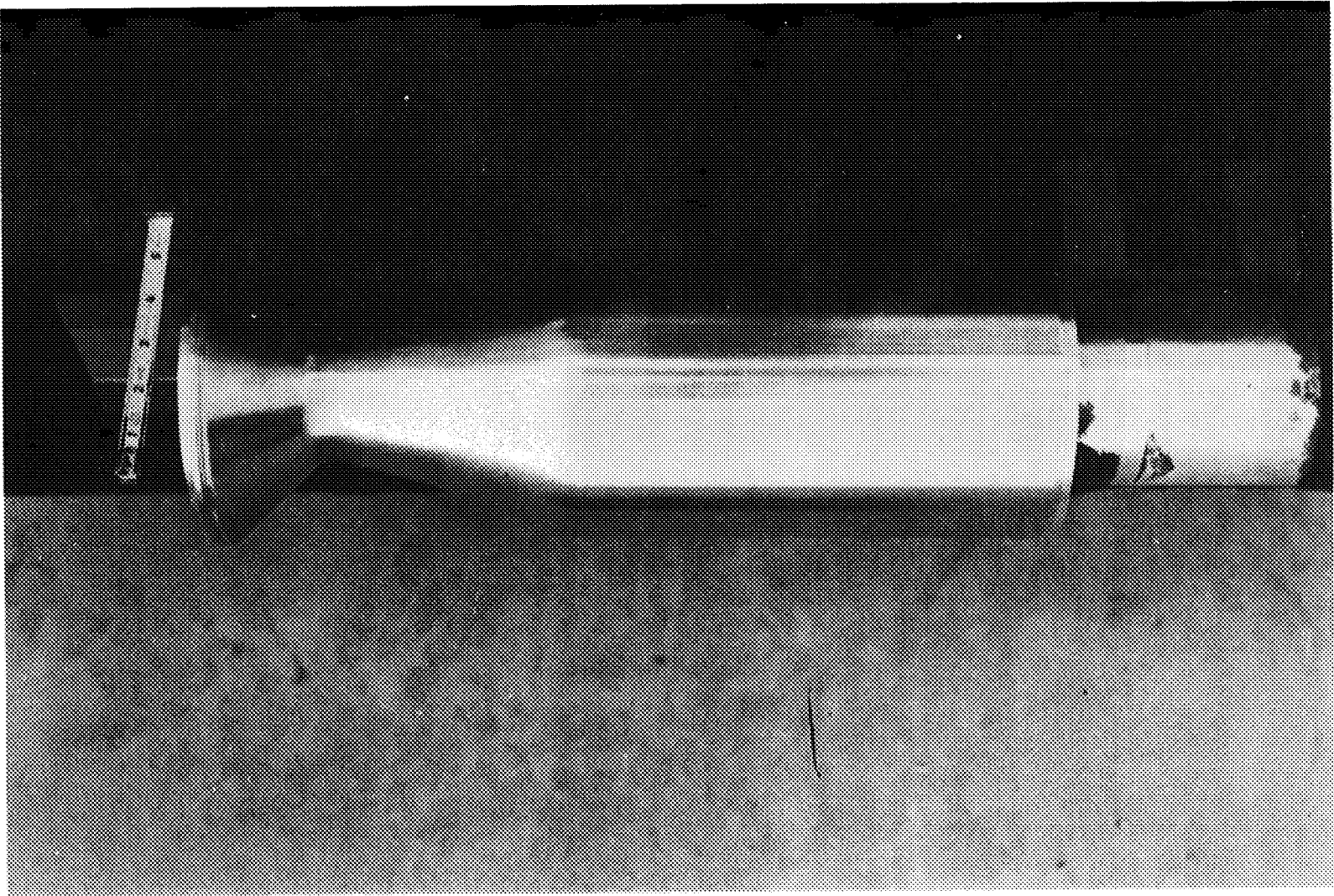
The machining of the manifold interface surfaces (Step (7)), which are limited to 0.004 in. (0.1016 mm) gap, was accomplished using the completed manifolds as a gauge. Using this approach, initial tolerances can be considerably looser than if the components were made independently but toleranced for maximum clearance.

#### (2) Problems in Electroforming Fabrication

The dye penetrant inspection operations specified in the manufacturing plan turned up one discrepancy which required rework and which if not discovered could have caused a catastrophic failure. This was the crack in the aft section of the chamber described in a previous paragraph and shown in Figure 41. Other discrepancies attributable to electroforming operations were discovered during subsequent fabrication and testing operations.

During welding of the manifolds to the chamber by the electron beam process, excessive out-gassing of the nickel was observed. Weld appearance was poor with excessive surface porosity. To obtain a

Figure 42. Electroformed Chamber Contour Machined to "K" Diameter



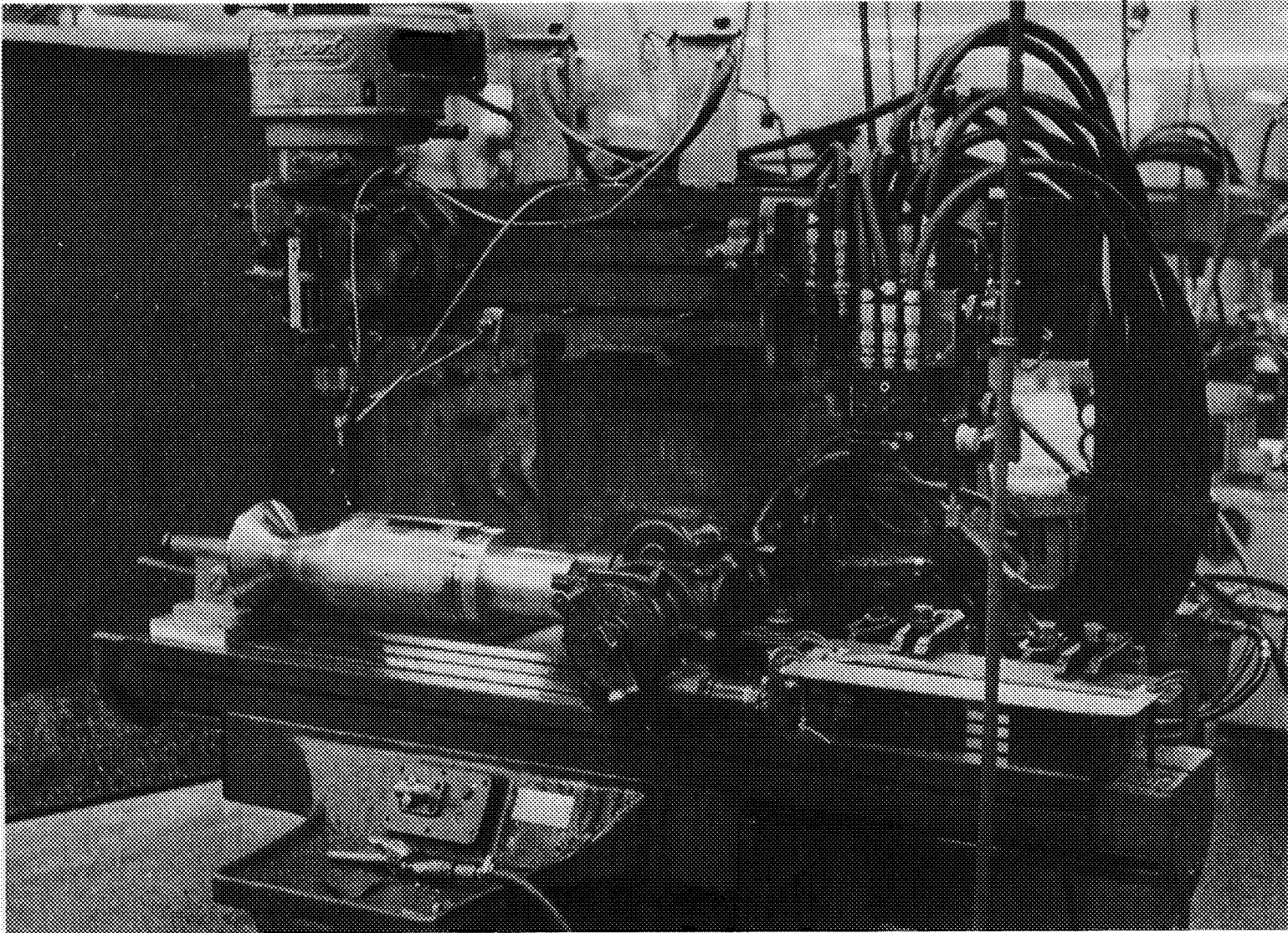
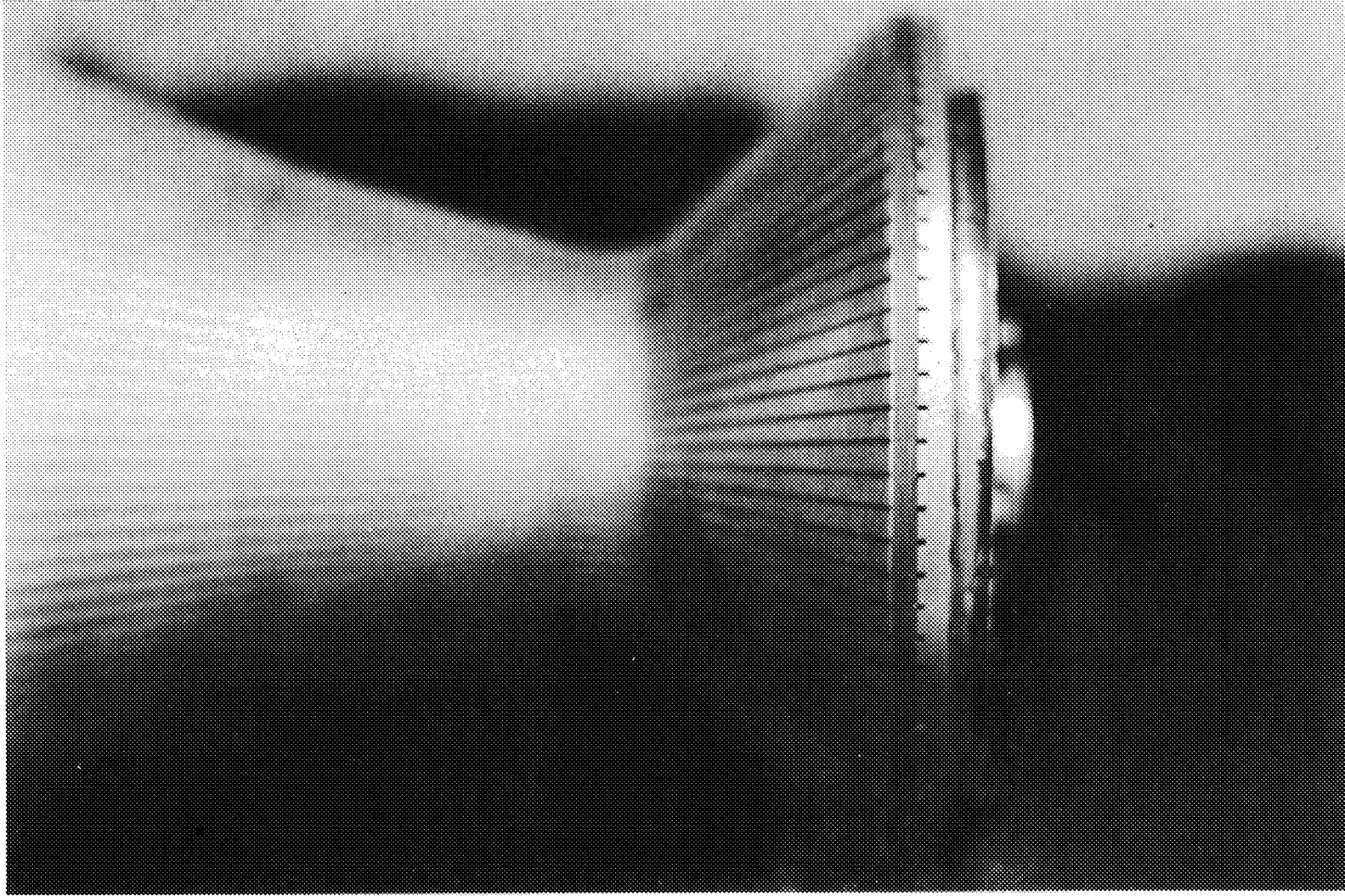


Figure 43. Milling Coolant Channels



Figure 44. Chamber with Core Material in Slots Before Closeout Electroforming



#### IV, B, Cooled Chamber Fabrication (cont.)

satisfactory joint, a procedure of welding in three passes was developed. The first pass was made to approximately 1/2 the joint depth. After repumping the welding chamber down to  $10^{-4}$  Torr during which time the joint cooled to ambient, the second pass was made to the full joint depth. After re-establishing vacuum and cooling, the third pass was made to 1/2 depth. The three-pass procedure described had the effect of reducing porosity to acceptable levels and no leaks or failures were observed; however, it is felt that improvements in the electroformed nickel chemistry in the identification and elimination of constituents detrimental to welding should be the subject of additional investigation.

A discrepancy occurred in the area of the aft flange on SN 1. In leak testing at 50 psi ( $0.344 \times 10^6$  N/m<sup>2</sup>), leaks were found 360° around the flange approximately 1/8 in. (31 mm) inside the weld. Based on appearance and location, this discrepancy was assumed to be a lamination in the nickel that was opened by heat of welding. No indication of this lamination was evident at the dye penetrant inspection performed before welding.

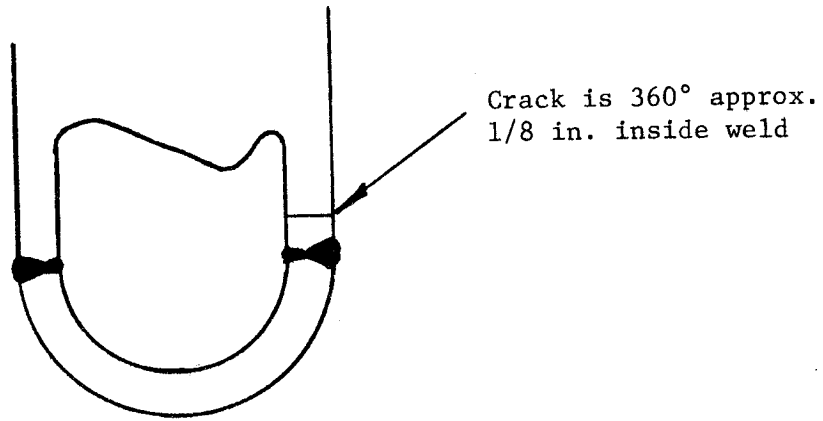
A machining error resulted in a 0.030-in.-deep (0.76 mm) undercut in the inside of the aft flange of SN 2. Examination of this area disclosed visible cracks at the root of the undercut.

Repairs for both thrust chambers were made by building up nickel on the face of the aft flange. Figures 45 and 46 illustrate the repair procedures adopted.

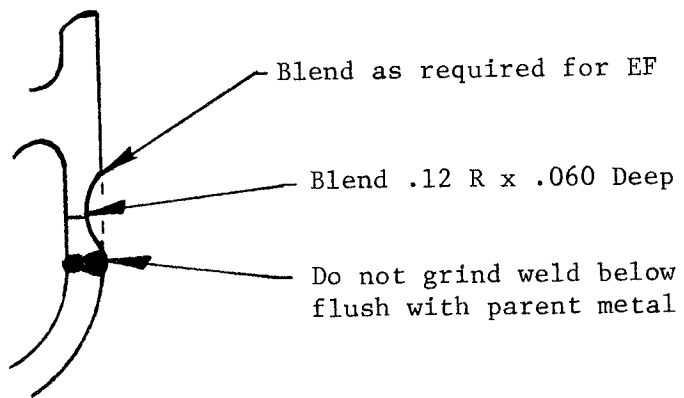
Leaks best described as weeping were observed in both chambers when pressure tested at 1900 psi ( $13.1 \times 10^6$  N/m<sup>2</sup>) with water. Dye penetrant inspection performed earlier showed no indication of the existence of porosity. Twenty-two holes were located and repaired by GTAW welding on SN 1. Only two weep holes were found on SN 2 and were not repaired. The photograph in Figure 47 is SN 2 after final machining prior to instrumentation.

#### d. Final Assembly

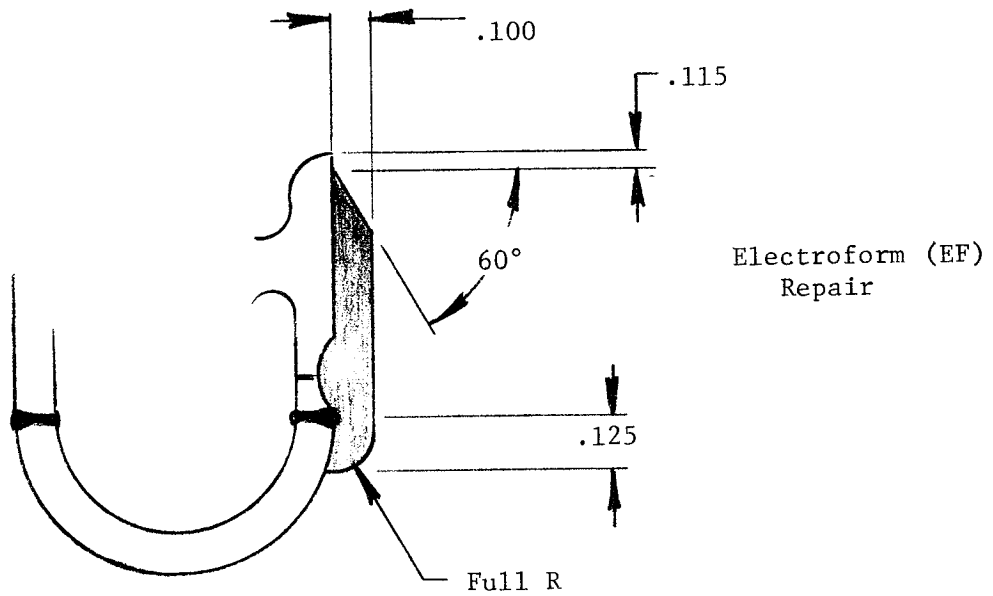
An important aspect of electroforming fabrication and final assembly of the thrust chamber was to ensure that coolant channels were to drawing requirement for size and free of filler material, chips or foreign matter that would prevent full and uniform coolant flow. Referring to the Manufacturing Plan (Figure 32) and the Discrepancy Analysis (Figure 33), several critical inspection points are noted. Flow testing and inspections were accomplished as planned; however, the pattern flow test in which it was planned to check the trajectory of each channel was determined to be inconclusive as the water coalesced and individual channel flow could not be observed. To ensure that each channel was open, a 0.032-in.-dia wire was passed through each channel. No evidence of core material or foreign matter was observed. Figure 48 illustrates the results of the pattern check flow test.



EXISTING



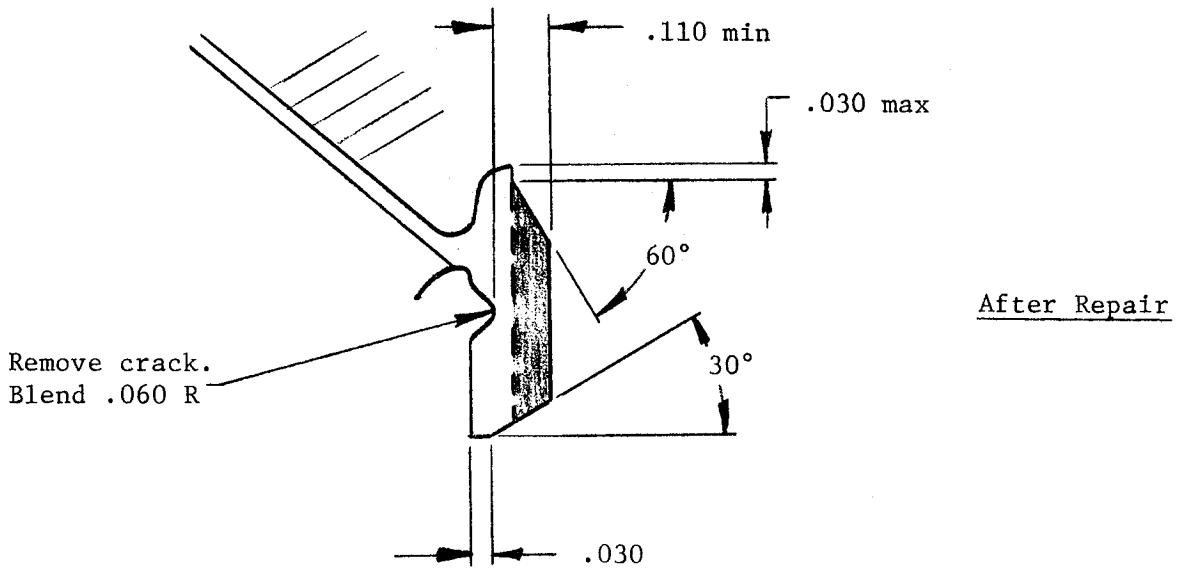
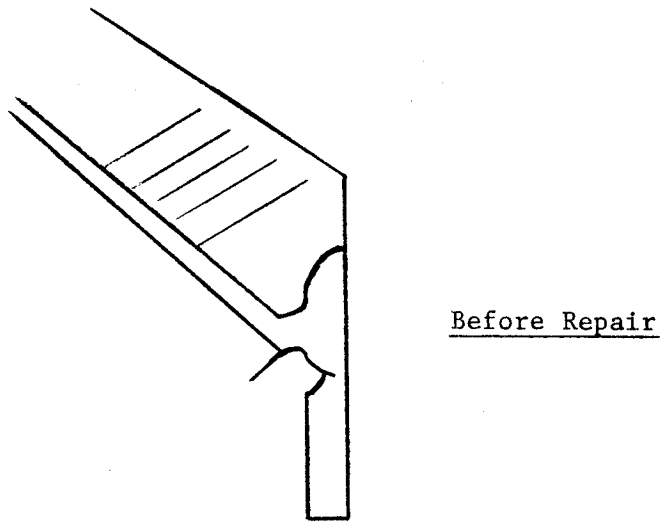
STEP 1



STEP 2

No scale

Figure 45. Electroform Repair, Aft Flange SN 1



No scale

Figure 46. Electroform Repair, Aft Flange SN 2

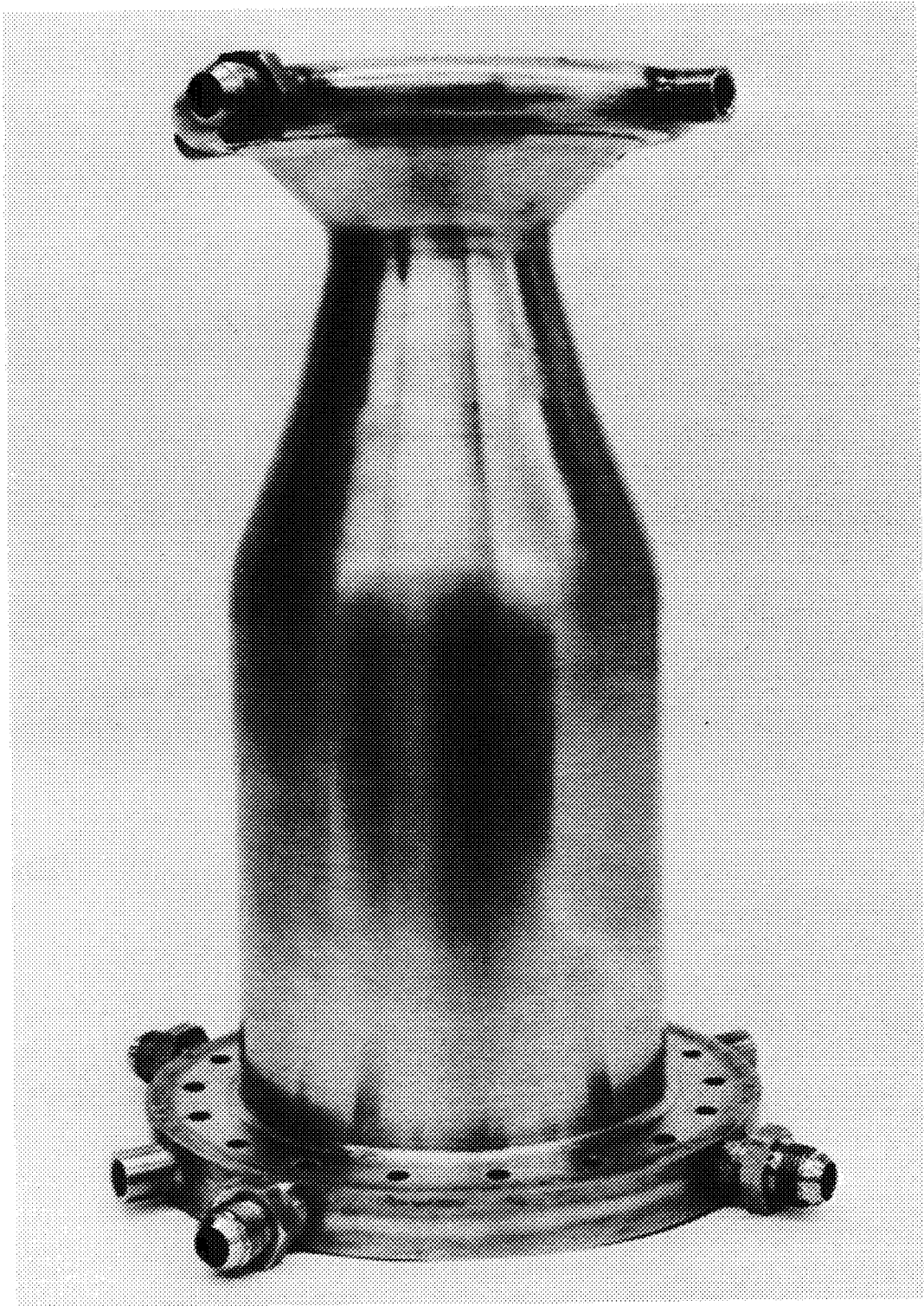


Figure 47. SN 2 After Final Machining

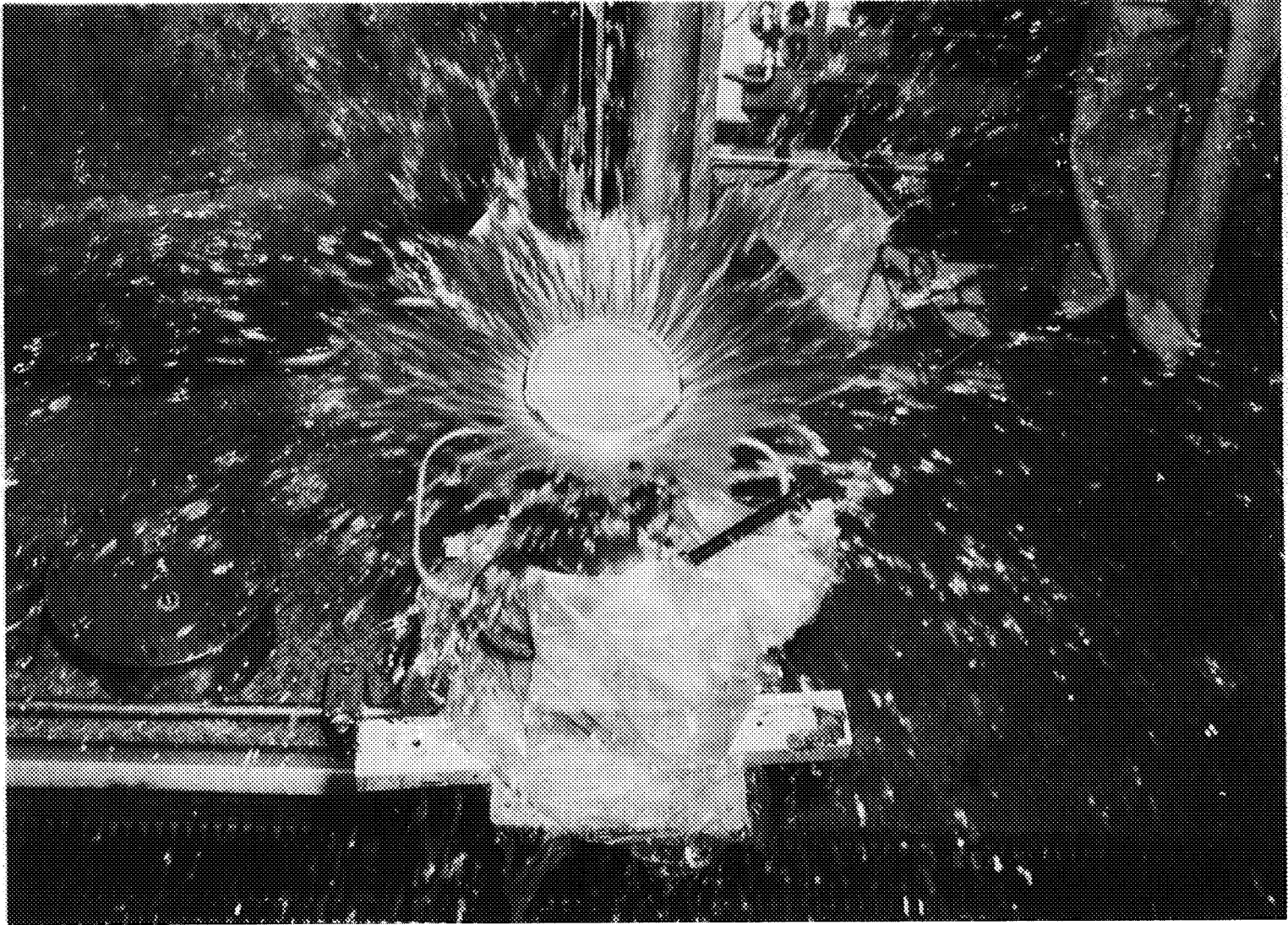


Figure 48. Pattern Flow Test

#### IV, B, Cooled Chamber Fabrication (cont.)

Welding of the flange and torus assembly to the chamber was accomplished as planned except for a change in procedure, noted previously, necessitated by excessive out-gassing of the nickel.

Leak testing was accomplished after the electroform repair described. Final flow testing was accomplished using the inlet and outlet plumbing fabricated for test firing. Flow testing was done with ambient water at a planned 4 lb/sec (1.81 kg/sec) and 135 psi ( $9.3 \times 10^6$  N/m<sup>2</sup>) back pressure. The pressure drop through the manifolds and thrust chamber was 176.7 psi for SN 1 and 182.5 psi for SN 2 ( $1.22 \times 10^6$  N/m<sup>2</sup> and  $1.26 \times 10^6$  N/m<sup>2</sup>, respectively).

Both chambers were subjected to ultrasonic testing to determine the extent of unbonded areas, if any, at the interface of the outer jacket and the rib lands. Results indicated apparent unbonded areas of approximately 1.0 in. length on one rib on SN 1 and on five ribs on SN 2. The discrepancies were located approximately 1.5 in. upstream of the throat. A standard was not available for proper calibration of the ultrasonic equipment prior to examination. For this reason, the validity of the readings has not been substantiated. Stress analysis of the unbonded areas indicated that a high margin of safety exists with 1.0-in. unbonds.

Final assembly was completed per the planning. Twelve thermocouples were installed as required on Drawing 1159636 and the thrust chamber was moved to the test area, J-4, for test firing.

## V. TASK III - FACILITY PREPARATION AND INJECTOR CHECKOUT

### A. FACILITY PREPARATION

The FLOX/methane hot test firings were planned for sea level conditions in Test Stand J-4, a steam ejector altitude facility utilizing a 98% efficient rocket exhaust scrubber system. The scrubber effluent is caught in a 200,000-gal (1136 m<sup>3</sup>) holding pond and treated with limestone prior to release.

The proepellant handling and flow system was completed to the test stand shown in Figure 49.

The FLOX propellant is supplied from a 1000-gal (4.54 m<sup>3</sup>), 2160 psi (14.89 x 10<sup>6</sup> N/m<sup>2</sup>) working pressure, triple jacketed, stainless steel tank through a 1.5-in. (0.038 m) LN<sub>2</sub> jacketed line and two flow meters with a 1-in. thrust chamber valve.

The methane propellant is supplied from a 100,000 standard cubic foot tube trailer with a working pressure of 2600 psi (17.92 x 10<sup>6</sup> N/m<sup>2</sup>) in parallel with a 1000-gal (4.54 m<sup>3</sup>), 2160 psi (14.89 x 10<sup>6</sup> N/m<sup>2</sup>) working pressure and a Corbin compressor. The methane is fed to the injector through a 2-in. (0.051 m) stainless line, 2-in. (0.051 m) pressure control regulator, a 2-in. (0.051 m) gas flow meter, and a 2-in. (0.051 m) cavitating venturi with a 1-in. (0.025 m) line with a 2-in. (0.051 m) pressure control regulator, through a pool boiling type heat exchanger which uses LN<sub>2</sub> as the cooling media. The coolant level in the heat exchanger was varied to change the temperature of the coolant. A calibrated flow orifice was used to maintain the required 600 (4.14 x 10<sup>6</sup> N/m<sup>2</sup>) psia coolant pressure out. The pressure control regulator was also used to control the coolant flow rate.

The test stand support equipment and systems includes a water-filled actuation tank pressurized with gaseous nitrogen for thrust chamber valve actuation. The injector purges are gaseous nitrogen supplied through 0.5-in. (12.7 mm) lines. A LN<sub>2</sub> bath is utilized to chill the backside of the injector to -40°F (233<sup>1</sup>/<sub>4</sub>K) prior to firing and is secured for the test.

Prior to conducting the cooled chamber tests, heat exchanger flow tests were conducted at various levels of LN<sub>2</sub> coolant to determine propellant temperatures. A helium purge is maintained on the heat exchanger during fill with LN<sub>2</sub> and pretest preparation to prevent freezing of atmosphere in the coolant tubes.

### B. INJECTOR CHECKOUT FIRING

The graphite-lined workhorse chamber (Figure 18) was designed and constructed to serve the dual purpose of demonstrating facility capability and determining injector performance in relation to possible detrimental streaking.





V, B, Injector Checkout Firing (cont.)

Testing was completed as shown in Table III with no evidence of corrosion or streaking on the graphite liner. The temperature of the steel shell was monitored during testing and for soakback after shutdown. The temperature stayed well below predicted levels. During the last test, the trailing edge of the graphite liner at the exit plane was ejected. The failure was by a clean fracture about 0.5 in. (12.7 mm) from the exit plane. Figure 50 shows the streak chamber in position for testing. Figure 51 shows the surface exposed by the failure and the buildup of soot in the throat area. The material on the outer perimeter of the exit flange is a trowelable material used to protect the metal flange from the radiant heat of the exhaust. The No. 12 denotes the 12 o'clock position of the chamber during testing.

Four test firings were planned:

<u>Test No.</u>	<u>Test Objective</u>	<u>O/F Mixture Ratio</u>	<u>Test Duration sec</u>
1	System check	5.25	1
2	System check and leak check	5.25	3
3	Streak check	5.25	6
4	Streak check	5.25	6

The results are summarized in Table III.

The copper heat sink chamber was installed on the test stand and leak tested at 50 psig ( $0.34 \times 10^6$  N/m<sup>2</sup>). Leaks were discovered in the spring-loaded thermocouples and between the chamber sections at the O-ring seal. Subsequently, a new seal was installed and the thermocouples removed and holes sealed; however, leakage still occurred at the seal joint. To avoid delay in the test firing schedule, the first cooled chamber (SN 2) was installed on the test stand. Initial success in its test firing resulted in a decision to delete heat sink chamber testing in favor of added duration, cooled test firings.

Figure 50. Graphite-Lined Workhorse Chamber on Test Stand

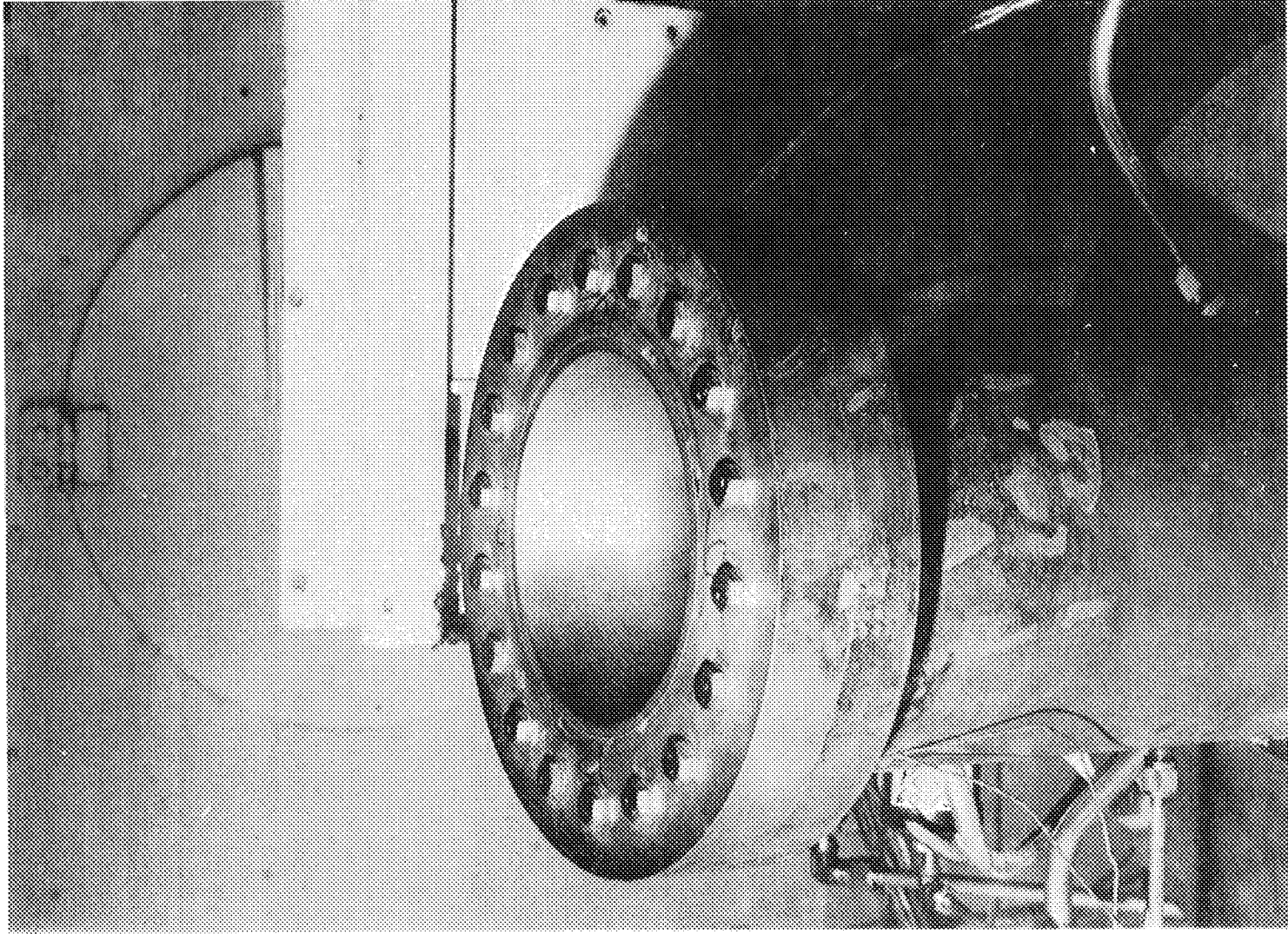




Figure 51. Graphite-Lined Workhorse Chamber, Posttest

TABLE III  
TEST RESULTS, GRAPHITE-LINED WORKHORSE THRUST CHAMBER

Test No.	Duration sec	$P_c$		Mixture Ratio	Remarks
		psia	$W/m^2 \times 10^6$		
1	0.62	--	--	--	Malfunction of FLOX pilot valve caused premature automatic shutdown.
2	1.52	445	3.07	4.56	No streaking, no throat erosion, slight sooting.
3	3.52	440	3.03	4.56	No streaking, no throat erosion, slight sooting.
4	6.52	480	3.31	4.68	No streaking, no throat erosion, slight sooting.
5	2.87	--	--	--	Premature shutdown due to failure to open fuel safety valve.
6	8.52	498	3.43	5.75	No streaking, no throat erosion, very slight sooting. Shear failure of graphite 0.5 in. (12.7mm) from exit.

All values are taken at FS<sub>2</sub>

FS<sub>2</sub> = fire switch 2, shutdown of run

VI. TASK IV - COOLED CHAMBER TESTS

A. TEST CONDITIONS

Two thrust chambers were completed to Drawing 1159636, including instrumentation. SN 2 was selected for the first planned series of tests to permit evaluation of the effect of delamination of the fibrous graphite liner in the divergent section (see Figure 39). The first test was a cold flow only, planned as a coolant system checkout with special regard to the function of the heat exchanger. Both ambient and cooled flow testing indicated the pressure drop of the methane coolant was higher than predicted. Due to the uncertainty in predictions and an inlet pressure limit of 1500 psia ( $10.3 \times 10^6 \text{ N/m}^2$ ), the required pressure at the exit manifold was reduced from 1000 psia ( $6.89 \times 10^6 \text{ N/m}^2$ ) to 600 psia ( $4.13 \times 10^6 \text{ N/m}^2$ ). This was accomplished by changing the downstream orifice. Inlet pressure was varied to obtain the desired flow rate. Overcooling was planned for the first hot tests.

Nominal test conditions were established as:

Thrust	5000 lb (22,240 N)
MR	5.25
Oxidizer, FLOX	82.67% $\text{F}_2$
Fuel temperature, methane	Ambient
$P_c$	500 psia ( $3.44 \times 10^6 \text{ N/m}^2$ )
Sea level	
Coolant inlet temperature, methane	-120°F (188°K)
Coolant pressure at exit	600 psia minimum ( $4.13 \times 10^6 \text{ N/m}^2$ )
$\dot{w}_T$ , coolant	2.02 lb/sec (0.091 kg/sec)
$\dot{w}_f$ , injector	2.02 lb/sec (0.091 kg/sec)
$\dot{w}_o$	10.62 lb/sec (4.81 kg/sec)
Injector	CJK 6901 100 SCFM

VI, A, Test Conditions (cont.)

1. Shutdown Parameters

- a. Use  $P_{fj}$  as CSM monitor and program shutdown for conditions in excess of the following:

<u>Amplitude of Oscillation</u>	<u>Frequency of Oscillation</u>	<u>Duration of Oscillation</u>
$\pm 50$ psi ( $0.34 \times 10^6$ N/m <sup>2</sup> )	1000 cps to limit of transducer	30 millisecc

- b. Monitor  $P_c$  and shut down if  $P_c$  drops below 450 psi ( $3.1 \times 10^6$  N/m<sup>2</sup>).
- c. Monitor TC5 and TC7; shut down if temperature exceeds 1300°F (977°K).

2. Start Procedure

- a. Coolant flow 2 sec minimum before fire switch. Coolant at full flow and at -120°F (188°K) to -150°F (172°K) before fire switch.
- b. Fuel and oxidizer circuit GN<sub>2</sub> prefire purge adjusted to a regulated pressure of 200 psig ( $1.38 \times 10^6$  N/M<sup>2</sup>). Purge to be initiated at least 3 sec before fire switch.
- c. Fuel TCV to lead oxidizer TCV by  $0.075 \pm 0.025$  sec (150 to 200 millisecc).
- d. TCV opening time is 0.45 to 0.50 sec.

3. Shutdown Procedure

- a. Postfire fuel and oxidizer circuit purge pressure 200 psig ( $1.38 \times 10^6$  N/m<sup>2</sup>).
- b. Leave fuel and oxidizer prefire purge "ON" (checked off) throughout test.

## VI, A, Test Conditions (cont.)

- c. Close oxidizer TCV 2 sec prior to closing fuel TCV. Minimum postfire fuel purge 5 sec. Minimum postfire oxidizer purge 5 sec. Minimum coolant flow 5 sec after closing fuel TCV.
- d. TCV closing time 150 to 170 millisec.

### 4. Passivation

Fluorine passivation of the injector oxidizer circuit is required prior to attachment of chamber. Continuous GN<sub>2</sub> purge of oxidizer circuit at 5 to 10 psig ( $0.034 \times 10^6$  N/m<sup>2</sup>) after passivation except during test firing.

The actual test firings were conducted as follows: The test procedure commenced with purging of the methane system feed lines with low pressure methane gas to remove air from the lines. The FLOX feed lines were bled at low pressure to prechill the system. The FLOX tank pressure was set to final test value, and the fuel line was set to final test pressure with the pressure control regulator; a final system bleed of both circuits was conducted. At this time, the helium purge to the heat exchanger was secured and the coolant regulator energized, and the FLOX bleed valve was opened. When the coolant outlet pressure and temperature were at prescribed limits, the countdown began, with the FLOX bleed being closed on the "2" count.

At FS<sub>2</sub>, the injector purges were sequenced on and a helium purge initiated through the heat exchanger to remove residual methane and prevent the coolant tubes in the heat exchanger from freezing.

Figure 52 shows the test stand and diffuser with the thrust chamber mounted for testing. Figure 53 shows the chamber in position with all plumbing and instrumentation complete.

### B. TEST RESULTS, COOLED CHAMBER TESTING

Test results are summarized in Tables IV and V.

Test 7 through 11 were conducted at planned parameters. Examination of data showed that thermocouples 5 and 7, which were monitored at 1400°F (1033°K for shutdown, were experiencing very erratic and dramatic variations in addition to indicating temperatures 300 to 500°F higher than thermocouples 6 and 8, which were located 180 degrees opposite. To determine whether the throat area at TC7 was actually experiencing the temperatures indicated, two thermocouples



## VI, B, Test Results, Cooled Chamber Testing (cont.)

(TC8a and TC7a) were installed on the outer nickel jacket surface near TC8 and TC7. When TC7a failed to show any significant temperature difference over TC8a, it was concluded that TC7 data were suspect. After Test 10, the shut-down monitor was changed to TC6. Posttest examination by X-ray indicated that TC7 was protruding approximately 0.040 in. (1.02 mm) into the graphite liner. For this reason, TC7 data are not valid for the interface temperatures. The erratic readings from all thermocouples were determined to be due to carbon soot buildup. Pieces of carbon to 1/8 in. (3.2 mm) thick were found in the diffuser and adhering to the cylindrical section of the chamber liner. Post-fire throat measurements indicated up to 3 mils (0.076 mm) deposit adhering. It is surmised that buildup and flaking off was a continuous process during test firing. Since soot is an excellent insulator, the variations in temperature in some cases exceeded 300°F (422°K) in 2 sec.

The pulse test summarized in Table V consisted of eight cycles of 5 sec on and 2 sec off. The test objective was to provide a thermal and mechanical shock on the thrust chamber. Posttest examinations indicated no visible change in the liner or jacket. Note that the coolant temperature out (TFCO) is actually lower than the coolant temperature in (TFCI) at 0.1 sec into the run. This is due to complete cooling occurring during the 2.0 sec off period plus the cooling effect of expanding methane while experiencing a pressure drop of approximately 650 psi from inlet to outlet.

Black and white photos were taken after each test and the throat diameter was measured. The throat measurements varied from 1 to 3 mils (0.025 to 0.076 mm) under prefire diameter measurements, indicating no throat erosion and varying soot buildup. Figures 52 and 53 show the thrust chamber in position on the test stand prior to the first test. Figure 54 shows the thrust chamber after the first cooled test (No. 7) of 5.5 sec duration. Figure 55 was taken after Test 13 and shows the carbon buildup in the cylindrical section of the thrust chamber. Figure 56, post-Test 14, shows a large carbon deposit just forward of the convergent section.

### C. POSTTEST ANALYSIS

Posttest analysis required was minimum and consisted of inspection of the hardware, particularly the liner throat and divergent section where a delamination was plainly visible in prefire photos, and X-rays to determine thermocouple locations. Figure 56 shows the throat and exit section after completion of all testing, 540 sec total duration. Figure 57 shows the throat and exit section after removal of soot by cleaning with soap, water, and steel wool. Reference can be made to Figure 39 for a before-and-after comparison.

X-rays taken axially through the throat showed that thermocouple 7 protruded approximately 0.042 in. (1.06 mm) into the graphite liner. This confirmed deductions based on the unusually high temperature readings recorded. Thermocouple 8, also at the throat and located 180 degrees from TC7, was not visible in X-rays, indicating it did not protrude into the graphite. The X-rays also established that the throat liner thickness was uniform and the liner was concentric with the nickel jacket.

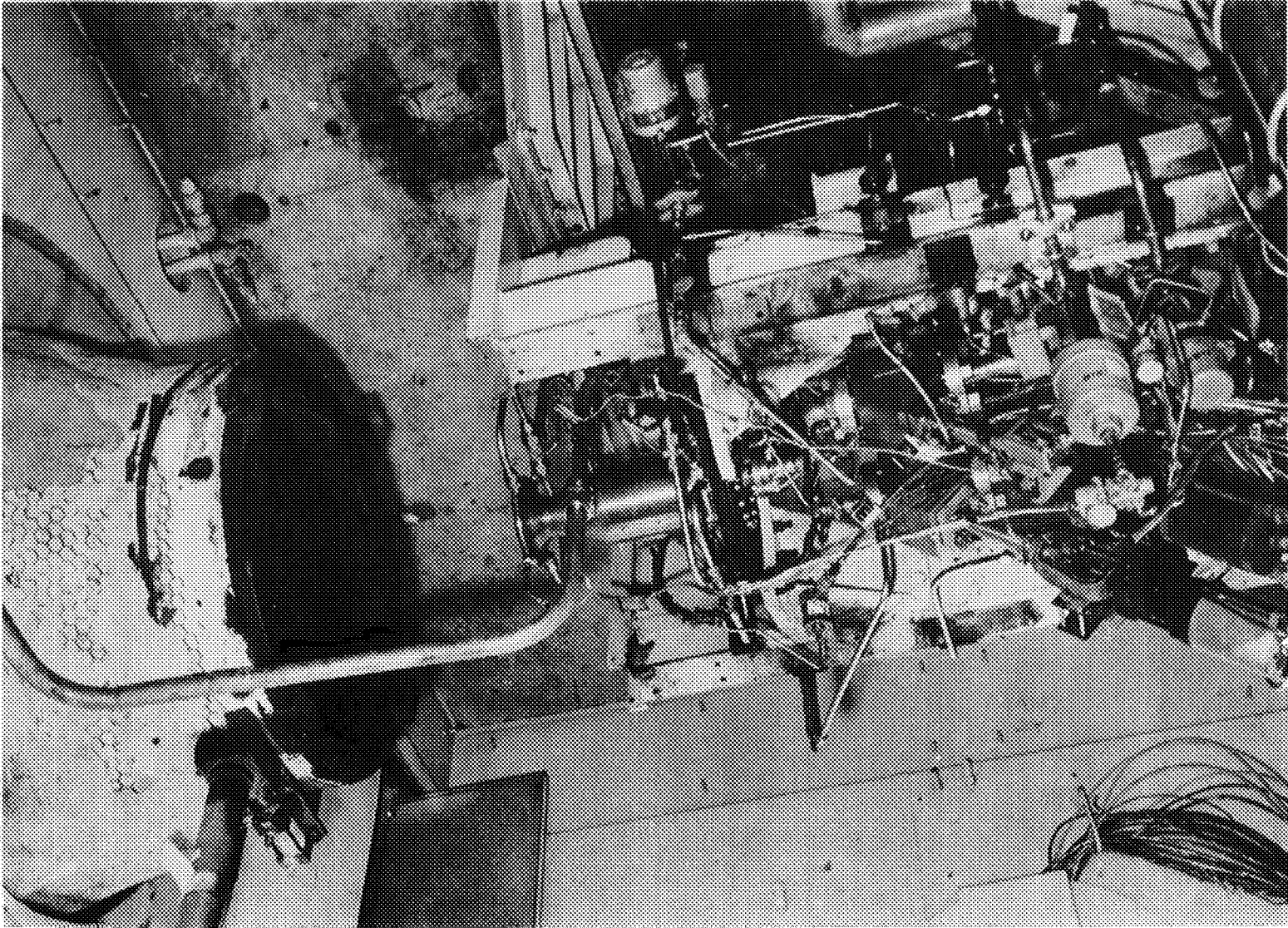


Figure 52. J-4 Test Stand

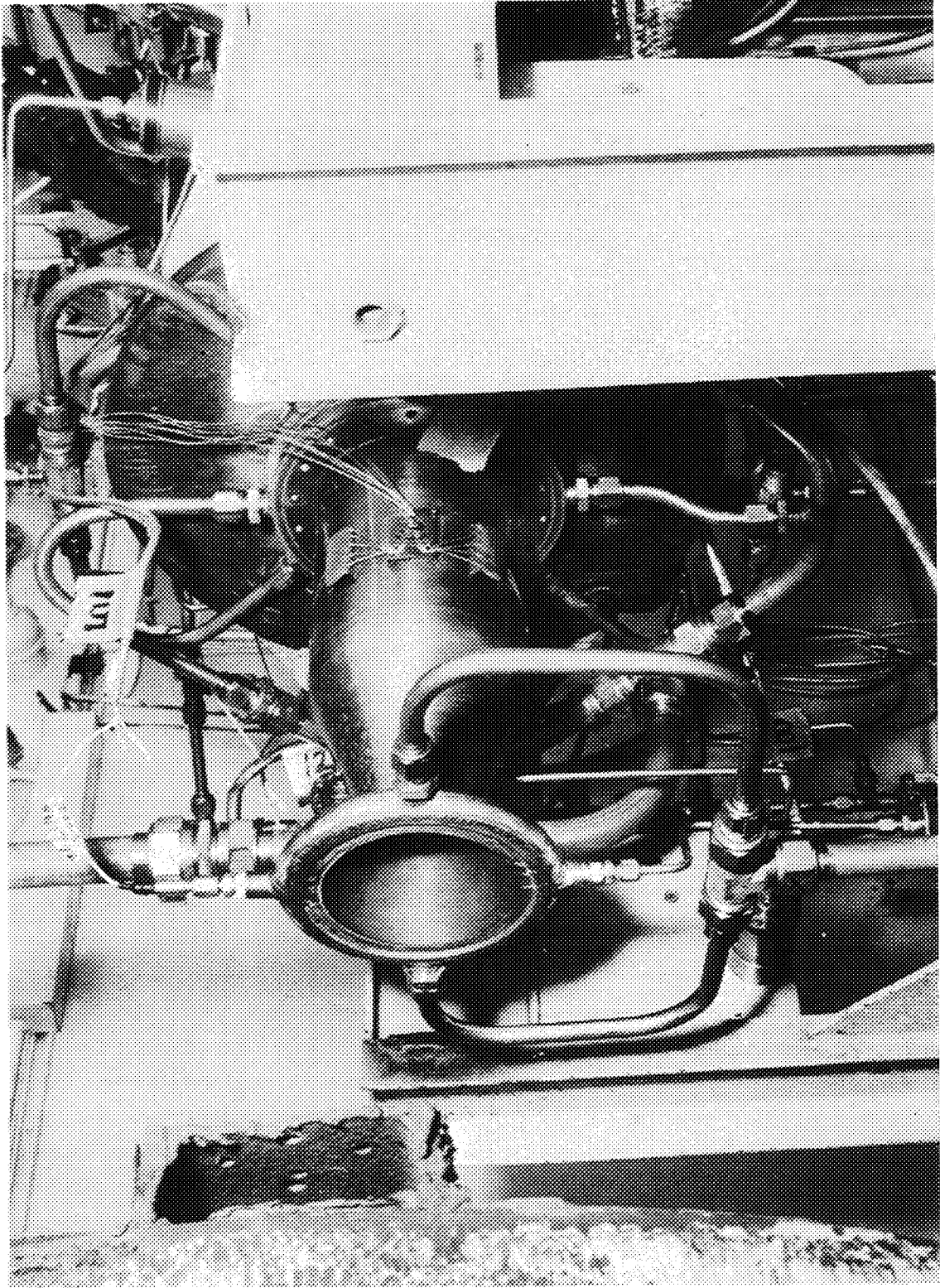


Figure 53. Thrust Chamber SN 2 on Test Stand

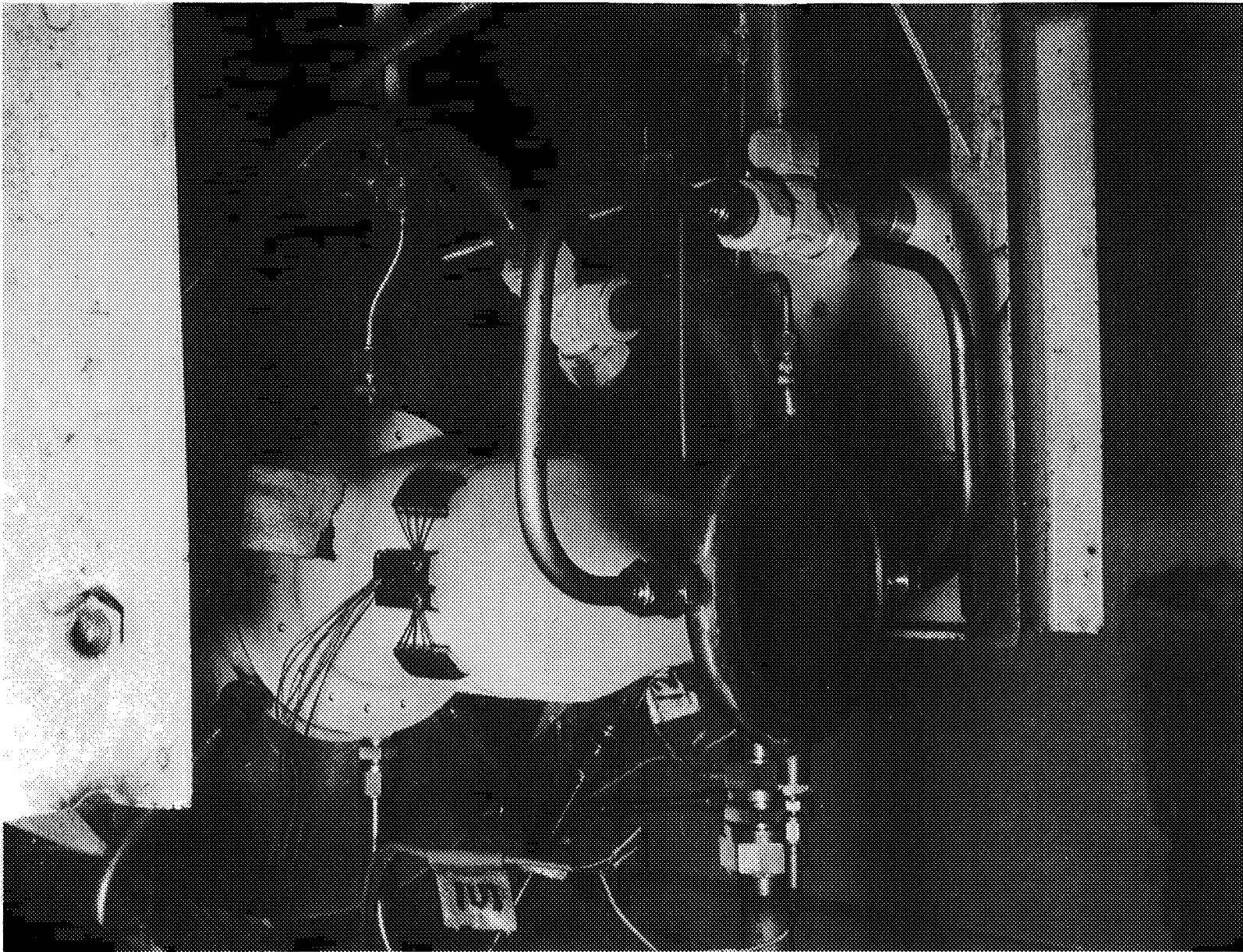


Figure 54. Posttest First Run, 5.5 sec

TABLE IV

SUMMARY OF MAJOR PARAMETERS OF COOLED TESTS

Test No.	Duration, sec	P <sub>c</sub>		MR	$\dot{w}_f$ Coolant		$\Delta P$ Coolant		TFCI		$\Delta T$ Coolant		c*	
		psia	N/m <sup>2</sup> x10 <sup>3</sup>		lb/sec	kg/sec	psi	N/m <sup>2</sup> x10 <sup>3</sup>	°F	°K	°F	°K	ft/sec	m/sec
7	5.5	494	3406	3.63	2.88	1.31	717	4973	-84	208	41	278	6840	2084
8 <sup>(2)</sup>	3.2	495	3412	4.60	2.03	0.92	739	5095	-43	231	73	296	6719	2048
9	100.5	523	3605	4.79	2.24	1.02	655	4516	-78	212	128	327	6866	2093
10 <sup>(3)</sup>	2.6	488	3364	5.32	2.09	0.95	932	6425	61	289	17	265	6805	2074
11	56.0	Pulse Test - See Table V												
12 <sup>(4)</sup>	0.4	--	--	--	--	--	--	--	--	--	--	--	--	--
13 <sup>(5)</sup>	160.5	486	3350	5.13	1.56	0.71	546	3764	-80	211	217	376	7033	2143
14 <sup>(6)</sup>	219.5	495	3412	5.50	1.85	0.84	600	4137	-77	213	181	356	6886	2098
13	10.0	491	3385	5.38	2.24	1.01	663	4571	-65 <sup>(1)</sup>	219	113 <sup>(1)</sup>	318	6802	2073
1-10 sec avg														
13	10.0	491	3385	5.11	1.60	0.72	552	3805	-80	211	214	374	6893	2101
150-159 sec avg														
14	10.0	515	3550	5.24	2.16	0.98	529	3647	-99	200	94	308	6819	2078
75-84 sec avg														
14	10.0	524	3612	5.42	1.91	0.87	594	4095	-80	211	159	344	7044	2147
190-199 sec avg														

Data are at FS<sub>2</sub> except as noted.

NOTES:

- (1) At 10 sec.
- (2) Shutdown by TC7 at 1400°F (1033°K).
- (3) Coolant ambient shutdown by TC7 at 1600°F (1144°K). Monitor changed to TC6 for next test.
- (4) Shutdown at 0.5 sec due to FLOX valve make before fuel valve. Delay timing had been set at 60 millisecc to attempt to shorten delay time. Due to lack of pressure (volume) in system, fuel valve failed to open. Delay was reset to 140 millisecc for next test.
- (5) Shutdown at 160.5 sec by TC6 at 1400°F (1033°K).
- (6) Shutdown at consumption of remaining FLOX.

NOMENCLATURE:

psia - Pounds per square inch atmosphere  
 N/m<sup>2</sup> - Newtons per square meter  
 MR - Mixture ratio  
 $\dot{w}_f$  Coolant - Weight flow, coolant  
 $\Delta P$  Coolant - Pressure drop, coolant  
 TFCI - Temperature, fuel coolant, in  
 $\Delta T$  Coolant - Temperature change, coolant in to coolant out

psi - Pounds per square inch  
 c\* - Characteristic velocity of propellant gases  
 kg/sec - Kilogram per second  
 lb/sec - Pounds per second  
 ft/sec - Feet per second  
 m/sec - Meters per second  
 °F - Degrees Fahrenheit  
 °K - Degrees Kelvin

TABLE V  
PULSE TEST

Function	Pulse 1		Pulse 2		Pulse 3		Pulse 4		Pulse 5		Pulse 6		Pulse 7		Pulse 8	
	$FS_{1+.1}$	$FS_2$	$FS_{1+.1}$	$FS_2$	$FS_{1+.1}$	$FS_2$	$FS_{1+.1}$	$FS_2$	$FS_{1+.1}$	$FS_2$	$FS_{1+.1}$	$FS_2$	$FS_{1+.1}$	$FS_2$	$FS_{1+.1}$	$FS_2$
$P_c$																
psia	478	489	487	487	466	465	450	447	448	448	448	448	450	450	446	446
$N/m^2 \times 10^6$	3.29	3.37	3.36	3.36	3.21	3.21	3.10	3.08	3.09	3.09	3.09	3.09	3.10	3.10	3.08	3.08
MR	5.1	5.4	5.3	5.3	5.3	5.3	5.0	5.0	5.0	5.0	5.0	5.0	5.0	5.0	5.0	5.0
$W_f$ Coolant																
lb/sec	3.02	2.98	3.01	2.95	3.06	2.95	2.88	2.93	2.99	2.90	2.98	2.85	2.98	2.66	2.88	2.71
kg/sec	1.37	1.35	1.36	1.34	1.39	1.34	1.31	1.33	1.35	1.32	1.35	1.29	1.35	1.21	1.31	1.23
TFCI																
°F	-100	-99	-99	-98	-97	-96	-96	-95	-95	-93	-93	-92	-90	-89	-89	-87
°K	200	201	201	201	202	202	202	203	203	204	204	204	205	206	206	207
TFCO																
°F	-120	-64	-107	-69	-107	-68	-107	-76	-107	-64	-106	-56	-104	-51	-107	-51
°K	189	220	196	217	196	218	196	219	196	220	195	224	198	227	196	227

TFCI = Temperature of coolant, in  
TFCO = Temperature of coolant, out

$FS_{1+.1}$  = Fire switch 1 plus 0.1 sec, start of run + 0.1 sec.

$FS_2$  = Fire switch 2, shutdown of run.



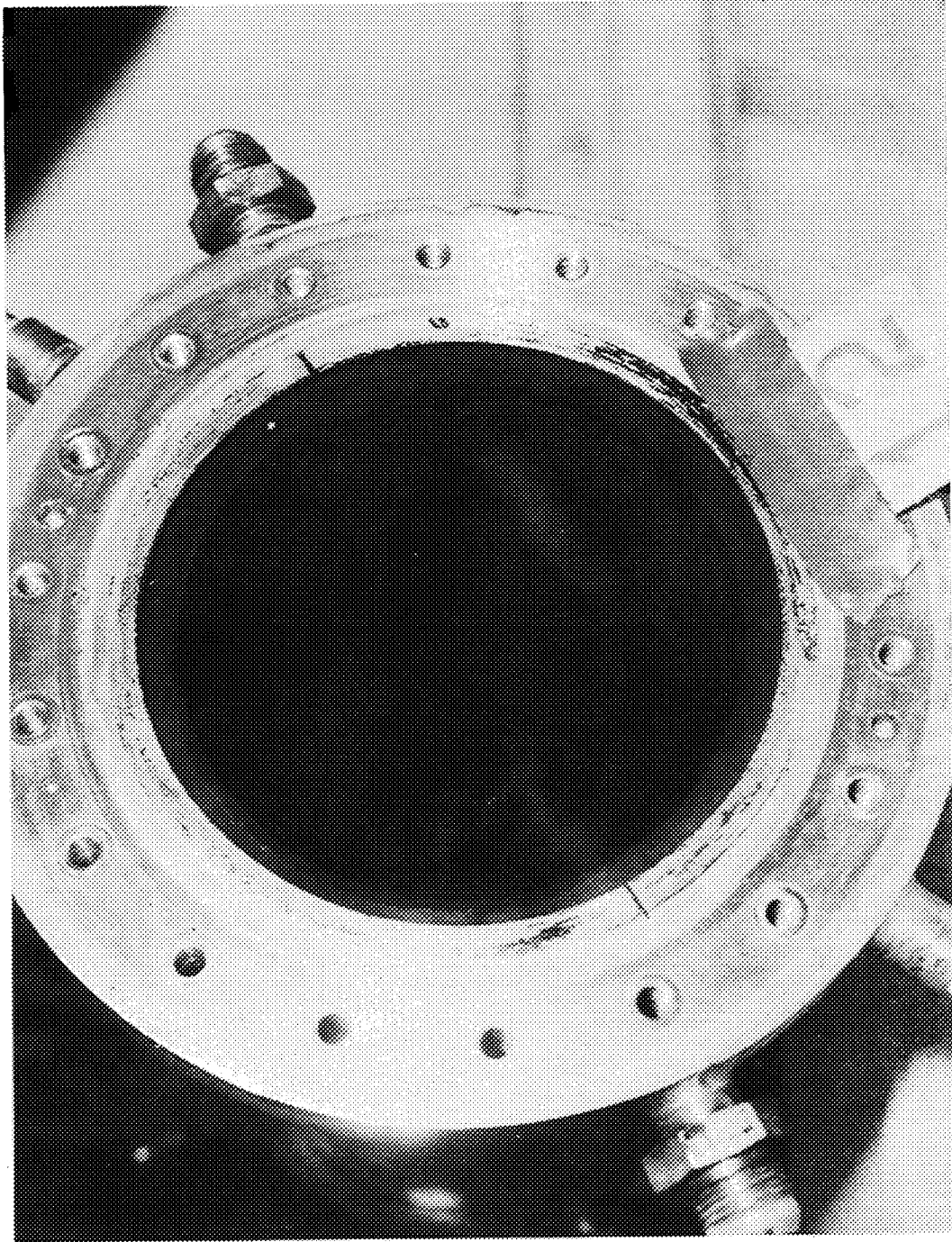


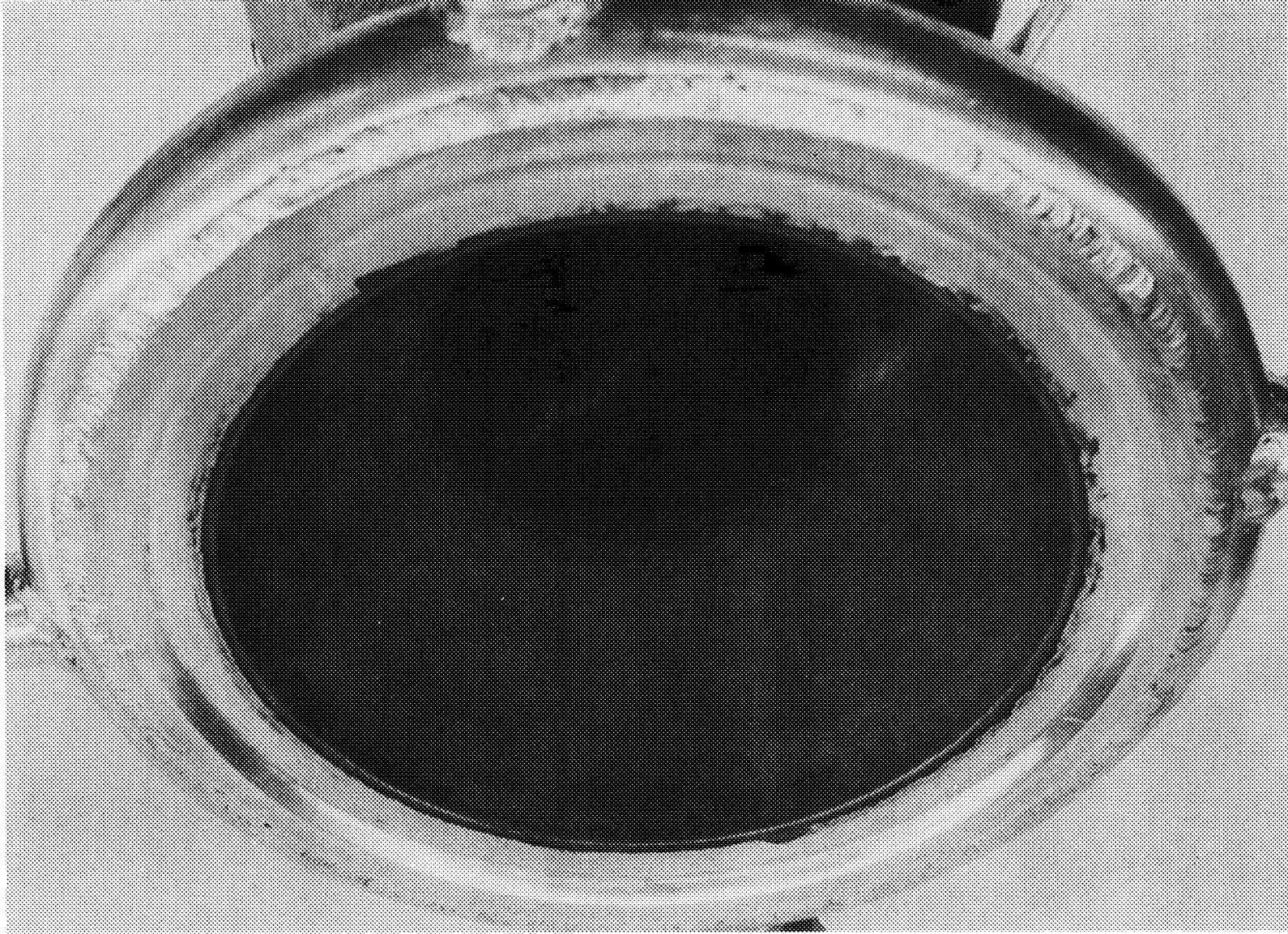
Figure 55. Posttest No. 13 Cylindrical Section



Figure 56. Posttest No. 14 Exit End Showing Carbon Deposit



Figure 57. Posttest No. 14 Exit End After Cleaning Liner



## VI, Task IV - Cooled Chamber Tests (cont.)

### D. ANALYSIS OF TEST RESULTS

#### 1. Instrumentation

Temperatures were measured at five axial stations along the contour with two measurements at each station 180 degrees apart. Ten thermocouples were inserted through the ribs nominally to the graphite-nickel interface. Two additional thermocouples were spot welded to the exterior surface of the electroformed nickel coolant jacket at the throat station. A postfire X-ray showed one of the throat thermocouples to be actually positioned 0.042 in. (1.06 mm) into the graphite.

#### 2. Test Results and Comparison to Predictions

Figure 58 shows typical temperature transients for Test No. 14 which was of 220-sec duration. The three thermocouples shown are the temperature at the throat station 0.042 (1.06 mm) into the AGCarb, the exterior of the throat, and the interface 2 in. (50.8 mm) upstream of the throat on the same side of the chamber. The wall temperatures are noted to oscillate throughout the test with all instrumentation on one side of the chamber and in the throat region showing similar response with time. Thermocouples located on the opposite side of the chamber also oscillate with time but phased independent of the transients shown.

Review of the coolant inlet and discharge pressures and coolant flow rates revealed the flow and pressures to be very steady during the periods when temperatures were changing rapidly, while the coolant bulk temperature rise increased only 11% with the largest wall temperature rises. The wall temperature oscillation phenomena observed are clearly due to the local building up and flaking off of soot deposits on the gas-side surface. This conclusion is supported by the following facts:

(1) The peak temperatures measured just after the soot flakes off are very close to the values predicted for a clean wall and are very repeatable.

(2) The temperatures drop slowly, reflecting a slow buildup rate; reach a minimum value which is also repeatable each cycle, reflecting the maximum soot thickness which is structurally stable under the gas shearing forces.

(3) The wall temperatures rise rapidly following stripping of the soot layer.

(4) Large shingles of carbon deposits were found on the AGCarb liner surface following each test. The fact that the soot flakes off supports the basic design criteria adopted--that soot deposits should not be depended upon to prevent chamber wall overheating.

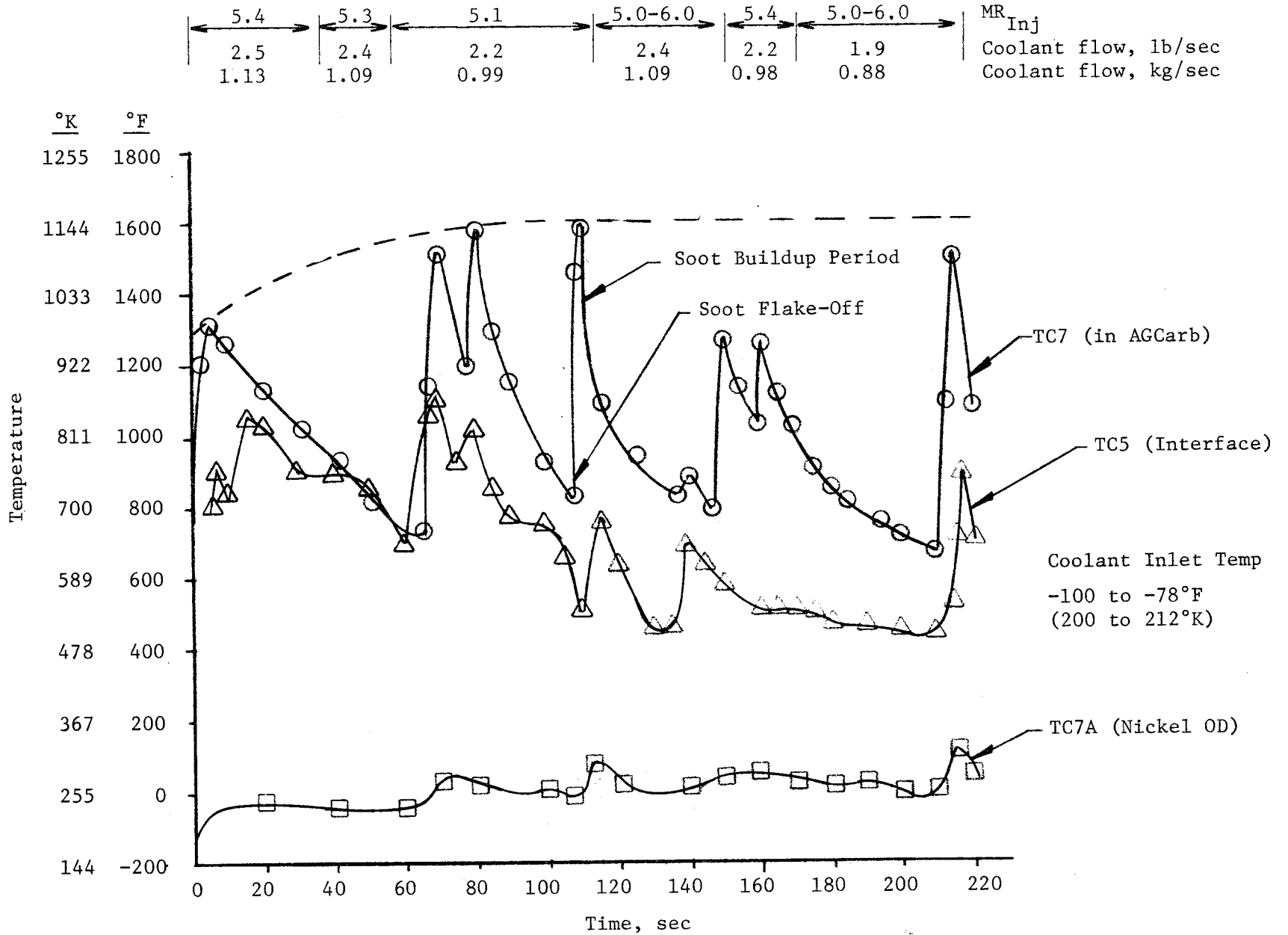


Figure 58. Temperature Transients at the Throat, Test No. 14

VI, D, Analysis of Test Results (cont.)

Figure 59 provides test data and the axial wall temperature profiles as computed from the two-dimensional heat conduction analysis prior to testing. Data are from Test No. 14 with TC7 thermocouple values adjusted to account for junction depth. The following information can be noted from this figure:

(1) Predicted wall temperatures for a no-soot condition on the gas-side of the AGCarb, the exterior of the nickel, and the interface of the AGCarb liner and the nickel jacket.

(2) Predicted temperatures for an injector with a 40 scfm (9.1 m<sup>3</sup>) face plate for which the chamber was designed and predicted temperature for the same injector with the 100 scfm (22.8 m<sup>3</sup>) face plate that was employed in testing.

(3) Measured wall temperatures which represent the maximum values in the time-temperature history. These are most appropriate since they represent the nearly clean wall condition for which the analysis was conducted.

The injector face plates are porous, sintered materials which provide a fuel-rich zone around the periphery of the injector. The greater porosity, 100 scfm (22.8 m<sup>3</sup>) face plate results in a longer fuel-cooled length in the cylindrical region of the chamber. At the start of the convergent nozzle, the unreacted oxidizer burns off the fuel-rich barrier and the wall temperatures rise rapidly such that, at the throat station and beyond, there is no predictable difference between the thermal characteristics of the two injectors. Since the throat station results in both the maximum wall temperatures, maximum temperature gradients and maximum thermal stresses, either injector assembly is considered to be suitable for evaluating the adequacy of the materials, the design and the fabrication approach, and analytical techniques.

In general, the measured temperatures are in good agreement with the predictions for the 100 scfm (22.8 m<sup>3</sup>) injector which was tested. The throat was running slightly cooler than predicted as verified by both the external thermocouple and the one located within the AGCarb liner. These temperatures are as follows:

<u>Location</u>	<u>Predicted</u>	<u>Measured</u>
External	264°F (402°K)	100°F (311°K)
AGCarb internal	1850°F (1283°K)	1600°F (1144°K)
AGCarb surface	4619°F (2821°K)	4000-4450°F (2477-2725°K)

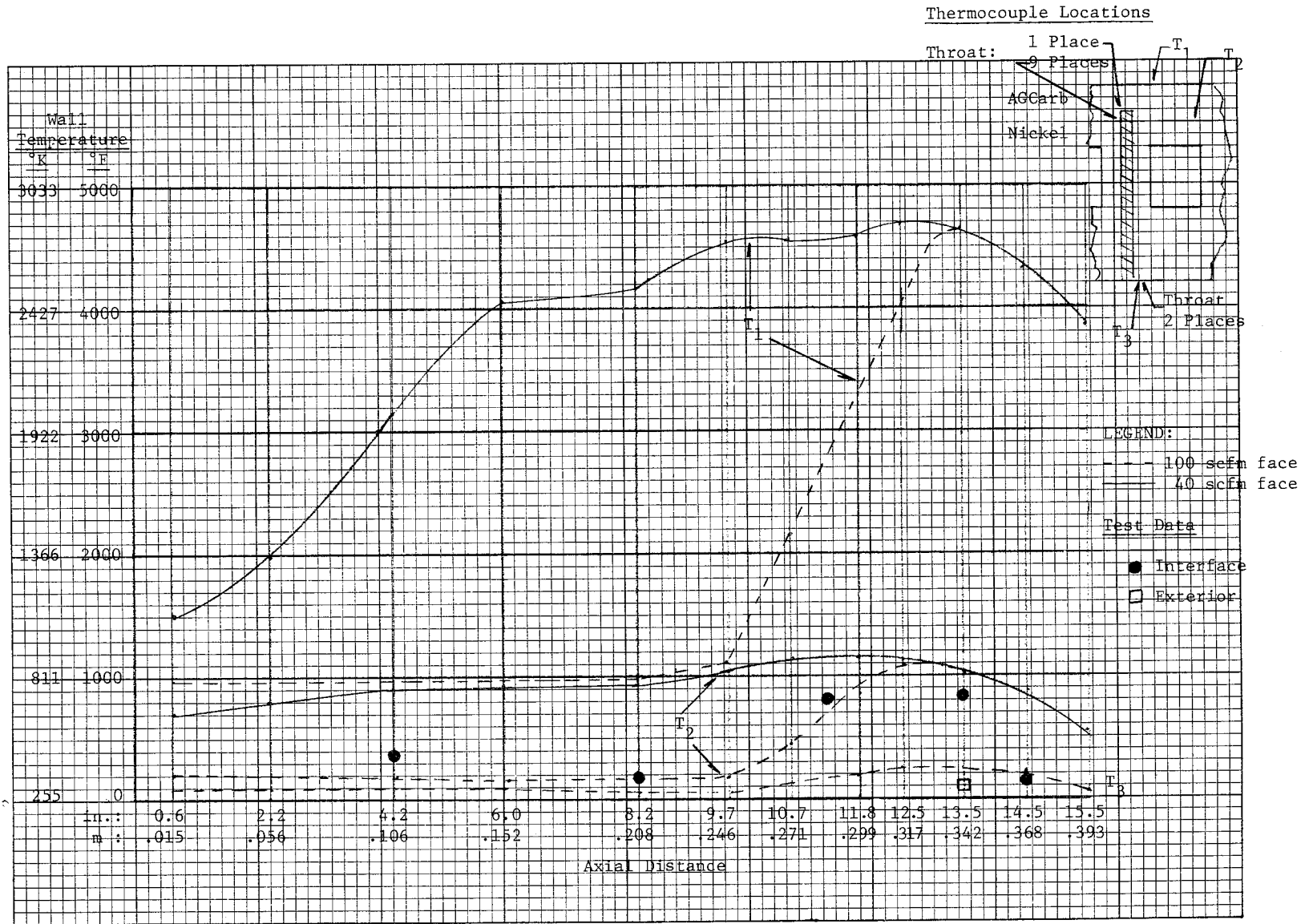


Figure 59. Predicted vs Actual Temperature Conditions

## VI, D, Analysis of Test Results (cont.)

The AGCarb surface temperature, which can be inferred from these results, range from 4000°F (2477°K) to 4450°F (2725°K), depending on which of the wall resistances or coefficients are assumed to be in error. Another possibility is that some soot always remains on the wall such that a really clean wall condition is never achieved.

The one region where a significant difference in predicted (760°F [678°K]) and measured (150°F [339°K]) nickel wall temperatures is noted is downstream of the throat. This may be due to the loss of good thermal contact at the bond line downstream of the throat. Reduced thermal contact will cause the nickel to run cooler and the AGCarb hotter. Complete separation would result in the AGCarb surface temperature rising to the order of 5000°F (3033°K) with radiation being the only cooling mode. The success of this material is not surprising since many previous applications in an uncooled configuration have been demonstrated at operating temperatures to 5500°F (3310°K). The lack of material removal under these severe conditions is credited to the compatibility of the graphite fibers with the products of combustion which are already saturated with the carbon supplied in the fuel.

An overall comparison of the accuracy of the thermal analysis can be obtained by comparing the predicted and measured coolant temperature rise as follows:

	<u>Predicted</u>		<u>Measured*</u>
Injector face, scfm (scmm)	40 (9.1)	100 (22.8)	100 (22.8)
Coolant inlet temperature, °F (°K)	-120 (188)	-120 (188)	-78 (212)
Coolant discharge temperature, °F (°K)	+357 (453)	+60 (288)	+92 (306)
Coolant temperature rise, °F (°K)	477 (520)	180 (355)	170 (350)

\*Test No. 14 at 215 sec.

### 3. Transient Analysis

A portion of the thermal design effort was devoted to consideration of the thermal transients of the chamber. One of the items of interest was the ability of the two-dimensional heat conduction program for regeneratively cooled chambers to predict the wall heating rates. Figure 60 provides a comparison of the predicted and measured throat station heating rates. Since the coolant flows were slightly higher during the engine start transient than those employed in the original design analysis, it was necessary to correct the test data to a lower flow condition. The top solid line in

— Predicted for TC location in AGCarb

- - - Actual; corrected to coolant flow of 2.05 lb/sec (9.29 kg/sec)

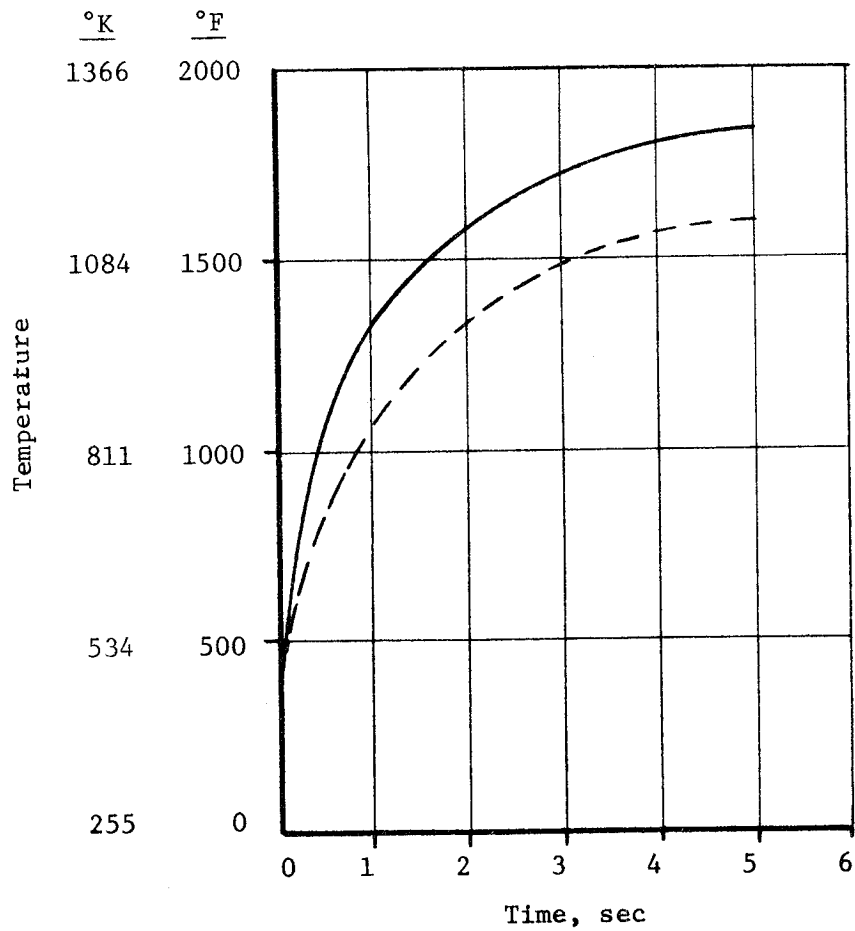


Figure 60. Predicted vs Actual Transient Temperature Conditions

#### VI, D, Analysis of Test Results (cont.)

Figure 60 shows the predicted time-temperature history of a point in the AGCarb liner which corresponds to the thermocouple position as located by a chamber X-ray. The dashed line shows the test results corrected to the proper coolant flow rates.

The time-temperature histories predicted by the computer model in the transient mode are noted to accurately define the wall heating rates and time required to reach steady state.

#### 4. Conclusions

- (a) The thermal design is satisfactory.
- (b) Soot reduces wall temperatures but not predictably.
- (c) Thermal resistance at interface was as predicted except for region downstream of the throat.
- (d) AGCarb properties are adequately defined.
- (e) Methane cooling characteristics used are confirmed by test results.

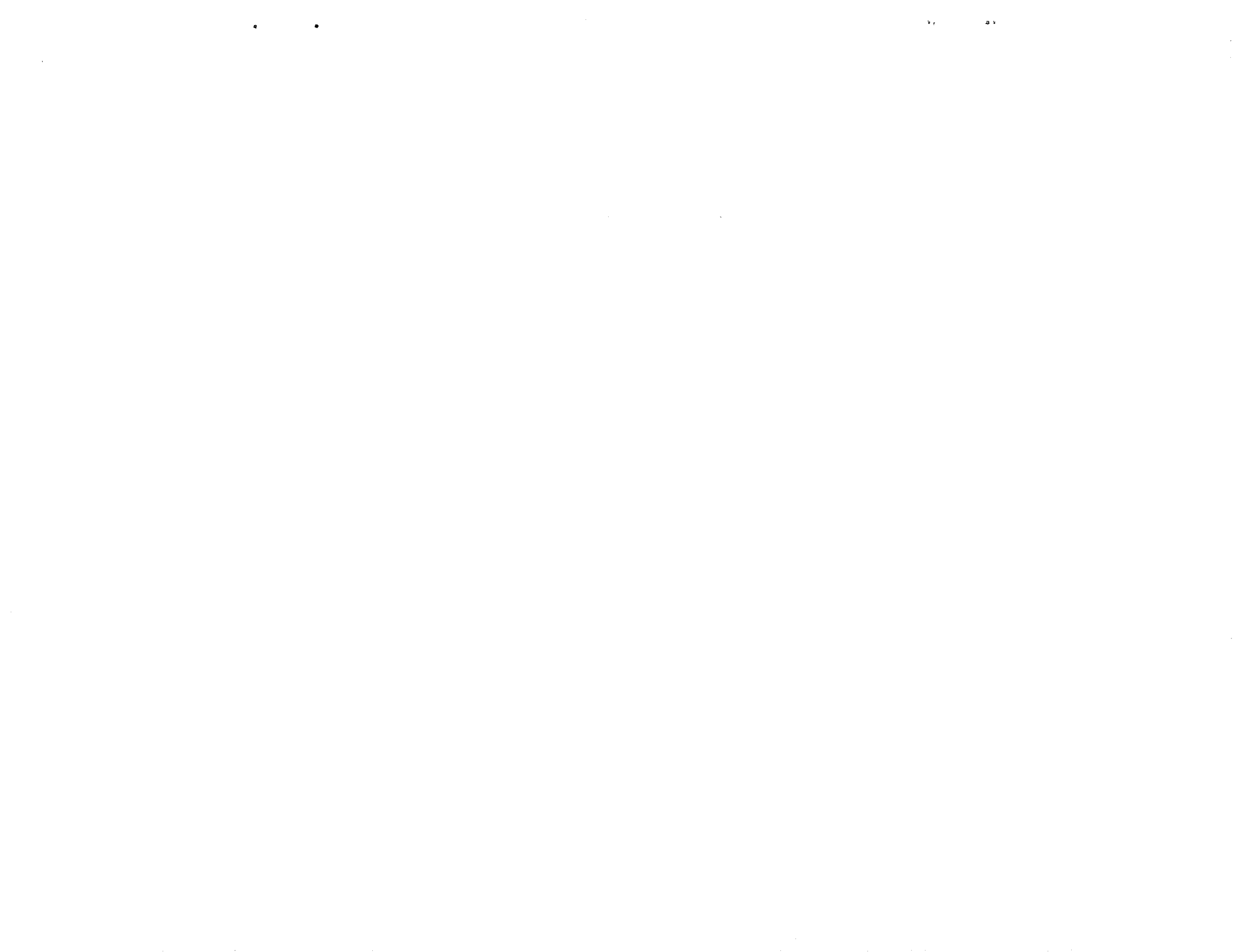


## VII. CONCLUSIONS

To meet the objectives of the program (i.e., to demonstrate the feasibility of operating a graphite-lined thrust chamber with FLOX-methane propellants) required the integrated efforts of several technical disciplines. The use of unique materials and fabrication methods required the development of special construction and assembly techniques by materials and fabrication specialists. Likewise, the design, development and analyses required application of special methods of analysis to account for and predict the performance of the materials and material combinations involved. Two thrust chambers were fabricated using fibrous graphite as a thermal barrier liner and nickel electroformed over the liner containing passages for regenerative cooling. One of these thrust chambers was test fired with FLOX-methane for a total duration of 540 sec, thus demonstrating the feasibility of the concept and methods of analysis. No throat erosion or other physical damage was evident, thus demonstrating the potential of the fibrous graphite and electroformed nickel as liquid rocket engine construction materials, either singly or in combination. There is a need, however, to improve the physical and chemical properties of these materials to further increase their potential. At the same time, the manufacturing methods used in producing fibrous graphite and electroformed nickel should be the subject of additional research with the objective of upgrading the consistency and reliability of physical properties.

#### REFERENCES

1. Kura, J. G., et al., "The Making of Nickel and Nickel-Alloy Shapes by Casting, Powder Metallurgy, Electroforming, Chemical Vapor Deposition, and Metal Spraying," NASA Technical Memorandum TM X-53430.
2. Kotfila, R. J., Davis, H.O., and Schleicher, W. J., "The Fabrication and Properties of the Fibrous Reinforced Graphite Composite, AGCarb-101," Aerojet Internal Report, August 1969.
3. Stubbs, V. R., Investigation of Advanced Regenerative Thrust Chamber Designs, Final Report, NASA CR-72742, 15 November 1971.



APPENDIX A

THERMAL AND MECHANICAL EVALUATIONS  
OF AGCARB MATERIAL



App A

THERMAL AND MECHANICAL EVALUATIONS  
OF AG CARB MATERIAL

Final Report

to

Aerojet Liquid Rocket Company  
Sacramento, California

Purchase Order L-801442-2022  
Prime Contract NAS3-13315

Southern Research Institute  
Birmingham, Alabama  
A-528-2550-I  
February 21, 1971



TABLE OF CONTENTS

	<u>Page</u>
INTRODUCTION . . . . .	1
MATERIAL AND SPECIMEN PREPARATION . . . . .	1
APPARATUS AND PROCEDURES . . . . .	3
Tension . . . . .	3
Compression . . . . .	3
Thermal Conductivity . . . . .	4
Weight/Volume Bulk Density . . . . .	5
Ultrasonic Velocity . . . . .	5
Electrical Resistivity . . . . .	6
DATA AND RESULTS . . . . .	7
Tension . . . . .	7
Compression . . . . .	8
Thermal Conductivity . . . . .	10
APPENDICES . . . . .	31



## LIST OF ILLUSTRATIONS

<u>Figure</u>		<u>Page</u>
1	Construction of Specimen Blanks . . . . .	11
2	Tensile Specimen Configuration . . . . .	12
3	Compressive Specimen Configuration . . . . .	13
4	Top View of Strip Specimen Assembly Employed in Radial Inflow Apparatus . . . . .	14
5	Tensile Strength versus Temperature for "A" and "B" Constructions of AG Carb . . . . .	15
6	Tensile Elastic Modulus versus Temperature for "A" and "B" Constructions of AG Carb . . . . .	16
7	Tensile Total Strain to Failure versus Temperature for "A" and "B" Constructions of AG Carb . . . . .	17
8	Failed "A" and "B" Construction Tensile Specimens . . . . .	18
9	Compressive Strength versus Temperature for "B" and "D" Constructions of AG Carb . . . . .	19
10	Compressive Elastic Modulus versus Temperature for "B" and "D" Constructions of AG Carb . . . . .	20
11	Failed "B" and "D" Construction Compressive Specimens . . . . .	21
12	Thermal Conductivity of "AG Carb" Material with Heat Flow 30° from Lamina . . . . .	22

App A

LIST OF TABLES

<u>Table</u>		<u>Page</u>
1	Test Matrix for AG Carb Materials . . . . .	23
2	Results of Tensile Evaluations of "A" and "B" Construction of AG Carb Material. . . . .	24
3	Results of Compressive Evaluations of "B" and "D" Construc- tions of AG Carb Material . . . . .	25
4	Thermal Conductivity of "AG Carb" Material with Heat Flow 30° from Lamina Determined using the Comparative Rod Apparatus with Armco Iron References . . . . .	26
5	Thermal Conductivity of "AG Carb" Material with Heat Flow 30° from Lamina Determined Using Strip Technique of Radial Inflow Apparatus . . . . .	27

App A

APPENDICES

- A' ULTIMATE STRENGTH, ELASTIC MODULUS AND POISSON'S RATIO TO 5500°F  
IN TENSION
- B' ULTIMATE STRENGTH, ELASTIC MODULUS AND POISSON'S RATIO TO 5500°F  
IN COMPRESSION
- C' A COMPARATIVE ROD APPARATUS FOR MEASURING THERMAL CONDUCTIVITY  
TO 2000°F
- D' THERMAL CONDUCTIVITY TO 5500°F BY RADIAL INFLOW METHOD

## App A

### THERMAL AND MECHANICAL EVALUATIONS OF AG CARB MATERIAL

#### INTRODUCTION

This is the final report to Aerojet Liquid Rocket Company, Division of Aerojet General Corporation, for work performed under Purchase Order Number L-801442-2022, Prime Contract NAS3-13315. The object of the program was to perform tensile, compressive and thermal conductivity evaluations of AG Carb nozzle material at room and elevated temperatures. As shown in the test matrix (Table 1), tensile and compressive evaluations were conducted at 70°F, 3000°F and 5000°F and thermal conductivity was measured from 70°F to 5000°F.

#### MATERIAL AND SPECIMEN PREPARATION

The material evaluated was identified as AG Carb and was furnished by Aerojet Liquid Rocket Company; the San Rafael Plastics Company in San Rafael, California was the manufacturer.

Five different constructions of the material were evaluated, but common denominators for all the specimens were that they were carbon-carbon composites constructed from National Carbon's WCA carbon tape and graphitized at a minimum temperature of 5000°F. The differences were the layups (flat, 30° or 60°), or biases (each layer biased 45°, alternate layers biased 15°, successive layers biased 15° or fabric randomly oriented). These different constructions for each evaluation are noted in the test matrix in Table 1; sketches of each construction are displayed in Figure 1 for further clarification. Also listed in Table 1 is the location and orientation of the material in the nozzle that each type specimen duplicates.

The material was received in the form of machined specimen blanks; the size of these blanks may be noted in Table 1 also. There were nine tensile and compressive specimens and one thermal conductivity specimen for each construction tested.

These mechanical specimens are identified throughout the report by the Aerojet designations that were on the blanks. These designations are explained as follows:

A1 - 4

Specimen number for this construction and type specimen

Aerojet type specimen number (1 and 12 were tensile specimens, 4 and 13 were compressive specimens and 9, 10, 14 and 15 were thermal conductivity specimens)

Construction of material from which specimen was fabricated ("A" construction was flat layup with 45° bias, "B" construction was flat layup with alternate layers rotated 15° clockwise, "D" construction was flat layup with straight fabric)

The thermal specimens did not fit within the nomenclature of the mechanical specimens; these specimens are identified as follows:

- B9 - a radial chamber specimen with plys oriented 30° to the longitudinal axis with random tape orientation. Heat flow was 30° to plys
- B10 - a radial throat specimen with plys 30° to the longitudinal axis with alternate tape layers rotated 15° clockwise. Heat flow was 30° to plys.
- C15 - a radial throat specimen with plys 60° to the longitudinal axis with successive plys rotated 15°. Heat flow was 30° to plys.
- D14 - a radial throat specimen with plys oriented 60° to the longitudinal axis with random tape orientation. Heat flow was 30° to plys.

As already mentioned the specimens were received as blanks, the size and configuration of which may be noted in the test matrix. Bulk density and sonic velocity measurements were made on these blanks. Sonic velocity measurements were accomplished by a through-transmission, elapsed-time technique. After the tensile specimens were final machined the electrical resistivities of some specimens were measured by the potentiometer method. All of these values are noted on the appropriate tables.

APPARATUS AND PROCEDURESTension

The tensile evaluations were conducted in a gas-bearing tensile facility. This apparatus utilizes gas-bearing universals in the load train to help detect misalignments which cause unknown bending stresses in the specimen. Primary components, other than the gas bearings, are the load frame, the mechanical drive system, the 5500°F furnace, the optical strain analyzers and associated instrumentation for measurement of load and strain. The complete facility is discussed in detail in Appendix A'.

Figure 2 is a sketch of the tensile specimen configuration utilized for the two material constructions evaluated in tension. This specimen is a 4-inch modification of the standard 6-inch configuration discussed in the appendix. The primary differences between the standard and the 4-inch specimen are the reduced L/D ratio in the gripping area and a lack of a double breakdown radius. A study (using graphite) to compare the two has been conducted to establish any differences, if they existed between the two configurations. Briefly, it was found that:

1. The specimen configuration (4-inch versus 6-inch) does not affect the tensile strength.
2. The 4-inch specimen gives about 6 percent lower modulus values, perhaps, because of the decreased gripping area and problems associated with specimen motion during initial loading and graphically interpreting the initial part of the curve.
3. Total strain was not affected by the problems of initial loading.

Compression

The compressive evaluations were performed in a gas-bearing compressive facility much like the tensile facility. This facility also has gas-bearings in the load train to eliminate misalignments and unknown bending stresses. Strains were measured with optical strain analyzers and elevated temperatures were supplied by an electrical resistance furnace with a graphite element. Appendix B' is a complete discussion of the facility. The standard "dumbbell" specimen configuration as discussed in the appendix was utilized for these evaluations; the configuration is shown in Figure 3.

## Thermal Conductivity

The thermal conductivity of the "AG Carb" composite was determined in the direction  $30^\circ$  from the lamina. The comparative rod and radial inflow apparatuses were employed to make the determinations from  $150^\circ\text{F}$  to  $5000^\circ\text{F}$ .

The material was supplied in the form of blanks and, as discussed previously, Blanks B9-1 and B10-1 were used to prepare the specimens for the comparative rod apparatus. Several blanks designated as C15 and D14 were employed to prepare the specimens for the radial inflow apparatus. These blanks were considered to be the same material and therefore were used to obtain duplicate data; however, there was a slight difference of fabric orientation between the blanks. The layers of the fabric in B9-1 and D14 were laid up with a random orientation of the warp direction; whereas, the alternate layers of the fabric in B10-1 and successive layers of the fabric in C15 were rotated  $15^\circ$  clockwise. This was not expected to affect the conductivity of the material and the good repeatability of the runs confirmed this expectation.

A description of the comparative rod apparatus used from  $150^\circ\text{F}$  to  $1500^\circ\text{F}$  is included in Appendix C'. The normal procedures and specimen configuration discussed in the appendix were employed for these determinations, therefore the estimated uncertainty of  $\pm 5$  percent applies to these runs.

For the temperatures above  $1500^\circ\text{F}$  the radial inflow apparatus was employed. A description of this apparatus and procedure is included in Appendix D'. Normally a cylindrical specimen is employed and the heat flows radially inward through the specimen, where it is monitored by a water calorimeter situated along the axial centerline of the specimens. Due to the anisotropic nature of this material the normal cylindrical specimen could not be employed, therefore, the strip assembly was used. This assembly consisted of four strips boxed around the central calorimeter as shown in Figure 4. The heat flowing radially inward toward the calorimeter transfers through the thickness of each strip. The temperature gradient across each strip is measured and the average value is used to calculate the thermal conductivity.

The uncertainty from all sources for the radial inflow apparatus is  $\pm 7$  percent when employing the normal cylindrical specimen configuration. For the strip assembly employed for these runs, two additional sources of error must be considered. The first is the amount of heat that bypasses the specimen strips and flows through the insulated corners of the assembly. This error is a function of the ratio of the conductivity of the corner insulation (thermatomic carbon) to that of the specimen. Due to the relatively

high conductivity of the specimens this error was negligible. The second source of error concerns the formation of isotherms within the strips that are not normal to the assumed direction of the heat flow. This error would be random and experience has shown that the error is probably less than  $\pm 3$  percent. Combining this with the uncertainty of  $\pm 7$  percent for the basic apparatus yields a total uncertainty of only  $\pm 8$  percent.

#### Weight/Volume Bulk Density

The bulk density of each specimen blank was determined from direct measurements of weight and dimensions. Weight measurements were made on an analytical balance having a sensitivity of 0.0001 gram. Dimensional measurements were made to the nearest 0.0005 inch using micrometers.

#### Ultrasonic Velocity

The through-transmission, elapsed-time technique was used for measuring the acoustic velocity. In this method, a short pulse of longitudinal-mode sound was transmitted through the specimen. An electric pulse was originated in a pulse generator and was applied to a ceramic piezoelectric crystal (SFZ). The pulse generated by this crystal was transmitted through a short delay line and inserted into the specimen. The time of insertion of the leading edge of this sound beam was the reference point on the time base of the oscilloscope which was used as a high-speed stopwatch. When the leading edge of this pulse of energy reached the other end of the specimen, it was displayed on the oscilloscope. The difference between the entrance and exit times was used with the specimen length in calculating ultrasonic velocity. A short lucite delay line was used to allow time isolation of the sound wave from electrostatic coupling and to facilitate clear presentation of the leading edge of the entrant wave resulting in a more accurate "zero" for time. Transducers having resonance frequencies of 1MHz and a 1/2-inch diameter cross-section were used. Alcohol was used as a couplant to reduce errors incurred by solid couplants. The precision of the measurement for tensile test blanks is  $\pm 0.002$  inch per micro-second.



Electrical Resistivity

Electrical resistivity was measured by the potentiometer method. The test specimen may be either a specimen blank or a finished specimen configuration having a uniform gage length of 1 inch or more. The attachment taps to the specimen were spring-loaded graphite discs. Potential taps were normally clipped to the specimen and had a gage length of 1 inch.

The procedure used in the potentiometer method involved comparing the voltages for a standard resistor with a specimen of unknown resistance when a common, known current flowed through both. With 1 amp flowing through the specimen and a standard 5000 ohm resistor, the potentiometer was set at 5000  $\mu$ V, and the rheostat adjusted until there was no current flow through the galvanometer. Then, the potentiometer leads were switched to the specimen. The potentiometer was adjusted for zero current flow through the galvanometer, and the voltage across the specimen was read.

From the relation

$$R = \frac{E}{I}$$

the relationship between the standard resistance, the unknown resistance and the associated voltages could be expressed as

$$\frac{R_x}{R_s} = \frac{E_x}{E_s} \quad \text{or} \quad R_x = R_s \frac{E_x}{E_s}$$

where

$R_x$  = resistance of specimen

$R_s$  = resistance of standard resistor (5000 ohm in this case)

$E_x$  = voltage drop across specimen

$E_s$  = voltage drop across standard resistor

A full-wave rectified dc power supply operated by an ac regulated power source was used to induce current flow through the specimen. A galvanometer having a sensitivity of 0.8  $\mu$ V per millimeter with a 1000 ohm series resistor was used with a potentiometer having a dial graduation of 0.0005  $\mu$ V to measure voltage.

Using the measured voltage drop across the specimen, the known current flow, and the dimension measurements from the specimen, the volume electrical resistivity was calculated using the equation

$$\rho = \frac{A}{L} \frac{V_x}{I}$$

where

- $\rho$  = volume electrical resistivity
- A = cross-sectional area of specimen
- $V_x$  = voltage drop across gage length of specimen (corrected for open-circuit voltage)
- I = current flow through specimen
- L = gage length of specimen

The normal uncertainty for the value of electrical resistivity determined from this apparatus is  $\pm 2$  percent.

#### DATA AND RESULTS

The results of the mechanical, thermal and nondestructive test evaluations obtained with the various constructions of AG Carb material are presented in Tables 2 through 5 and Figures 5 through 12.

#### Tension

The results of the tensile evaluations of the "A" and "B" constructions of the AG Carb are exhibited in Table 2 and Figures 5 through 8.

As shown in Figure 5, the strength of both constructions increased approximately 20 percent with each increase in temperature from 70°F to 5000°F. Also evident, is the fact that the "B" construction specimens (flat layup with alternate layers rotated 15° clockwise) were 20 to 25 percent stronger than the "A" construction specimens (flat layup with 45° fabric bias). At 70°F the respective values were 6790 psi and 5360 psi; at 5000°F these comparative values were 9770 psi and 8050 psi.

In Figure 6 the tensile elastic moduli for both constructions are plotted against temperature. At 70°F and 3000°F the "B" construction specimens again exhibited higher values. Comparative

values at 70°F were  $1.48 \times 10^6$  psi for the "A" and  $1.75 \times 10^6$  psi for the "B"; at 3000°F the comparative values in the same respective order were  $1.19 \times 10^6$  psi and  $1.46 \times 10^6$  psi. At 5000°F both constructions exhibited the same value of  $0.55 \times 10^6$  psi. As one can note by this discussion each increase in temperature resulted in a lower modulus for each construction.

Figure 7 is a plot of total strain to fracture versus temperature for each construction. The results are confusing here because of scatter in the data and there were no absolute values obtained at 5000°F. This latter phenomena was due to the strain targets falling off or sliding down the specimens before fracture occurred. At 70°F both constructions exhibited a value of approximately 0.007 in./in. Increasing the temperature to 3000°F caused the values to increase to 0.008 in./in. for the "A" construction and 0.010 in./in. for the "B" construction. It is evident that increasing the temperature further to 5000°F caused the total strain values of both constructions to increase greatly (greater than 0.060 in./in.).

Photographs of the fractured specimens may be seen in Figure 8. As shown, the specimens from the "A" construction failed along an approximate angle of 45°. This would be expected since the "A" construction was a flat layup with a 45° tape bias. The specimens from the "B" construction did not seem to fail at a definite angle - part of the fracture (individual laminae) was approximately 75° to the longitudinal axis while the other part of the fracture was torn straight across (90° to the longitudinal axis). This reflects this material's construction of flat layup with alternating layers offset 15° to the longitudinal axis; in-between layers were straight.

### Compression

The results of the compressive evaluations of the with lamina specimens from the "B" construction and the across lamina specimens from the "D" construction are displayed in Table 3 and Figures 9 through 11.

The compressive strength versus temperature plot is shown in Figure 9. As anticipated the strength of the across lamina specimens ("D" construction) was approximately double that of the with lamina specimens ("B" construction). Also as anticipated (from the tensile behavior), each temperature increase from 70°F to 5000°F resulted in successively higher strengths for both type specimens.

At 70°F the strength of the across lamina and with lamina specimens respectively were 13,590 psi and 7,790 psi. In the same order the values were 18,500 psi and 9,870 at 3000°F. Only one fracture was obtained at 5000°F due to the physical limits of load train travel being exceeded by the specimen deformations. The single fracture was obtained with a with lamina specimen ("B" construction); the value was 11,800 psi.

Compressive moduli are plotted against temperature for each type specimen in Figure 10. The moduli of the with lamina specimens were greater than those of the across lamina specimens at all three test temperatures. Respectively at 70°F, 3000°F and 5000°F the comparative values were  $1.50 \times 10^6$  psi to  $0.30 \times 10^6$  psi,  $1.54 \times 10^6$  psi to  $0.44 \times 10^6$  psi and  $0.86 \times 10^6$  psi to  $0.18 \times 10^6$  psi. This also shows that the moduli of both constructions increase slightly with the temperature increase from 70°F to 3000°F. Further increasing the temperature to 5000°F caused a drastic reduction in moduli for both constructions.

A plot of compressive strain to failure versus temperature is not included because there is a lack of data from which to produce one. We were able to measure total strain with only the "B" construction specimens and then only at 70°F and 3000°F. Measurements of strain were usually terminated by the strain targets breaking off the specimens. For this reason the values with the "greater than" notations in the tables mean this was as far as we could follow the targets; the actual total strain at failure would be much higher.

The specimens from the "B" construction exhibited a total strain of 0.0074 in./in. at 70°F and 0.0093 in./in. From this it should be safe to say that total strain increased with each increase in temperature from 70°F to 5000°F as was the case in tension. The across lamina specimens ("D" construction) exhibited very high total strain at each test temperature. In fact the specimens evaluated at 70°F strained so much that the strain targets fell (approximately 0.040 in./in.) before fracture occurred.

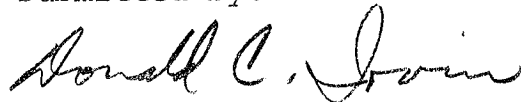
Figure 11 is a photograph of the failed specimens. All of the failures obtained with the "B" construction material (with lamina) occurred along a shear line angularly located at approximately 30° to the longitudinal axis. The across lamina specimens ("D" construction) failed in a compaction manner. It may be noted that most of these specimens have also failed in an inter-laminar mode. These failures occurred as secondary breaks and in removing the specimens from the push rods.

Thermal Conductivity

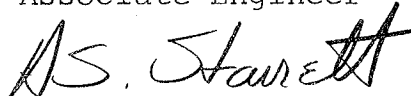
The thermal conductivity of the "AG Carb" with the heat flow in the direction of  $30^\circ$  from the lamina is shown in Figure 12 and Tables 4 and 5. The values decreased from 425 Btu in./hr ft<sup>2</sup>°F at 200°F to 182 Btu in./hr ft<sup>2</sup>°F at 4500°F. These values were extrapolated to 190 Btu in./hr ft<sup>2</sup>°F at 5000°F. The extrapolation was based on the character of two runs made initially during this program using a strip assembly that did not monitor the temperature gradient across each strip. These initial runs were not reported due to a higher random uncertainty that resulted.

The slight increase in the conductivity at the elevated temperatures, although being less than the uncertainty of the measurement, is believed to exist since all data points (for the initial unreported runs and those shown in Figure 2) taken in this temperature range consistently increased. Previous evaluations on this type of composite have also exhibited increasing conductivity with temperature above 3500°F. This increase is attributed to the further graphitization of the material in addition to a slight contribution by radiant transport.

Submitted by:



Donald C. Irvin  
Associate Engineer



H. S. Starrett, Head  
Solid Mechanics Section

Approved by:

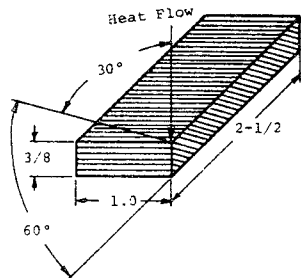


C. D. Pears, Head  
Mechanical Engineering Division

A-528-2550-I

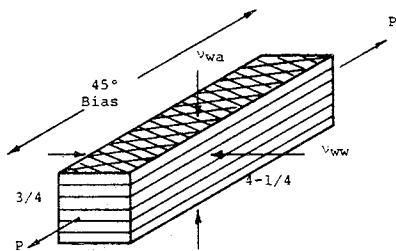
(5:12)

klr



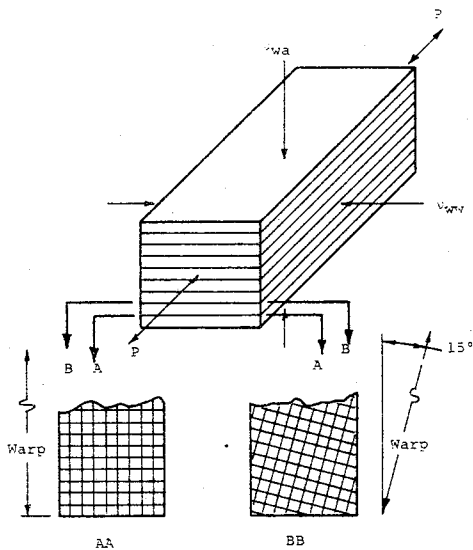
Evaluation: 30° to Lamina Thermal Conductivity - Radial Inflow Apparatus (2000°F to 5000°F) - Chamber Radial and Throat Radial

Construction: Plys 60° to longitudinal axis, National Carbon WCA carbon tape randomly oriented in radial chamber specimen (D14) and successive layers rotated 15° clockwise in radial throat specimens (C15)



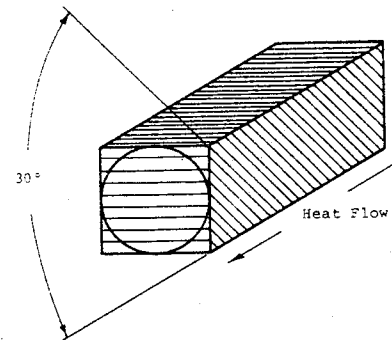
Evaluation: With Lamina Tensile ("A") Chamber Hoop

Construction: Flat layup, National Carbon WCA carbon tape with 45° bias



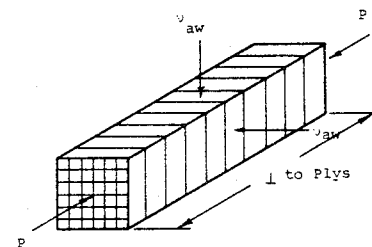
Evaluation: With Lamina Tensile and Compressive ("B") Throat Hoop

Construction: Flat layup with National Carbon WCA carbon tape with alternate layers rotated 15°



Evaluation: 30° to Lamina Thermal Conductivity - Comparative Rod Apparatus (70°F to 2000°F) - Chamber Radial and Throat Radial

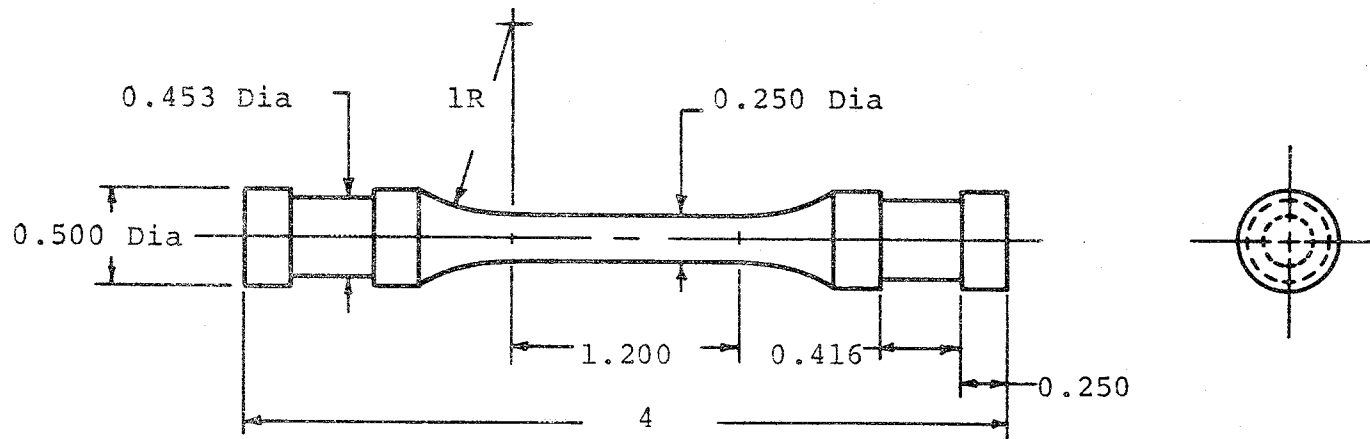
Construction: Plys 30° to longitudinal axis, National Carbon WCA carbon tape randomly oriented in radial chamber specimen (B9) and alternate layers rotated 15° clockwise in radial throat specimens (B10)



Evaluation: Across Lamina Compressive ("D")

Construction: Flat layup with National Carbon WCA carbon tape

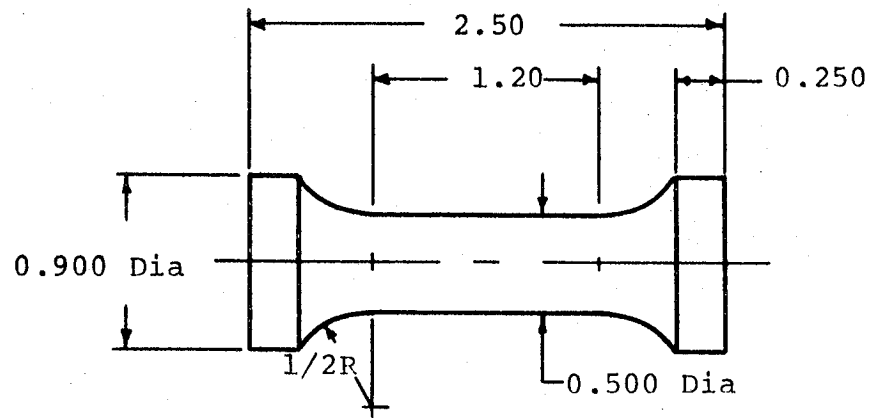
Figure 1. Construction of Specimen Blanks



Notes:

1. All diameters must be true and concentric to within 0.0005 inch
2. Both ends flat and perpendicular to  $\text{C}$  to within 0.0005 inch
3. Do not undercut radii at tangent points. Contour grind
4. All dimensions are in inches. Tolerances are  $\pm 0.001$  inch on diameters,  $\pm 0.005$  inch on lengths.

Figure 2. Tensile Specimen Configuration



Notes:

1. All diameters true and concentric to 0.0005 inch
2. Both ends flat and perpendicular to 0.0005 inch
3. Do not undercut in gage length

Figure 3. Compressive Specimen Configuration



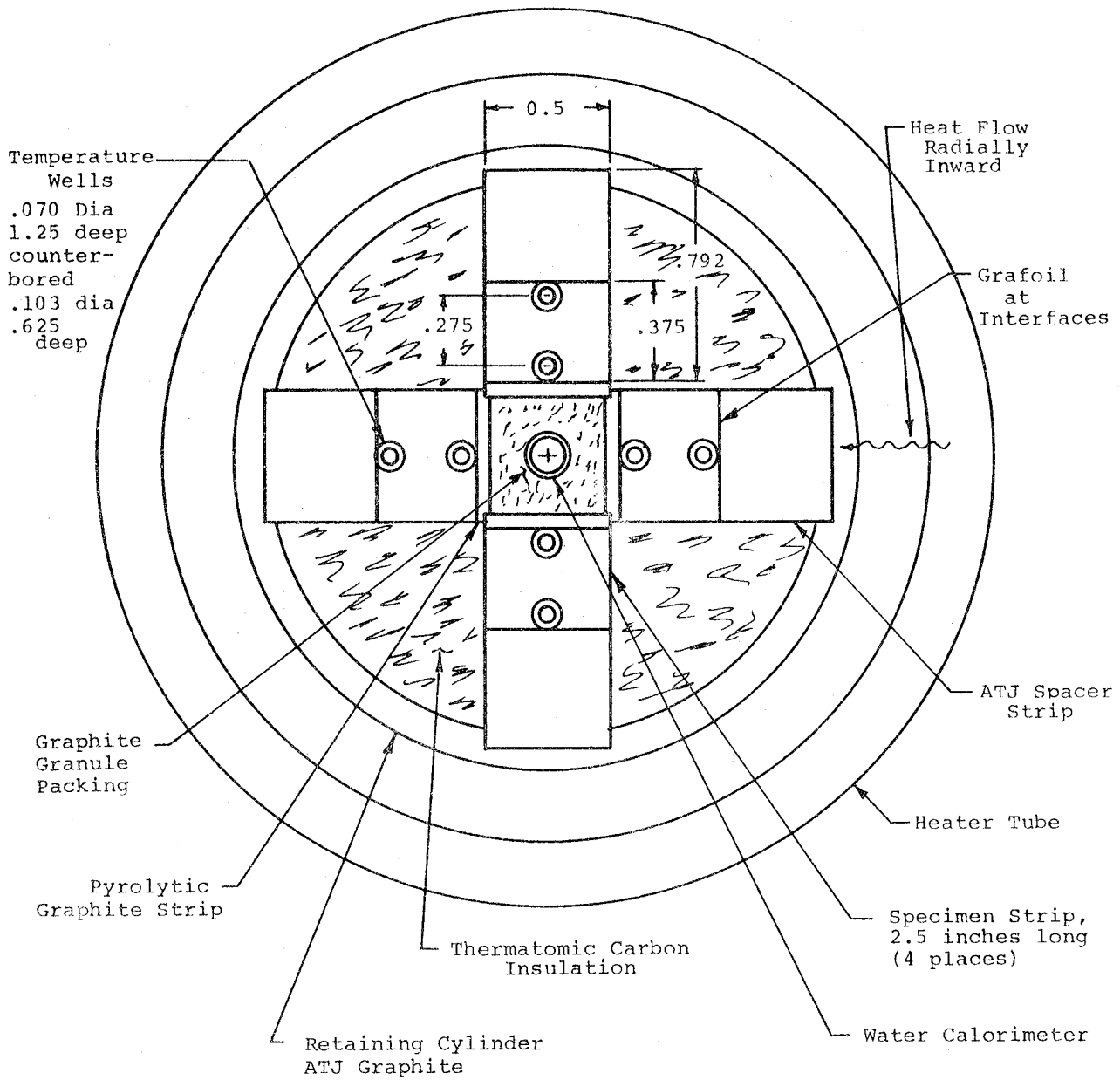


Figure 4. Top View of Strip Specimen Assembly Employed in Radial Inflow Apparatus

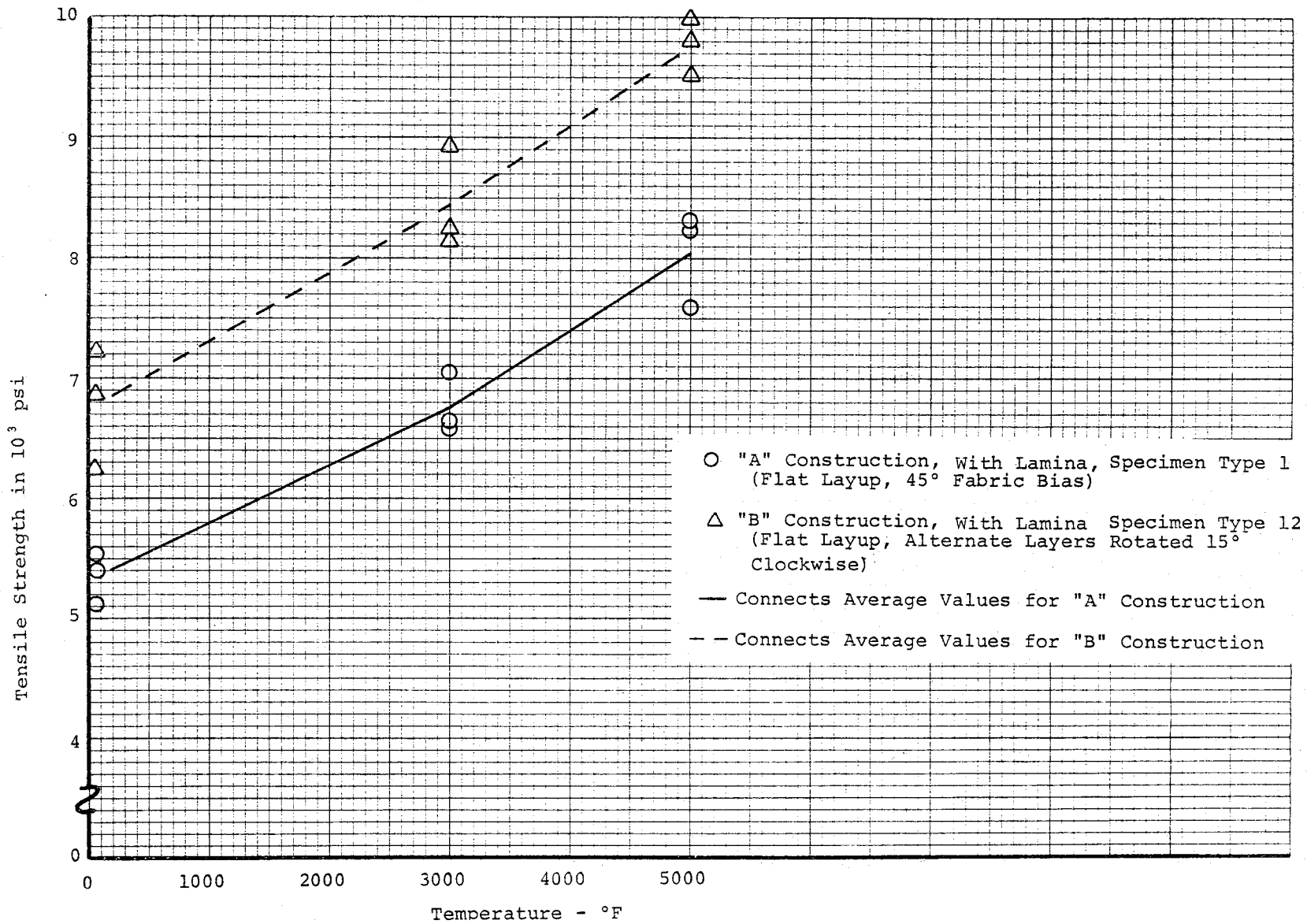


Figure 5. Tensile Strength versus Temperature for "A" and "B" Constructions of AG Carb

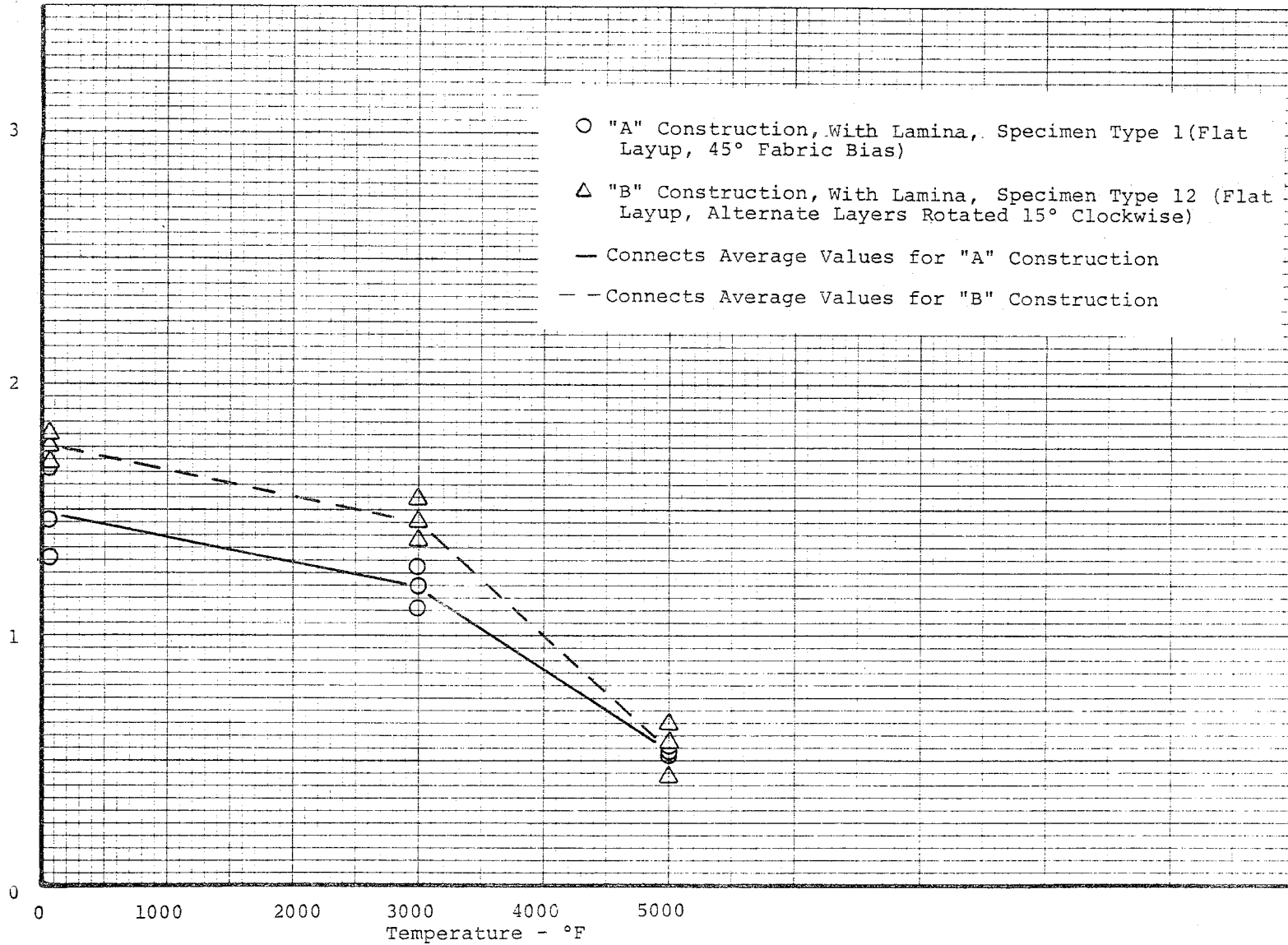
Tensile Elastic Modulus in  $10^6$  psi

Figure 6. Tensile Elastic Modulus versus Temperature for "A" and "B" Constructions of AG Carb

Tensile Total Strain to Failure in  $10^{-3}$  in./in.

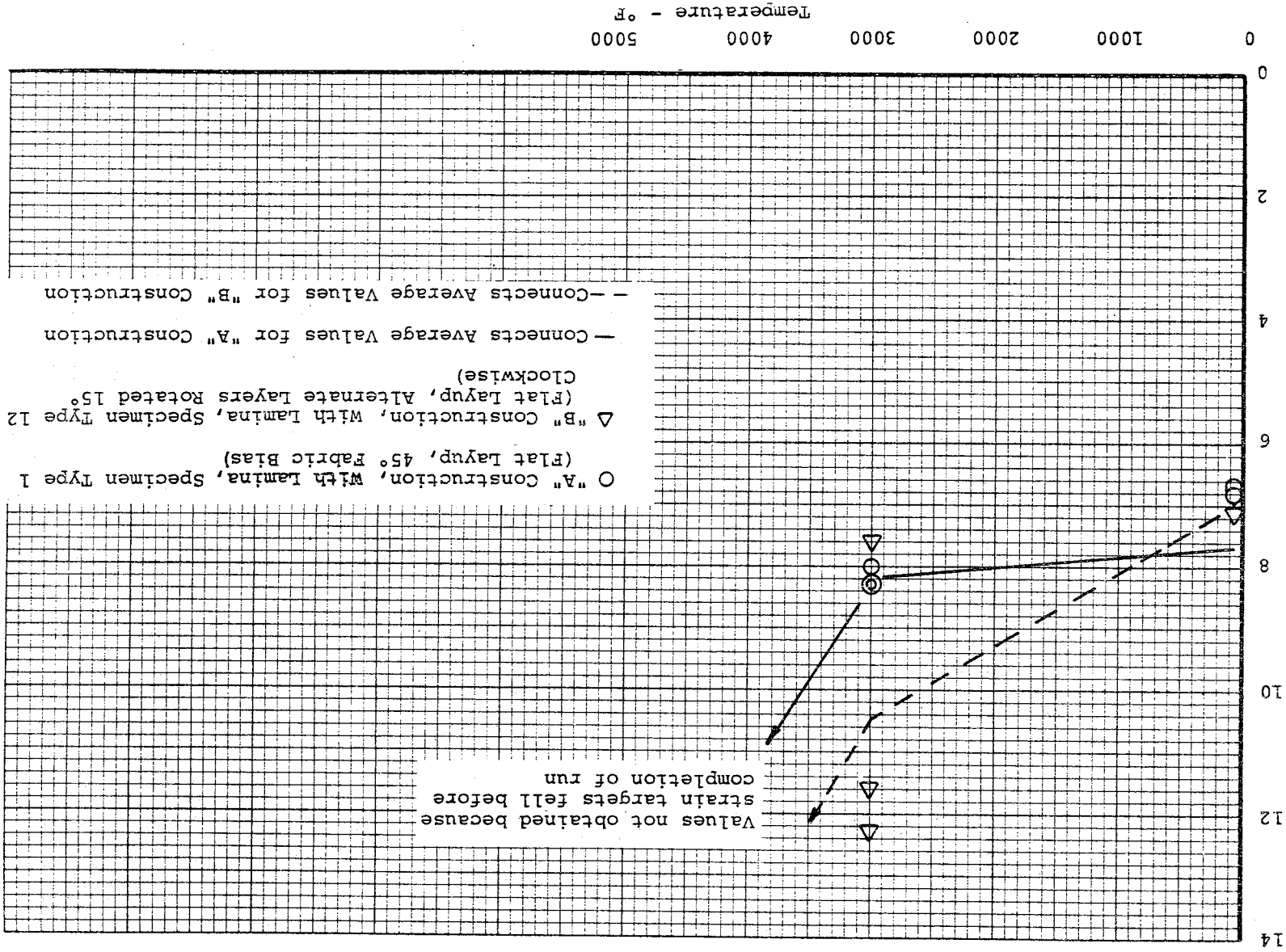
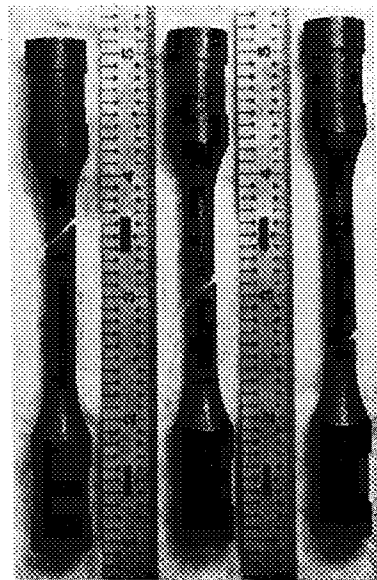
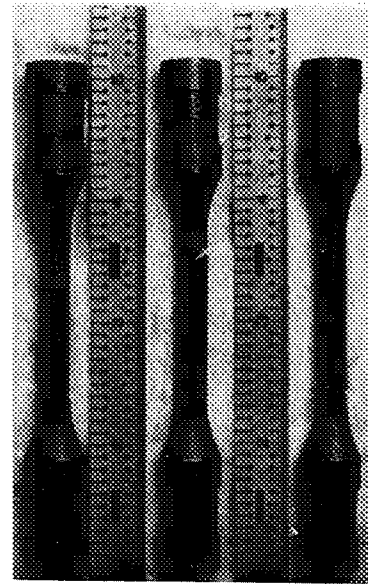


Figure 7. Tensile Total Strain to Failure versus Temperature for "A" and "B" Constructions of Ag Carb

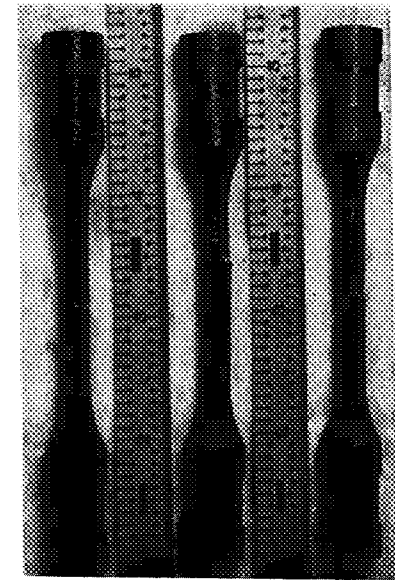
With Lamina Tension  
Flat Layup, National  
Carbon WCA Carbon Tape  
with 45° Bias



A1-1      A1-4      A1-8

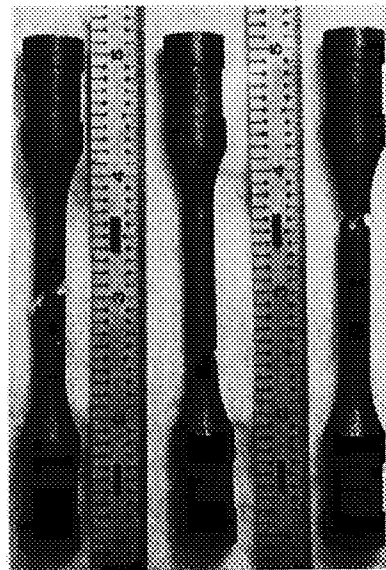


A1-3      A1-5      A1-7



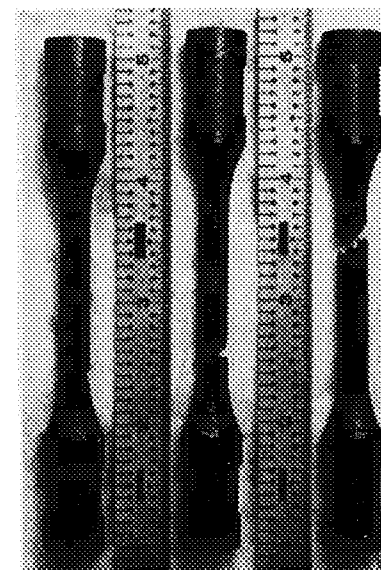
A1-2      A1-6      A1-9

With Lamina Tensile  
Flat Layup, National  
Carbon WCA Carbon Tape  
with Alternate Layers  
Rotated 15° Clockwise



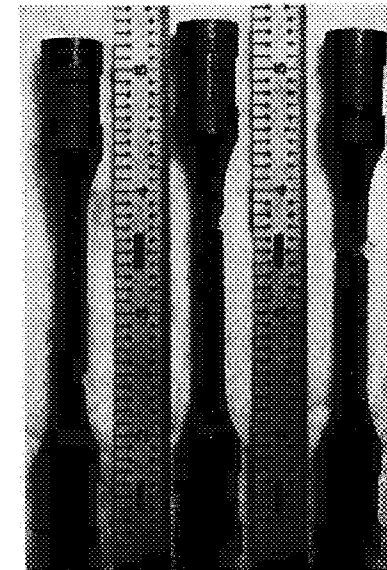
B12-1      B12-4      B12-7

70°F



B12-2      B12-5      B12-9

3000°F



B12-3      B12-9      B12-8

5000°F

Figure 8. Failed "A" and "B" Construction Tensile Specimens

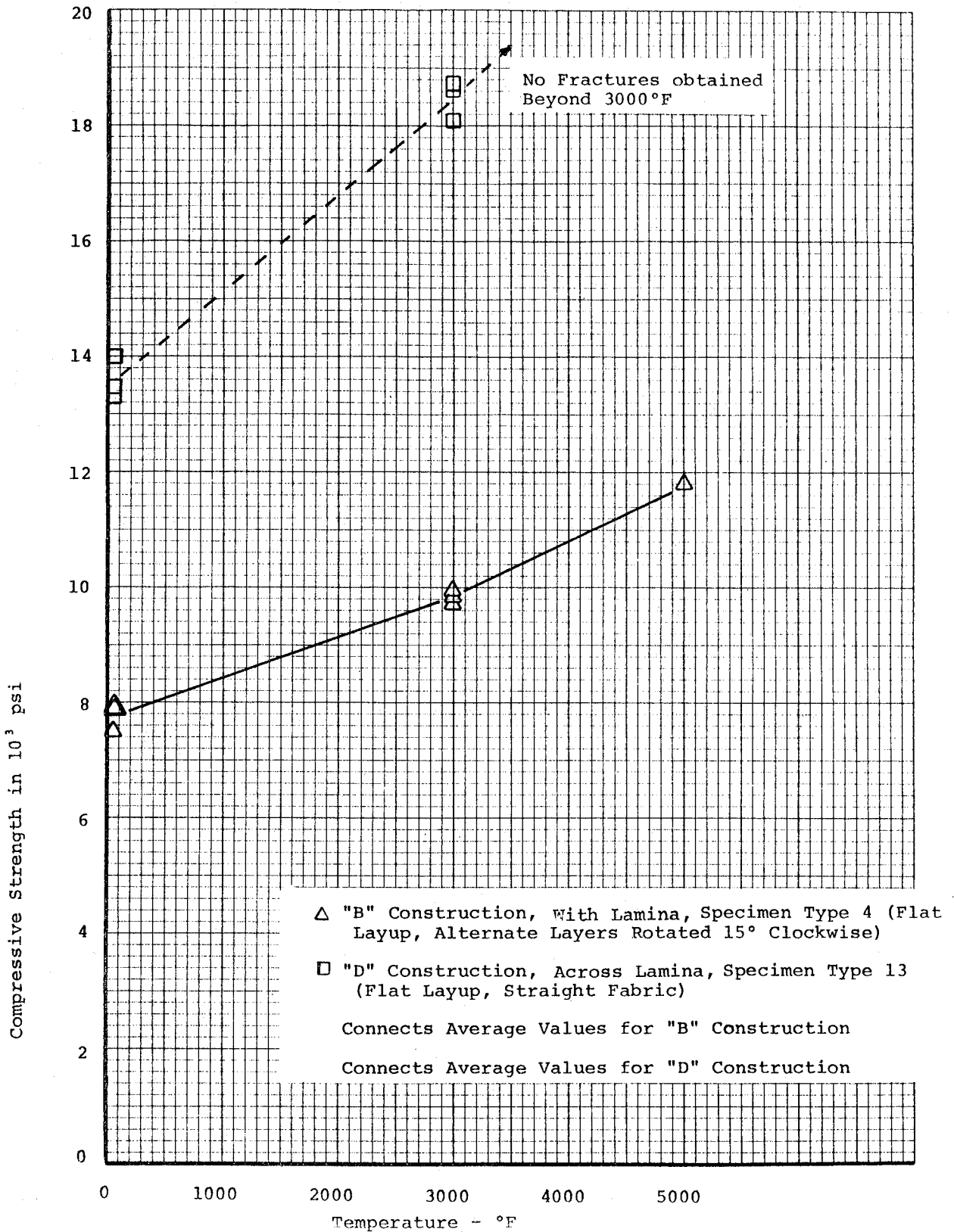


Figure 9. Compressive Strength versus Temperature for "B" and "D" Constructions of AG Carb

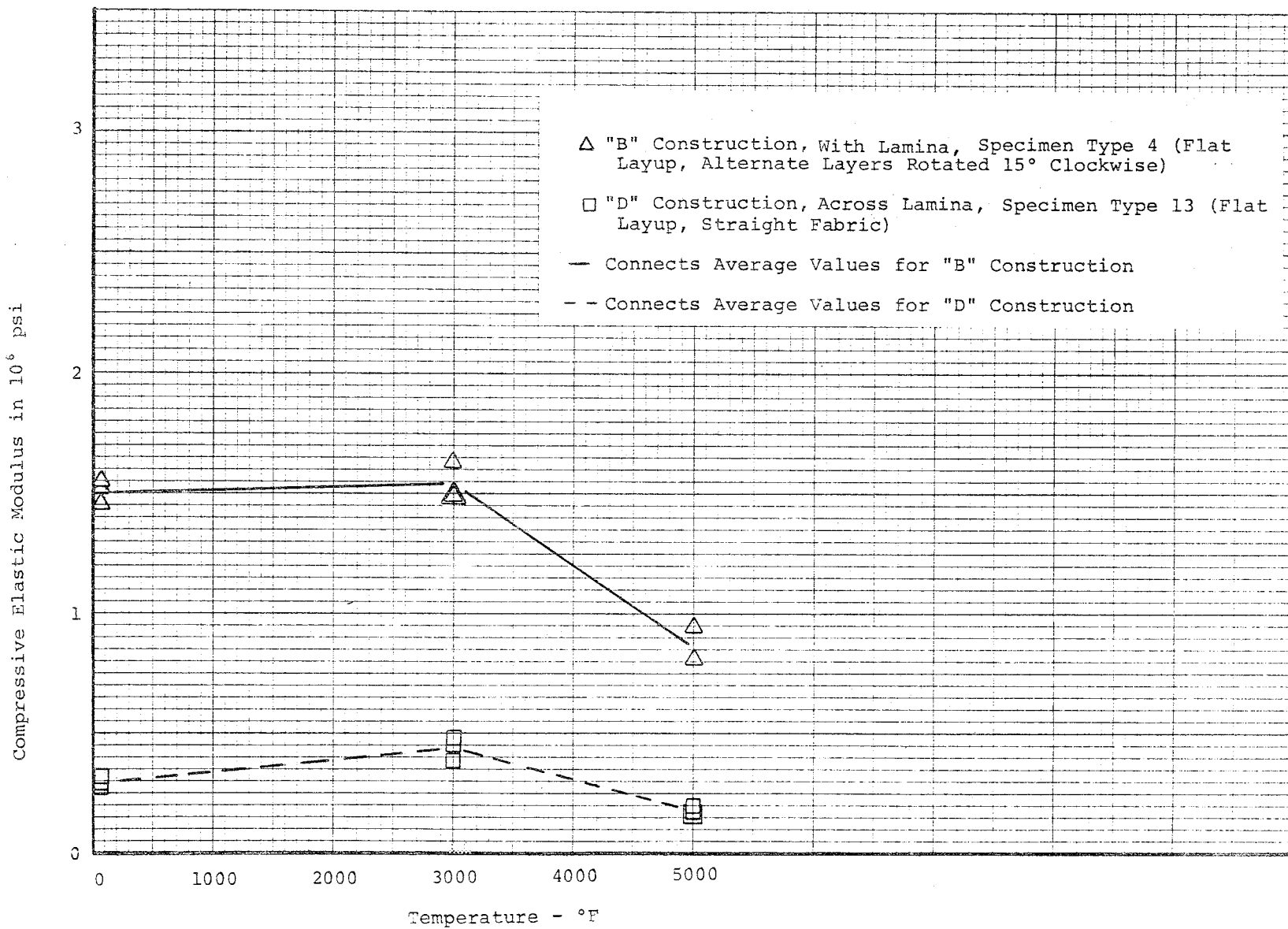
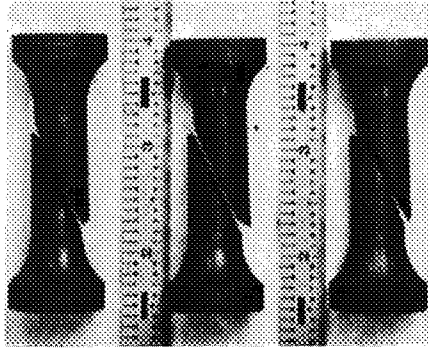
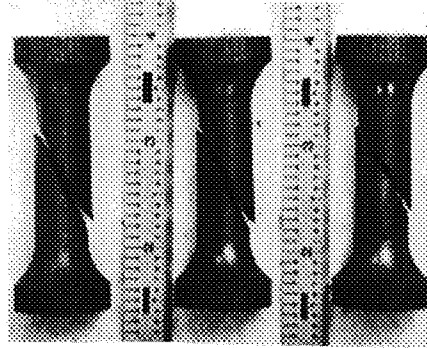


Figure 10. Compressive Elastic Modulus versus Temperature for "B" and "D" Constructions of AG Carb

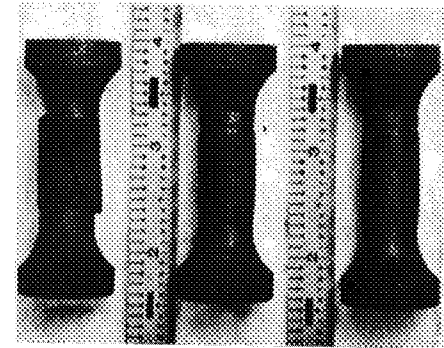
With Lamina  
 Compression  
 Flat Layup,  
 National  
 Carbon WCA  
 Carbon Tape  
 Alternate  
 Layers Rotated  
 15° Clockwise



B4-1      B4-2      B4-3

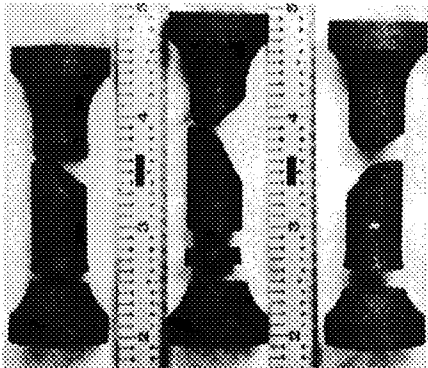


B4-4      B4-5      B4-6



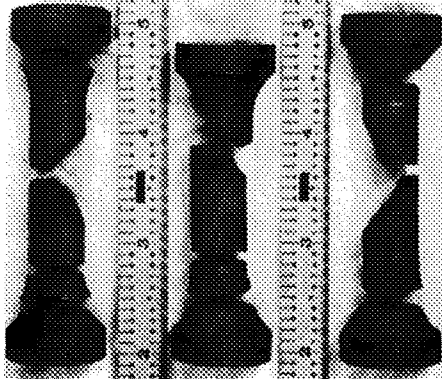
B4-7      B4-8      B4-9

Across Lamina  
 Compression  
 Flat Layup,  
 National  
 Carbon WCA  
 Carbon Tape  
 Straight



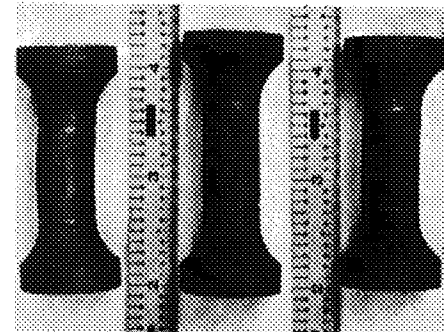
D13-1      D13-4      D13-8

70°F



D13-2      D13-6      D13-9

3000°F



D13-3      D13-5      D13-7

5000°F

Figure 11. Failed "B" and "D" Construction Compressive Specimens



Thermal Conductivity - Btu in./hr ft<sup>2</sup>°F

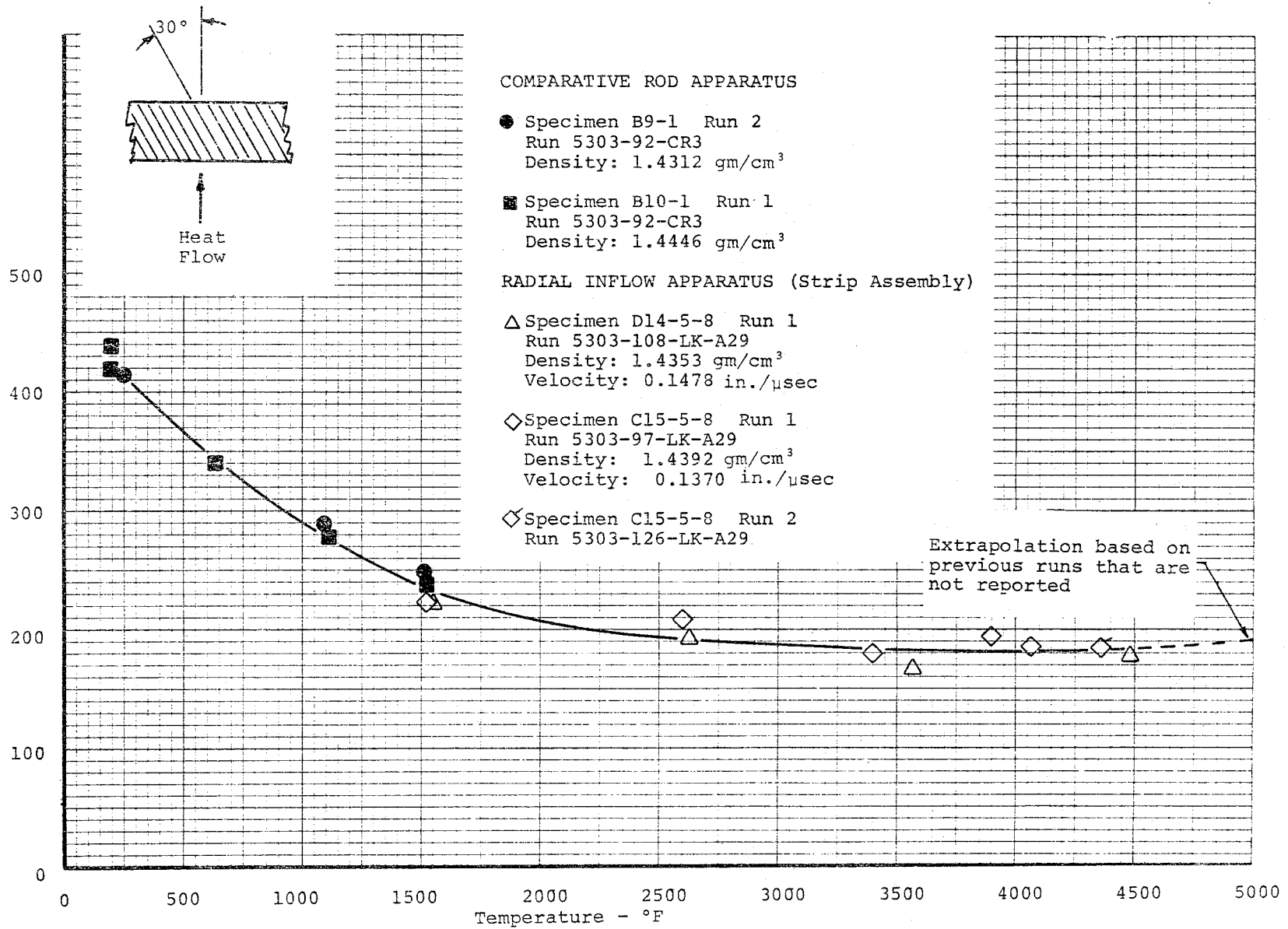


Figure 12. Thermal Conductivity of "AG Carb" Material with Heat Flow 30° from Lamina

Table 1

Test Matrix for AG Carb Materials

Evaluation	Specimen Orientation	Material Construction	Location of Type Material in Nozzle	Specimen Designation	Number of Runs Per Temperature			Size of Specimen Blank
					70°F	3000°F	5000°F	
Tension (ultimate strength, elastic modulus, Poisson's ratio and strain to fracture)	With Lamina	Flat layup with National Carbon WCA carbon tape with 45° bias	Chamber hoop	A1-1 through A1-9	3	3	3	3/4"x3/4"x4-1/4"
Tension (ultimate strength, elastic modulus, Poisson's ratio and strain to fracture)	With Lamina	Flat layup with National Carbon WCA carbon tape with alternate layers rotated 15° clockwise	Throat hoop	B12-1 through B12-9	3	3	3	3/4"x3/4"x4-1/4"
Compression (ultimate strength, elastic modulus, Poisson's ratio and strain to fracture)	With Lamina	Flat layup with National Carbon WCA carbon tape with alternate layers rotated 15° clockwise	Throat hoop	B4-1 through B4-9	3	3	3	1-1/8"x1-1/8"x2-1/2
Compression (ultimate strength, elastic modulus, Poisson's ratio and strain to fracture)	Across Lamina	Flat layup with National Carbon WCA carbon tape straight	-----	D13-1 through D13-9	3	3	3	1-1/8"x1-1/8"x2-1/2
Thermal Conductivity (comparative rod apparatus - 70°F to 2000°F)	30° to Lamina <sup>1</sup>	Plys 30° to longitudinal axis, National Carbon WCA carbon tape in random orientation	Radial Chamber	B9	← 1 →			1.0" dia x 1.0" lg
Thermal Conductivity (radial inflow apparatus - 2000°F to 5000°F)	60° to Lamina <sup>1</sup>	Plys 60° to longitudinal axis, National Carbon WCA carbon tape in random orientation	Radial Chamber	D14	← 1 →			5/8" tk x 1.0" wide x 2-1/2" long
Thermal Conductivity (comparative rod apparatus - 70°F to 2000°F)	30° to Lamina <sup>1</sup>	Plys 30° to longitudinal axis, National Carbon WCA carbon tape with alternate layers rotated 15° clockwise	Radial Throat	B10	← 1 →			1.0" dia x 1.0" lg
Thermal Conductivity (radial inflow apparatus - 2000°F to 5000°F)	60° to Lamina <sup>1</sup>	Plys 60° to longitudinal axis, National Carbon WCA carbon tape with successive layers rotated 15° clockwise	Radial Throat	C15	← 1 →			3/8" tk x 1.0" wide x 2-1/2" long

1. The manner in which heat was introduced to the specimens resulted in the heat flowing 30° to lamina.

Table 2

Results of Tensile Evaluations of "A" and "B" Constructions  
of AG Carb Material

Loading Direction	Temperature °F	Stress Rate psi/min	Specimen Number	Bulk Density gm/cm <sup>3</sup>	Ultimate Strength psi	Initial Elastic Modulus in 10 <sup>6</sup> psi	Total Unit Axial Strain to Failure in./in.	Poisson's Ratio		Sonic Velocity in./usec	Electrical Resistivity μhm cm
								v <sub>wa</sub>	v <sub>ww</sub>		
Flat layup 45° Bias Fabric With Lamina (with warp)	70	10,000	Al-1	1.450	5550	1.32	0.0095	0.10		0.1242	1281
			Al-4	1.452	5410	1.67	0.0068	0.22		0.1253	1281
			Al-8	1.432	5130	1.46	0.0067		0.40	0.1230	----- <sup>1</sup>
			Average	1.445	5360	1.48	0.0077	0.16	0.40		
	3000	10,000	Al-3	1.447	7040	1.27	0.0083		0.13	0.1245	1314
			Al-7	1.444	6600	1.11	0.0080		0.19	0.1228	----- <sup>1</sup>
			Al-5	1.449	6650	1.20	0.0083	0.07		0.1236	1260
			Average	1.447	6760	1.19	0.0082	0.07	0.16		
	5000	10,000	Al-2	1.444	8320	0.53	>0.033 <sup>2</sup>	0.05		0.1247	----- <sup>1</sup>
			Al-6	1.450	8240	0.54	>0.062 <sup>2</sup>	0.10		0.1238	1264
			Al-9	1.440	7600	0.56	>0.066 <sup>2</sup>	0.22		0.1219	1305
			Average	1.445	8050	0.54		0.14	0.10		
Flat layup Alt. layers rotated 15° clockwise With Lamina (with warp)	70	10,000	B12-1	1.446	6260	1.81	-0.005 <sup>3</sup>	0.43	0.1285	1283	
			B12-4	1.446	6870	1.68	0.0071	0.46		0.1284	----- <sup>1</sup>
			B12-7	1.440	7230	1.76	0.0068		0.05	0.1280	1244
			Average	1.444	6790	1.75	0.0070	0.46	0.24		
	3000	10,000	B12-2	1.443	8150	1.46	0.0076	0.27		0.1283	----- <sup>1</sup>
			B12-5	1.449	8260	1.55	0.0116	0.20		0.1278	1238
			B12-9	1.443	8930	1.38	0.0123	0.22		0.1280	1267
			Average	1.445	8450	1.46	0.0105	0.24	0.20		
	5000	10,000	B12-6	1.444	9990	0.44	>0.070 <sup>2</sup>		0.17	0.1290	----- <sup>1</sup>
			B12-3	1.447	9520	0.65	>0.066 <sup>2</sup>		0.22	0.1293	1247
			B12-8	1.437	9800	0.57	>0.066 <sup>2</sup>	0.23		0.1285	1268
			Average	1.443	9770	0.55		0.23	0.20		

1. Data not obtained with this specimen.

2. Strain targets fell before completion of run.

3. Strain approximated because specimen tore making accurate measurement impossible.

Table 3

Results of Compressive Evaluations of "B" and "D" Constructions  
of AG Carb Material

Loading Direction	Temperature °F	Stress Rate psi/min	Specimen Number	Bulk Density gm/cm <sup>3</sup>	Ultimate Strength psi	Initial Elastic Modulus in 10 <sup>6</sup> psi	Total Unit Axial Strain to Failure in./in.	Poisson's Ratio			Sonic Velocity in./μsec
								v <sub>wa</sub>	v <sub>ww</sub>	v <sub>aw</sub>	
Flat layup Alt. layers rotated 15° clockwise With Lamina (with warp)	70	10,000	B4-1	1.448	7920	1.52	0.0077		0.41		0.1321
			B4-2	1.451	7920	1.54	0.0082		0.43		0.1311
			B4-3	1.442	7520	1.45	0.0062	0.13			0.1327
			Average	1.447	7790	1.50	0.0074	0.13	0.42		
	3000	10,000	B4-4	1.452	9740	1.63	0.0098		0.34		0.1331
			B4-5	1.450	9960	1.49	0.0099		0.31		0.1341
			B4-6	1.452	9900	1.49	0.0083	0.10			0.1344
			Average	1.451	9870	1.54	0.0093				
	5000	10,000	B4-7	1.448	11,800	0.82	>0.030 <sup>2</sup>		0.47		0.1343
			B4-8	1.454	>7500 <sup>1</sup>	0.94	>0.020 <sup>2</sup>		0.42		0.1333
			B4-9	1.462	>6900 <sup>1</sup>	0.83	>0.020 <sup>2</sup>	0.26			0.1334
			Average	1.455	11,800	0.86	-----	0.26	0.44		
Flat layup straight fabric Across Lamina	70	10,000	D13-1	1.434	13,300	0.28	>0.064 <sup>2</sup>		0.09		0.0687
			D13-4	1.427	14,000	0.32	>0.044 <sup>2</sup>		0.19		0.0736
			D13-8	1.440	13,480	0.29	>0.019 <sup>2</sup>		0.05		0.0687
			Average	1.434	13,590	0.30	-----		0.11		
	3000	10,000	D13-2	1.433	18,750	0.39	>0.033 <sup>2</sup>		0.10		0.0681
			D13-6	1.439	18,100	0.47	>0.044 <sup>2</sup>		0.09		0.0686
			D13-9	1.432	18,650	0.45	>0.045 <sup>2</sup>		0.13		0.0678
			Average	1.435	18,500	0.44	-----		0.11		
	5000	10,000	D13-3	1.436	>8550 <sup>1</sup>	0.20	>0.036 <sup>2</sup>		0.12		0.0688
			D13-5	1.435	>5360 <sup>1</sup>	0.17	>0.027 <sup>2</sup>		0.13		0.0709
			D13-7	1.432	>7990 <sup>1</sup>	0.17	>0.061 <sup>2</sup>		0.25		0.0712
			Average	1.434	-----	0.18	-----		0.17		

1. Specimen deformation exceeded limits of load train travel.
2. Strain targets fell before completion of run.

Table 4

Thermal Conductivity of "AG Carb" Material with Heat Flow 30° from Lamina  
Determined using the Comparative Rod Apparatus with Armco Iron References

Specimen and Time	Mean Temperature of Specimen °F	Thermal Conductivity of Specimen $k_s$ Btu in./hr ft <sup>2</sup> °F	$\Delta T$ through Specimen °F	Mean Temperature of Lower Reference °F	Thermal Conductivity of Lower Reference $k_1$ Btu in./hr ft <sup>2</sup> °F	$\Delta T$ through Lower Reference $\Delta T_1$ °F	Mean Temperature of Upper Reference °F	Thermal Conductivity of Upper Reference $k_2$ Btu in./hr ft <sup>2</sup> °F	$\Delta T$ through Upper Reference $\Delta T_2$ °F
Spec B9-1 Run 2 Run 5303-92-app 2		Initial thickness: 0.9994 in. Final thickness: 0.9995 in.			Initial weight: 17.8815 gm Final weight: 17.8619 gm				
9:00 am	223	417	8.62	209	466	7.68	237	459	7.88
9:20 am	222	415	8.85	209	466	7.83	237	459	8.05
1:35 pm	1072	289	43.08	1005	288	44.40	1141	261	46.39
1:55 pm	1073	290	43.12	1006	288	44.82	1142	261	46.35
4:15 pm	1515	251	75.07	1393	220	87.25	1642	195	95.00
4:30 pm	1519	251	74.27	1396	219	86.85	1644	195	93.65
Spec B10-1 Run 1 Run 5303-90-app 3		Initial thickness: 0.9974 in. Final thickness: 0.9975 in.			Initial weight: 18.5392 gm Final weight: 18.5317 gm				
7:45 pm	193	421	6.00	184	472	5.25	202	468	5.50
8:15 pm	192	444	5.97	183	472	5.63	702	468	5.65
8:30 am	632	342	37.77	575	376	33.03	692	350	38.35
9:15 am	631	341	37.82	575	376	33.00	692	350	38.35
12:30 pm	1108	277	26.08	1022	282	53.35	1200	251	64.05
12:55 pm	1111	278	36.07	1025	281	53.70	1203	251	64.13
2:45 pm	1521	238	75.75	1401	220	81.00	1650	195	93.70
3:15 pm	1526	239	75.48	1405	220	81.12	1654	195	93.60

- Notes: 1. All measurements made with helium purge. Apparatus was not evacuated prior to determination  
2. Thermal conductivity ( $k_s$ ) of specimen calculated from following equation

$$k_s = \left[ \frac{k_1 \Delta T_1}{l_1} + \frac{k_2 \Delta T_2}{l_2} \right] \frac{l_s}{2\Delta T_s}$$

where

$k$  = thermal conductivity  
 $\Delta T$  = temperature drop over gage length  
 $l$  = gage length

and subscripts 1, 2, and s refer to lower reference, upper reference, and specimen, respectively.

Table 5

Thermal Conductivity of "AG Carb" Material with Heat Flow 30° from Lamina  
Determined Using Strip Technique of Radial Inflow Apparatus

Specimen and Run Number	Time	Strip Location	Average $\Delta T$ for Each Strip	Heat Flow to Calorimeter Btu/hr	Specimen Average Mean Temperature	Average Thermal Conductivity Btu in./hr ft <sup>2</sup> .°F	
Spec D-14-5-8 Run 1 Run 5303-108-A29 Density: 1.4353 gm/cm <sup>3</sup> Velocity: 0.1478 in./usec	<u>9:35</u>	Front	53	240	<u>1548</u>	<u>221</u>	
		Left	47	252			
		Back	49	258			
		Right	45	290			
				297			
	<u>12:30</u>			<u>49</u>	<u>306</u>		
		Front	105	455			
		Left	76	459			
		Back	97	473			
		Right	88	449			
	<u>2:45</u>			<u>91</u>	<u>411</u>		
		Front	149	630			
		Left	143	589			
		Back	140	590			
		Right	125	578			
	<u>4:30</u>			<u>139</u>	<u>556</u>		
		Front	150	666			
		Left	137	640			
		Back	156	650			
		Right	136	640			
			<u>145</u>	<u>668</u>			
				<u>648</u>			
				<u>651</u>	<u>4492</u>	<u>178</u>	



Table 5 - Concluded

Specimen and Run Number	Time	Strip Location	Average $\Delta T$ for Each Strip	Heat Flow to Calorimeter Btu/hr	Specimen Average Temperature	Average Thermal Conductivity Btu in./hr ft. <sup>2</sup> °F
C-15-5-8 Run 2 Run 5303-126-LK-A29	1:00	Front Left Back Right	115 123 112 112	535 536 549 530	4364	184
	3:45	Front Left Back Right	115 123 112 112	535 536 549 530		
C-15-5-8 Run 2 Run 5303-126-LK-A29	1:00	Front	201	899	4060	185
		Left	170	873		
		Back	210	925		
		Right	190	945		
				887		
				909		
				884		
				876		
				884		
				873		
				873		
				896		

Mean temperature calculated as the average of temperatures measured in inside and outside temperature wells

$$k = \frac{t \cdot Q}{A \Delta T}$$

where

k = thermal conductivity  
 t = distance between outside and inside hole = 0.275 in.  
 Q = heat to calorimeter gage  
 A = area of specimen = 1.00 in.<sup>2</sup>  
 $\Delta T$  = temperature drop from outside to inside hole





App A

- 31 -

APPENDICES



## APPENDIX A'

### ULTIMATE STRENGTH, ELASTIC MODULUS, AND POISSON'S RATIO TO 5500°F IN TENSION

---

A typical tensile facility is shown in the photograph in Figure 1 and in the schematic in Figure 2. The primary components are the gas-bearings, the load frame, the mechanical drive system, the 5500°F furnace, the optical strain analyzers, and associated instrumentation for measurement of load and strain. The load capacity is 15,000 pounds.

The load frame and mechanical drive system are similar to those of many good facilities. The upper crosshead is positioned by a small electric motor connected to a precision screw jack. This crosshead is stationary during loading and is moved only when assembling the load train. The lower crosshead is used to apply the load to the specimen through a precision screw jack chain driven by a variable speed motor and gear reducer.

Nonuniaxial loading, and therefore bending stresses, may be introduced in tensile specimens not only from (1) misalignment of the load train at the attachment to the crossheads, but also from (2) eccentricity within the load train, (3) unbalance of the load train, and (4) external forces applied to the load train by such items as electrical leads and clip-on extensometers. Although the bending moments from some of these sources may seem relatively slight, the resulting stress distortions are quite significant in the evaluation of the extremely sensitive brittle materials. Now consider each individually.

To confirm that the gas-bearings had eliminated nonuniaxial loading at the point of attachment of the load train to the crossheads, the frictional moment was determined at a load of 5000 pounds by measuring the torque required to produce initial motion within the system with the bearings in operation. This torque was found to be a maximum of  $6.6 \times 10^{-3}$  inch-pounds. The equation

$$M_O = \frac{2\mu P}{3} \left[ \frac{R_2^3 - R_1^3}{R_2^2 - R_1^2} \right] \quad (1)$$

was then applied to the system to calculate the kinetic friction where  $M_O$  was the resisting moment due to kinetic friction and  $\mu$  represented the coefficient of kinetic friction. The calculated value of  $\mu$  was then equal to a maximum of only  $4.5 \times 10^{-7}$ .

The classic equation

$$S = \frac{Mc}{I} \quad (2)$$

was then employed to obtain the stress that could be induced in the specimen due to this bending moment. This value was 0.16 psi, or less than 0.002 percent of the tensile stress produced within a typical graphite specimen. These low values clearly indicate the elimination of problems of bending stress in the specimen imposed by misalignment at the crosshead attachments, either initially or during loading.

Emphases in the design of the load train were placed on (1) large length-to-diameter ratios at each connection, (2) close sliding fits (less than 0.005 inch) of all mating connections, (3) the elimination of threaded connections, (4) the use of pin connections wherever possible, and (5) increasing the size of components to permit precise machining of all mating surfaces. All members were machined true and concentric to within 0.0005 inch, and the entire load train was checked regularly to ensure overall alignment following assembly of the individual members. This process ensures concentricity and no kinks in the system.

The problems of unbalance within the load train and of external forces applied to the load train have been explored and corrected. The entire load train is statically balanced to less than 0.01 inch-pound for normal operation.

One configuration of the tensile specimen is shown in Figure 3. This specimen provides a relatively large L/D ratio in the gripping area to ensure good alignment. All surfaces in the gripping area are cylindrical in order to make precision machining easier and repeatable from specimen to specimen. This specimen also has double breakdown radii from the gripping area to the gage section. This double breakdown allows a uniform transition of the stress pattern and reduces the frequency of radius (out of gage) fractures. This specimen provides a uniform gage section which gives a definable volume of material under stress and permits accurate measurements of strain. The flags for the measurement of axial strain are positioned one inch apart so that unit strain is recorded directly. The flag attachment for measurement of lateral strain is positioned between the flags for axial strain; see Figure 4.

## App A'

A schematic of the precision tensile grip is shown in Figure 5. The design is much like the jaws of a lathe head or the chuck of a drill motor made with precision. Observe from the figure the long surface contact of the mating parts and the close fits to establish precise alignment with the specimen. As the load is applied, the wedges maintain alignment to fracture.

Figure 6 is a sketch of the 5500°F furnace used for tension showing the basic components. The furnace consists of a resistively heated graphite element insulated from a water-cooled shell by thermatomic carbon. The furnace and specimen are purged with helium to provide an inert atmosphere. Ports with visual openings are provided on opposite sides of the furnace as a means of allowing the strain analyzers to view the gage flags on the specimen. Specimen temperatures are determined by optical pyrometer readings taken through another small sight port containing a sapphire window. A calibration curve was established for the loss through the sapphire window, and since the furnace cavity acts essentially as a blackbody, true temperature readings are obtained. Power is supplied to the heating element by means of a 25 KVA variable transformer.

Strain measurement consists of measuring optically the elongation between two flags, or targets, which are mounted on the specimen and separated initially by a predetermined gage length. The travel of the targets is measured by sensing the displacement of the image of the edge of the targets and then electromechanically following the image displacement. The relative travel of the two targets provides the strain. Readout is continuous and automatic on a millivolt recorder. A schematic of the analyzer is shown in Figure 7.

A brief summary of the mechanical motions of the components involved in monitoring the strain is helpful in understanding the detailed performance. A tracking telescope follows the upper target and carries a second telescope mounted on its carriage. The second telescope is capable of independent motion to follow the lower target. The relative displacement between the upper and lower telescope, as strain occurs, defines the strain. The system usually is operated so that the tracking telescope follows the upper target and the strain is monitored by the relative displacement of the aperture rather than the telescope following the lower target. With this procedure the maximum range is the maximum displacement available for the lower aperture, of about 1/8 inch, and the sensitivity is limited by the optics and the noise level of the detector. Using both telescopes, the range is about 3/4 inch.

## App A'

To provide optical references on the specimens, targets are affixed to the test specimen as mentioned. When the specimen is heated to temperature, the targets are self-luminous and are observed optically. The optics view past the luminous targets into a cooled cavity in the opposite furnace wall. The self-luminous targets are then visible against a dark background. To obtain data below 2000°F, a light beam is directed from behind the flags providing a shadow image for the detection system.

The image of the flowing target is focused through a rotating shutter (chopper) and onto a rectangular aperture. Small slits in the aperture pass a portion of the upper and lower edges of the light beam. A photocell receives the light thus transmitted, and an electronic circuit detects whether the energy passed by the two slits is equal. A servo drives the apertures to let a balanced quantity of light pass through the two slits and thus maintains an optical null.

To obtain lateral strain, a strain analyzer is supported horizontally on the tensile frame to view the diametrical or lateral strain of the specimen. A flag attachment, with the general configuration as shown in Figure 8, was developed to follow and transmit lateral motions of up to a few mils. The three-piece assembly consists of a ring and two rams bearing on the specimen.

Calibrations of the analyzers are performed in various ways including absolute correlations to precision micrometers, strain gage extensometers, and direct plots of stress-strain for reference materials such as steel, plexiglas, magnesium, and aluminum. Precision is within  $\pm 0.000020$  inch.

Instrumentation includes primarily a stress-strain measurement system composed of a 1000-pound SR-4 Baldwin load cell, constant d. c. voltage power supply, two optical strain analyzers, and two X-Y recorders. Specimen temperature is monitored with an optical pyrometer. Stress (load) is measured by a commercial load cell. The cell receives a constant d.c. voltage input from the power supply and transmits a millivolt signal (directly proportional to load) to an X-Y recorder. Simultaneously, the optical strain analyzers measure both the axial and lateral strain and transmit a millivolt signal (proportional to strain) to the X-Y recorders. Thus, continuous plots of stress-axial strain and axial strain-lateral strain are recorded simultaneously.

11/69  
200

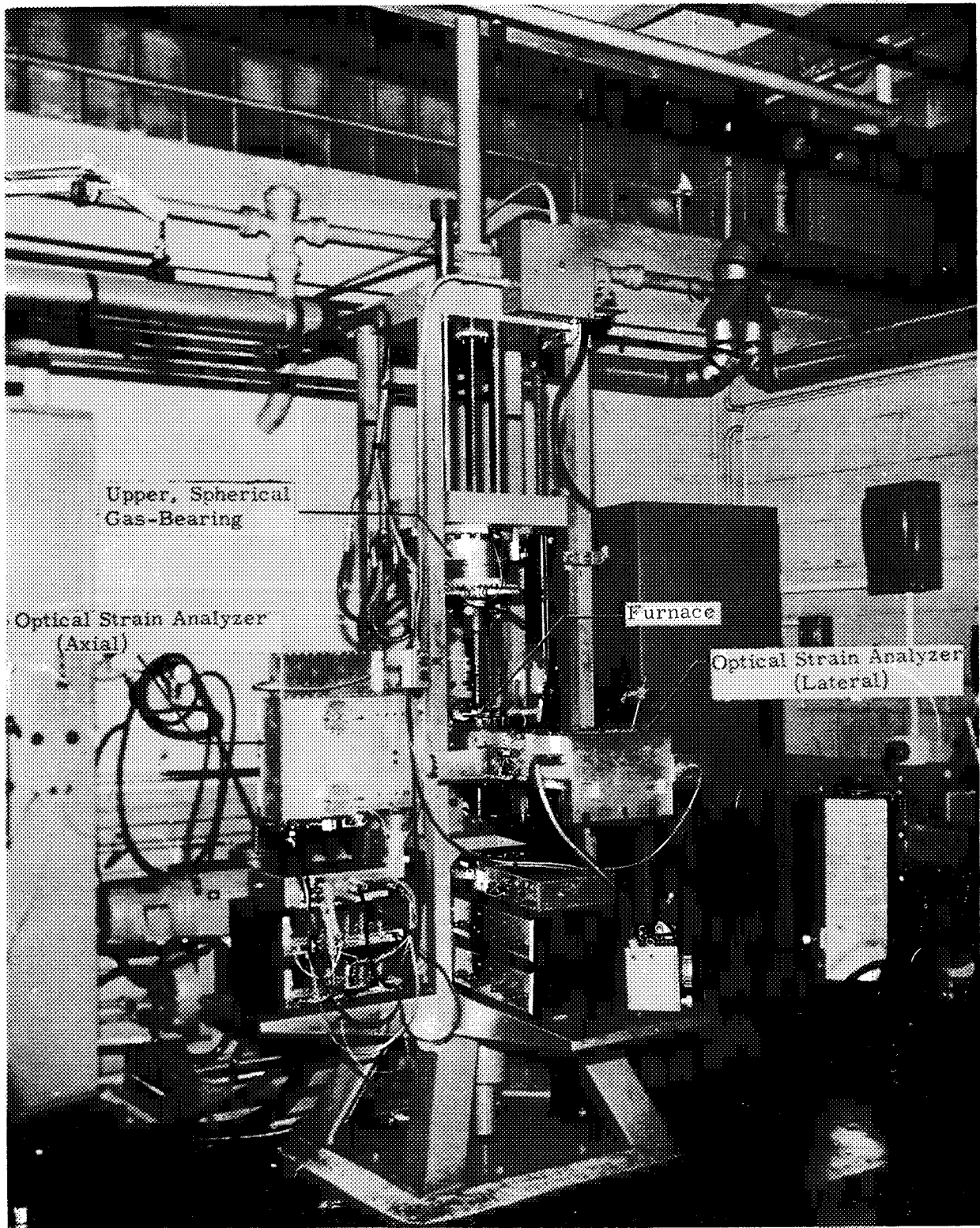


Figure 1. Picture of a Tensile Stress-Strain Facility





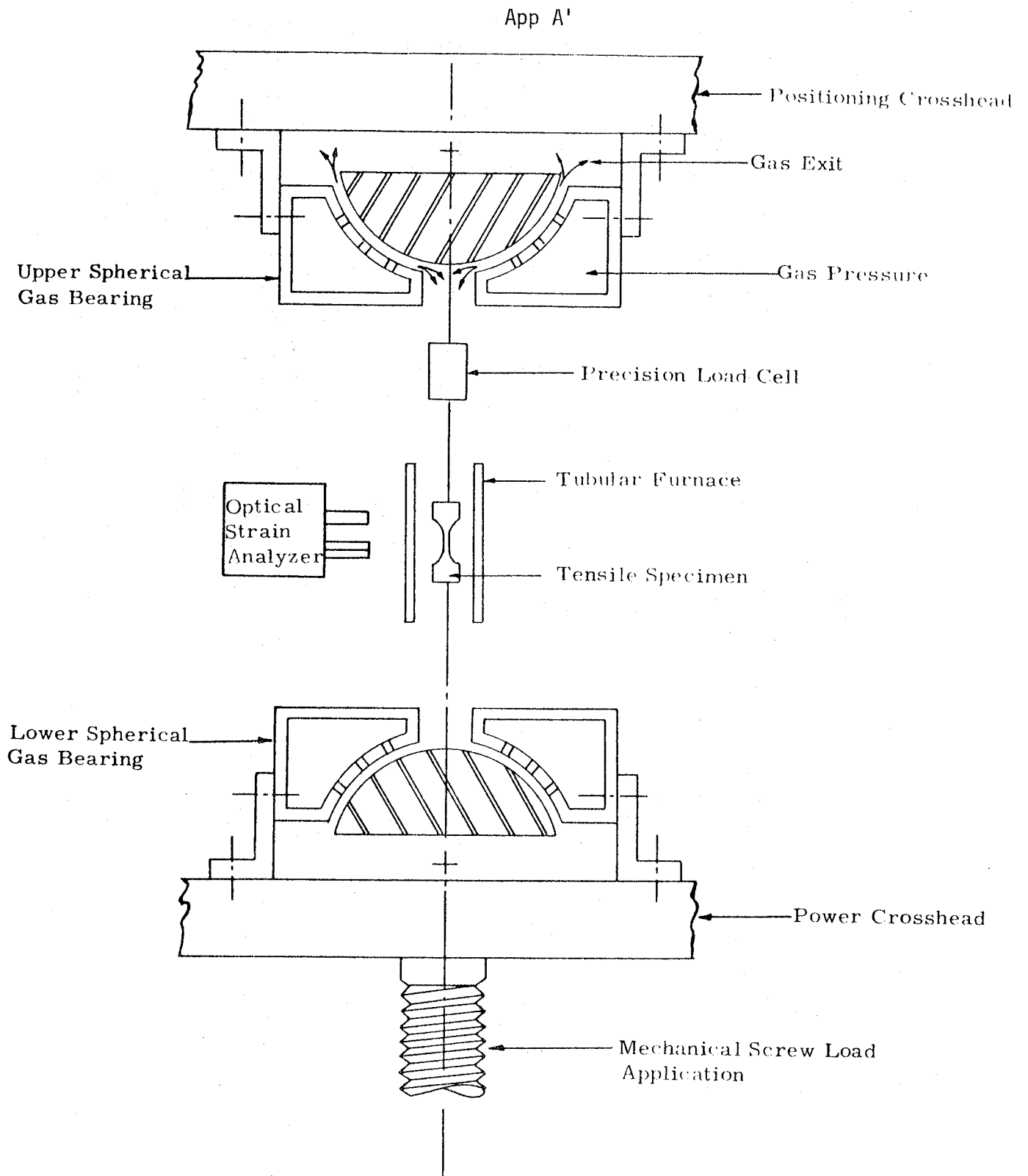


Figure 2. Schematic Arrangement of Gas-Bearing Universals, Specimen, Load Train, and Grips

Notes:

1. All Diameters True and Concentric to Within 0.0005"
2. Do Not Undercut Radii At Tangent Points
3. Both Ends Flat and Perpendicular to and to Within 0.0005"
4. All Dimensions are in Inches
5. Tolerances are  $\pm 0.001$  on Diameters  
 $\pm 0.005$  on Lengths  
 $\pm \frac{1}{64}$  on Fractions

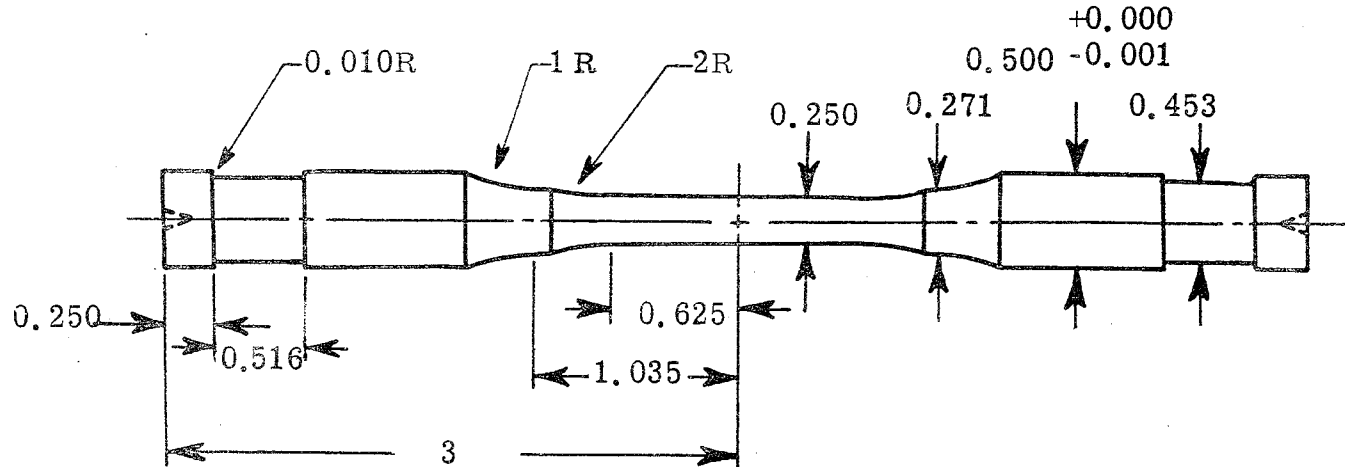


Figure 3. Tensile Specimen Configuration

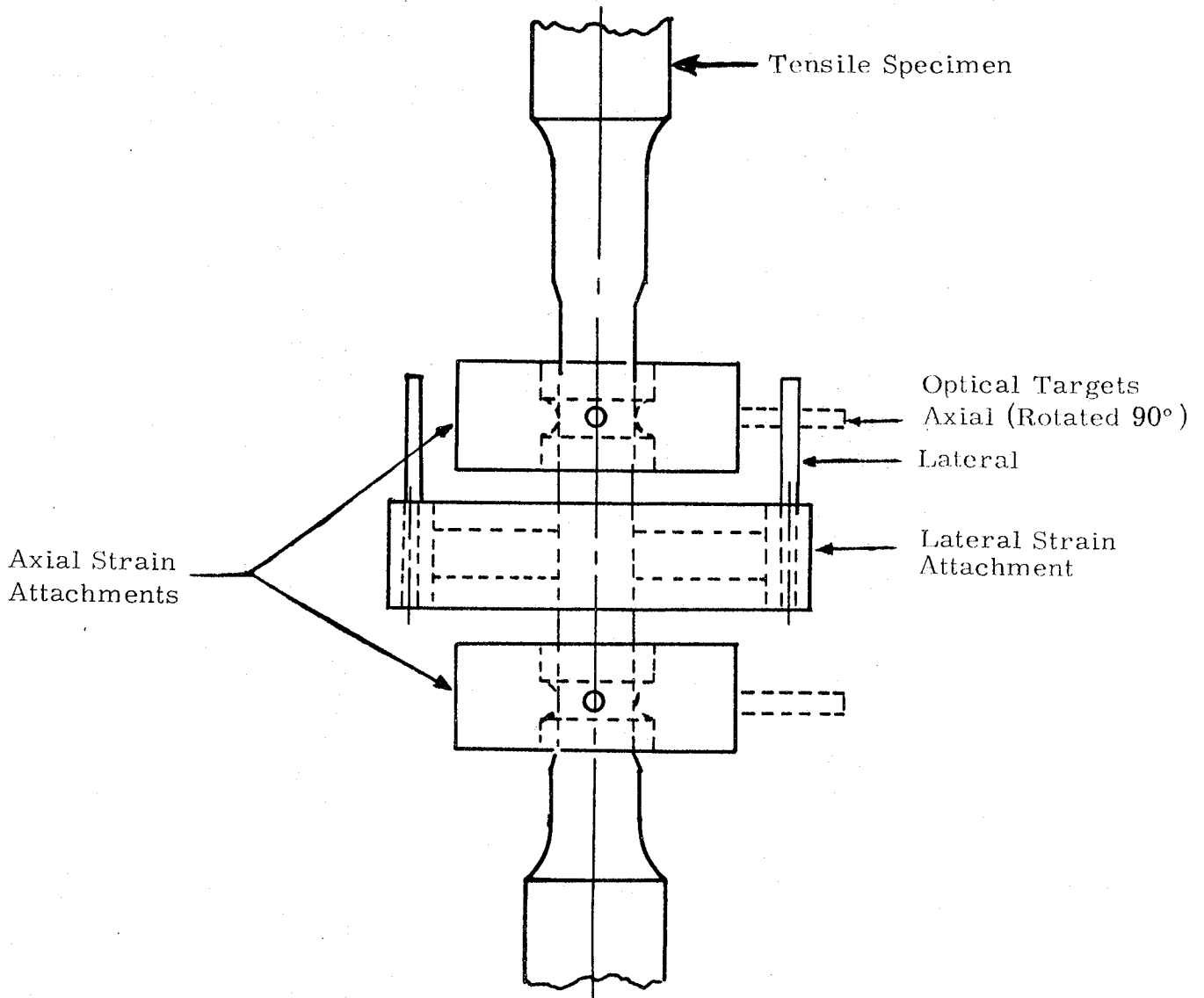


Figure 4. Location of the Flag Attachments on the Tensile Specimens

App A'

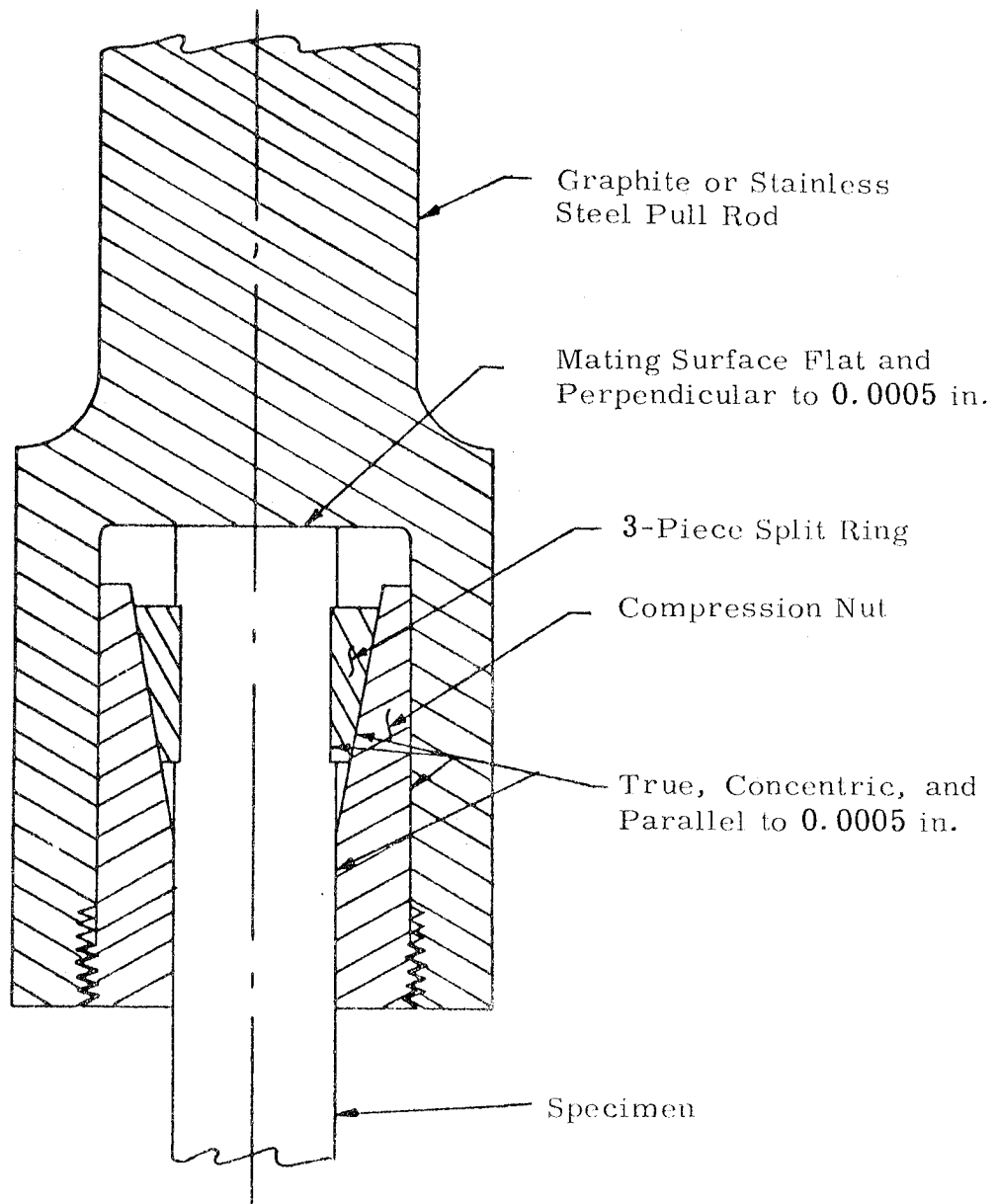
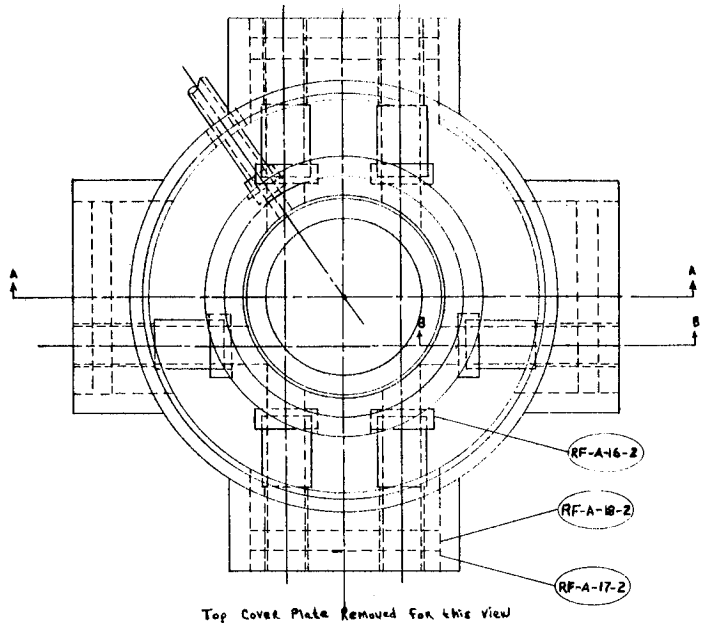
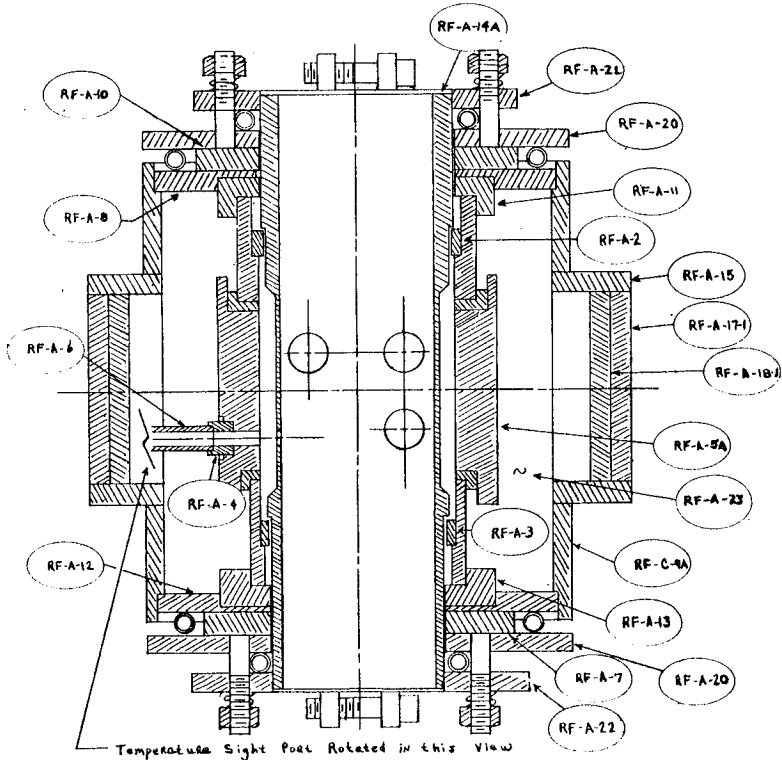


Figure 5. Precision Collet Grip for Tensile Specimens 2:1 Scale

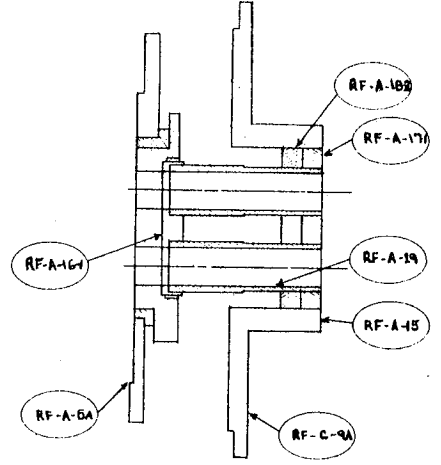
# App A'



Assy.	Item	Quan.	Description
A-2	1	1	Top pyrolytic graphite ring
A-3	1	1	Bottom pyrolytic graphite ring
A-4	1	1	Pyrolytic graphite temperature sight plate
A-5A	1	1	CS graphite protector tube
A-6	1	1	CS graphite temperature sight tube
A-7	1	1	Bottom Micarta insulating disc
A-8	1	1	Top steel base plate
C-9A	1	1	Steel shell
A-10	1	1	Top Micarta insulating disc
A-11	1	1	Top zirconia disc
A-12	1	1	Bottom steel base plate
A-13	1	1	Bottom zirconia disc
A-14A	1	1	CS graphite heater tube
A-15	2	2	Steel sight port tube
A-16-1	2	2	CS graphite sight port plate
A-16-2	2	2	CS graphite sight port plate
A-17-1	2	2	Firebrick sight port plate
A-17-2	2	2	Firebrick sight port plate
A-18-1	2	2	Zirconia sight port disc
A-18-2	2	2	Zirconia sight port disc
A-19	4	4	CS graphite sight tube
A-20	2	2	Fiberfrax insulator
A-21	1	1	Top electrode
A-22	1	1	Bottom electrode
A-23	1	1	Thermatomic carbon



Section A-A



Section B-B

Figure 6. Small 5500° F Graphite Resistance Furnace



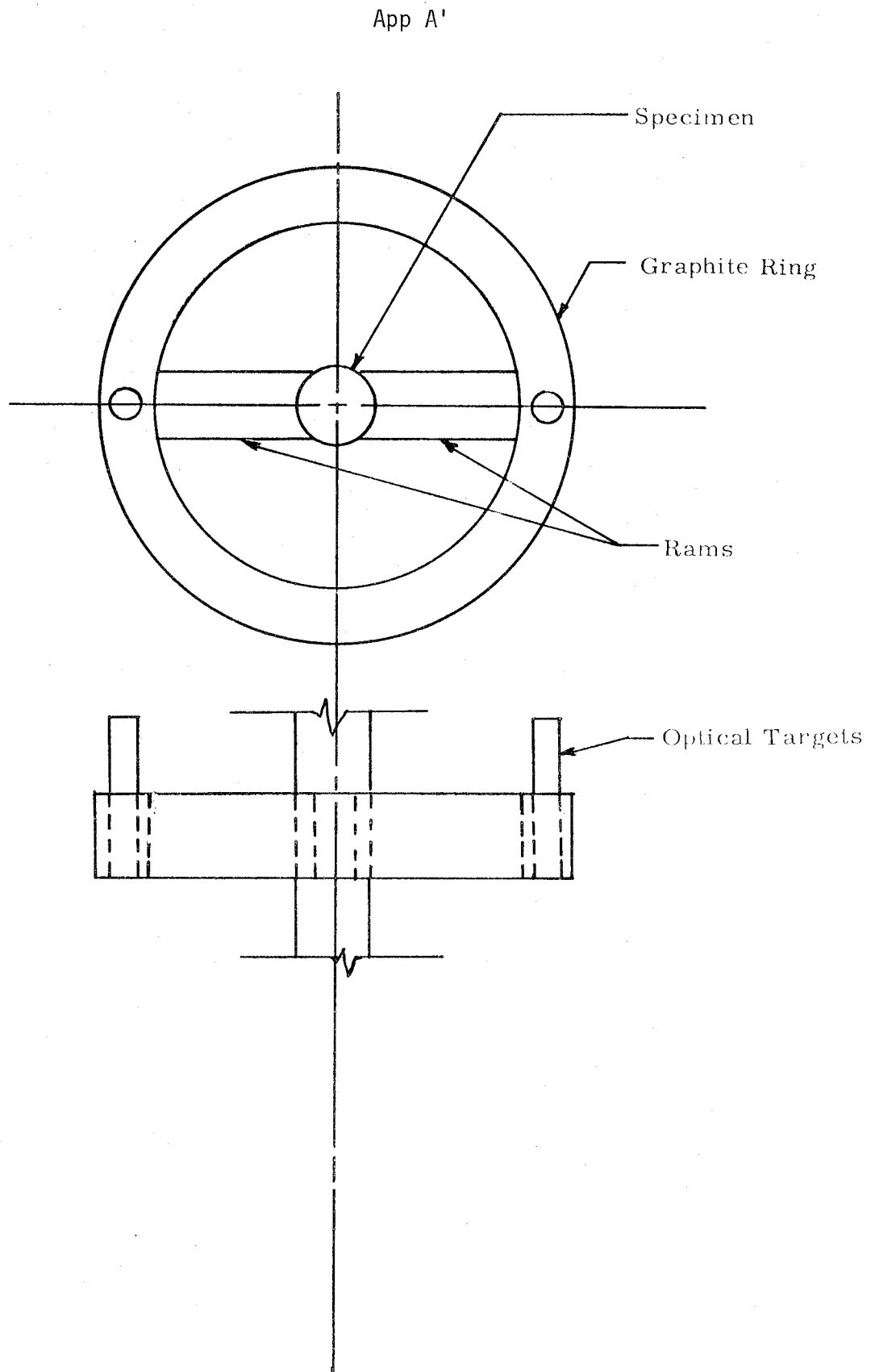


Figure 8. General Configuration of the Flag Attachment to Monitor Lateral Strain in Tension





## APPENDIX B'

### ULTIMATE STRENGTH, ELASTIC MODULUS, AND POISSON'S RATIO TO 5500°F IN COMPRESSION

The compressive apparatus is shown in the photograph in Figure 1 and in the schematic in Figure 2 and consists primarily of a load frame, gas bearings, load train, 50-ton screw jack, variable speed mechanical drive system, strain analyzers, 5500°F furnace, and associated instrumentation for the measurement of load and strain.

The load frame is similar to most standard frames. It was designed to carry a maximum load of 100,000 pounds and to support the furnace, optical strain analyzers, and other related equipment.

Gas bearings are installed at each end of the load train to permit precise alignment of the loading train to the specimen. The upper bearing is spherical on a radius of 6.5 inches. This radius is the distance from the top of the specimen to the spherical bearing surface. The load train, not the specimen, shifts to maintain radial alignment. The lower bearing is flat and is about 6 inches in diameter. The lower bearing permits transverse alignment of the load train. The gas bearings are floated for only a small initial amount of load so that precise alignment of the load train can be attained.

The load train near the furnace consists of the specimen loaded on each side by graphite and water-cooled steel push rods. The graphite push rods are counter-bored to permit insertion of a pyrolytic graphite disc which serves as a heat dam and to align the specimen to the center-line of the load train. Extreme care is exercised in the preparation of all parts of the load train to ensure concentricity of the mating parts to less than 0.0005 inch.

The 50-ton jack is a power screw type. The mechanical drive system consists of a gear reducer driven by a Louis Allis Synchro-Spede Unit (300-3000 rpm). The gear reducer is connected to the Synchro-Spede Unit through a chain coupling and to the 50-ton jack by a single roller chain and sprocket system. Different load rates are obtained by adjustment of the variable speed setting on the Synchro-Spede and by changeout of sprockets on the gear reducer and screw jack.

## App B'

Figure 3 shows details of the "dumbbell" specimen which maintains a 0.500 inch diameter over the 1.2 inch long gage section. The specimen provides sufficient room for the flag attachments that follow the axial and lateral strains and also minimizes the influence of end restraint.

The flag attachments for the measurement of axial strain are positioned one inch apart so that unit strain is recorded directly. The flag attachment for the measurement of lateral strain is positioned between the flags for axial strain; see Figure 4. The lateral flag attachment used in compression is shown in Figure 5. The 4-piece assembly consists of a ring, two rams bearing on the specimen, and a screw to adjust the contact pressure. The ring was designed to track lateral motions as great as 0.030 inch without breaking.

The furnace and strain measurement system is the same as described in Appendix A'.

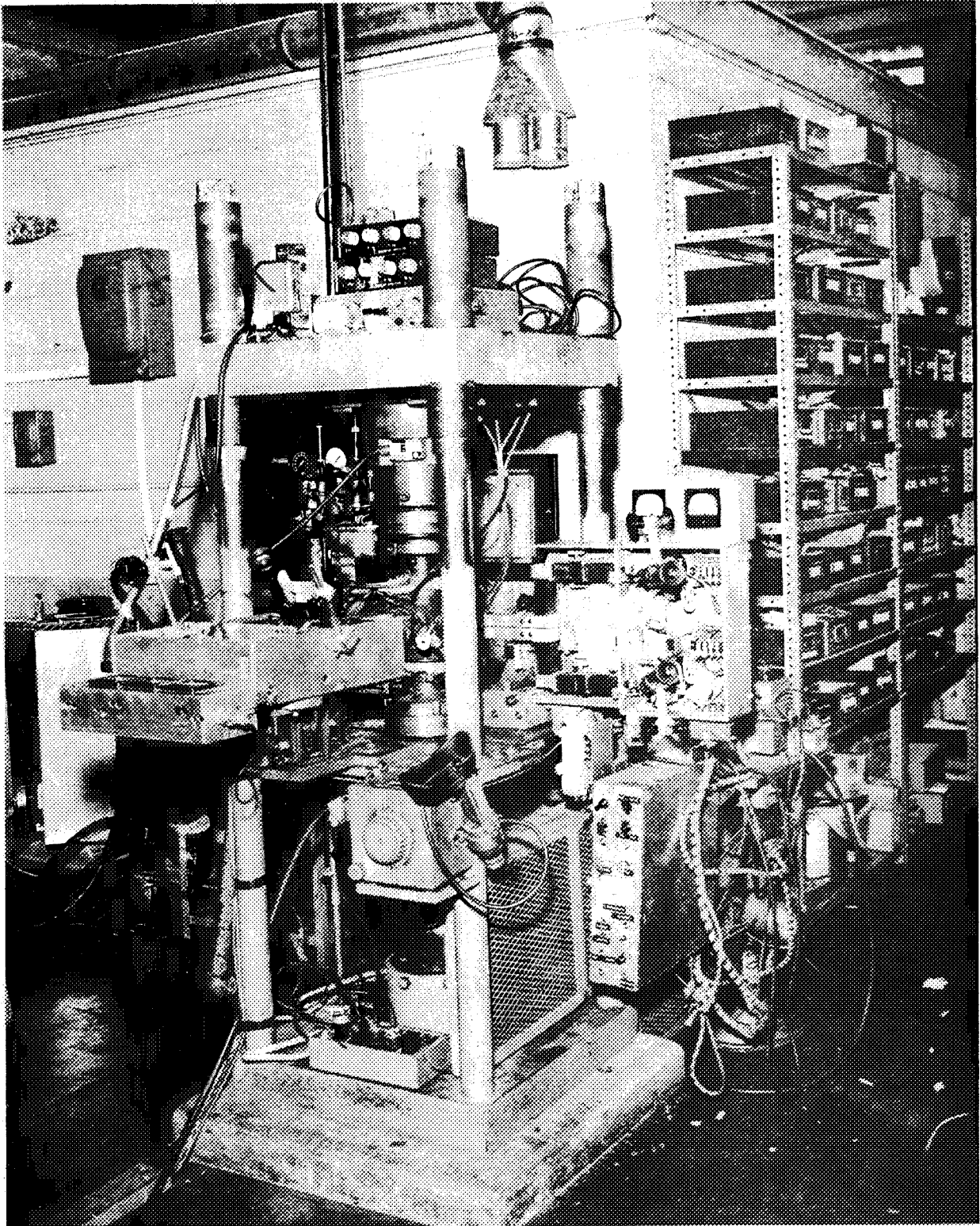


Figure 1. Picture of the Compressive Facility with Gas Bearings and Optical Strain Analyzer

App B'

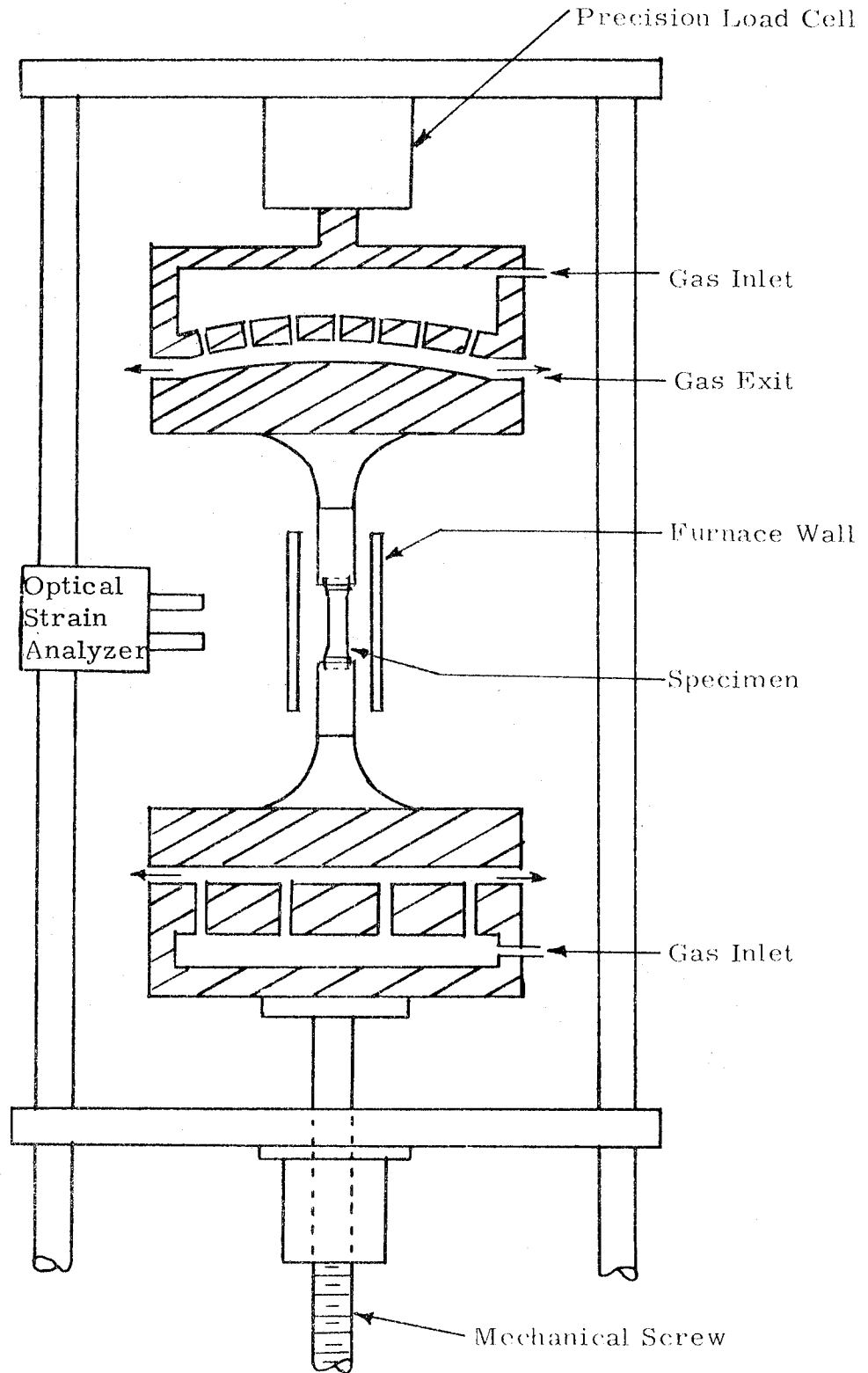


Figure 2. Schematic Arrangement of Gas-Bearing Universals, Specimen, and Load Train

App B'

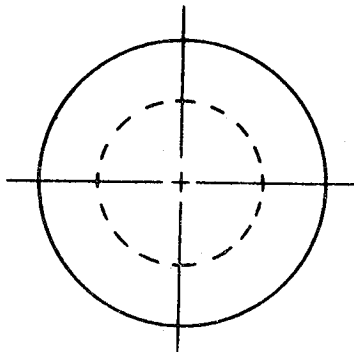
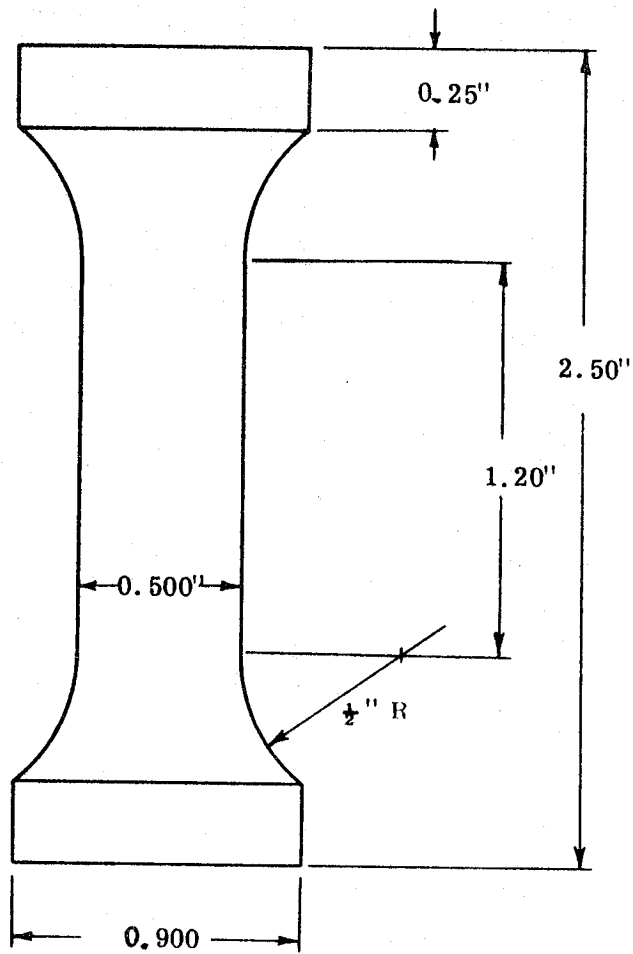


Figure 3. Compressive Specimen Configuration

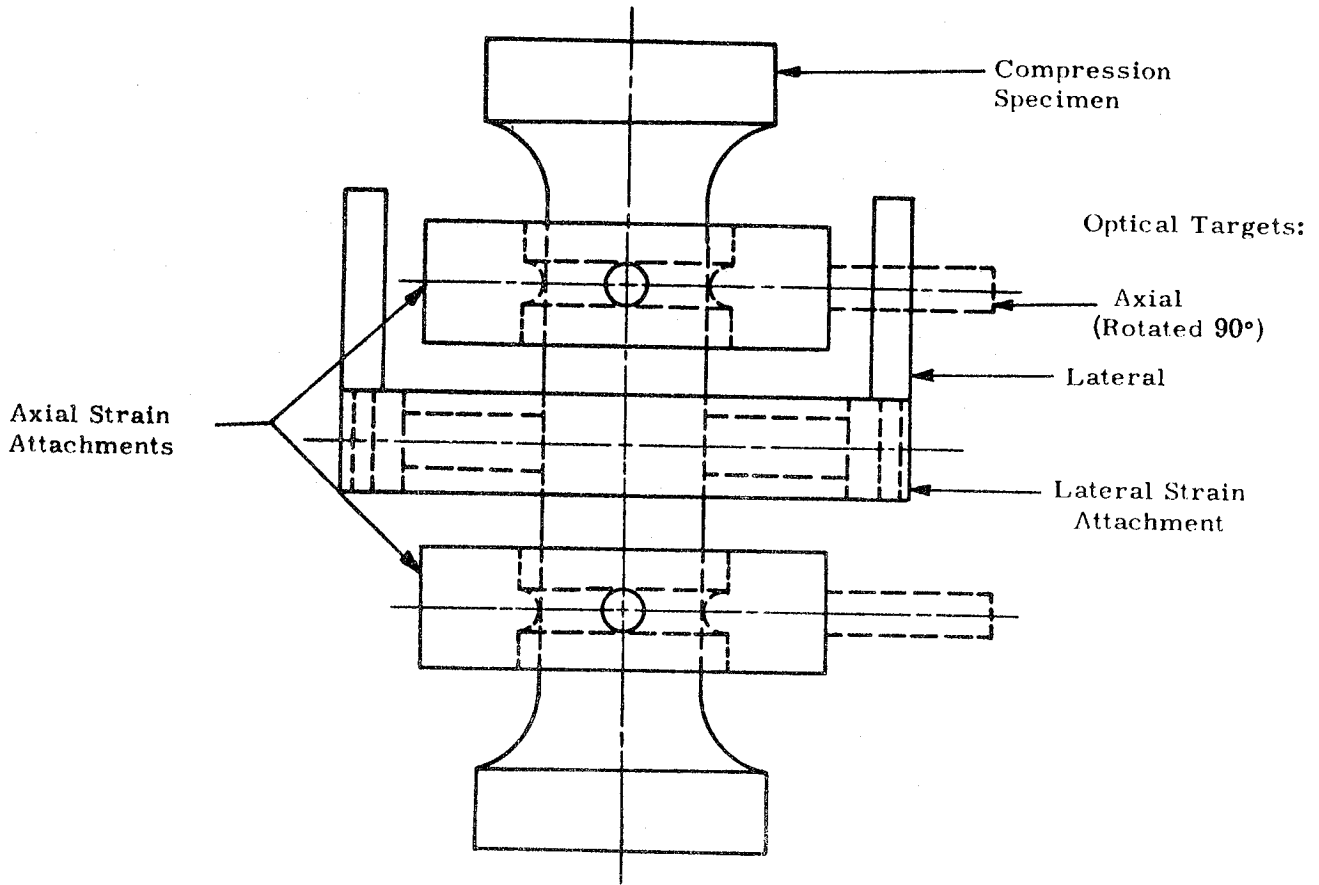


Figure 4. Location of the Flag Attachments on the Compressive Specimen

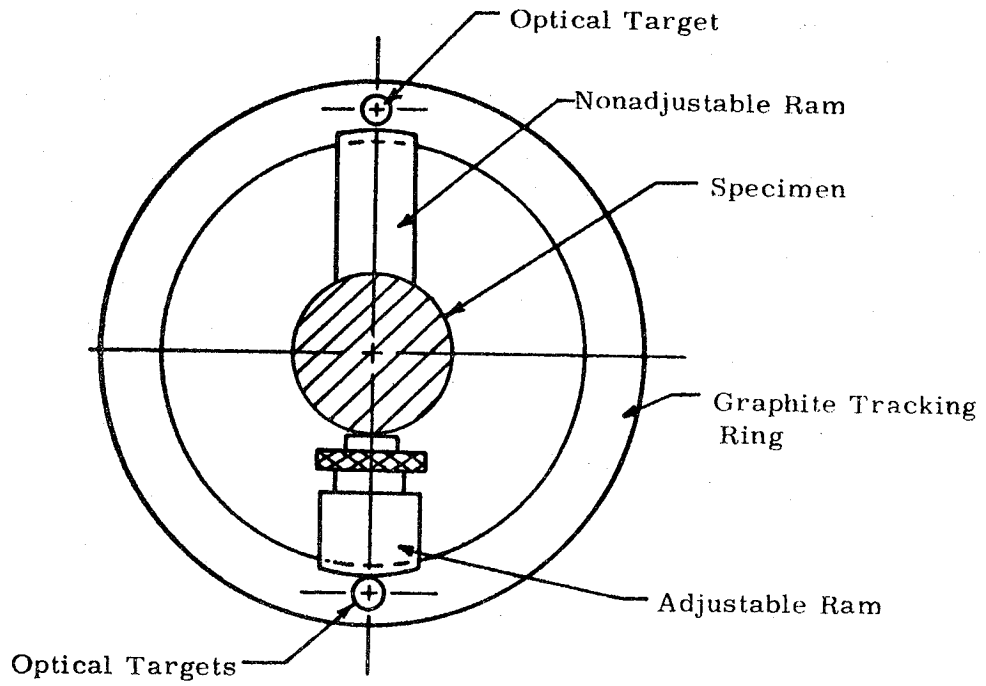


Figure 5. Lateral Strain Flag Attachment for Compressive Specimen





## APPENDIX C

### A COMPARATIVE ROD APPARATUS FOR MEASURING THERMAL CONDUCTIVITY TO 2000°F

Southern Research Institute's comparative rod apparatus is used to measure thermal conductivities of a wide variety of materials from -300°F to 2000°F. This apparatus, shown schematically in Figure 1, consists basically of two cylindrical reference pieces of known thermal conductivity stacked in series with the cylindrical specimen. Heat is introduced to one end of the rod, composed of the references and specimen, by a small electrical heater. A cold sink or heater is employed at the opposite end of the rod as required to maintain the temperature drop through the specimen at the preferred level. Cylinders of zirconia may be inserted in the rod assembly to assist in controlling the temperature drop. Radial losses are minimized by means of radial guard heaters surrounding the rod and consisting of three separate coils of 16, 18 or 20-gage Kanthal wire wound on a 2 or 4-inch diameter alumina core. The annulus between the rod and the guard heaters is filled with diatomaceous earth, thermatomic carbon, bubbled alumina or zirconia powder. Surrounding the guard is an annulus of diatomaceous earth enclosed in an aluminum or transite shell.

The specimens and references (see Figure 2) are normally 1-inch diameter by 1-inch long. Thermocouples located 3/4 inch apart in radially drilled holes measure the axial temperature gradients. Thermocouples located at matching points in each guard heater are used to monitor guard temperatures, which are adjusted to match those at corresponding locations in the test section.

In operation, the apparatus is turned on and allowed to reach steady state. The guard and rod heaters are adjusted to minimize radial temperature gradients between the rod and guard sections consistent with maintaining equal heat flows in the references. Temperatures are measured on a Leeds and Northrup Type K-3 potentiometer, and the temperature gradients calculated. A typical temperature profile in the test section is shown in Figure 3.

The thermal conductivity of the specimen is calculated from the relation

$$K_S = \frac{K_1 \Delta T + K_2 \Delta T}{2 \Delta T_S} \frac{\Delta X_S}{\Delta X_R}$$

## App C'

where  $K_1$  and  $K_2$  are the thermal conductivities of the upper and lower references;  $\Delta T_1$ ,  $\Delta T_2$  and  $\Delta T_S$  are the temperature differences in the upper and lower references and specimen, respectively;  $\Delta X_S$  and  $\Delta X_R$  are the distances between thermocouples in the specimen and references.

Note that for purely axial heat flow, the products  $K_1 \Delta T_1$  and  $K_2 \Delta T_2$  should be equal. Due to imperfectly matched guarding and other factors, this condition is seldom attained in practice; therefore, the average of the two values is used in the calculations. Their difference is maintained as small as possible, usually within 5 percent of the smaller.

For identical specimens, the ratio  $\Delta X_S / \Delta X_R$  should be unity but may vary due to the uncertainty in hole locations. To prevent introducing an additional error in calculations,  $\Delta X$  is determined as follows: the depth of the hole is measured by inserting a snugly fitting drill rod in the hole, measuring the projecting length and subtracting it from the total length of the rod. The slope, or angle the hole makes with the perpendicular to the specimen axis, is determined by making measurements to the face of the hole and the outer end of the drill rod with respect to a datum plane, using a dial gage. From these measurements, the location of the bottom of the hole can be calculated.

Generally, measurements with the comparative rod apparatus are performed in an inert helium environment. The apparatus can also be operated in vacuum and at gas pressures of up to 100 psig. We have had experience operating under all conditions.

The primary reference materials which we use are Code 9606 Pyroceram and Armco iron for measurements on materials with low and high thermal conductivities, respectively. Primary standard reference sets are kept and are used to calibrate other references made from the same materials. The standards of Code 9606 Pyroceram were made from a batch of material which NBS purchased shortly after their measurements on a sample of Code 9606 Pyroceram. The curve which Flynn presented for the thermal conductivity of the Pyroceram is given in Figure 4.<sup>1</sup> Note that the curve is in good

---

<sup>1</sup> Robinson, H. E. and Flynn, D. R., Proceedings of Third Conference on Thermal Conductivity, pages 308-321, 1963 (with author's permission)

agreement with the recommended values from NSRDS-NBS 8<sup>2</sup>. The standards of Armco iron were made from the stock which was used in the round-robin investigations from which Powell<sup>3</sup> developed the most probable values for Armco iron. The curve used for the Armco iron standards is shown in Figure 5. Powell estimated the uncertainty to be within  $\pm 2$  percent over the temperature range from 0° to 1000°C. Note in Figure 5 that numerous evaluations of Armco iron from other batches of material have agreed within  $\pm 3$  percent (coefficient of variation about curve) with Powell's original data.

In addition to Code 9606 Pyroceram and Armco iron, several other materials have been used as references. These include copper for high conductivity specimens, 316 stainless steel for specimens of intermediate thermal conductivity and Teflon or Pyrex for low conductivity materials.

Copper references have been calibrated against Armco iron and excellent agreement with literature data has been obtained. Thermal conductivity values obtained from calibrations of 316 stainless steel against Pyroceram, Armco iron and a set of 316 stainless steel standards are presented in Figure 6. Note the consistency of the data obtained with the three different sets of references. The coefficient of variation of the data shown in Figure 6, about the curve value, was  $\pm 3.3$  percent. These data indicate the internal consistency of the stainless steel and the reference materials. Note that the thermal conductivity values for 316 stainless steel presented in Figure 6 lie between values reported by several steel manufacturers and Lucks and Deem.<sup>4</sup>

The calibrations indicate that for materials with moderate to high thermal conductivities the apparatus operates with a precision of about  $\pm 3$  percent and a total uncertainty of about  $\pm 5$  percent at temperatures above 0°F if temperatures between the guard and test section are closely matched. Below 0°F, the precision achieved to date has been about  $\pm 7$  percent with a total uncertainty of about  $\pm 10$  percent. We anticipate that the precision and uncertainty at cryogenic temperatures can be improved by additional calibrations.

---

<sup>2</sup> Powell, R. W., C. Y. Ho and P. E. Liley, Thermal Conductivity of Selected Materials, NSRDS-NBS 8, Department of Commerce, November 25, 1966.

<sup>3</sup> Powell, R. W., Proceedings of Third Conference on Thermal Conductivity, pages 322-341, 1963.

<sup>4</sup> WADC TR58-476, "The Thermophysical Properties of Solid Materials", Armour Research Foundation, November, 1960.

Some additional data obtained on the comparative rod apparatus are shown in Figures 7 and 8. Figure 7 shows thermal conductivity data for ATJ graphite, with grain, using Armco iron as the reference material. These data show excellent agreement with earlier data obtained here and by other sources<sup>5-7</sup>. The maximum scatter of the comparative rod points was about 5 percent.

Figure 8 shows data for thermocouple grade constantan obtained on the comparative rod apparatus using Armco iron references and on Southern Research Institute's high temperature radial inflow apparatus. Note the excellent agreement. These data also show close agreement with data obtained by Silverman<sup>4</sup> on an alloy of very similar composition.

---

<sup>5</sup> ASD-TDR-62-765, "The Thermal Properties of Twenty-Six Solid Materials to 5000°F or Their Destruction Temperatures," Southern Research Institute, August, 1962.

<sup>6</sup> Pears, C. D., Proceedings of Third Conference on Thermal Conductivity, 453-479, 1963.

<sup>7</sup> NSRDS-NBS 16, "Thermal Conductivity of Selected Materials", Part 2, by C. Y. Ho, R. W. Powell and P. E. Liley, National Bureau of Standards, 1968.

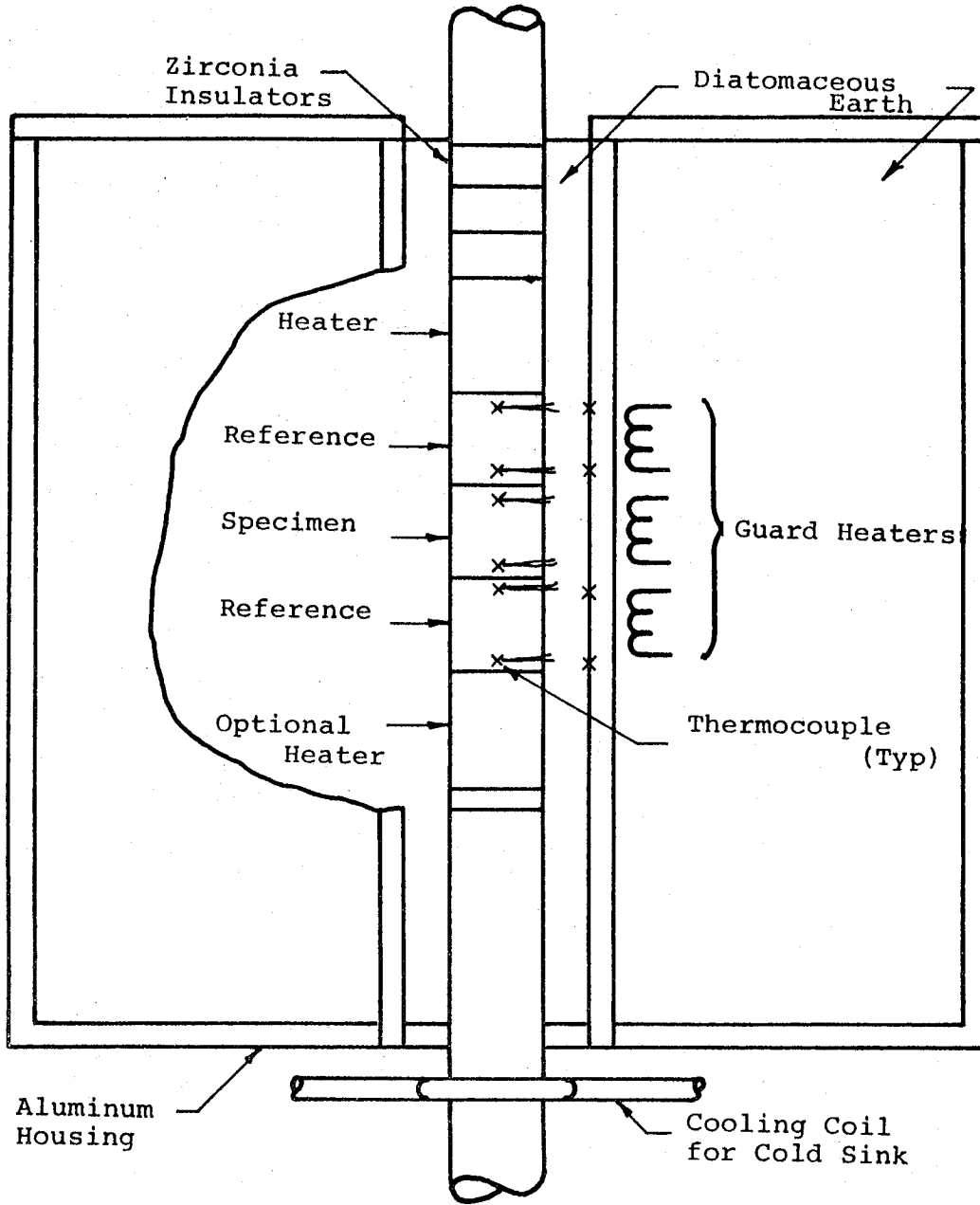
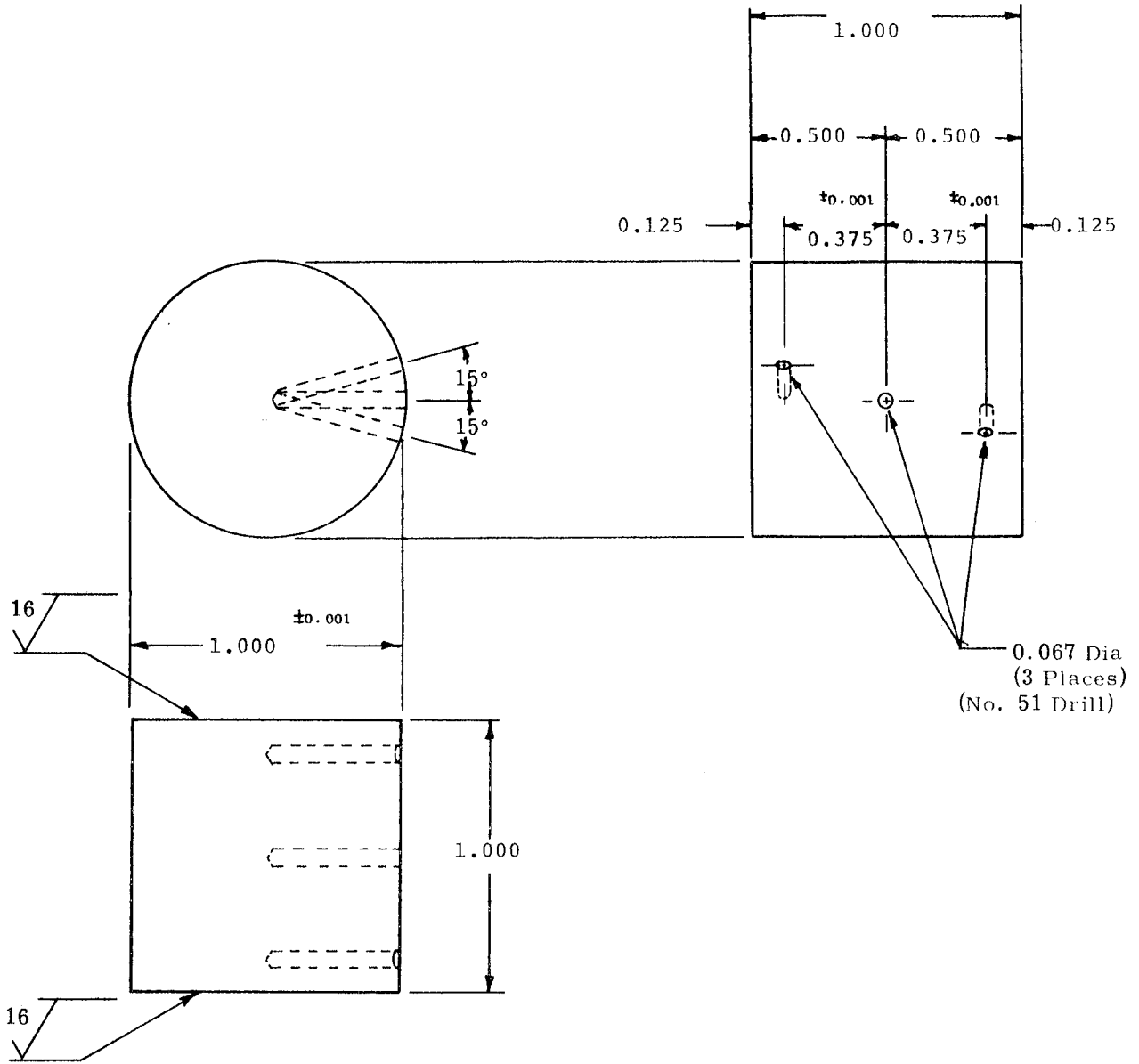


Figure 1. Schematic of Comparative Rod Thermal Conductivity Apparatus



Note: All dimensions  $\pm 0.005$  except where noted

Figure 2. Drawing of Specimen for Thermal Conductivity Measurements in Comparative Rod Apparatus to 1800°F

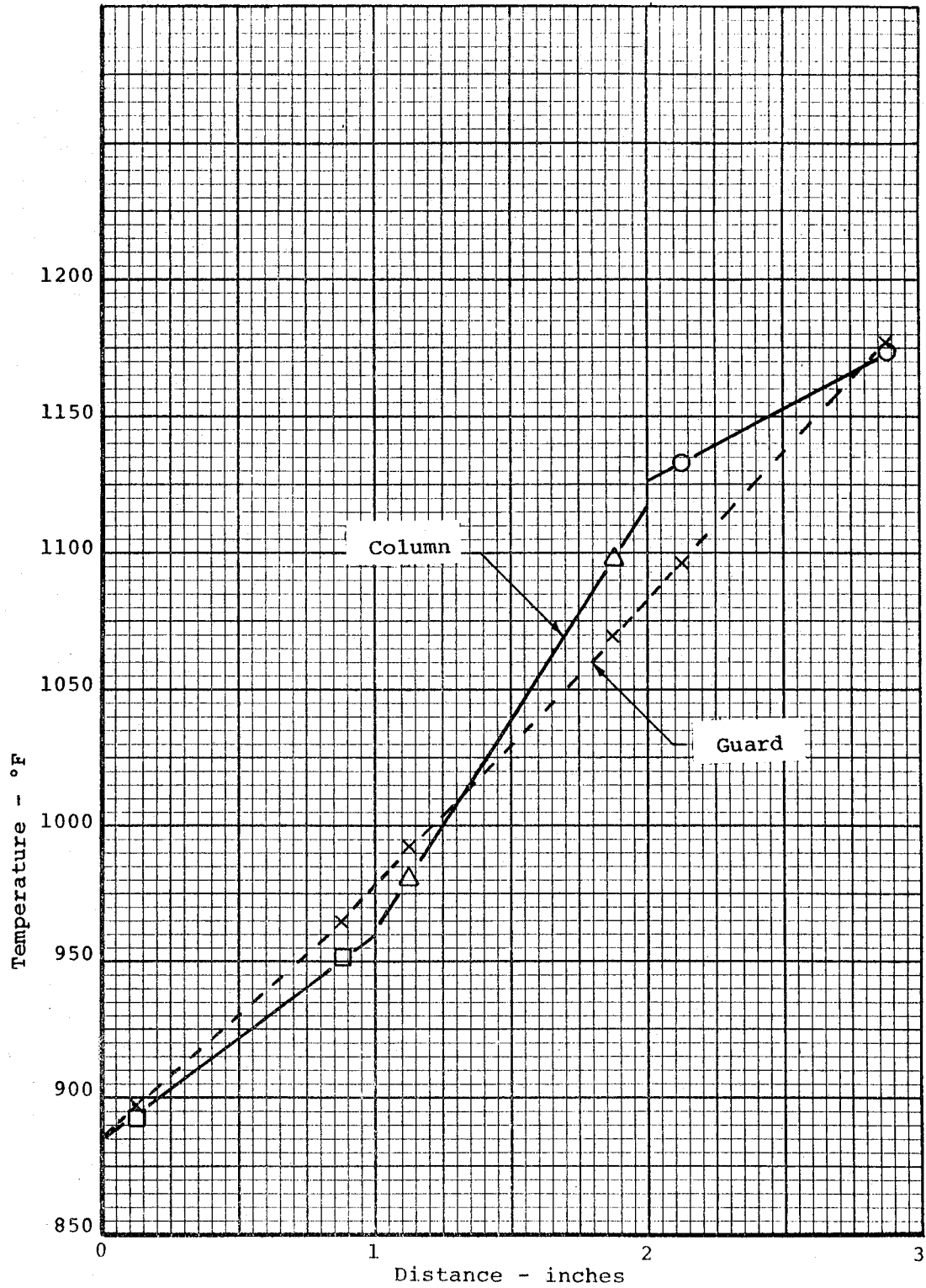


Figure 3. Typical Temperature Profile in Test Section



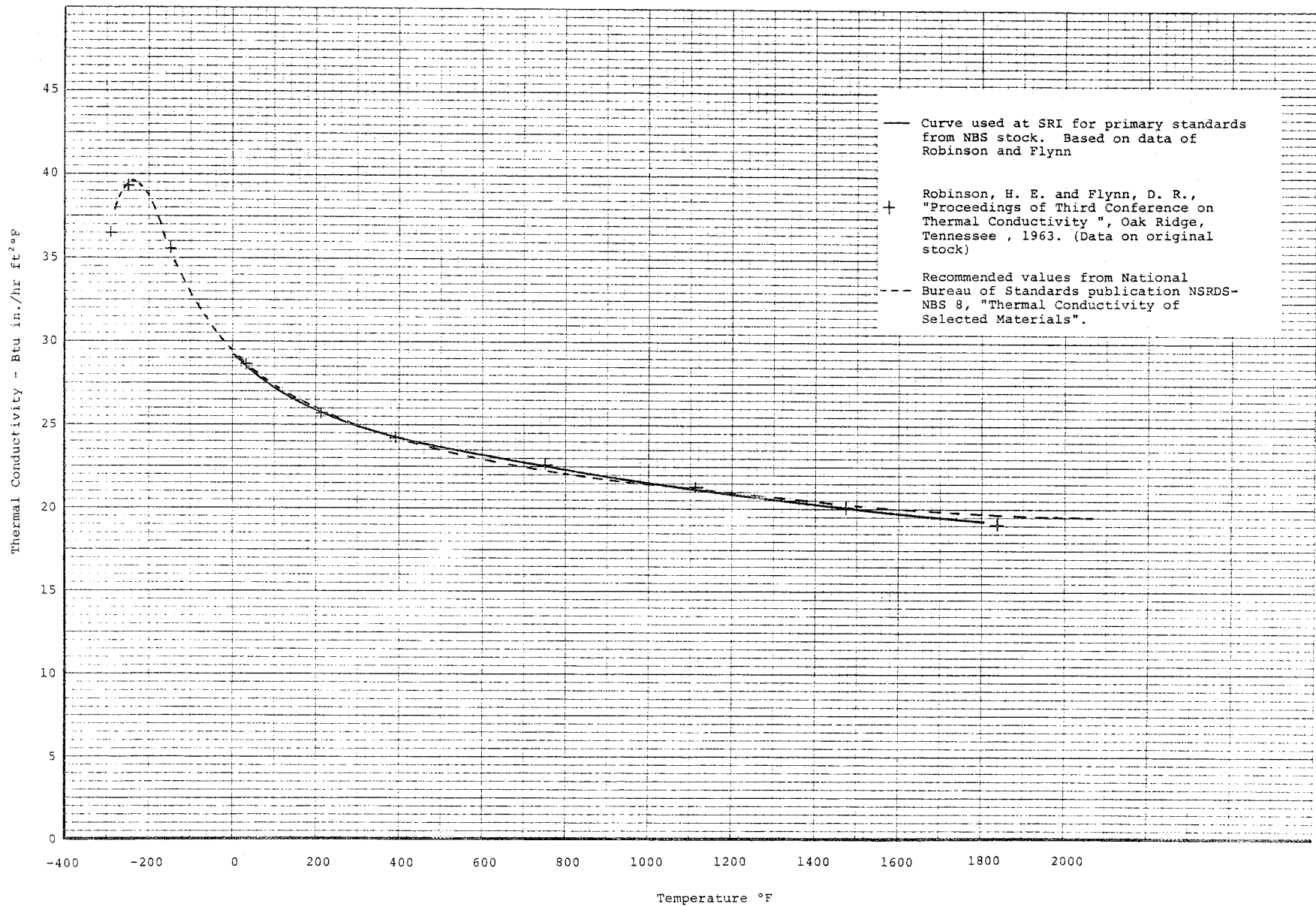
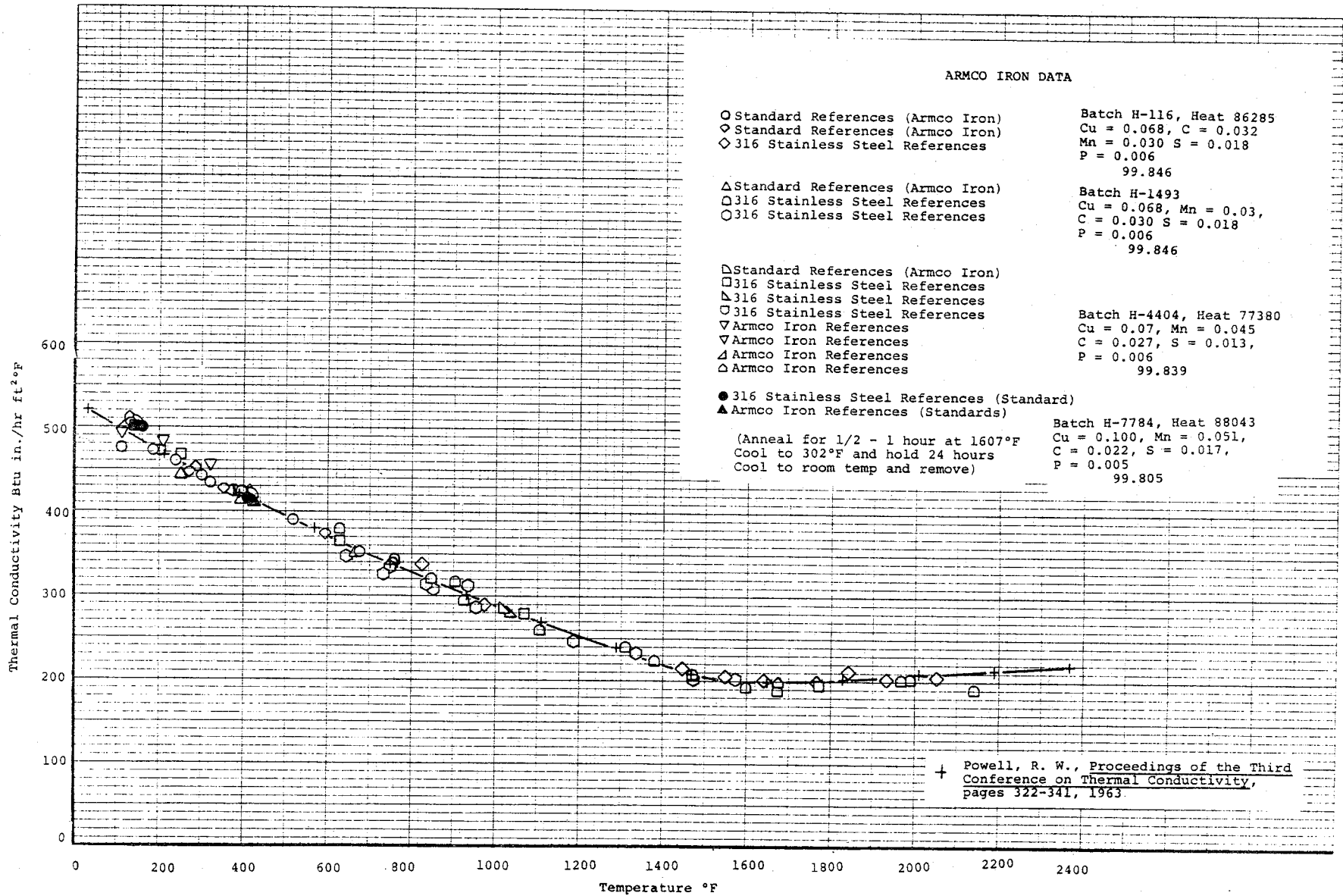


Figure 4. The Thermal Conductivity of Primary SRI Standards from NBS Stock of Code 9606 Pyroceram



App C1

Figure 5. The Thermal Conductivity of Armco Iron

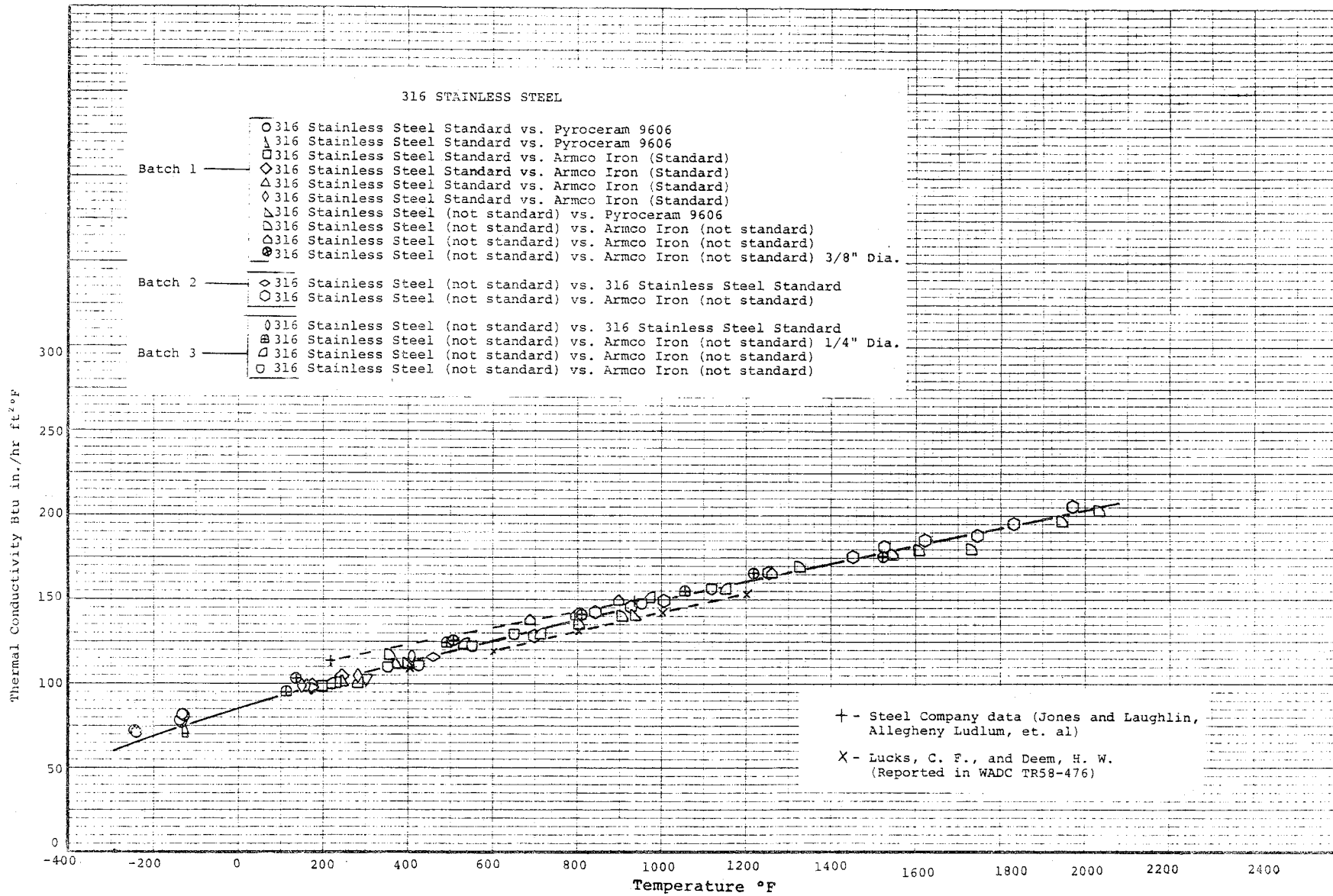


Figure 6. The Thermal Conductivity of 316 Stainless Steel

Thermal Conductivity - Btu in./hr ft<sup>2</sup>°F

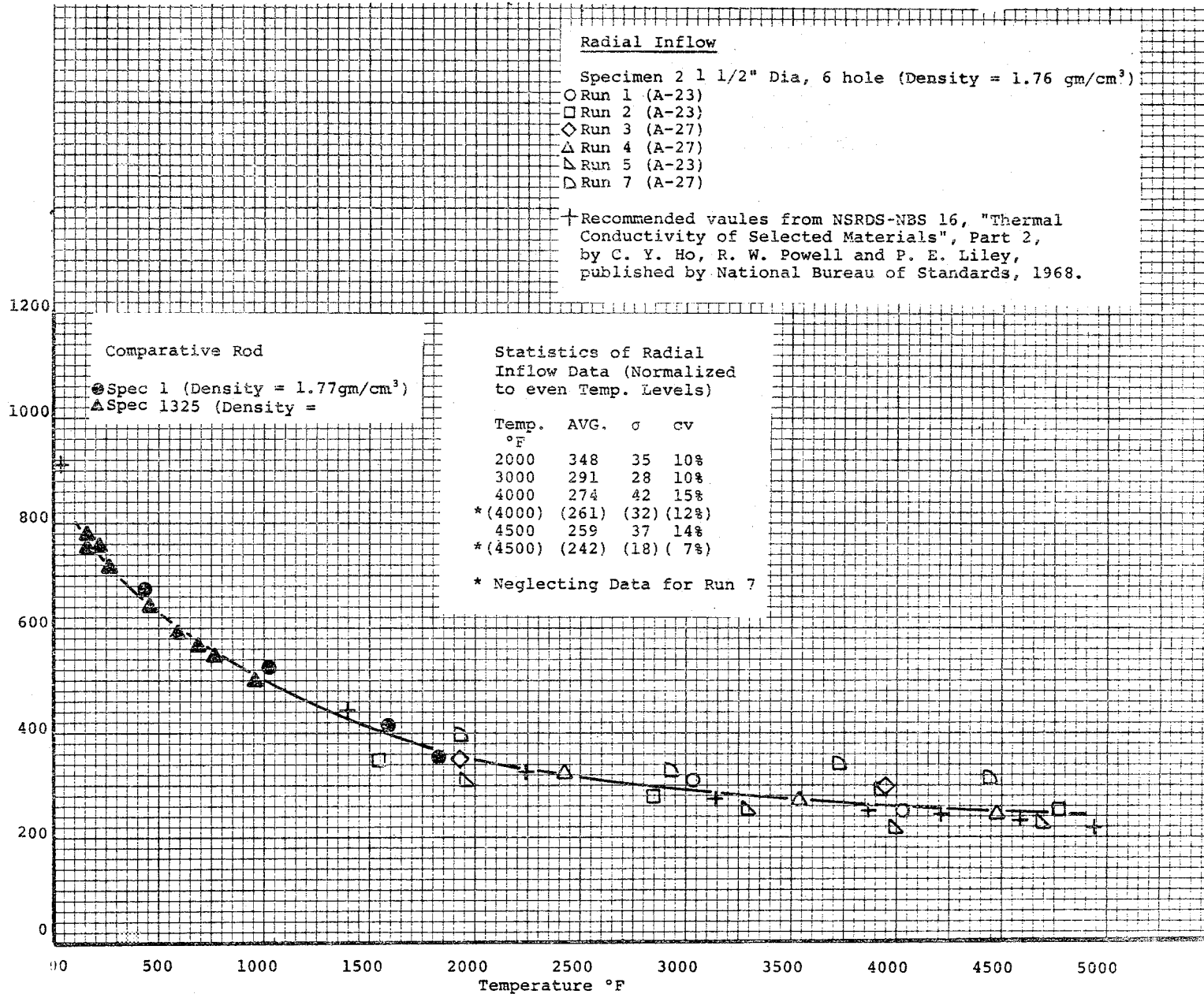


Figure 7. The Thermal Conductivity of ATJ Graphite, With Grain

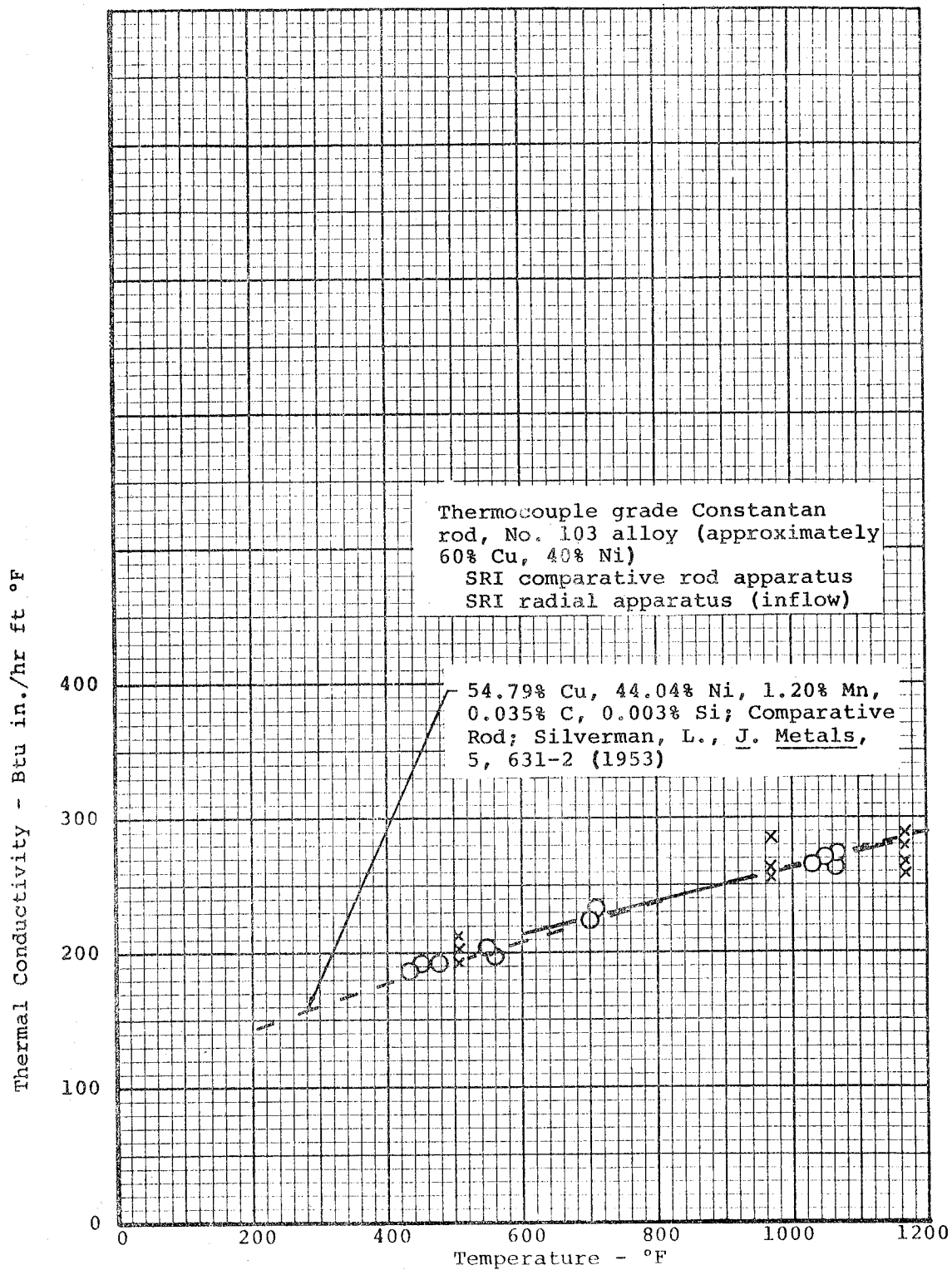


Figure 8. The Thermal Conductivity of Thermocouple Grade Constantan Rod

## APPENDIX D'

### THERMAL CONDUCTIVITY TO 5500°F BY RADIAL INFLOW METHOD

The thermal conductivity is determined with a radial heat inflow apparatus that utilizes a central specimen 1" long. This apparatus is normally employed for measurements over the temperature range from 1500°F to 5500°F. Comparative rod apparatus is used at temperatures below 1500°F where radiant heating is less effective. The radial inflow apparatus gives a direct measurement of the thermal conductivity rather than a measurement relative to some standard reference material. A picture of the apparatus ready to be installed in the furnace is shown in Figure 1. The furnace and associated equipment for the thermal conductivity work is shown in Figure 2. In addition to the specimen, the apparatus consists primarily of (1) a water calorimeter that passes axially through the center of the specimen, (2) guards made from the same specimen material at both ends of the specimens to reduce axial heat losses, (3) sight tubes that allow the temperature at selected points in the specimen to be determined either by thermocouples or optical pyrometer and (4) an external radiant heat source (see Figure 3). The water calorimeter provides a heat sink at the center of the specimen to create a substantial heat flow through the specimen and allows the absolute value of the heat flow to be determined. Thermocouples mounted 1/2" apart in the calorimeter water stream measure the temperature rise of the water as it passes through the gage portion of the specimen. By metering the water flow through the calorimeter, it is possible to calculate the total radial heat flow through the 1/2" gage section of the specimen from the standard relationship  $Q = MC\Delta T$ .  $M$  is the weight of water flowing per hour,  $C$  is the specific heat of water and  $\Delta T$  is the temperature rise of the water as it passes through the gage section.

The standard specimen configuration is shown in Figure 4. The specimen is 1.062" O.D. x 0.250" I.D. x 1" long. Holes 0.073" in diameter are drilled on radii of 0.233 and 0.437" to permit measurement of the radial temperature gradient. In specimens which are anisotropic in the diametral plane (for example, certain graphites) a second pair of holes is drilled 90° to the first pair. The diameters joining each pair of holes is located to coincide with the principal planes of anisotropy in the material.

A 1/2" long upper guard and a 1/2" long lower guard of specimen material are placed above and below the 1" long specimen to maintain a constant radial temperature gradient throughout the entire specimen length and thereby prevent axial heat flow in the

## App D'

specimen. The outer ends of the specimen guards are insulated with graphite tubes filled with thermatomic carbon. These tubes also hold the specimen in alignment. The combined effect of specimen guards and thermatomic carbon insulation permits a minimum axial temperature gradient within the specimen. This gradient is not detectable by optical pyrometer readings. Visual inspection of the specimens after runs have verified that no large axial temperature gradient exists in the specimen. The guards, made of specimen material, display axial distortion of the isothermal lines for approximately 1/4" from the outer ends before reaching an apparent constant axial temperature.

When sufficient material is available the alternate specimen configuration shown in Figure 5 is employed. This specimen, being 1.5" in diameter, provides a larger gage length (0.357") between temperature wells and allows the installation of three holes on each radius without excessively distorting the radial temperature profiles. Thus this specimen configuration permits a more precise measurement of the average temperature at each radial location. As with the smaller specimen, the location of the temperature wells must be altered for transversely anisotropic specimens.

The annulus between the specimen inside diameter and the 7/32" outside diameter of the calorimeter tube is packed with either copper granules, graphite or zirconia powder. This packing provides a positive method for centering the calorimeter within the specimen and promotes good heat transfer between specimen and calorimeter.

Temperatures up to 2000°F are measured with Chromel/Alumel thermocouples inserted into the specimen through the sight tubes. At high temperatures, the temperatures are measured through the vertical sight tubes using a right-angle mirror device and optical pyrometer.

In Figures 1 and 3 showing a typical conductivity calorimeter apparatus ready for insertion into a furnace for a run, a water-cooled copper section can be seen at the top of the unit. This section provides permanent sight tubes to within about 2-1/2" of the guard specimen, in addition to a permanent mount for the right-angle mirror device used with the optical pyrometer. Within the short zone between the water-cooled section and the top guard, thin-walled graphite sight tubes are fitted. The remainder of the annulus is filled with thermatomic carbon insulation.

During thermal conductivity runs, the following data are recorded: (1) power input, (2) specimen face temperature, (3) specimen temperatures in the gage section at the two radii, (4) temperature of the calorimeter water at two points 1/2" apart axially within the specimen center and (5) water flow rate through the calorimeter. At least 5 readings are made at each general temperature range to determine the normal data scatter and to minimize the error that might be encountered in a single reading.

## App D'

All thermocouple readings are measured on a Leeds and Northrup K-3 null balance potentiometer used in conjunction with a galvanometer of 0.43 microvolts per mm deflection sensitivity. All optically measured temperatures are read with a Leeds and Northrup Type 8622 optical pyrometer. The flow rate of the calorimeter water is measured with a Fischer and Porter Stabl-Vis Flowrater.

The thermal conductivity values are computed from the relation

$$\kappa = \frac{QL}{\Delta T A_{1m}}$$

where  $Q$  is the heat flow to the calorimeter within the specimen gage section,  $A_{1m}$  is the log mean area for the specimen gage length,  $\Delta T$  is the specimen temperature change across the specimen gage length and  $L$  is the gage length over which the specimen  $\Delta T$  is measured.

The heat flow  $Q$  is determined by the calorimeter.  $A_{1m}$  and  $L$  are calculated directly for the particular specimen configuration.  $\Delta T$  is determined directly from the observed temperature difference across the specimen gage length.

Based on an extensive error analysis and calibrations on homogeneous isotropic materials of known thermal conductivities, such as Armco iron and tungsten, the precision (coefficient of variation) in the measurements has been established at  $\pm 7$  percent over the temperature range. For multiple runs on samples having similar properties, the uncertainty in a smooth curve through the data can be established to within  $\pm 7$  percent. A detailed error analysis has been presented in a paper by Mann and Pears.<sup>1</sup>

Data obtained here on several high temperature materials are presented in Figures 6, 7 and 8. Figure 6 is a plot of data obtained here on tungsten. The specimen for these determinations were fabricated from stacks of 0.060" washers cut from hot rolled sheet stock. Also plotted are values reported by other investigators including "recommended values" given by Powell, Ho and Liley<sup>2</sup> based on a compilation of 103 sets of data. Agreement between our data and

---

<sup>1</sup>Mann, W. H. Jr., and C. D. Pears, "A Radial Heat Flow Method for the Measurement of Thermal Conductivity to 5200°F", presented at the Conference on Thermal Conductivity Methods, Battelle Memorial Institute, October 26-28, 1961.

<sup>2</sup>Powell, R. W., C. Y. Ho and P. F. Liley, "Thermal Conductivity of Selected Materials" NSRDS-NBS 8, National Standard Reference Data Series - National Bureau of Standards - 8, 1966, pp. 11, 54-59.



the recommended values is excellent throughout the temperature range.

Figure 7 shows data obtained here on ATJ graphite, with grain. This material is premium grade, medium grain graphite having a density range of 1.73 to 1.78 gm/cm<sup>3</sup>. The crosses (+) shown in the figure are "recommended values" given by Ho, Powell and Liley.<sup>3</sup> Again agreement is excellent.

Figure 8 shows data obtained on AXM-501. These data were obtained under a program sponsored by the Air Force Materials Laboratory to develop high temperature thermal conductivity standards. Measurements were made on this material by four laboratories in addition to Southern Research Institute. The bands shown in Figure 8 represent the range of data reported by the other participating organizations. A complete presentation and discussion of the data are given in AFML-TR-69-2.<sup>4</sup>

---

<sup>3</sup>Ho, C. Y., R. W. Powell and P. E. Liley, "Thermal Conductivity of Selected Materials, Part 2," NSRDS-NBS 16 National Standard Reference Data Series - National Bureau of Standards-16, pp. 89-128.

<sup>4</sup>AFML-TR-69-2, "Development of High Temperature Thermal Conductivity Standards" submitted by Arthur D. Little, Inc., under Contract AF33(615)-2874, 1969, pp. 115-127.

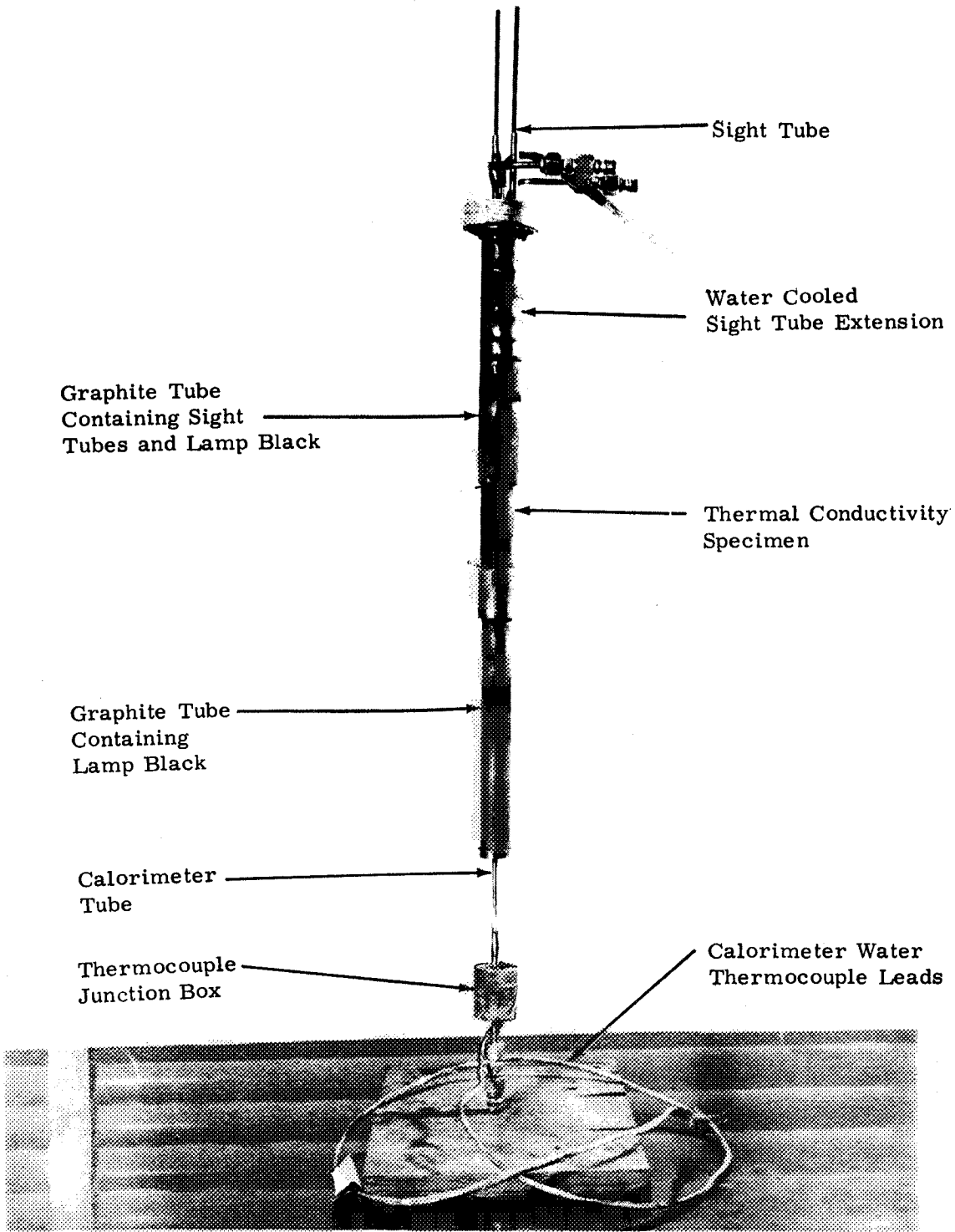


Figure 1. Picture of the Radial Thermal Conductivity Apparatus

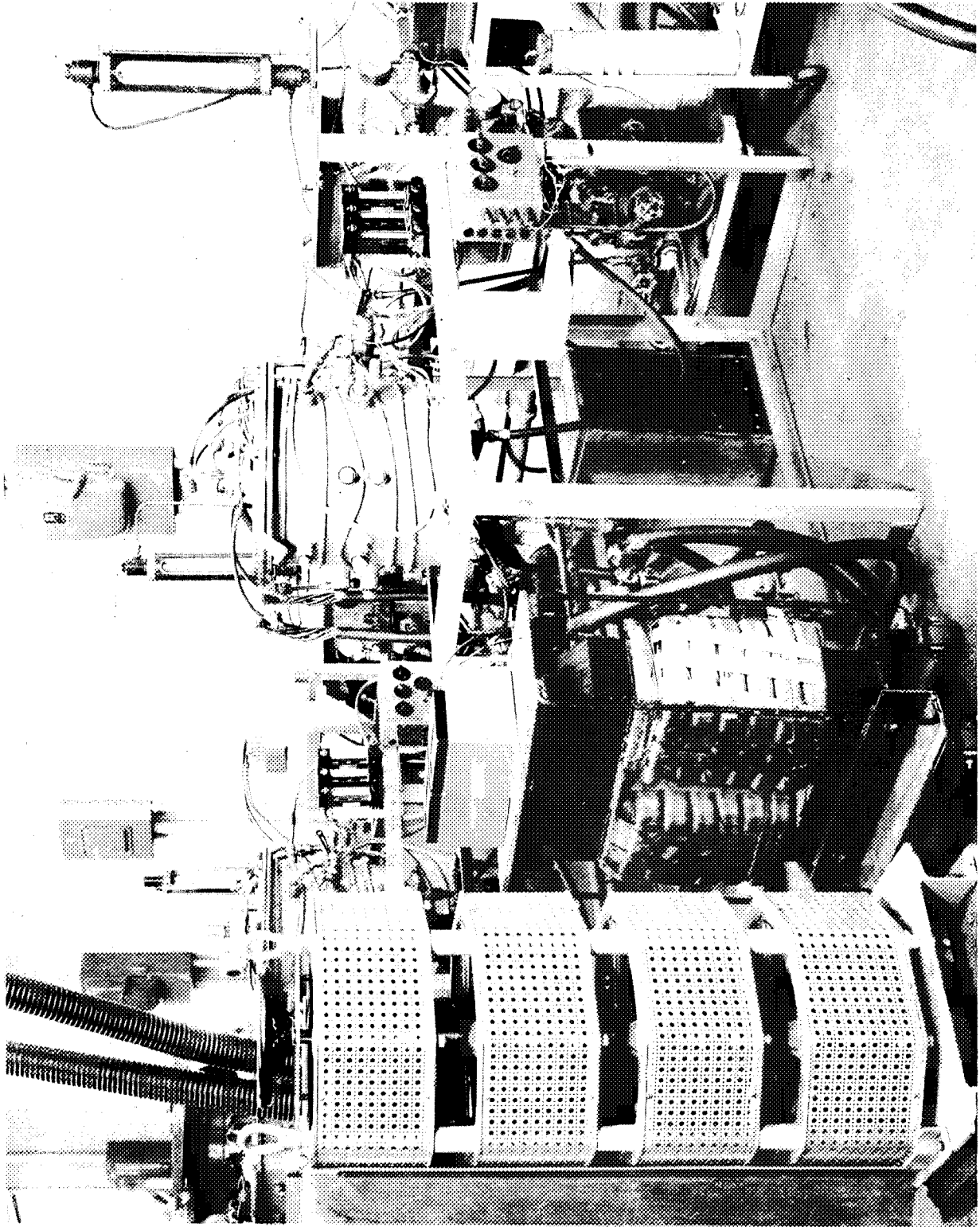


Figure 2. Furnace with Thermal Conductivity Apparatus Installed

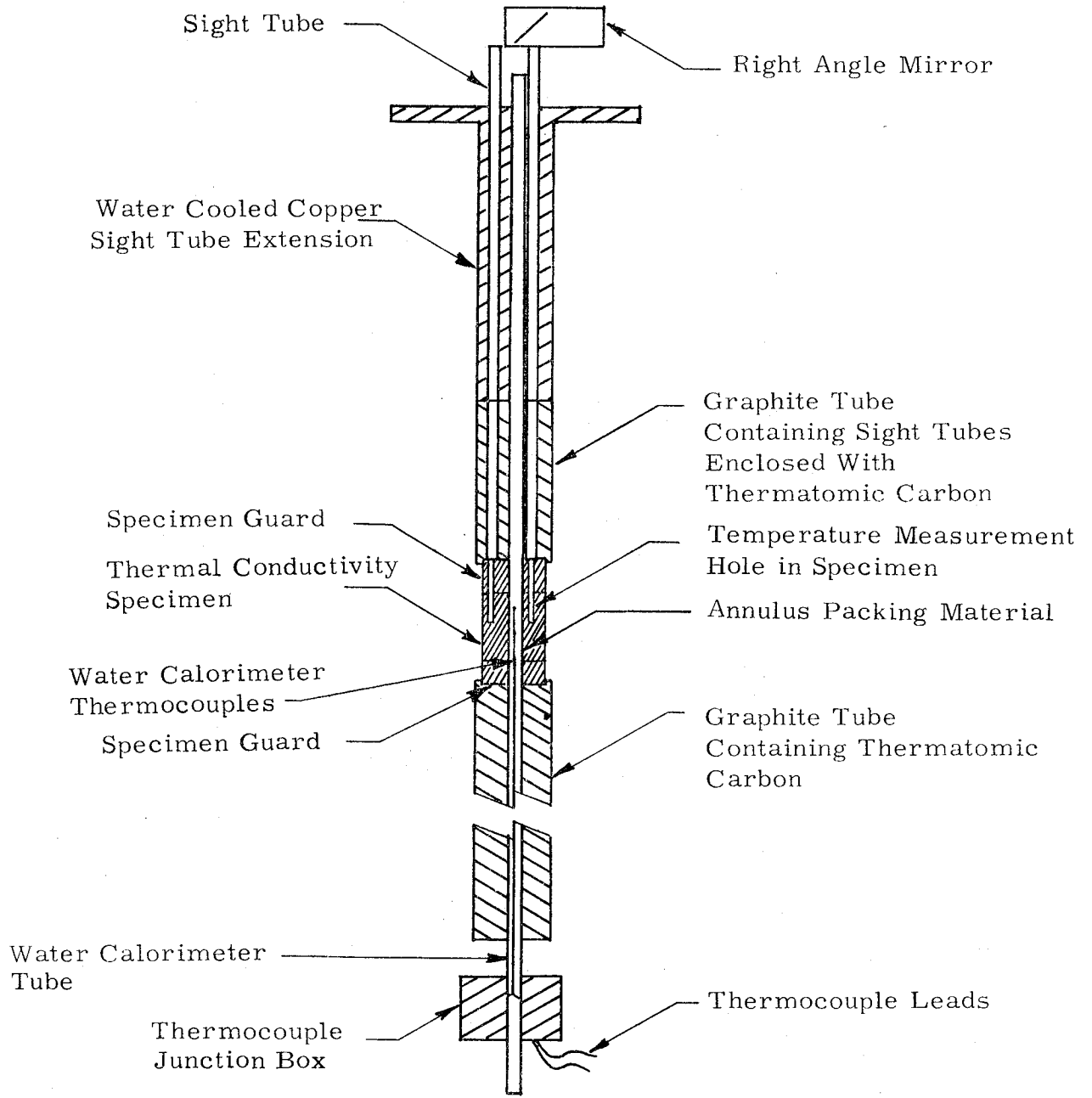


Figure 3. Cross-section Schematic of the Thermal Conductivity Apparatus

App D'

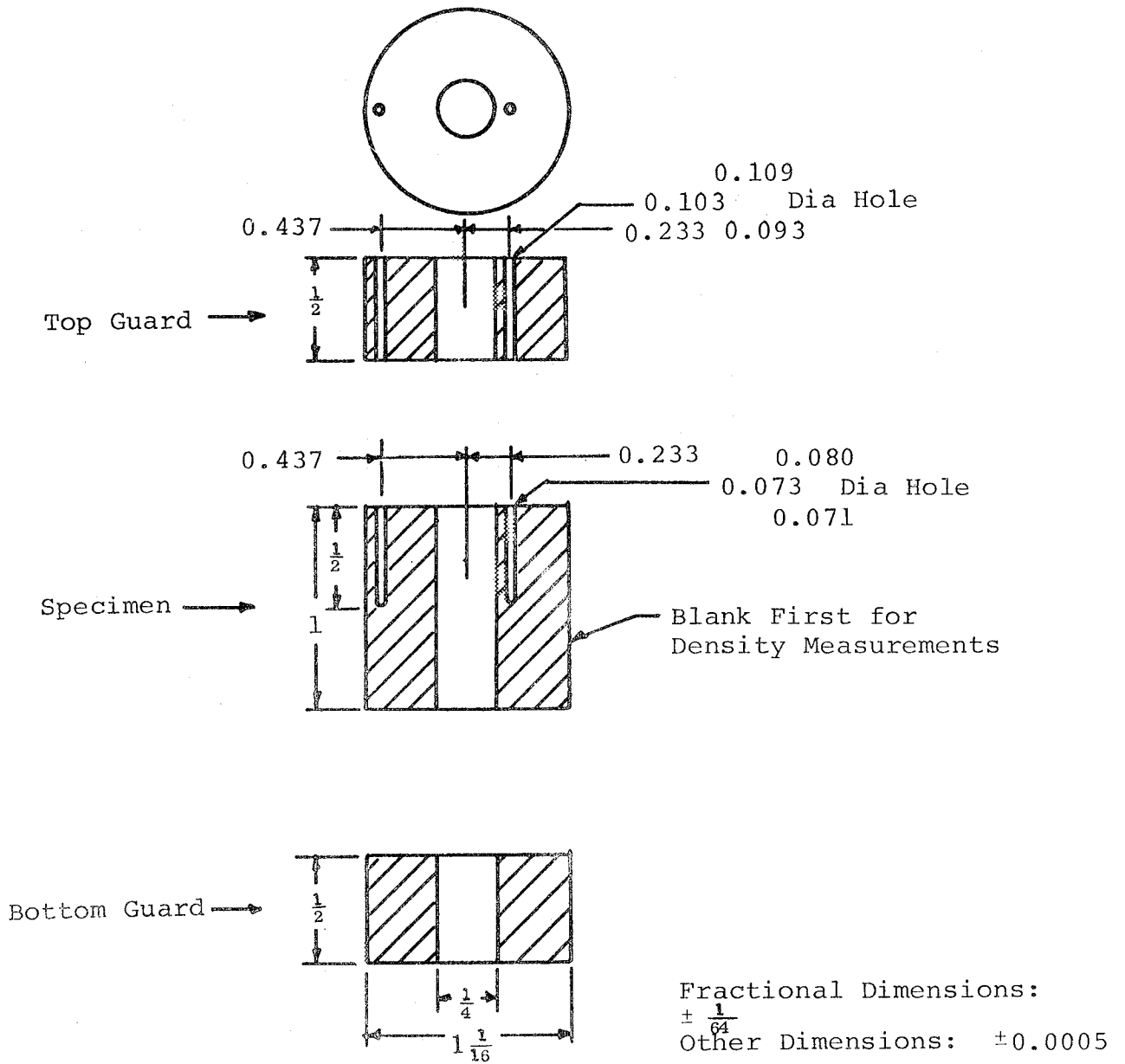


Figure 4. 1.06 Diameter Thermal Conductivity Specimen for Radial Inflow Apparatus

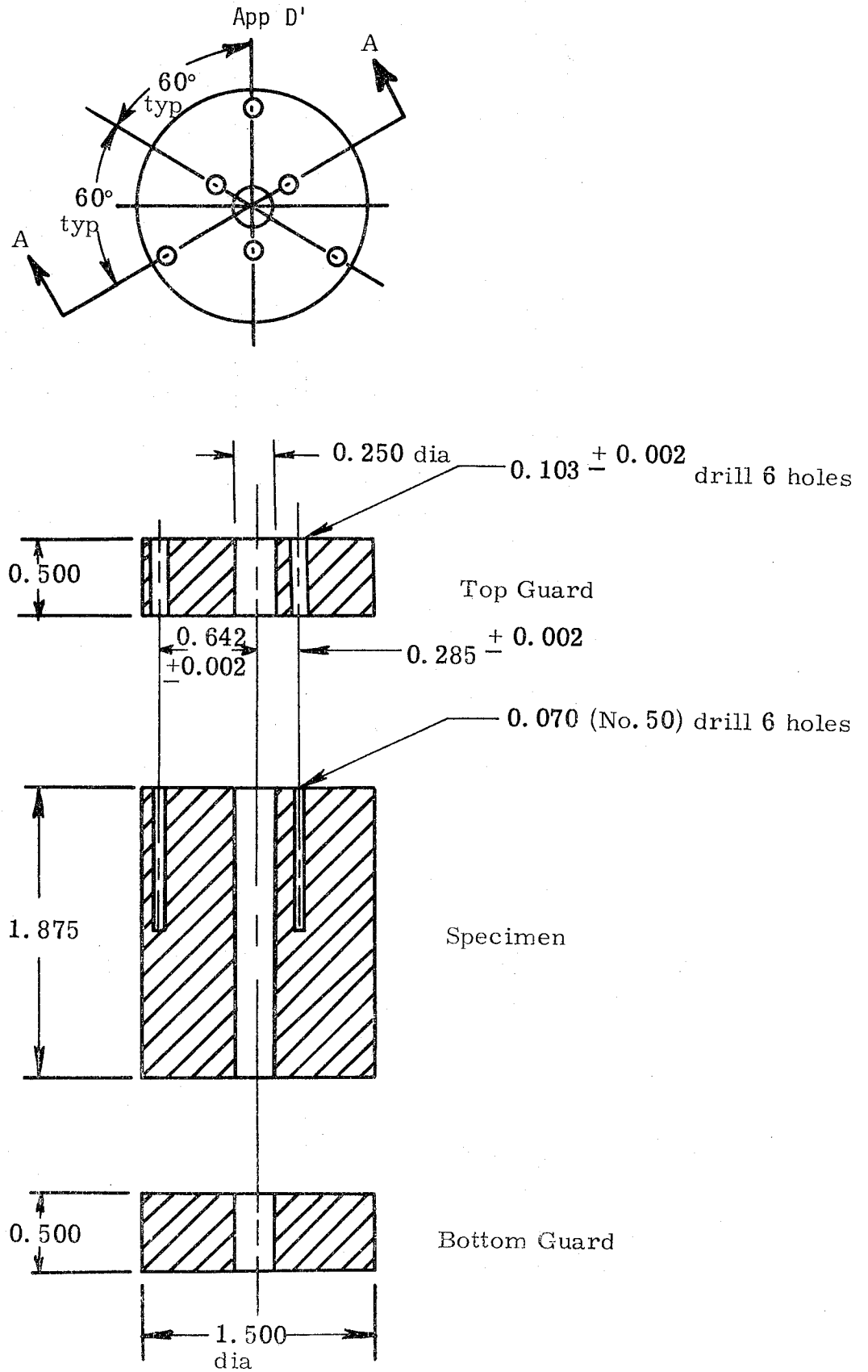


Figure 5. Dimensions of 1.50 Inch Diameter Specimen and Guards Used for Radial Inflow Thermal Conductivity Measurements

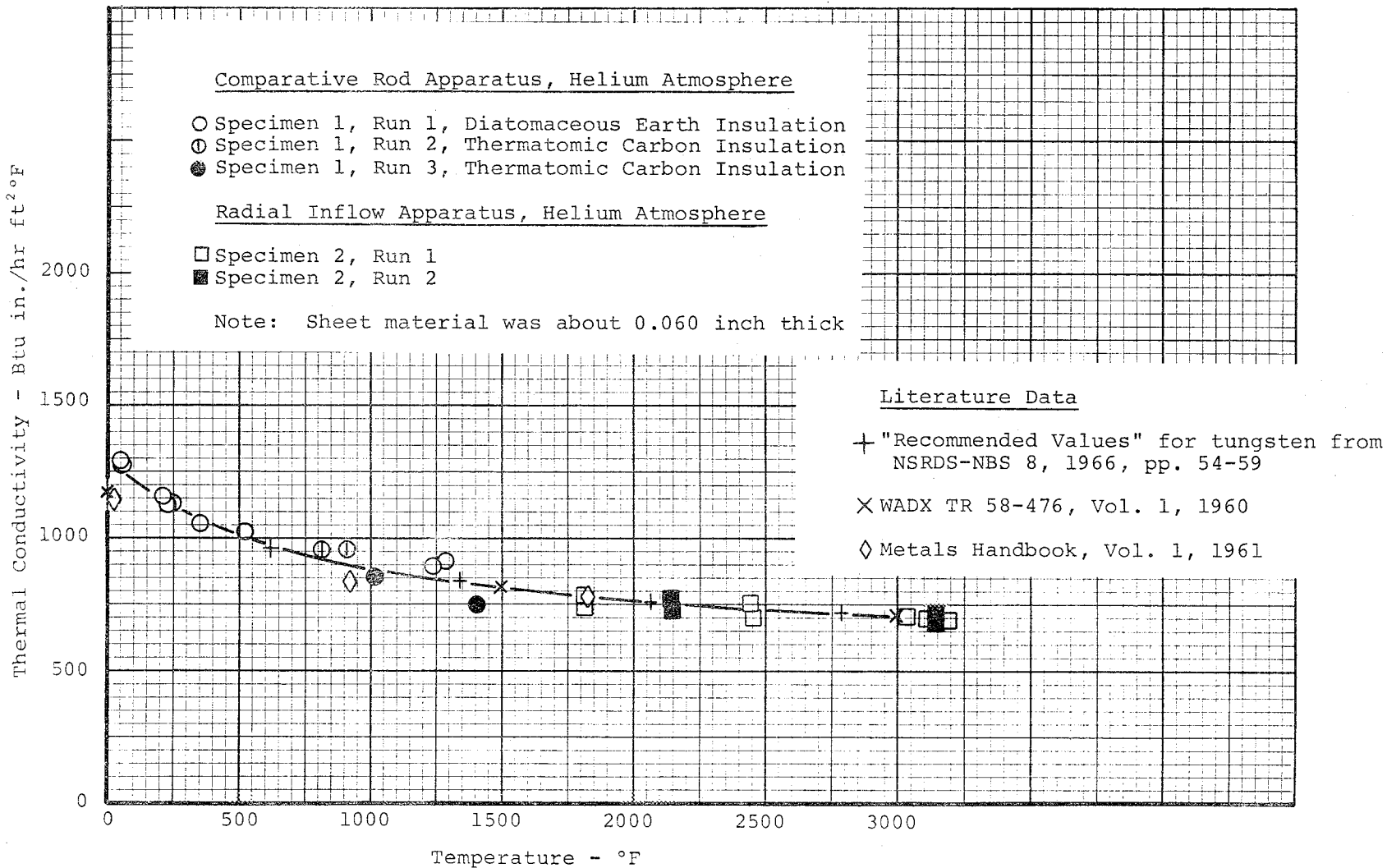
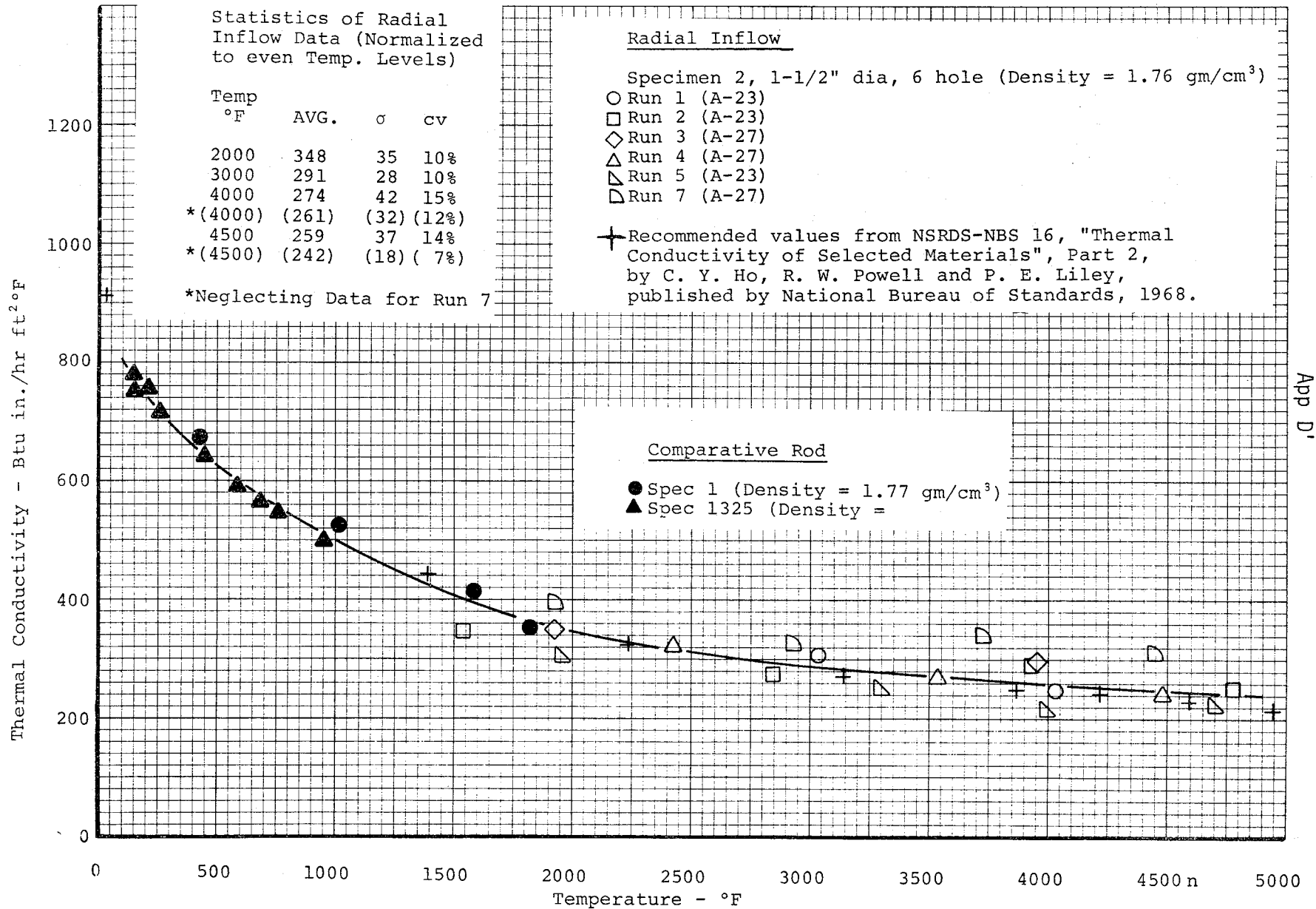


Figure 6. The Thermal Conductivity of Tungsten Sheet Parallel to the Plane of the Sheet



App D'

Figure 7. The Thermal Conductivity of ATJ Graphite, With Grain



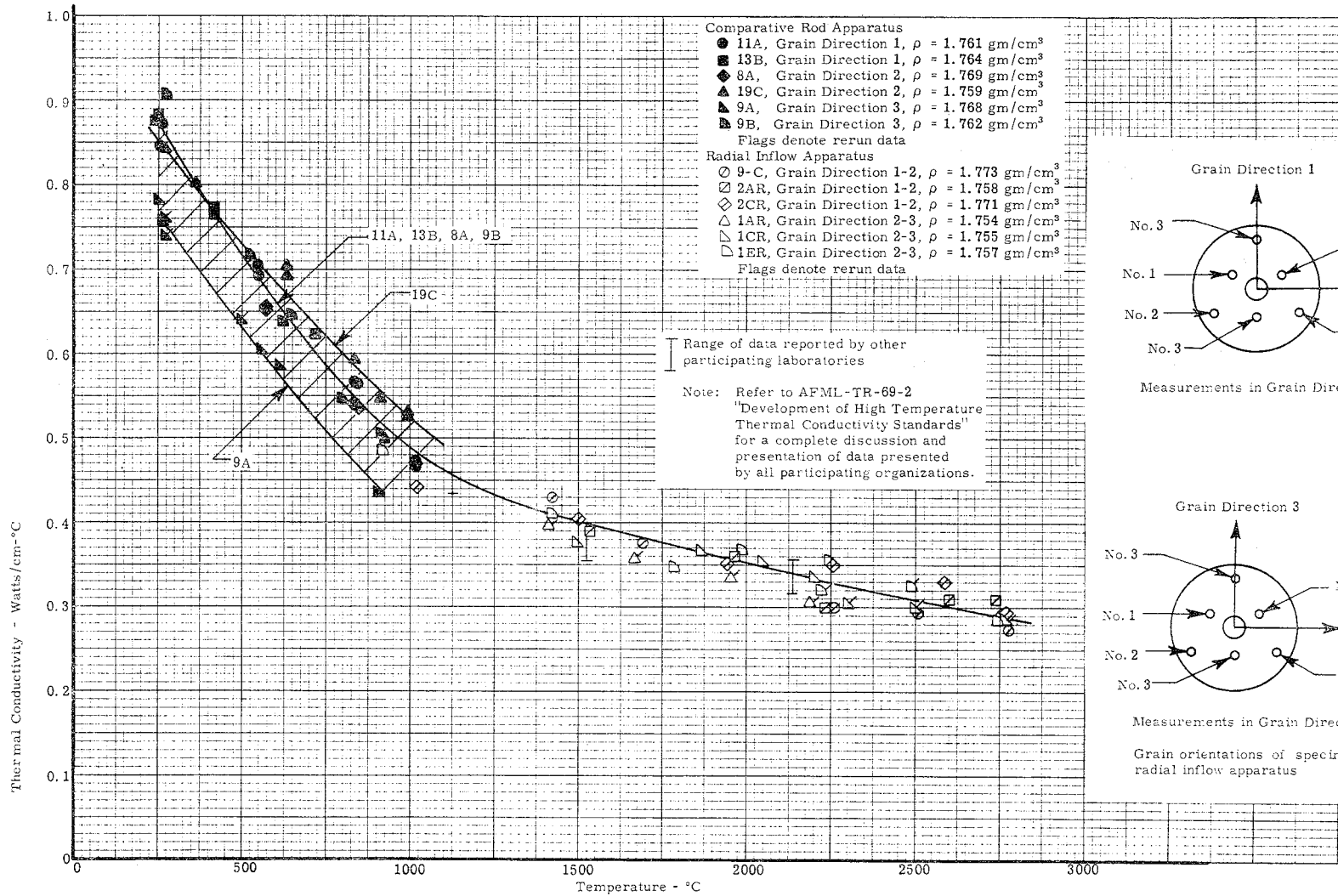
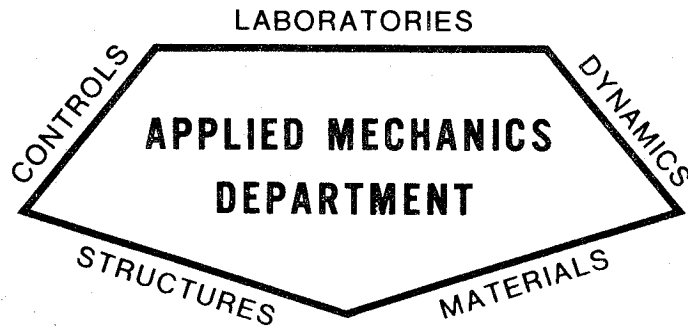


Figure 8. The Thermal Conductivity of AXM-5Q1 Graphite

APPENDIX B

STRUCTURAL ANALYSIS OF REGENERATIVELY COOLED  
AGCARB GRAPHITE-LINED THRUST CHAMBER





# STRUCTURAL ENGINEERING SECTION

Report No. SA-RTC-11

STRUCTURAL ANALYSIS OF  
REGENERATIVELY COOLED  
AGCARB GRAPHITE-LINED THRUST CHAMBER  
(NAS 3-13315)

PREPARED BY:

P. J. Krusi  
Senior Engineer  
Structural Engineering Section

PREPARED BY:

J. W. Starr, Supervisor  
Technology Components  
Structural Engineering Section  
Engineering Operations

APPROVED BY:

L. K. Severud, Manager  
Structural Engineering Section  
Engineering Operations

DATE 12 January 1971



**AEROJET LIQUID ROCKET COMPANY**

SACRAMENTO, CALIFORNIA



TABLE OF CONTENTS

	<u>Page</u>
I. Introduction	1
II. Summary of Results	1
A. Margins of Safety	3
III. Conclusions	5
IV. Analysis	
A. Design Criteria	6
B. Pressure and Thermal Conditions	6
C. Material Properties	7
D. Method of Analysis	8
E. Detailed Analysis	9
1. Finite Element Representation of Coolant Channel Stiffness	9
2. Forward End Region	10
3. Throat and Aft End Region	10
4. Coolant Channel	11
a. Steady State Thermal Conditions	11
b. Transient Thermal Conditions	11
5. Low Cycle Fatigue Life	12
V. References	13

App B

LIST OF SYMBOLS AND SUBSCRIPTS

$F_{TU}$	Ultimate tensile strength (psi)
$F_{CU}$	Ultimate compression strength (psi)
$\tau_u$	Ultimate shear strength (psi)
$F_{TY}$	Yield tensile strength (psi)
$F_{CY}$	Yield compressive strength (psi)
$E_T$	Tensile modulus of elasticity (psi)
$E_C$	Compression modulus of elasticity (psi)
$G$	Shear modulus of elasticity (psi)
$\alpha$	Coefficient of thermal expansion (in./in./°F)
$\Delta T$	Change in temperature (°F)
$\epsilon$	Strain (in./in.)
$\sigma$	Stress (psi)
$\nu$	Poisson's ratio
$t$	Shell thickness (in.)
$p$	Pressure load (psi)
M.S.	Margin of safety
$\tau$	Shear stress (psi)
$P_B$	Coolant pressure (psig)

## App B

### LIST OF FIGURES

<u>Figure</u>	<u>Title</u>	<u>Page</u>
1	Design Configuration	14a
2	Gas Static Wall Pressure	15
3	Steady State Temperature Distribution at Various Locations Along AGCarb-101 Lined Electroformed Nickel Chamber P/N 1159525 (Reference 7)	16
4	Steady State Temperature Distribution at Various Locations Along AGCarb-101 Lined Electroformed Nickel Chamber P/N 1159525 (Reference 7)	17
5	Coolant Channel Temperature Distribution Steady State Condition Stress Model Station 5.1 (Reference 7)	18
6	Start-up Condition Transient Temperature Distribution (Reference 8)	19
7	Coolant Channel Temperature Distribution Transient Thermal Conditions Stress Model Station 5.1 (Reference 8)	20
8	Tensile Properties of Electroformed Nickel	21
9	Dynamic Modulus vs Temperature Electroformed Nickel	22
10	Thermal Coefficient of Expansion Electroformed Nickel	23
11	Compression Strength and Modulus AGCarb-101 Throat Configuration and Block Tests	24
12	Poisson's Ratio - AGCarb Compression Tests	25
13	AGCarb-101 Interlaminar Shear Strength	26
14	Regen Cooled AGCarb Lined Thrust Chamber Finite Element Model Axisymmetrical Analysis Forward End	27
15	Regen Cooled AGCarb Lined Thrust Chamber Finite Element Model Axisymmetrical Analysis Aft End	28
16	Regen Cooled AGCarb Lined Thrust Chamber Finite Element Model Plane Stress Analysis Coolant Channel Forward of Throat	29
17	Effective Stress Distribution Electroformed Nickel Forward Shell and CRES 304-L Manifold	30
18	Hoop and Meridional Stress Distribution AGCarb-101 Forward Liner	31
19	AGCarb-Nickel Bond Compressive and Shear Stress Distribution Forward End	32
20	Effective Stress Distribution Electroformed Nickel Aft Shell and CRES 304-L Manifold	33
21	Hoop and Meridional Stress Distribution AGCarb-101 Aft Liner	34
22	Iso-Stress Shear Distribution AGCarb-101 Liner Aft End	35



App B

LIST OF FIGURES (cont.)

<u>Figure</u>	<u>Title</u>	<u>Page</u>
23	AGCarb-Nickel Bond Compressive and Shear Stress Distribution Aft End	36
24	Effective Stress and Hoop Stress Distributions at Coolant Channel Stress Mode Station 5.1 Plane Stress Analysis for Steady State Temperature Conditions	37
25	Effective Stress and Hoop Stress Distributions at Coolant Channel Stress Model Station 5.1 Plane Stress Analysis for Transient Temperature Conditions (t = 1.8 sec)	38
26	Cycles to Failure vs Total Strain Electroformed Nickel	39

LIST OF TABLES

<u>Table</u>	<u>Title</u>	<u>Page</u>
I	Margins of Safety Steady State Temperature Conditions AGCarb Graphite Lined Thrust Chamber	3
II	Margins of Safety Maximum Transient Temperature Conditions t = 1.8 seconds AGCarb Graphite Lined Thrust Chamber	4
III	AGCarb Graphite Lined Electroformed Nickel Thrust Chamber 100 Channel Design	14

I. INTRODUCTION

The earlier structural analysis of the Regeneratively Cooled AGCarb Graphite-Lined Thrust Chamber is given in Reference 1. This analysis did not include the stiffening effects of the inlet and outlet coolant manifolds in the stress model of the structure and did not incorporate the measured compressive material properties of the AGCarb-101 liner material obtained from Southern Research Corporation. The purpose of this analysis is to complete a detailed structural evaluation of the entire design concept to determine structural adequacy and necessary design strength modifications. The design conditions consider a chamber operating pressure of 500 psia and the thermal conditions during steady state and transient operation.

II. SUMMARY OF RESULTS

Three finite element analyses were conducted to evaluate the thrust chamber structure. These analyses considered the forward chamber shell and outlet manifold; the throat region; the aft chamber shell and inlet manifold; and the stress distribution about the coolant channel at the axial station where the maximum radial thermal gradients are developed during steady state and transient thermal conditions after start-up. The results of the analysis are summarized in Tables I and II and indicate the following:

A. The inner diameter of the nickel shell will experience yielding during operation but the stress levels are well within allowable ultimate strength values. The outer diameter tensile stresses are within allowable values.

B. The stresses developed in the inlet and outlet manifolds are below allowable strength levels.

C. The meridional stresses in the AGCarb liner are low compression. The compressive hoop stresses developed in the liner at the throat where the 15° rotated layup is used are marginal in that they are equal to the ultimate compressive strength (M.S. = 0.0).

## App B

D. The shear stresses developed in the AGCarb liner are acceptable except aft of the throat region at the aft retaining flange where the shear locally exceeds the allowable value (M.S. = -0.37). The contact pressure between the liner and the nickel is less than the intended design value of 200 psi at this same location but is greater than the 200 psi value along all the other bondlines.

E. The stress developed in the thrust chamber during the transient thermal conditions after start-up are less severe than during steady state operation.

F. The stresses developed around the coolant channel are within allowable values.

G. The low cycle fatigue life associated with the maximum compressive strain in the nickel is approximately 80 cycles.

TABLE I  
MARGINS OF SAFETY  
STEADY STATE TEMPERATURE CONDITIONS  
AGCARB GRAPHITE LINED  
THRUST CHAMBER

Region	Material	Location			Maximum Conditions	Stresses				F <sub>tu</sub> Ult	Allowable		Max Strain ε%	Temp °F	M.S. Ult
		Radius (R) (in.)	Sta. (Z)* (in.)	Elem No.*		σ <sub>H</sub> Hoop	σ <sub>Z</sub> (psi) Meridional	τ Shear	σ <sub>e</sub> Effective		F <sub>ty</sub> Yield	τ <sub>u</sub> Shear Ult			
I. Fwd End Outlet Manifold	GRES 304L	3.17	15.75	542	Comp	-8,945	-19,370	--	-25,820	59,000	26,000	--	.09	350	+1.3
	Electroformed	2.94	10.52	28	Comp	-25,996	-25,160	--	-24,210	32,000	17,000	--	0.78	930	+0.27
	Shell Nickel	3.20	10.22	16	Tension	41,580	46,830	--	44,835	75,000	52,000	--	0.20	103	+ .67
	Liner AGCarb 15° Bias Layup At 60° to §	2.67	11.27	65	Hoop Comp	-7,980	-3,800	1350	--	-20,100	--	1550	.28	3929	+1.51
II. Throat Region Shell	Electroformed	1.91	5.02	536	Comp	-12,920	-12,740	--	11,058	18,000	8,000	--	1.26	1176	+0.63
	Nickel	2.67	6.67	628	Tension	34,840	38,580	--	41,036	72,000	50,000	--	0.20	420	+0.75
	Coolant Channel Electroformed	1.94**	5.1*	8**	Comp	-13,195	--	--	12,332	18,000	8,000	--	0.98	1171	+0.45
	Nickel	2.08**	5.1*	14**	Tension	33,729	--	--	33,809	71,000	49,000	--	0.12	154	+1.10
Liner	15° Bias Layup At 60° to §	1.38	3.65	438	Comp	-2,027	-4,937	594	--	21,700	--	1400	1.57	4551	+1.40
	AGCarb 15° Rotated Layup At 60° to §	2.04	5.77	574	Shear	-6,910	-2,713	801	--	18,700	--	1500	1.33	3133	+1.27
	Comp and Shear	1.56	2.65	310	Comp and Shear	-10,730	-2,389	1379	--	10,700	--	1550	1.07	3988	0.0
III. Aft End Inlet Manifold	GRES 304L	3.52	1.03	46	Tension	1,6450	2,300	--	45,760	140,000	35,000	--	0.11	-120	+2.06
	Shell Electroformed	2.77	1.53	125	Comp	-53,644	-13,112	--	47,540	70,000	49,000	--	0.18	490	+0.17
	Nickel	3.42	1.09	42	Tension	42,990	-8,305	--	48,180	92,000	59,000	--	0.11	-120	+0.81
	Liner AGCarb 15° Bias Layup At 60° to §	2.35	1.44	109	Comp	-11,179	-1,682	1140	--	21,200	--	1580	1.58	4572	+0.90
		2.80	1.09	34	Shear	-3,347	-838	2180	--	15,300	--	1380	0.74	1133	-0.37

\* See Figures 14 and 15.  
\*\* See Figure 16.

App B

TABLE II  
MARGINS OF SAFETY  
MAXIMUM TRANSIENT TEMPERATURE CONDITIONS  
t = 1.8 SECONDS  
AGCARB GRAPHITE LINED THRUST CHAMBER  
CHAMBER STATION Z = 5.1\*  
PLANE STRESS ANALYSIS

Material	Maximum Conditions	Location			Stress (psi)				Allowable (psi)			Max Strain $\epsilon$ (%)	Temp ( $^{\circ}$ F)	M.S. Ult.
		Radius (R) (in.)	Sta. (Z)* (in.)	Elem No.**	$\sqrt{H}$ Hoop	$\sqrt{Z}$ Meridional	$\Sigma$ Shear	$\sqrt{e}$ Effective	$F_{tu}$ Ult	$F_{ty}$ Yield	$\Sigma_u$ Shear Ult			
Electroformed Nickel Shell	Comp Tension	1.92	5.1	21	-37,380	--	256	38,220	60,000	40,000	--	.22	617	+ .57
		2.08	5.1	46	24,103	--	38	24,382	87,000	58,000	--	.08	180	+2.57
AGCarb Liner 45 $^{\circ}$ Bias Layup at 60 $^{\circ}$ to $\phi$	Comp Hoop	1.78	5.1	31	-10,220	--	243	--	20,600	--	1550	1.26	4213	+1.01

\* See Figures 14 and 15.

\*\* See Figure 16.

III. CONCLUSIONS

The finite element analyses of the AGCarb graphite-lined electroformed nickel thrust chamber indicate:

A. The structure will develop marginal hoop compressive stresses in the AGCarb throat liner. However, the AGCarb is in a state of compression and is contained by the nickel shell with the local shear stresses within allowable values. Therefore, the condition is considered acceptable.

B. The structure will develop excessive shear stresses in the aft AGCarb liner at the aft retaining flange. Since this is a very local condition, it is anticipated that the liner will probably delaminate locally (interlaminar) but not completely fracture. A possible means of alleviating this local excessive stress condition would be to provide an axial expansion relief, e.g., a Grafoil material insert.

IV. ANALYSIS

A. DESIGN CRITERIA

1. Configuration

a. Reference Drawings

1159525	Combustion Chamber
1159524	AGCarb Liner
1159636	Combustion Chamber Assembly

2. Geometry

The basic dimensions of the regeneratively cooled chamber are given in Figure 1.

B. PRESSURE AND THERMAL CONDITIONS

1. Pressure

The chamber pressure for FLOX/Methane propellant is  $P_c = 500$  psia.

The gas static wall pressure during firing is shown in Figure 2. The coolant channel and manifold pressure schedule is given in Table III.

2. Temperature

a. Steady State

The temperature data used in the analyses for the steady state firing condition are depicted in Figures 3 and 4. Figure 5

## App B

shows the temperature distribution used in the analysis of the coolant channel at chamber Station 12.5 (Stress Model Station 4.3). This particular axial location was selected because it is where the highest thermal gradient is developed across the AGCarb liner and nickel shell.

### b. Transient Analysis

A transient thermal analysis of a start-up condition was conducted at chamber Station 12.5. Figure 6 summarizes these data by showing the temperature distribution across the chamber wall with time. The stress analysis of the thermal transient condition was conducted for time  $t = 1.8$  seconds when the maximum thermal gradient is developed across the AGCarb liner. The temperature distribution used is shown in Figure 7.

### C. MATERIAL PROPERTIES

The material properties used in the analysis for the electroformed nickel are given in Figures 8 through 10. The AGCarb-101 material properties used in the analysis were obtained from the tests conducted at Southern Research (Reference 4). Figure 11 shows the compressive strength and modulus of the AGCarb for the 15 degree rotated layup used in the throat and the 45 degree bias layup used in the chamber. Figure 12 gives the corresponding Poissons' Ratio data for the two AGCarb materials. The interlaminar shear strength for both layups was assumed to be proportional to the warp direction tensile strengths as given by Reference 5 - and shown in Figure 13.

The material properties for the CRES 304 stainless steel were obtained from Reference 6.



D. METHOD OF ANALYSIS

The finite element method of analysis was used to evaluate the structural adequacy of the modified design. The particular computer routine considered the separate three dimensional (laminated orthotropic) radial, axial and hoop mechanical properties of the AGCarb liner wrapped at a 60 degree orientation. Also, the procedure accounted for the inelastic behavior (plasticity) of the nickel shell at high temperatures under high radial compressive load. The method has been described in previous reports (Reference 1).

1. Stress Models

In order to conduct a complete detailed analysis of the thrust chamber shell, liner and manifold, the structure was considered as two separate models coupled by appropriate boundary conditions. Figure 14 shows the finite element computer plot of the model for the forward end of the chamber and Figure 15 shows the similar model of the aft end. Since these models are axisymmetrical, the local radial reduction of stiffness in the electroformed nickel shell at the coolant channels was accounted for by using an equivalent radial and axial elastic modulus for the finite elements representing the channels. The derivation of this effective stiffness is given on page 9.

The local stress distribution about the channels during steady state and transient thermal conditions was evaluated by the plane-stress finite element model plotted in Figure 16. The geometry evaluated was at the axial station where the highest thermal gradient is developed across the nickel shell ( $Z = 4.3$ , Figure 15).

App B

E. DETAILED ANALYSIS

1. Finite Element Representation of Coolant Channel Stiffness

a. Material Properties for Effective Channel Stiffness in the Axisymmetrical Model

Electroformed nickel w/100 - .034 in. wide channels equally spaced.

Assume an average radius of 2.0 in.

$$\begin{aligned} C &= 2\pi R \\ &= 2\pi(2.0) \\ &= 12.57 \text{ in.} \end{aligned}$$

Effective Meridional and Radial Modulus:

$$\begin{aligned} E_{\text{eff}} &= \left[ \frac{12.57 - 100(.034)}{12.57} \right] E_{\text{nickel}} \\ &= .73(E_{\text{nickel}}) \end{aligned}$$

Hoop stiffness is  $E_{\theta} = 1000$

Temp °F	$E_{\text{nickel}}$ psi	Equivalent, Stiffness, psi			
		$E_R$ & $E_Z$	$E_{\theta}$	$G_{RZ}$	$\nu_{R,Z,\&\theta}$
70	29.4 E06	21.4 E06	1000	8.25 E06	0
400	28.0 E06	20.4 E06	1000	7.85 E06	0
800	25.8 E06	18.8 E06	1000	7.25 E06	0

Coefficient of expansion for equivalent material in the channel is assumed the same as for nickel.

## App B

### 2. Forward End Region

The results of the analysis are summarized in Tables I and II and Figures 17, 18 and 19. Figure 17 shows an iso-stress plot of the effective stresses in the CRES 304-L outlet manifold and electroformed nickel shell. These data show the inner diameter of the nickel shell will yield but the stress level is well within the allowable ultimate strength values. Figure 18 shows the hoop and meridional stress distributions in the AGCarb liner with all values well within allowable strength criteria. Figure 19 gives the compressive contact stress and the shear stress distribution in the AGCarb and the bond line between the nickel and the AGCarb. The bond contact pressure and shear stress in the AGCarb are all within allowable design conditions of 200 psi pressure and 1300 psi shear along the laminates (interlaminar).

### 3. Throat and Aft End Region

The results of the analysis are summarized in Table I and Figures 20, 21, 22 and 23. Figure 20 shows the isostress plot of the effective stresses in the CRES 304-L inlet manifold and electroformed nickel shell. These data show compressive stresses in the nickel exceeding yield values forward of the throat region. The minimum ultimate margin of safety in compression at the inner diameter is +0.45 at the throat. The minimum ultimate margin of safety in tension is at the same location at the outside diameter is +0.75. Figure 21 shows the hoop and meridional stress distribution in the AGCarb liner. The minimum ultimate margin of safety of 0.0 at the throat shows the design is structurally marginal at this location. However, since the AGCarb is in compression and contained by the nickel shell; and the local shear stresses are within allowable values; the condition is considered acceptable. A reduction in the nickel shell thickness at this region would partially alleviate the compressive hoop stress due to the liner bulk temperature but would have no effect on that portion of the total stress due to the temperature gradient.

## App B

Figure 22 gives the shear stress distribution in the AGCarb liner with the plasticity effects in the nickel being included in the analysis. These data indicate that high shear stresses exist in the liner aft of the throat region. These shear stresses are a maximum at the aft end where the retaining flange contains the liner. The maximum value is 2,180 psi giving a margin of safety of -0.37. Since this is a very local condition, it is anticipated that the liner will possibly delaminate locally (interlaminar) but not completely fracture. A possible means of alleviating this local excessive stress condition would be to provide an axial expansion relief, e.g., a Grafoil material insert.

Figure 23 gives the compressive contact stress and the shear stress distribution in the AGCarb at the bond line. The contact pressure is only below the design value of 200 psi at the retaining flange corner in the vicinity where the high bond shear stress was determined; as discussed above.

#### 4. Coolant Channel

##### a. Steady State Thermal Conditions

The results of the plane stress analysis of the stress distribution about the coolant channel during steady state thermal conditions are depicted in Figure 24 with maximum values shown in Table I. These data show no structural inadequacies.

##### b. Transient Thermal Conditions

The results of the analysis of the coolant channel for the maximum thermal gradients developed at  $t = 1.8$  seconds are shown in Figure 25. The maximum values are summarized in Table II and these data indicate that during the transient condition a greater compressive stress is developed on the inside surface of the AGCarb liner and the electroformed nickel. The higher compressive stress in nickel will occur at a lower thermal

## App B

condition which will result in higher margins of safety than for steady state conditions. The higher compressive stress in the AGCarb is still below the maximum value developed in the 45° bias layup aft of the throat (stress model Sta. Z = 1.44) where the minimum margin of safety (+0.90) occurs for this material.

### 5. Low Cycle Fatigue Life

Figure 26 shows the results of an evaluation of the low cycle fatigue life of the nickel shell inside diameter based on the Manson/NASA universal slopes equation:

$$\Delta \epsilon_{\text{total}} = \frac{3.5 F_{tu}}{E} N_f^{-0.12} + D^{0.6} N_f^{-0.6}$$

These data show that the maximum compressive strain of 1.26% developed in the nickel would result in a low cycle fatigue life of approximately 80 cycles.

App B

V. REFERENCES

1. V. Stubbs, L. Schoenman, R. Leary, G. Jacobson, Report Covering Subtask 2 of Task 1, Design Evaluation, NAS 3-13315, Contract for Regeneratively Cooled Graphite-Lined Thrust Chamber, 1 March 1970.
2. WADD TR60-438
3. Sample and Knapp on Properties of Electroformed Nickel, Table XI, p. 39.
4. Southern Research Institute, AGCarb-101 Data.
5. R. J. Kotfila, H. O. Davis, and W. J. Schleicher, The Fabrication and Properties of the Fibrous Reinforced Graphite Composite, AGCarb-101, Aerojet Internal Report, August 1969.
6. AGC Materials Properties Data Book, Report 2275, Vol. 2, NERVA Program, 31 July 1968.
7. AGC Memorandum, 9641:0558, V. R. Stubbs from J. A. Cunningham, Subj: "AGCarb-101 Lined Chamber Redesign Thermal Analysis," Contract NAS 3-13315, dtd 15 June 1970.
8. AGC Data, AGCarb-101 Lined Chamber Transient Temperature Analysis, dtd 11 November 1970.

App B

TABLE III

AGCARB GRAPHITE LINED  
ELECTROFORMED NICKEL  
THRUST CHAMBER  
100 CHANNEL DESIGN

COOLANT PRESSURE DISTRIBUTION

	Axial Dist From Outlet (in.)	Coolant Pressure $P_B$ (psi)
(Outlet)	0	1000
	.6	1001
	2.2	1012
	4.2	1031
	6.2	1048
	8.2	1063
	9.7	1078
	10.7	1003
	11.25	--
	11.8	1021
	12.5	1099
	13.0	1140
	13.5	1196
	14.0	1225
	14.5	1246
	15.0	1256
	15.5	1263
(Inlet)	15.8	1263

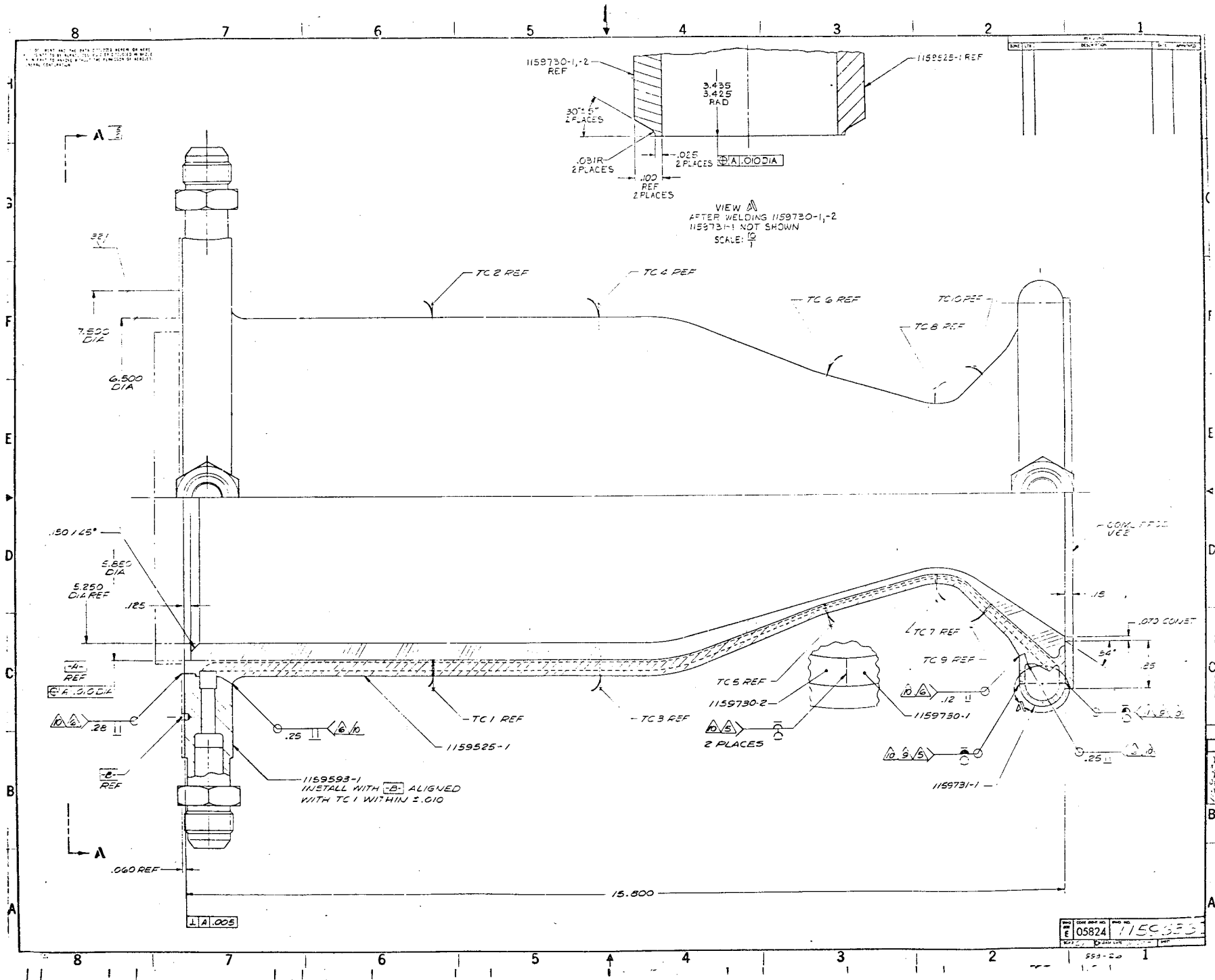
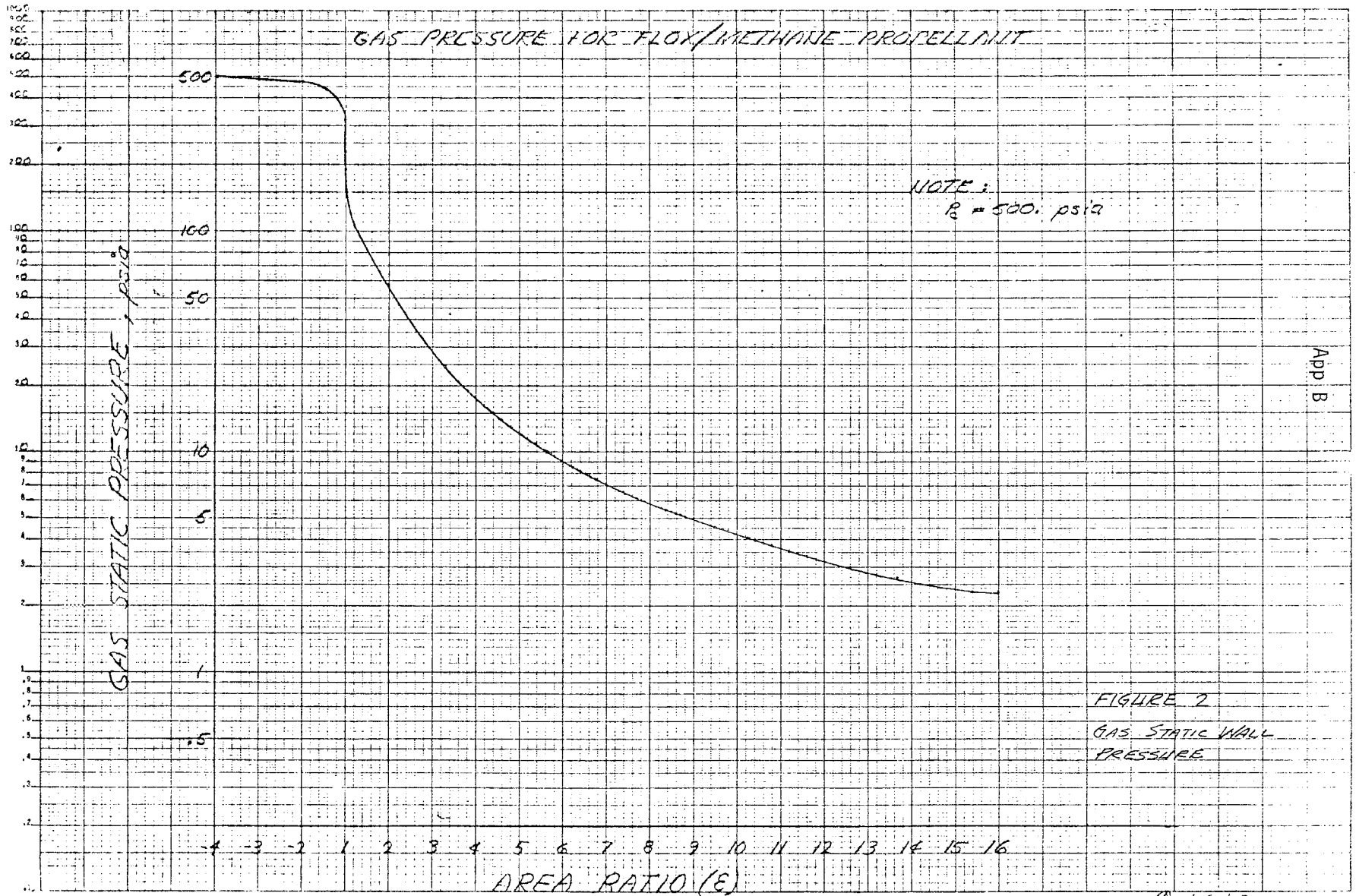


Figure 1 Design Configuration

REV	DATE	BY	CHK	APP
1	05824	1159525-1		

593-2-0





App B

14 Sept 70

AGCS-0800-11

SUBJECT

BY

KRUI

CHK. BY

REPORT NO.

PAGE

OF

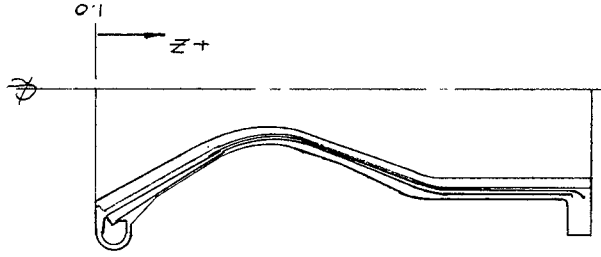
DATE

WORK ORDER

DATE

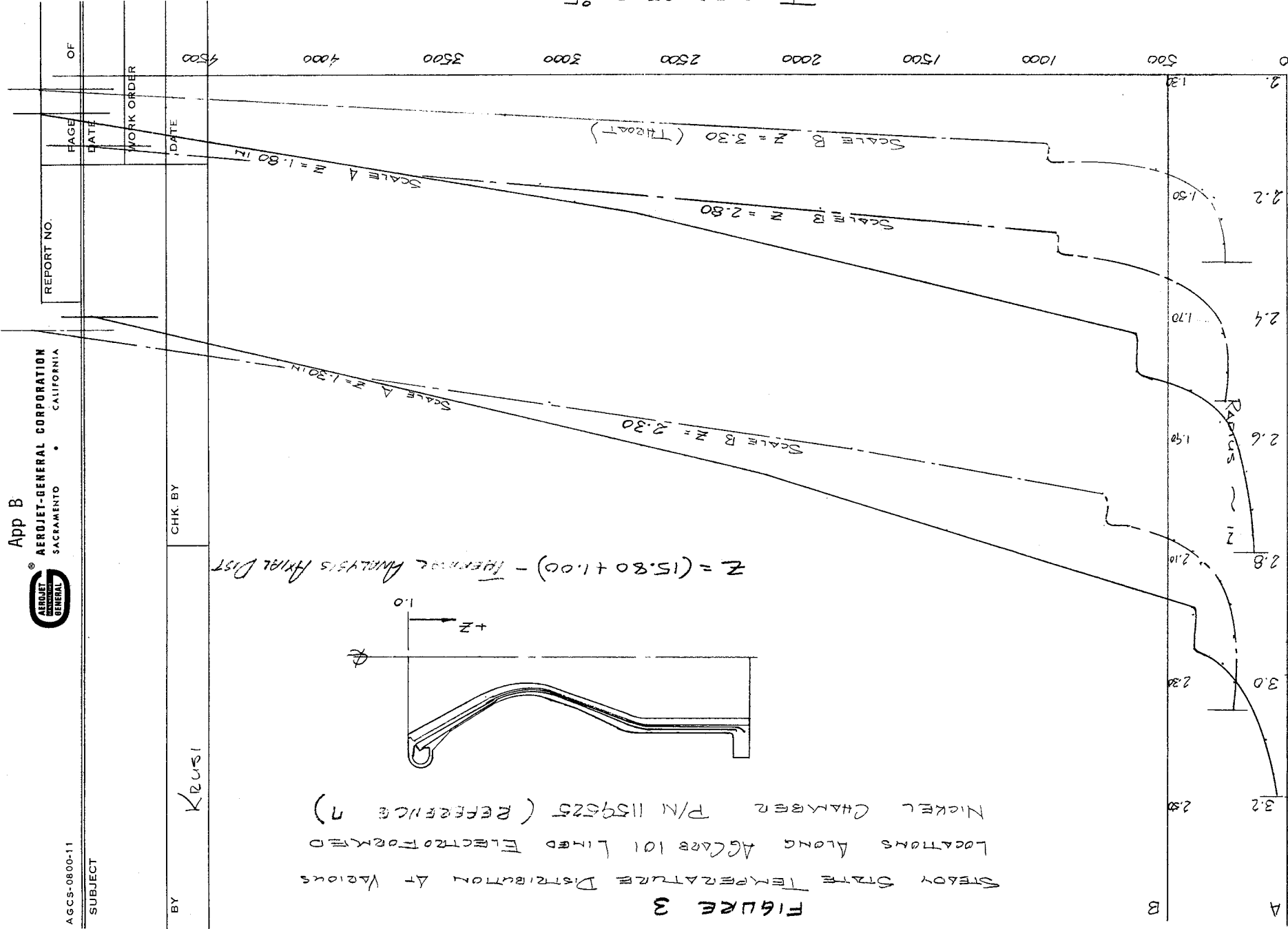
4500

STEADY STATE TEMPERATURE DISTRIBUTION AT VARIOUS  
 LOCATIONS ALONG AGCARE 101 LINED ELECTROFORMED  
 NICKEL CHAMBER P/N 1159525 (REFERENCE 7)



$Z = (15.80 + 1.00) - \text{TEMPERATURE ANALYSIS AXIAL DIST}$

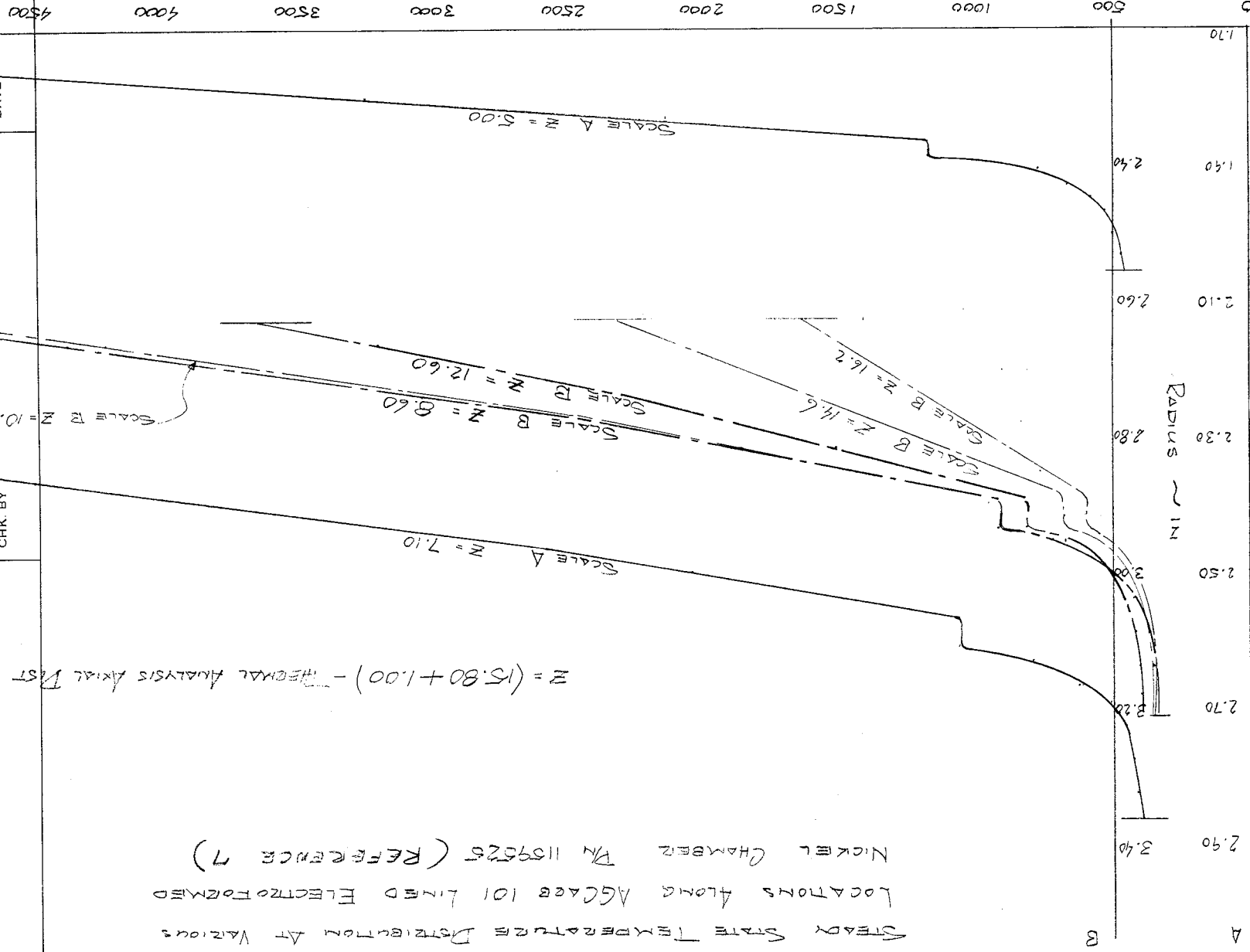
FIGURE 3



STEADY STATE TEMPERATURE DISTRIBUTION AT VARIOUS LOCATIONS ALONG AGCAGE 101 LINED ELECTROFORMED NICKEL CHAMBER IN 1109525 (REFERENCE 7)

FIGURE 4

$Z = (15.80 + 1.00) - \text{THERMAL ANALYSIS AXIAL DIST}$



App B  
**AERJET-GENERAL CORPORATION**  
 SACRAMENTO CALIFORNIA



AGCS-0800-11

SUBJECT

BY

CHK. BY

REPORT NO.

PAGE

OF

DATE

WORK ORDER

DATE

4500

4000

3500

3000

2500

2000

1500

1000

500

0

TEMPERATURE ~ °F

RADIUS ~ IN

2.90 2.70 2.50 2.30 2.10 1.90 1.70

A

B

17

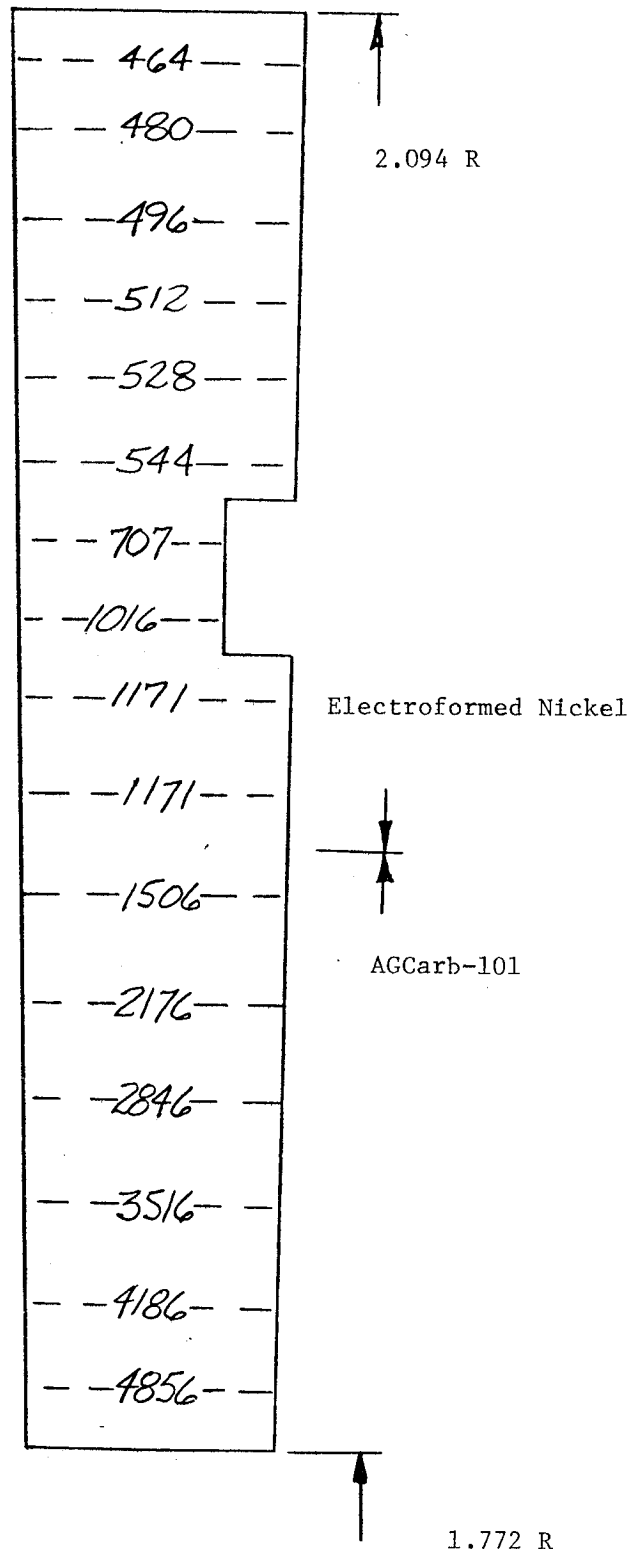


Figure 5 Coolant Channel Temperature Distribution Steady State Condition, °F, Stress Model Station 4.3 (Reference 7)

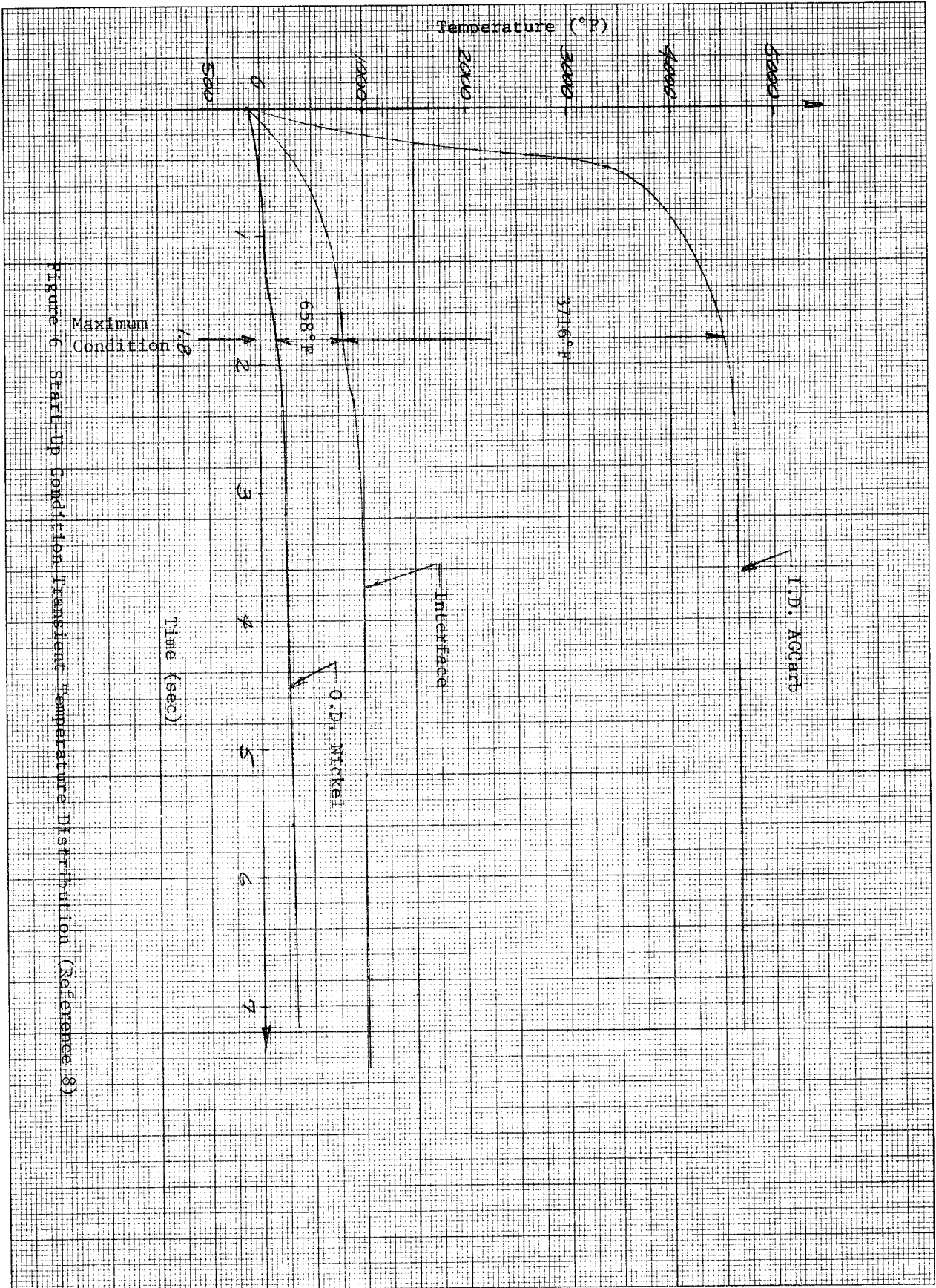


Figure 6 Start-Up Condition Transient Temperature Distribution (Reference 8)

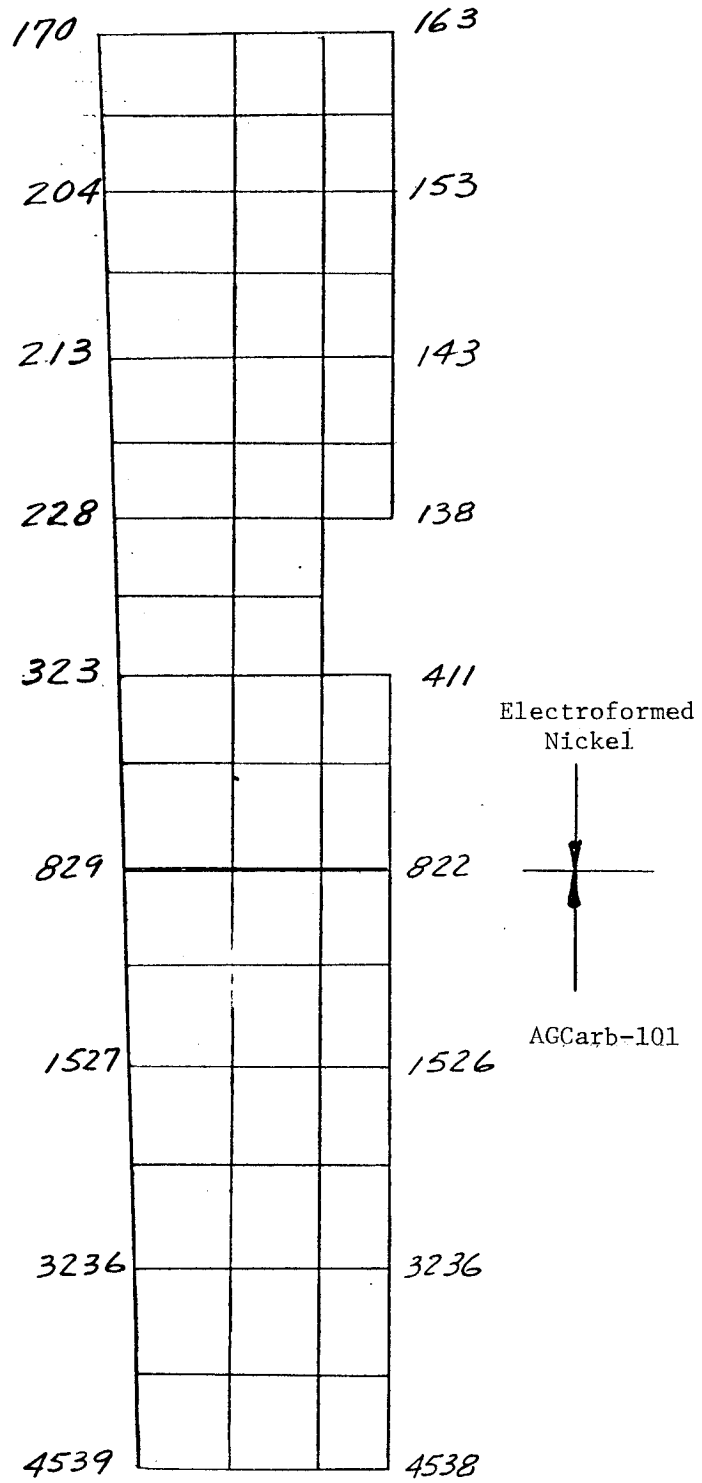


Figure 7 Coolant Channel Temperature Distribution  
 Transient Thermal Conditions, °F, Stress-Model  
 Station 4.3 (Reference 8)

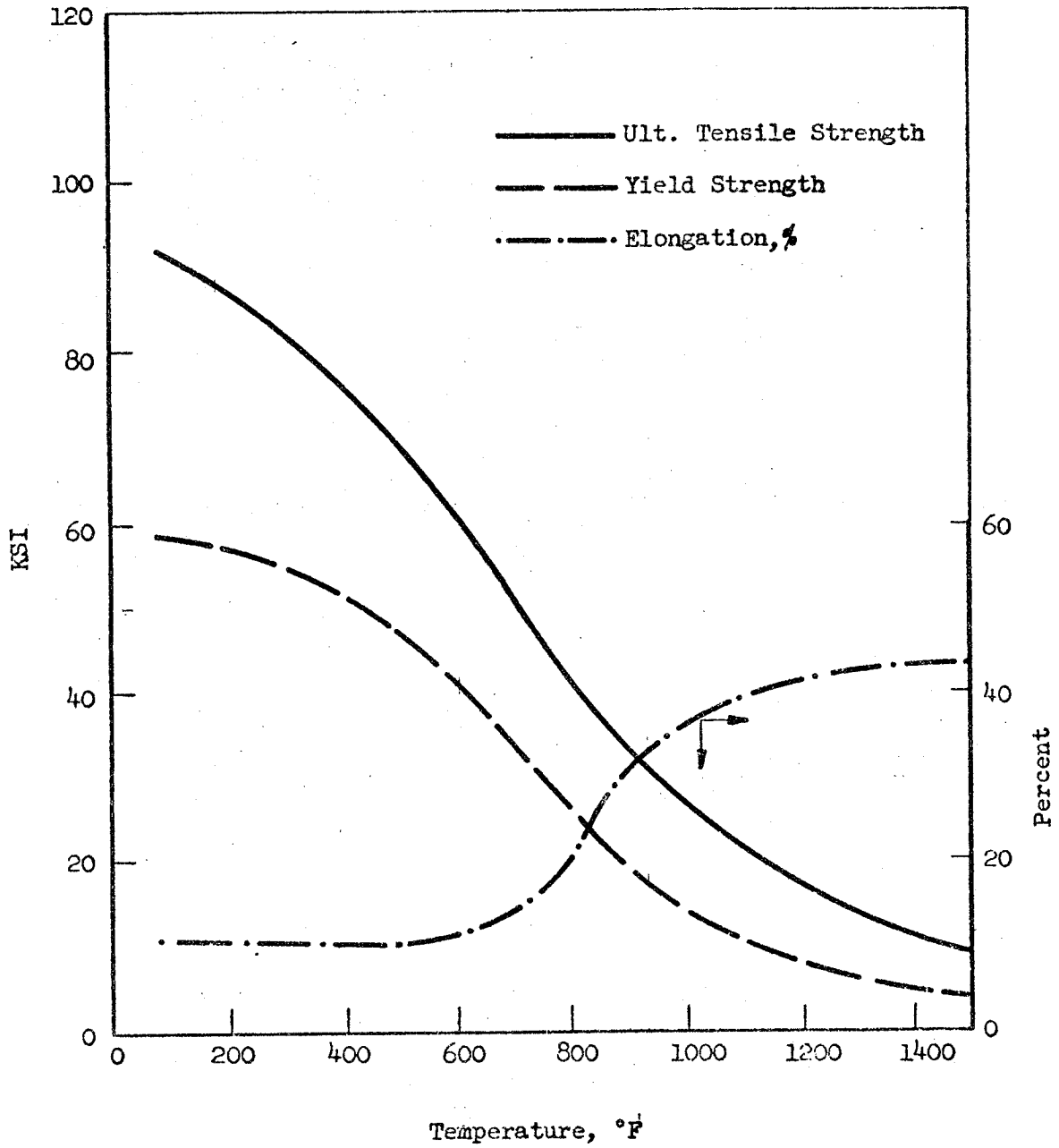


Figure 8  
Tensile Properties of Electroformed Nickel

DYNAMIC MODULUS  
VS  
TEMPERATURE  
ELECTROFORMED NICKEL

REFERENCE 2

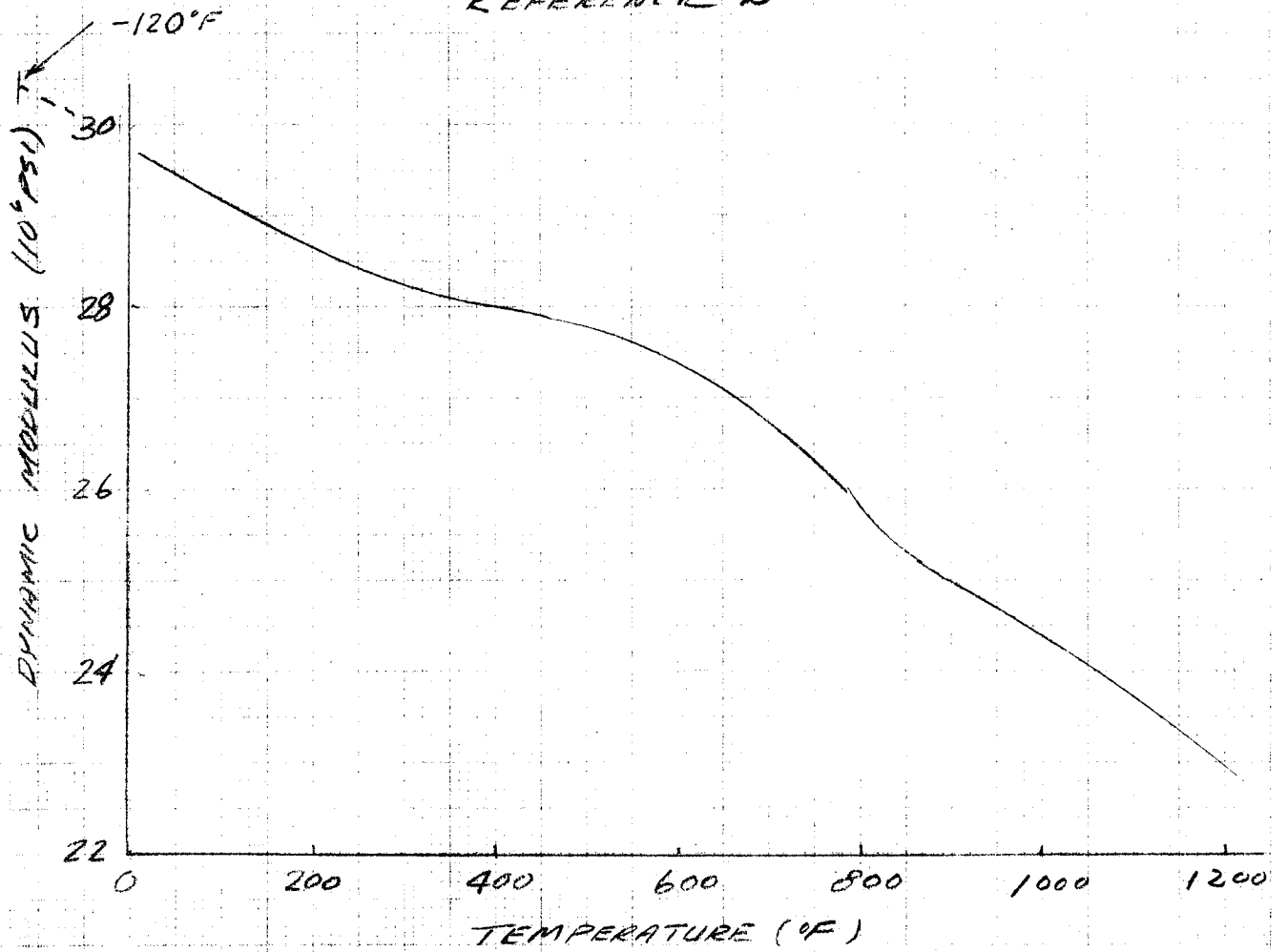
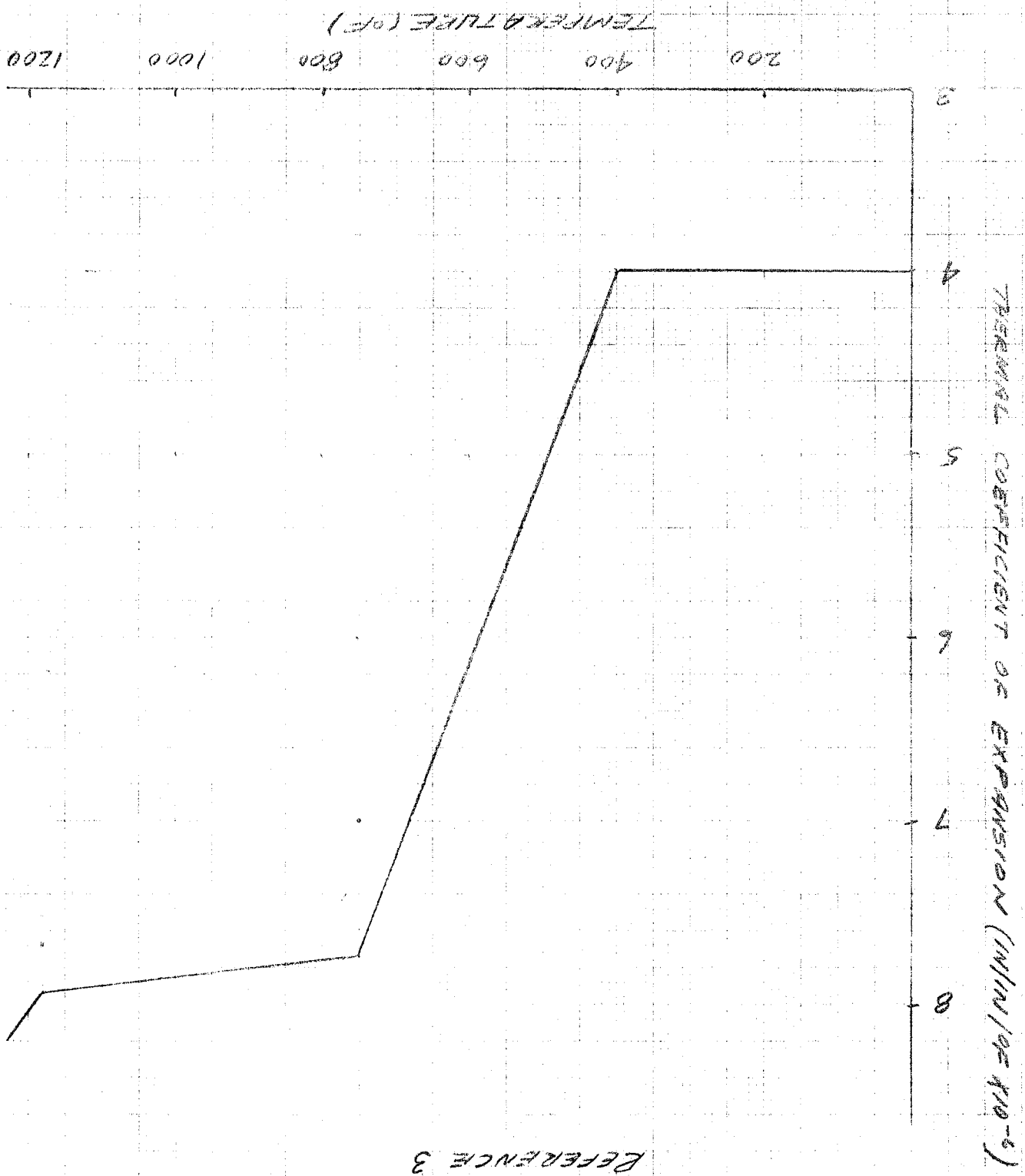


FIGURE 9

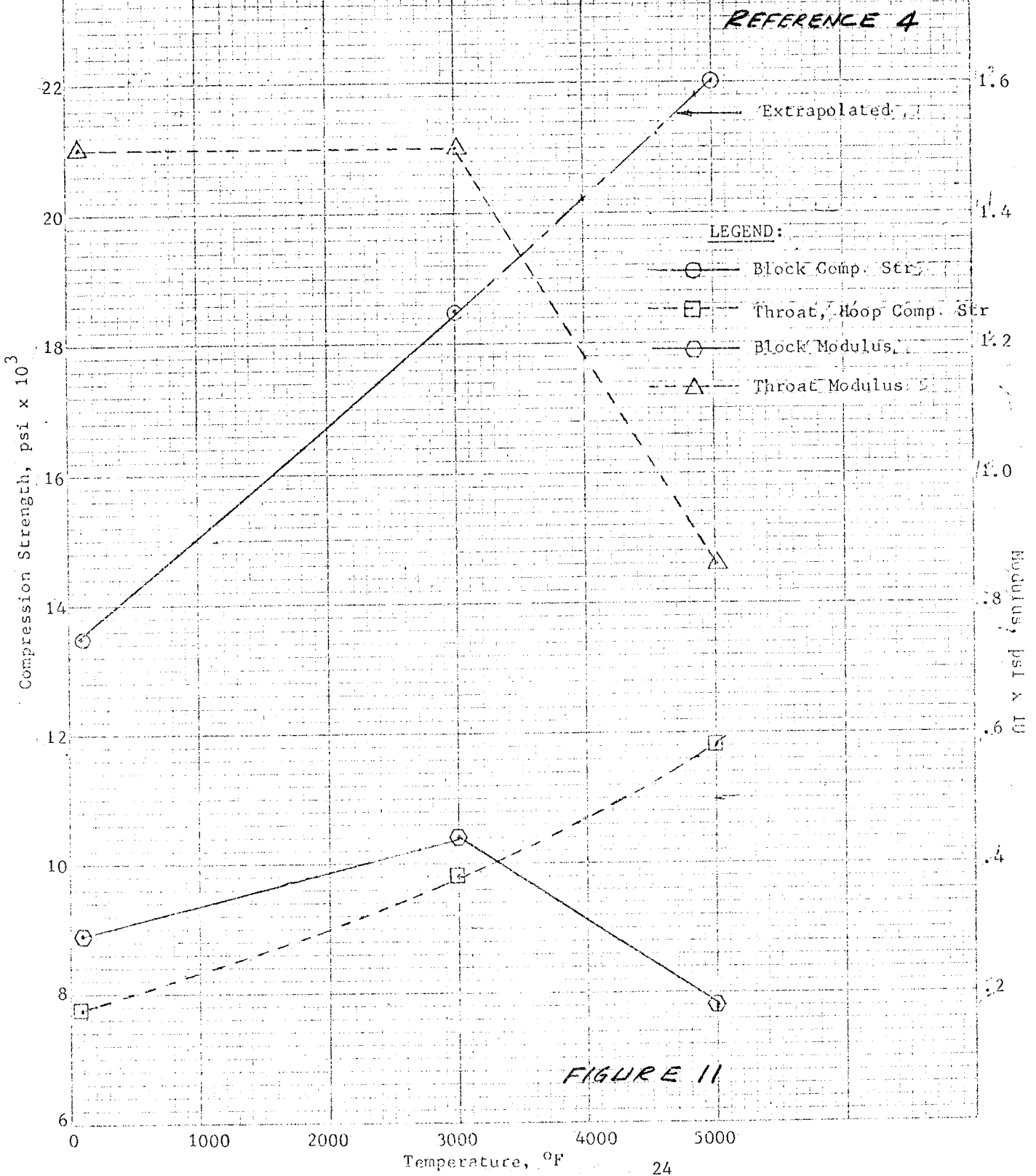


FIGURE 10



THE THERMAL COEFFICIENT  
OF  
EXPANSION  
OF  
ELECTROFORMED NICKEL

COMPRESSION STRENGTH AND MODULUS  
AGCarb-101 THROAT CONFIGURATION AND BLOCK  
TESTS



POISSON'S RATIO - AGCarb COMPRESSION TESTS

CONFIDENCE 4

LEGEND:

- Throat, hoop across plies
- Throat, hoop with plies
- Block, across plies

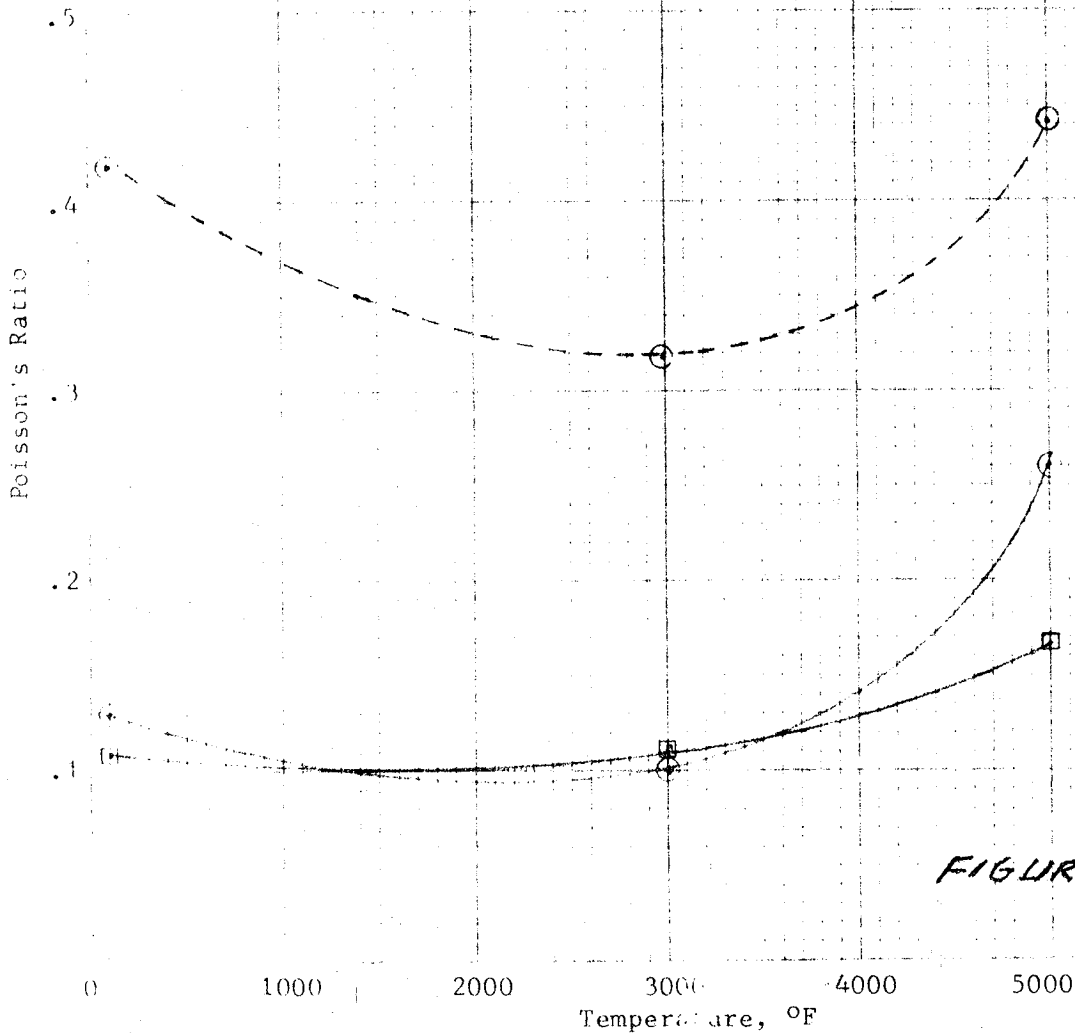


FIGURE 12

AGCARE-101  
INTERLAMINAR SHEAR  
STRENGTH  
REFERENCE 5

INTERLAMINAR SHEAR STRENGTH (PSI)

2000

1500

1000

500

0

1000

2000

3000

4000

5000

TEMPERATURE (°F)

FIGURE 13

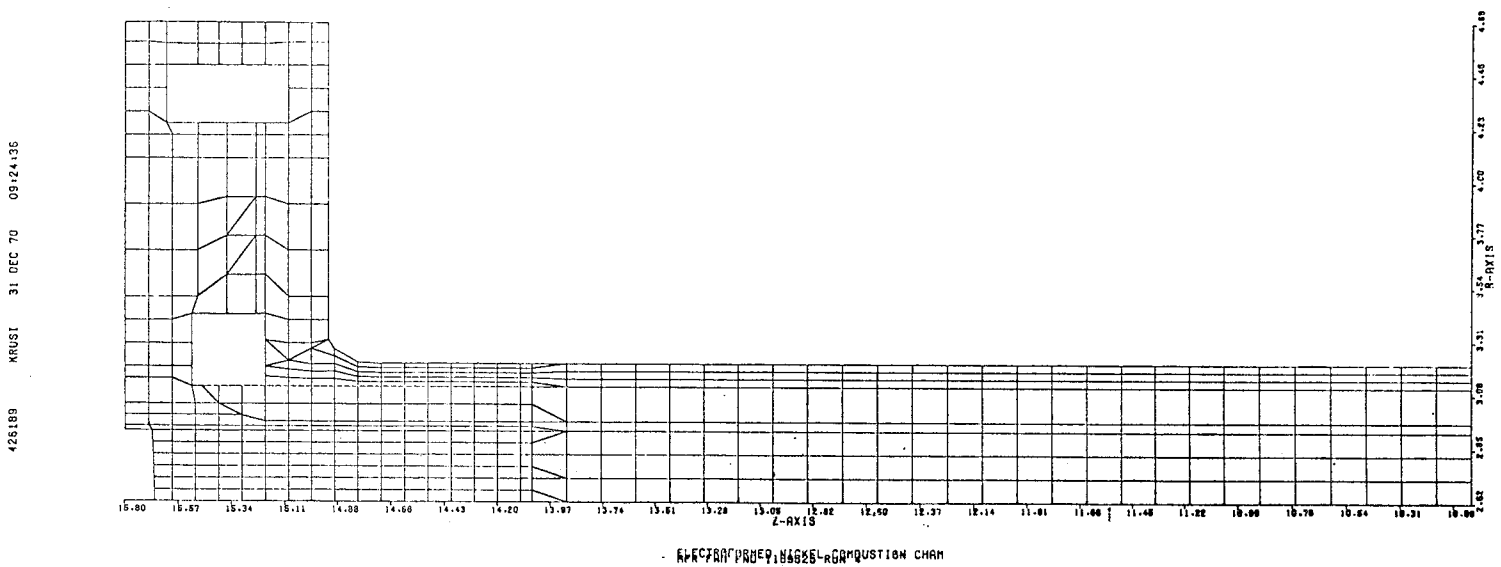
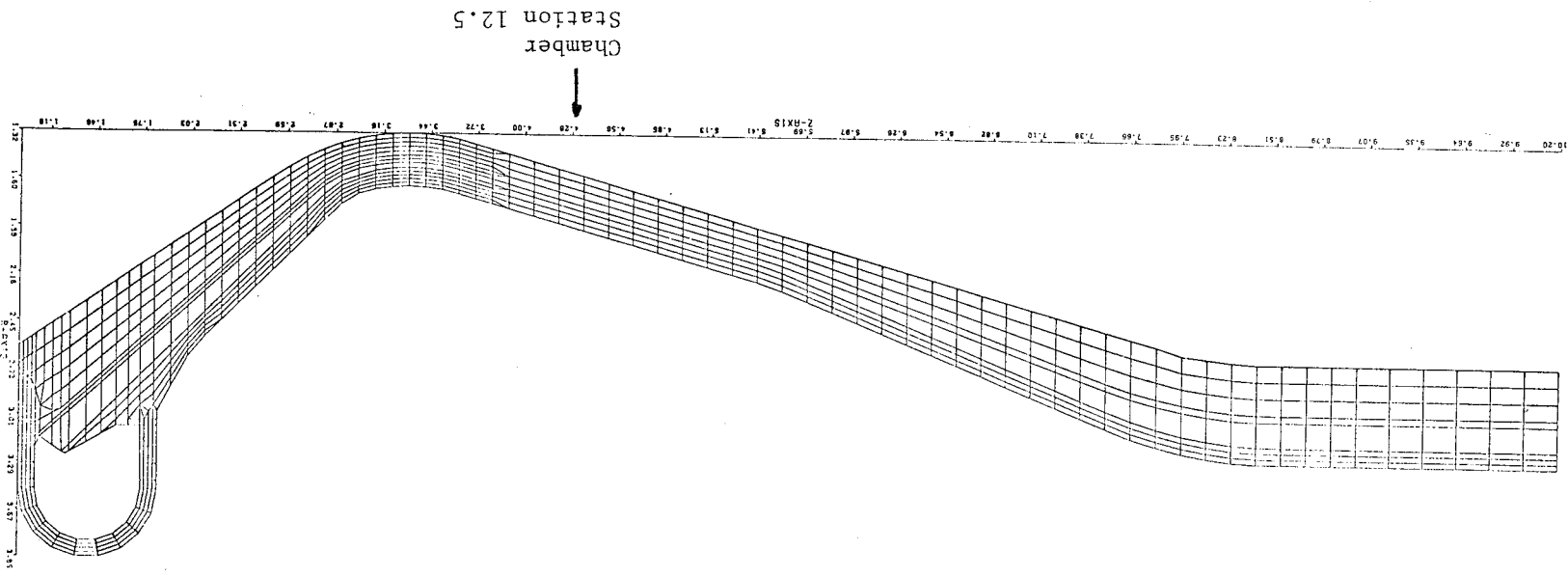


Figure 14 Regen Cooled AGCarb Lined Thrust Chamber Finite Element Model  
Axisymmetrical Analysis Forward End

Figure 15 Regen Cooled AGCarb Lined Thrust Chamber Finite Element Model  
Axisymmetrical Analysis Aft End



App B

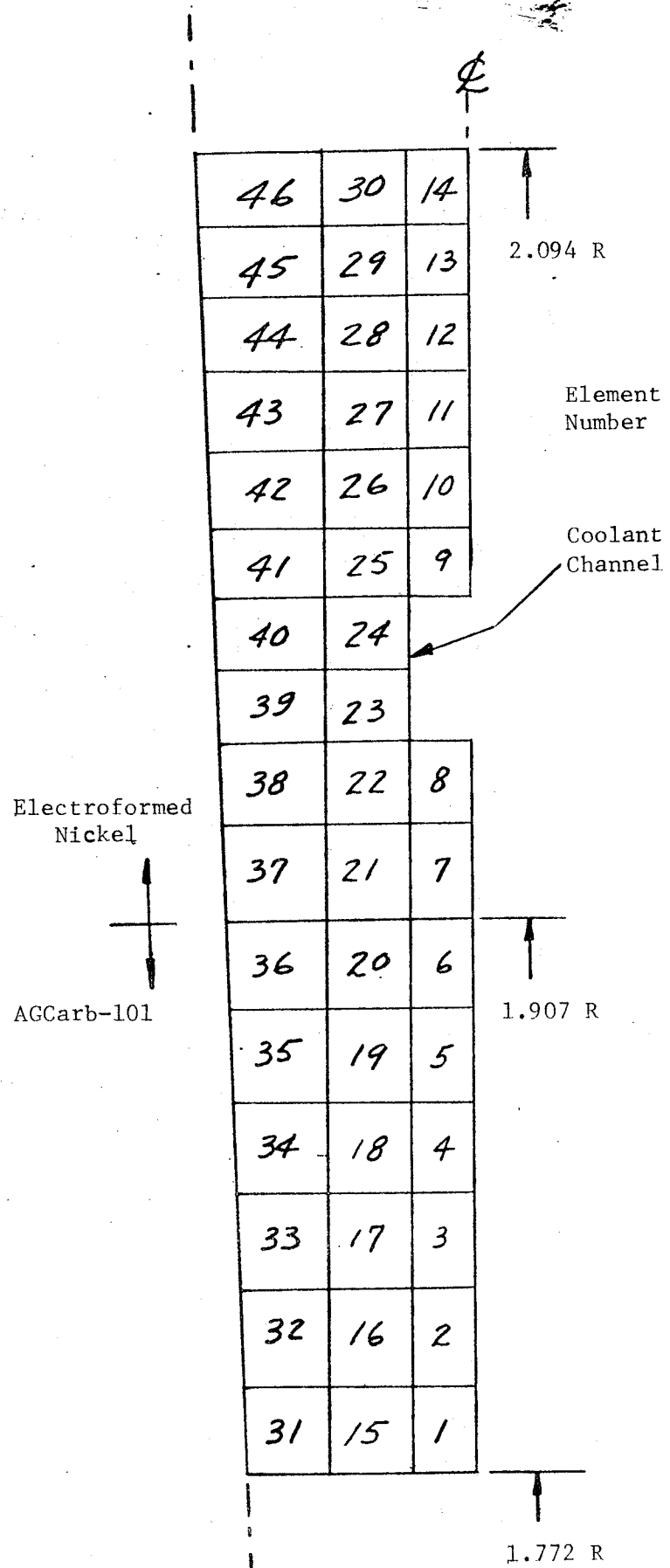


Figure 16 Regen Cooled AGCarb Lined Thrust Chamber Finite Element Model Plane Stress Analysis Coolant Channel Forward of Throat

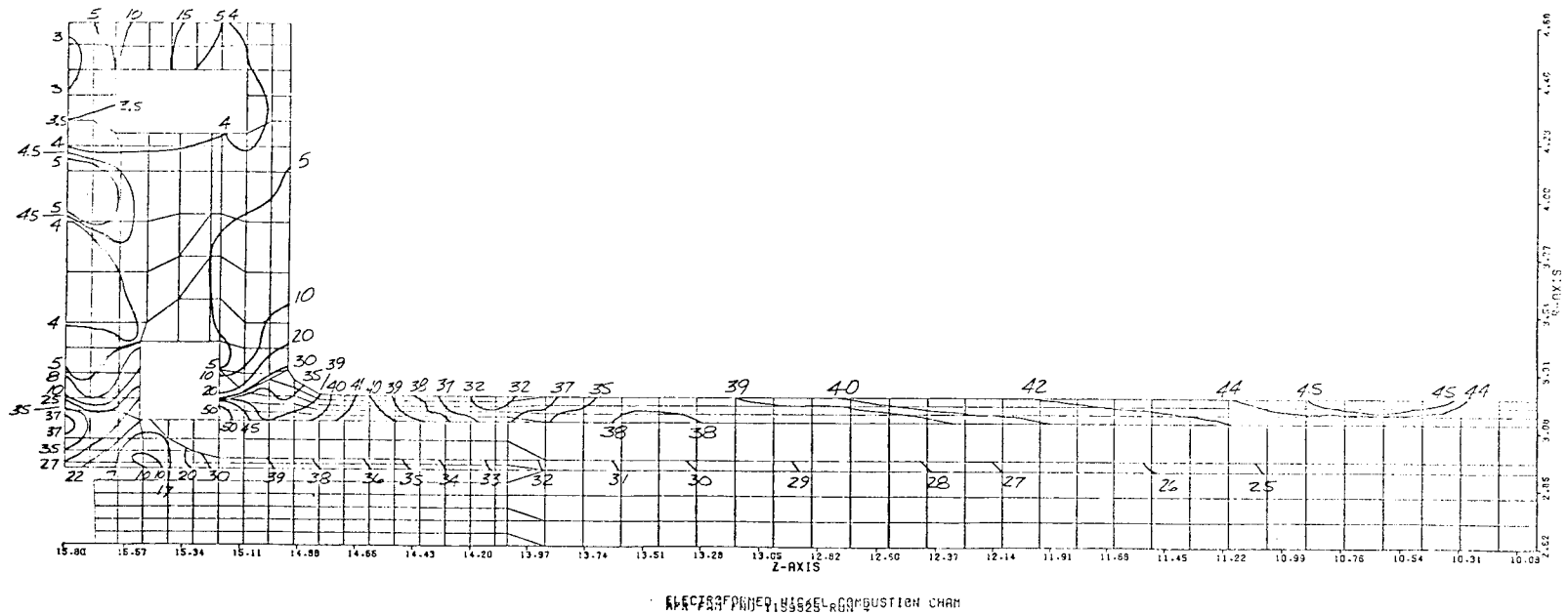


Figure 17 Effective Stress Distribution Electroformed Nickel Forward Shell and CRES 304-L Manifold, ksi



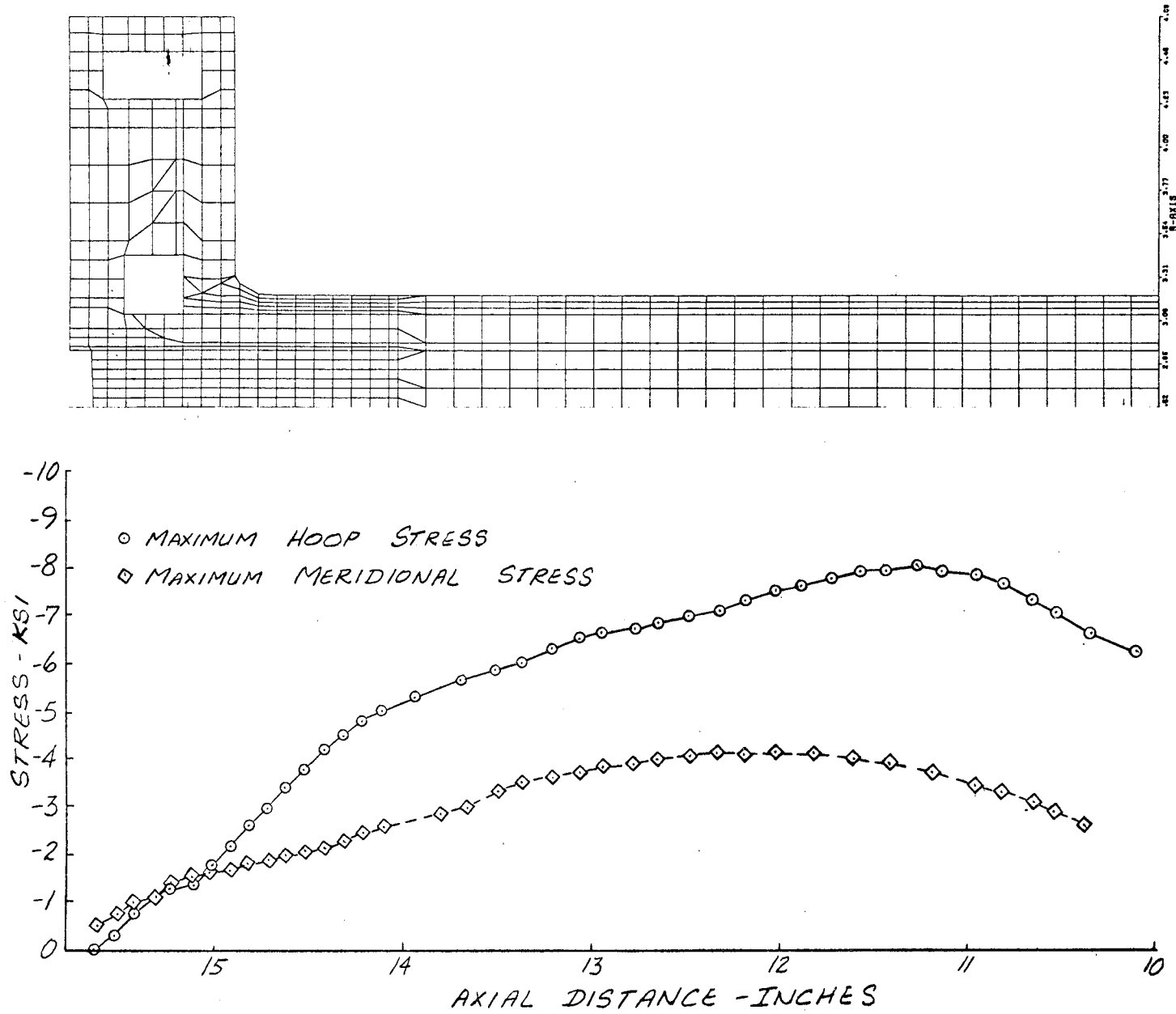
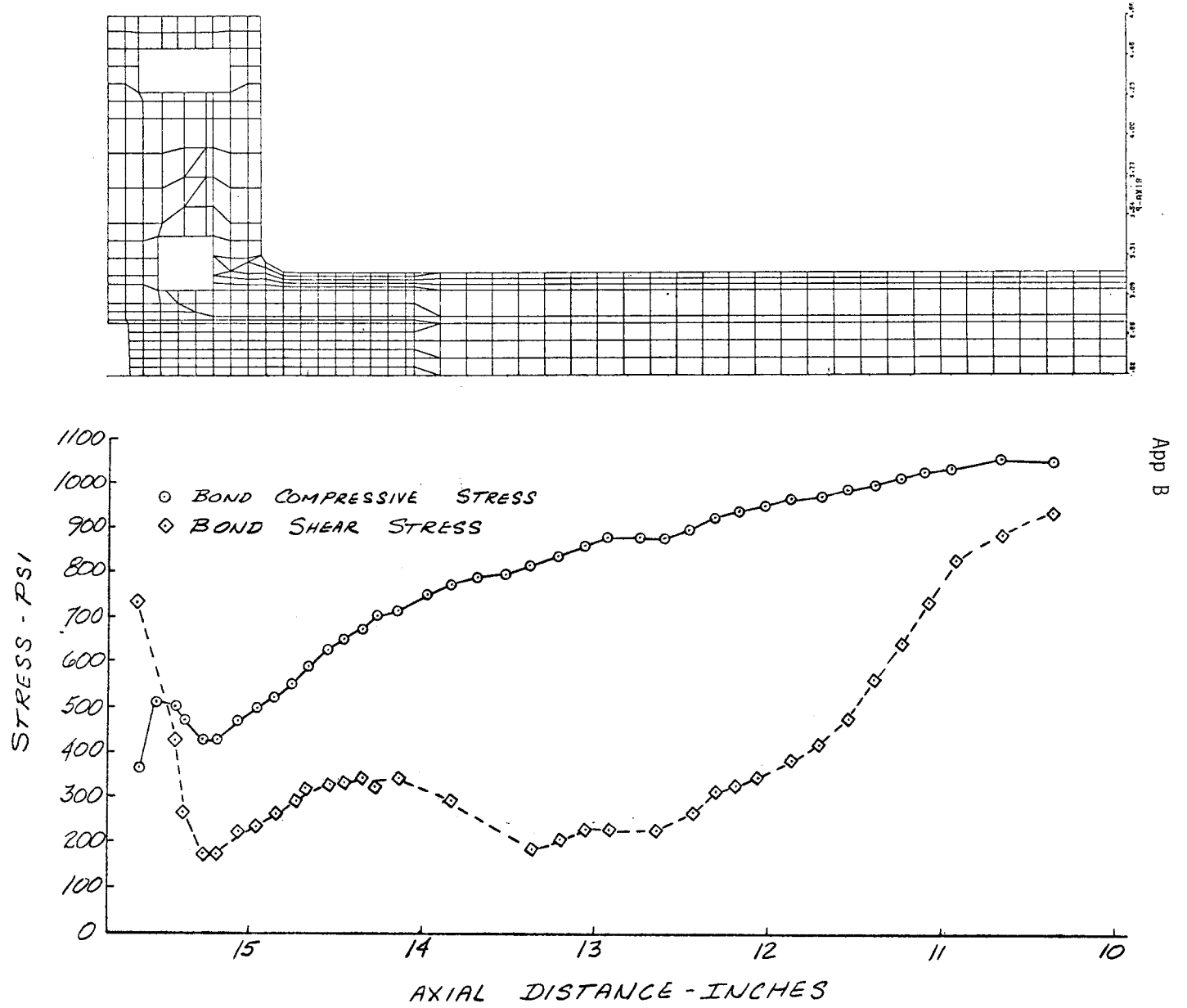


Figure 18 Hoop and Meridional Stress Distribution AGCarb-101 Forward Liner



App B

Figure 19 AGCarb-Nickel Bond Compressive and Shear Stress Distribution Forward End



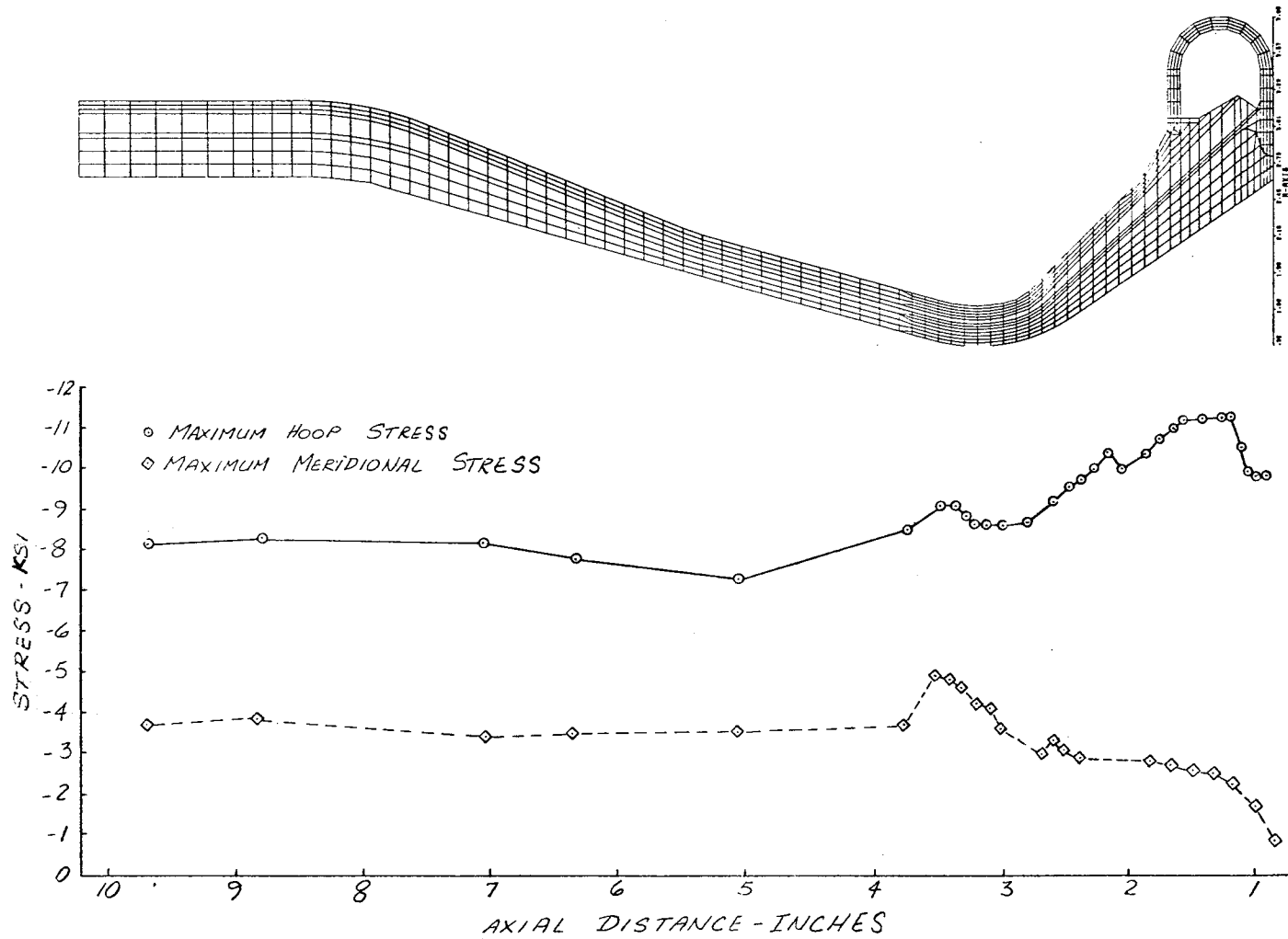


Figure 21 Hoop and Meridional Stress Distribution AGCarb-101 Aft Liner

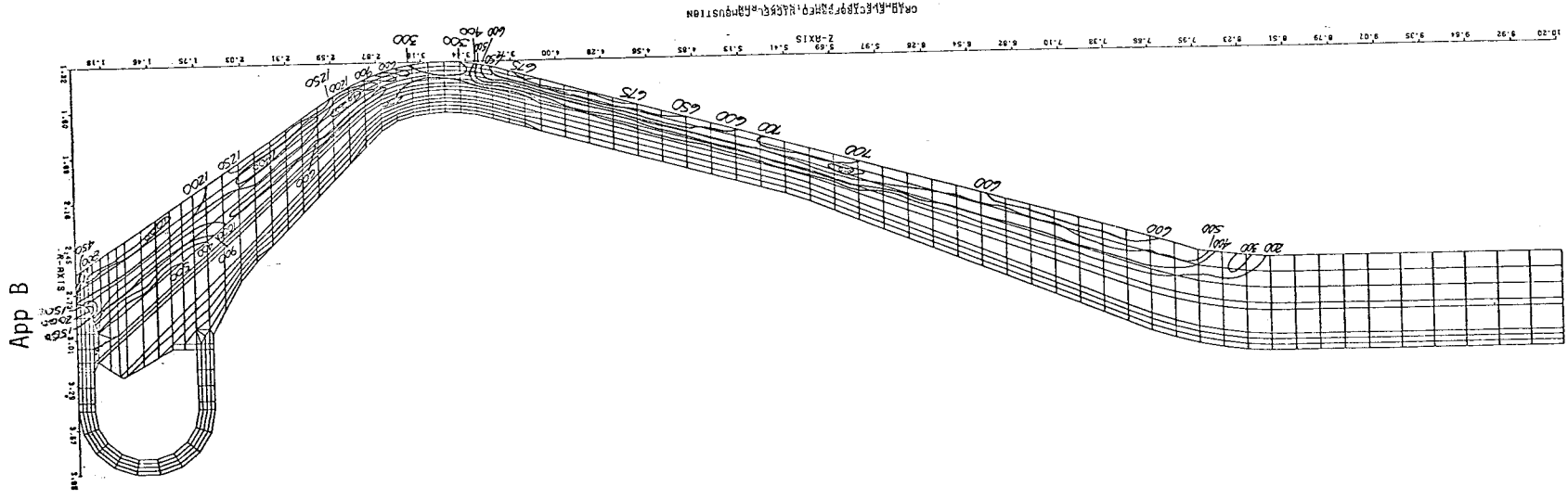


Figure 22 Iso-Stress Shear Distribution AGCarb-101 Liner Aft End, psi

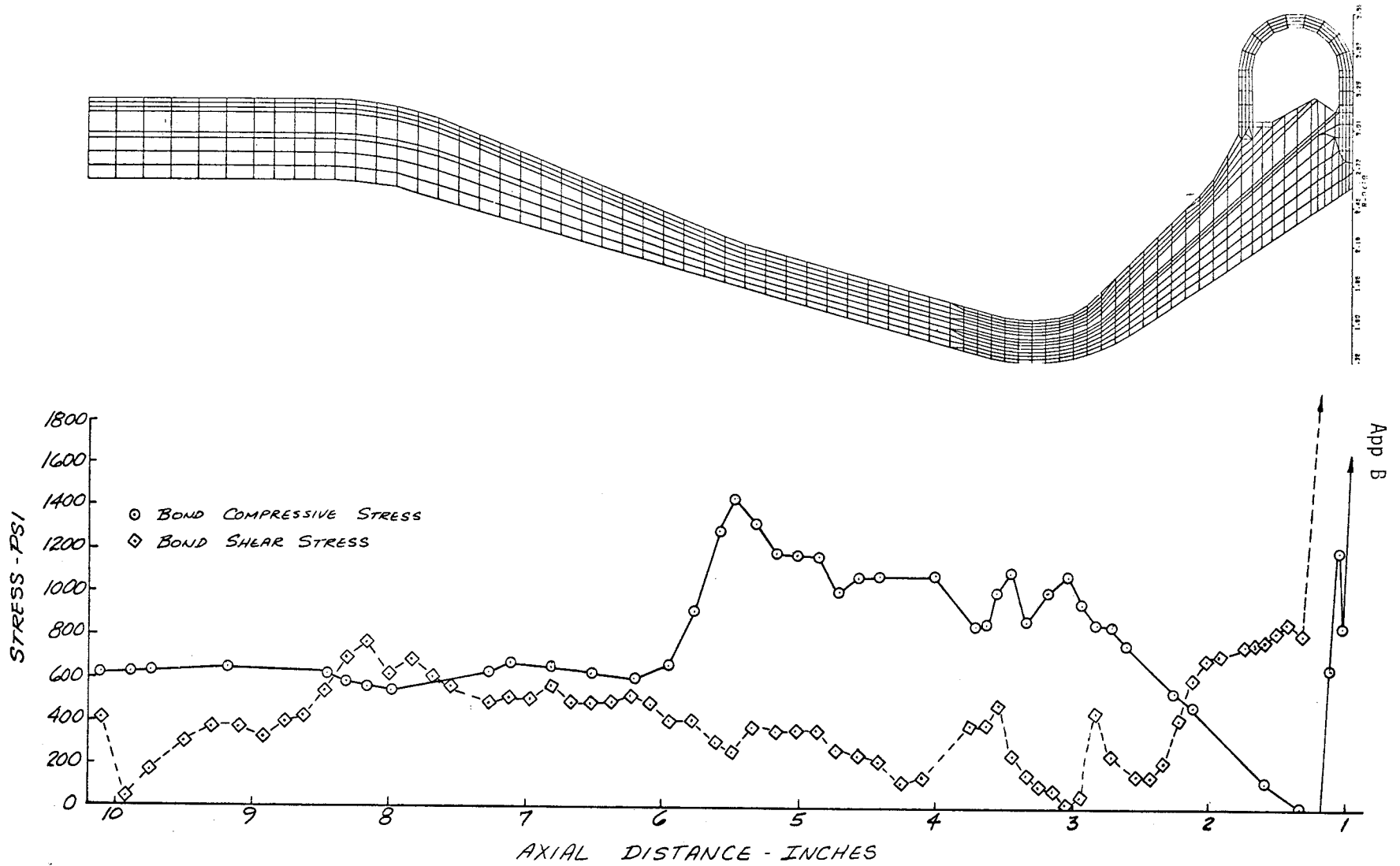


Figure 23 AGCarb-Nickel Bond Compressive and Shear Stress, Distribution Aft End

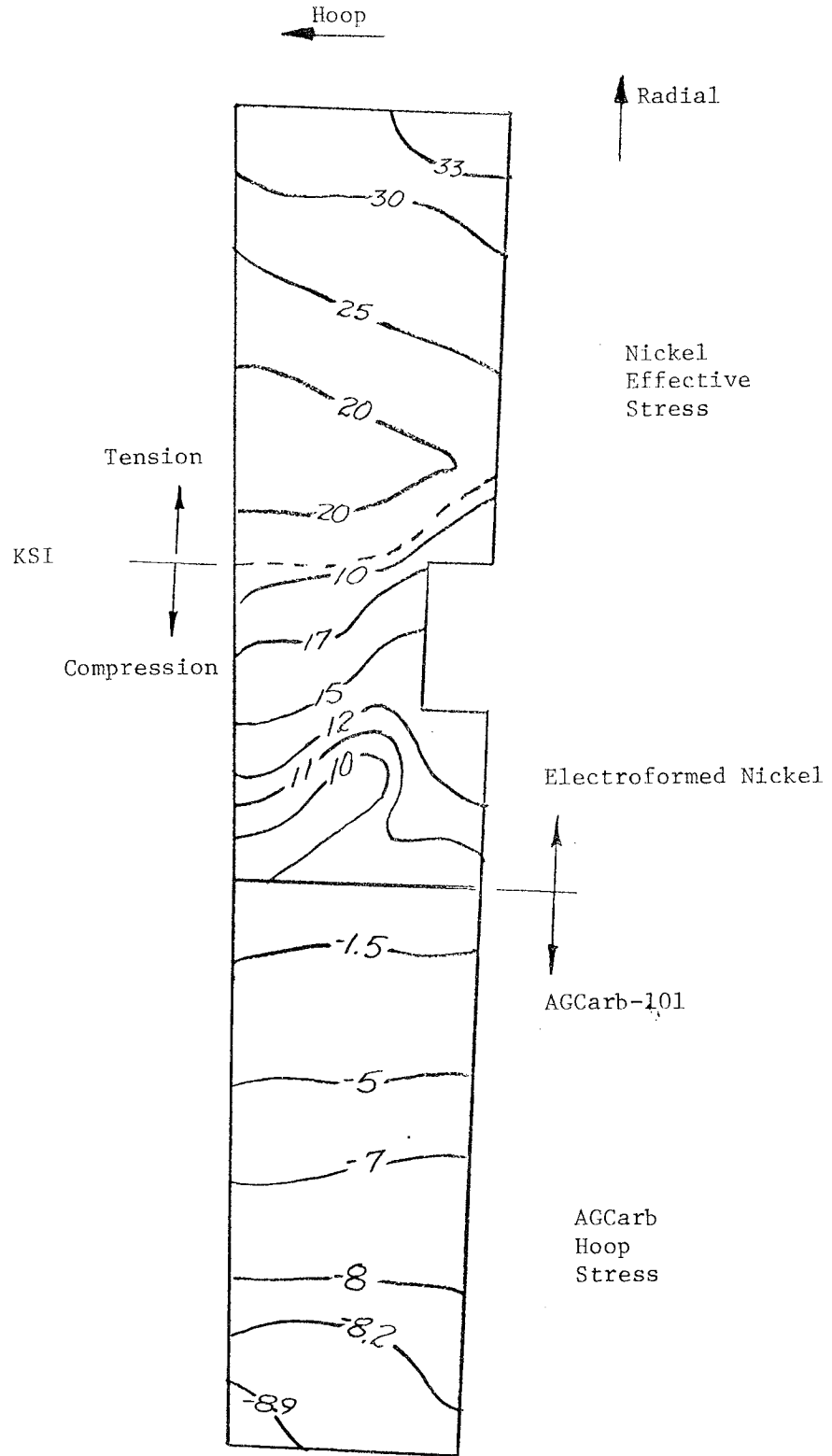


Figure 24 Effective Stress and Hoop Stress Distributions at Coolant Channel Stress Mode Station 4.3 Plane Stress Analysis for Steady State Temperature Conditions, °F

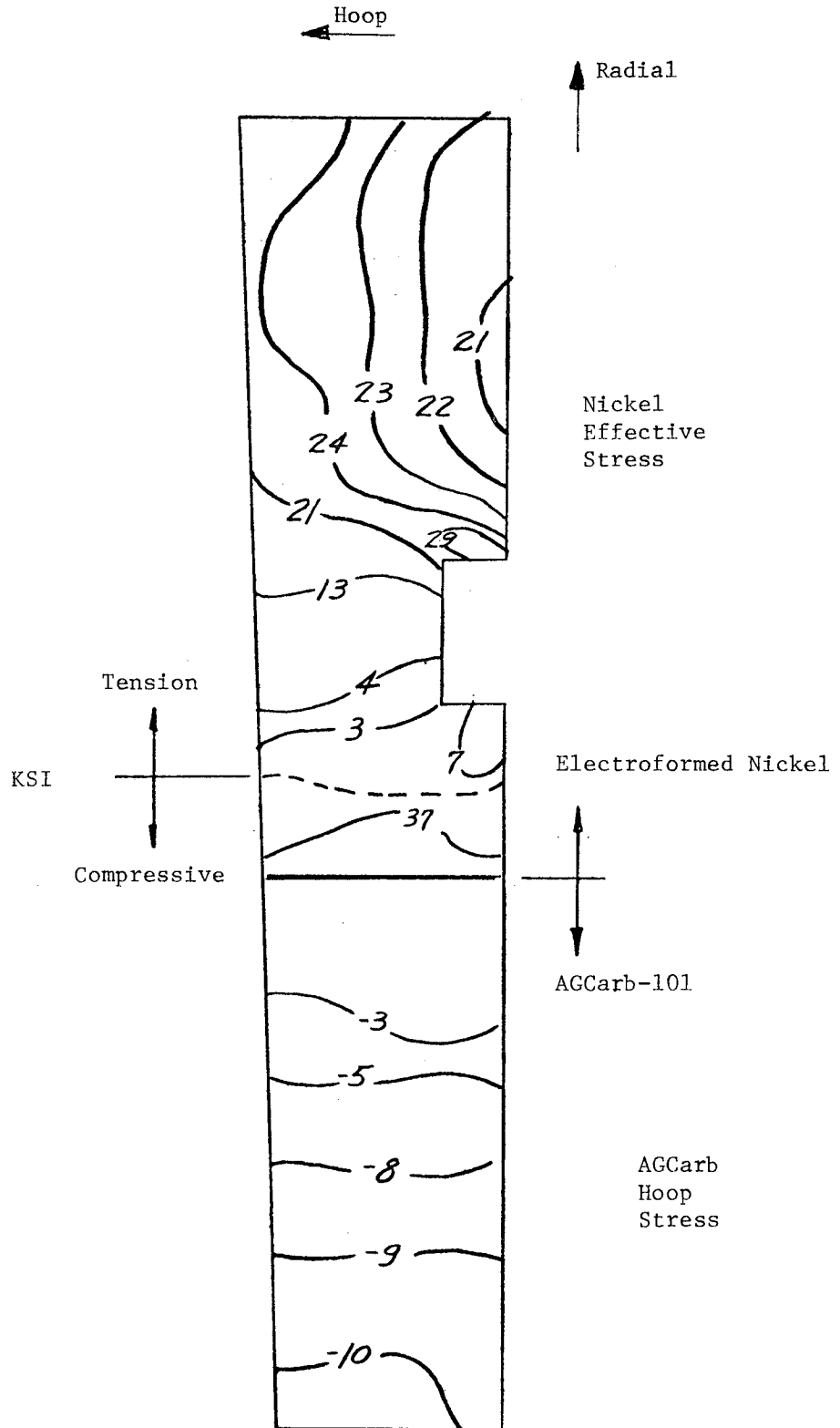


Figure 25 Effective Stress and Hoop Stress Distributions at Coolant Channel Stress Model Station 4.3 Plane Stress Analysis for Transient Temperature Conditions ( $t = 1.8$  sec)





APPENDIX C

DISTRIBUTION LIST



DISTRIBUTION LIST FOR FINAL REPORTInstructions:

Final reports are to be sent directly to the "Recipient" and the "Designee" per the quantities specified in the respective columns, R and D. When no copies are specified in column D, a carbon copy of the letter of transmittal should be sent to the person named as the "Designee". The letter of transmittal should contain the contract number and complete title of the final report.

The distribution list, indicating all of the Recipients and Designees, should be included in the final report as an appendix.

<u>REPORT COPIES</u>		<u>RECIPIENT</u>	<u>DESIGNEE</u>
<u>R</u>	<u>D</u>		
		National Aeronautics & Space Administration	
		Lewis Research Center	
		21000 Brookpark Road	
		Cleveland, Ohio 44135	
1		Attn: Contracting Officer, MS 500-313	
2		Liquid Rocket Technology Branch, MS 500-209	
1		Technical Report Control Office, MS 5-5	
1		Technology Utilization Office, MS 3-16	
2		AFSC Liaison Office, 501-3	
2		Library	
1		Office of Reliability & Quality Assurance, MS 500-111	
1		D. L. Nored, Chief, LRTB, MS 500-209	
10		<u>R. A. Duscha</u> Project Manager, MS 500-209	
1		E.W.Conrad, MS 500-204	
1		J.W.Gregory, MS 500-209	
1		J.M.Kazaroff, M.S. 500-204	
2		Chief, Liquid Experimental Engineering, RPX Office of Advanced Research & Technology NASA Headquarters Washington, D.C. 20546	

App C

REPORT  
COPIES  
R D

RECIPIENT

DESIGNEE

2	Chief, Liquid Propulsion Technology, RPL Office of Advanced Research & Technology NASA Headquarters Washington, D.C. 20546	
1	Director, Launch Vehicles & Propulsion, SV Office of Space Science & Applications NASA Headquarters Washington, D.C. 20546	
1	Chief, Environmental Factors & Aerodynamics Code RV-1 Office of Advanced Research & Technology NASA Headquarters Washington, D.C. 20546	
1	Chief, Space Vehicles Structures Office of Advanced Research & Technology NASA Headquarters Washington, D.C. 20546	
1	Director, Advanced Manned Missions, MT Office of Manned Space Flight NASA Headquarters Washington, D.C. 20546	
20	National Technical Information Service Springfield, Virginia 22151	
1	Director, Technology Utilization Division Office of Technology Utilization NASA Headquarters Washington, D.C. 20546	
1	National Aeronautics & Space Administration Ames Research Center Moffett Field, California 94035 Attn: Library	
1	National Aeronautics & Space Administration Flight Research Center P.O. Box 273 Edwards, California 93523 Attn: Library	

Hans M. Mark  
Mission Analysis  
Division

REPORT  
COPIES  
R D

RECIPIENTDESIGNEE

1	Aerospace Corporation 2400 E. El Segundo Blvd. Los Angeles, California 90045 Attn: Library-Documents	J. G. Wilder
1	Arthur D. Little, Inc. 20 Acorn Park Cambridge, Massachusetts 02140 Attn: Library	A. C. Tobey
1	Astropower Laboratory McDonnell-Douglas Aircraft Company 2121 Paularino Newport Beach, California 92163 Attn: Library	
1	DCIC, Battelle Memorial Institute Columbus Lab. - Room 11-9021 505 King Ave. Columbus, Ohio 43201 Attn: Library	J. F. Lynch
1	ARO, Incorporated Arnold Engineering Development Center Arnold AF Station, Tennessee 37389 Attn: Library	
1	Susquehanna Corporation Atlantic Research Division Shirley Highway & Edsall Road Alexandria, Virginia 22314 Attn: Library	
1	Battelle Memorial Institute 505 King Avenue Columbus, Ohio 43201 Attn: Report Library, Room 6A	
1	Beech Aircraft Corporation Boulder Facility Box 631 Boulder, Colorado Attn: Library	Douglas Pope
1 1	Bell Aerospace Company Box 1 Buffalo, New York 14240 Attn: Library	A. E. Leach

REPORT  
COPIES  
 R D

RECIPIENTDESIGNEE

1	Bendix Systems Division Bendix Corporation 3300 Plymouth Street Ann Arbor, Michigan Attn: Library	John M. Brueger
1	Bellcomm 955 L'Enfant Plaza, S. W. Washington, D.C. Attn: Library	H. S. London
1	Boeing Company Space Division P.O. Box 868 Seattle, Washington 98124 Attn: Library	J. D. Alexander C. F. Tiffany
1	Boeing Company 1625 K Street, N.W. Washington, D.C. 20006	
1	Boeing Company P.O. Box 1680 Huntsville, Alabama 35801	Ted Snow
1	Chemical Propulsion Information Agency Applied Physics Laboratory 8621 Georgia Avenue Silver Spring, Maryland 20910	Tom Reedy
1	Chrysler Corporation Missile Division P.O. Box 2628 Detroit, Michigan Attn: Library	John Gates
1	Chrysler Corporation Space Division P.O. Box 29200 New Orleans, Louisiana 70129 Attn: Librarian	
1	Electroforms, Inc. 239 East Gardena Blvd. Gardena, California 90247 Attn: Paul Silverstone	

REPORT  
COPIES  
R    D

RECIPIENTDESIGNEE

1	Radio Corporation of America Astro-Electronics Products Princeton, New Jersey Attn: Library	
1	Rocket Research Corporation Willow Road at 116th Street Redmond, Washington 98052 Attn: Library	F. McCullough, Jr.
1	Stanford Research Institute 333 Ravenswood Avenue Menlo Park, California 94025 Attn: Library	Dr. Gerald Marksman
1	San Rafael Plastics Co 97 Jordan St. Box 2908 San Rafael, California 94902	Peter Bayliss
1	Thiokol Chemical Corporation Redstone Division Huntsville, Alabama Attn: Library	John Goodloe
1	TRW Systems Inc. 1 Space Park Redondo Beach, California 90278 Attn: Tech. Lib. Doc. Acquisitions	Curtis Watts
1	TRW TAPCO Division 23555 Euclid Avenue Cleveland, Ohio 44117	P. T. Angell
1	United Aircraft Corporation Corporation Library 400 Main Street East Hartford, Connecticut 06108 Attn: Library	Dr. David Rix Erle Martin Frank Owen Wm. E. Taylor
1	United Aircraft Corporation Pratt & Whitney Division Florida Research & Development Center P. O. Box 2691 West Palm Beach, Florida 33402 Attn: Library	J. P. Mitchell Dr. Schmitke



REPORT

COPIES

R     D

RECIPIENT

DESIGNEE

1

United Aircraft Corporation  
United Technology Center  
P. O. Box 358  
Sunnyvale California 94038  
Attn: Library

Dr. David Altman

1

Vickers Incorporated  
Box 302  
Troy, Michigan

1

Vought Astronautics  
Box 5907  
Dallas, Texas  
Attn: Library

1

Union Carbide Corporation  
Carbon Products Division  
Parma Technical Center  
P. O. Box 6116  
Cleveland, Ohio 44101  
Attn: Library

J. M. Criscione

REPORT  
COPIES  
R    D

RECIPIENTDESIGNEE

1	Martin-Marietta Corporation (Baltimore Division) Baltimore, Maryland 21203 Attn: Library	
1	Denver Division Martin-Marietta Corporation P. O. Box 179 Denver, Colorado 80201 Attn: Library	Dr. Morgenthaler F. R. Schwartzberg
1	Orlando Division Martin-Marietta Corporation Box 5827 Orlando, Florida Attn: Library	J. Fern
1	Western Division McDonnell Douglas Astronautics 5301 Bolsa Ave Huntington Beach, California 92647 Attention: Library	R. W. Hallet G. W. Burge P. Klevatt
1	McDonnell Douglas Aircraft Corporation P. O. Box 516 Lambert Field, Missouri 63166 Attn: Library	R. A. Herzmark
1	Rocketdyne Division North American Rockwell Inc. 6633 Canoga Avenue Canoga Park, California 91304 Attn: Library, Department 596-306	Donald Fulton
1	Space & Information Systems Division North American Rockwell 12214 Lakewood Blvd. Downey, California Attn: Library	
1	Northrop Space Laboratories 3401 West Broadway Hawthorne, California Attn: Library	Dr. William Howard
1	Purdue University Lafayette, Indiana 47907 Attn: Library (Technical)	Dr. Bruce Rouse

REPORT  
COPIES  
R D

RECIPIENTDESIGNEE

1	Grumman Aircraft Engineering Corporation Bethpage, Long Island, New York Attn: Library	Joseph Gavli
1	Hercules Powder Company Allegheny Ballistics Laboratory P. O. Box 210 Cumberland, Maryland 21501 Attn: Library	
1	Honeywell Inc. Aerospace Division 2600 Ridgeway Road Minneapolis, Minnesota Attn: Library	
1	IIT Research Institute Technology Center Chicago, Illinois 60616 Attn: Library	C. K. Harsh
1	Kidde Aer-Space Division Walter Kidde & Company, Inc. 567 Main Street	R. J. Hanville
1	Ling-Temco-Vought Corporation P. O. Box 5907 Dallas, Texas 75222 Attn: Library	
1	Lockheed Missiles and Space Company P. O. Box 504 Sunnyvale, California 94087 Attn: Library	
1	Poco Graphite, Inc. 1200 Jupiter Rd. P. O. Box 1524 Garland, Texas 75040	R. F. Wehrmann
1	Lockheed Propulsion Company P. O. Box 111 Redlands, California 92374 Attn: Library, Thackwell	H. L. Thackwell
1	Marquardt Corporation 16555 Saticoy Street Box 2013 - South Annex Van Nuys, California 91409	L. R. Bell Jr.

REPORT  
COPIES  
R D

	<u>RECIPIENT</u>	<u>DESIGNEE</u>
1	National Aeronautics & Space Administration Goddard Space Flight Center Greenbelt, Maryland 20771 Attn: Library	Merland L. Moseson, Code 620
1	National Aeronautics & Space Administration John F. Kennedy Space Center Cocoa Beach, Florida 32931 Attn: Library	Dr. Kurt H. Debus
1	National Aeronautics & Space Administration Langley Research Center Langley Station Hampton, Virginia 23365 Attn: Library	E. Cortwright Director
1	National Aeronautics & Space Administration Manned Spacecraft Center Houston, Texas 77001 Attn: Library	J. G. Thibodaux, Jr. Chief, Propulsion & Power Division
1	National Aeronautics & Space Administration George C. Marshall Space Flight Center Huntsville, Alabama 35812 Attn: Library	Hans G. Paul James Thomas
2	NASA Scientific & Technical Information Facility P.O. Box 33 College Park, Maryland 20740 Attn: NASA Representative	
1	Jet Propulsion Laboratory 4800 Oak Grove Drive Pasadena, California 91103 Attn: Library	Henry Burlage, Jr. Duane Dipprey
1	Defense Documentation Center Cameron Station Building 5 5010 Duke Street Alexandria, Virginia 22314 Attn: TISIA	
1	Office of the Director of Defense Research & Engineering Washington, D.C. 20301 Attn: Office of Asst. Dir. (Chem. Technology)	

REPORT  
COPIES  
R D

RECIPIENTDESIGNEE

1	RTD (RTNP) Bolling Air Force Base Washington, D.C. 20332	
1	Arnold Engineering Development Center Air Force Systems Command Tullahoma, Tennessee 37389 Attn: Library	Dr. H. K. Doetsch
1	Advanced Research Projects Agency Washington, D.C. 20525 Attn: Library	
1 1	Nonmetallic Materials Division Air Force Materials Lab (AFSC) Wright-Patterson Air Force Base, Dayton, Ohio 45433 Attn: Library	D. L. Schmidt Code MANC
1	Air Force Missile Test Center Patrick Air Force Base, Florida Attn: Library	L. J. Ullian
1	Air Force Systems Command Andrews Air Force Base Washington, D.C. 20332 Attn: Library	Capt. S. W. Bowen SCLT
1 1	Air Force Rocket Propulsion Laboratory (RPR) Edwards, California 93523 Attn: Library	Donald Penn Robert Wiswell
1	Air Force Rocket Propulsion Laboratory (RPM) Edwards, California 93523 Attn: Library	
1	Air Force FTC (FTAT-2) Edwards Air Force Base, California 93523 Attn: Library	Donald Ross
1	Air Force Office of Scientific Research Washington, D.C. 20333 Attn: Library	SREP, Dr. J. F. Masi

REPORT  
COPIES  
R D

RECIPIENT

DESIGNEE

1	Space & Missile Systems Organization Air Force Unit Post Office Los Angeles, California 90045 Attn: Technical Data Center	
1	Office of Research Analyses (OAR) Holloman Air Force Base, New Mexico 88330 Attn: Library RRRD	
1	U. S. Air Force Washington, D.C. Attn: Library	Col. C. K. Stambaugh, Code AFRST
1	Commanding Officer U. S. Army Research Office (Durham) Box CM, Duke Station Durham, North Carolina 27706 Attn: Library	
1	U. S. Army Missile Command Redstone Scientific Information Center Redstone Arsenal, Alabama 35808 Attn: Document Section	Dr. W. Wharton
1	Bureau of Naval Weapons Department of the Navy Washington, D.C. Attn: Library	J. Kay, Code RTMS-41
1	Commander U. S. Naval Missile Center Point Mugu, California 93041 Attn: Technical Library	
1	Commander U. S. Naval Weapons Center China Lake, California 93557 Attn: Library	
1	Commanding Officer Naval Research Branch Office 1030 E. Green Street Pasadena, California 91101 Attn: Library	

REPORT  
COPIES  
R D

RECIPIENTDESIGNEE

1	Director (Code 6180) U. S. Naval Research Laboratory Washington, D.C. 20390 Attn: Library	H. W. Carhart J. M. Krafft.
1	Picatinny Arsenal Dover, New Jersey 07801 Attn: Library	I. Forsten
1	Air Force Aero Propulsion Laboratory Research & Technology Division Air Force Systems Command United States Air Force Wright-Patterson AFB, Ohio 45433 Attn: APRP (Library)	R. Quigley C. M. Donaldson
1	Electronics Division Aerojet-General Corporation P.O. Box 296 Azusa, California 91703 Attn: Library	
1	Space General Corporation  9100 East Flair Drive El Monte, California 91734 Attn: Library	
1	Aerojet Liquid Ordnance and Manufacturing 11711 South Woodruff Avenue Fullerton, California 90241 Attn: Library	
1	Aerojet Liquid Rocket Company P. O. Box 13222 Sacramento, California 95813 Attn: Technical Library 2484-2015A	
1	Aeronutronic Division of Philco Ford Corp. Ford Road Newport Beach, California 92663 Attn: Technical Information Department	Dr. L. H. Linder